Vol. 14 • No. 2 • October 2020

ISSN: 0976 - 1330

Journal of GEOMATICS

INDIAN SOCIETY OF GEOMATICS

Journal of Geomatics

(A publication of the Indian Society of Geomatics)

Secretary: (address for correspondence)
6202, Space Applications Centre, ISRO, Bopal Campus, Ahmedabad-380058, India
Email: secretary@isgindia.org; sasharma@sac.isro.gov.in

Journal of Geomatics

(A Publication of the Indian Society of Geomatics)
Vol. 14. No. 2 Research articles October 2020

Filtering of quantified solid earth tidal data for deformation monitoring

I. Yakubu* and B. Kumi-Boateng
Department of Geomatic Engineering, University of Mines and Technology, Tarkwa, Ghana
*Email: yissaka@umat.edu.gh

(Received: Jan 29, 2020; in final form: July 16, 2020)

Abstract: Data filtering is the process of defining, detecting and correcting errors in a raw survey data in order to minimize the impact on succeeding analyses. Filtering of noise is an important feature in a dataset because noise limits the relevance of the data. In deformation monitoring, the need to remove/reduce all noise associated with raw data before further processing and interpretations on the data cannot be underestimated. Several techniques have been used by researchers to filter survey data. These include; model-free techniques, model-based techniques, and techniques based on empirical models. The researcher in previous studies had quantified tidal effect on the earth crust for various geographic locations in the five (5) Regions of Ghana using the theory of Love. Also, further research conducted by the researcher used three mathematical methods namely; Auto-Regressive Integrated Moving Average (ARIMA) Time Series, Non-Linear Auto-Regressive Neural Network (NARNET), and Hybrid ARIMA and Neural Network to model and predict the tidal effect on the earth crust for geodetic deformation monitoring. This research will use the Empirical Mode Decomposition, Kalman Filter, Moving Average Filter and Savitzky-Golay Filter on computed solid earth tidal data for varying geographic locations and predicted monthly for five years. The solid earth tidal effect data values in the study area were categorized into three main groups; those along the coastal line (COAST), those away from the coastline (INLAND) and those in between Coastal line and Inland (MIDDLE). The Relative Error Correction (REC) of the INLAND displacements when the various filtering techniques were adopted resulted in; 97.47, 76.69, 75.47 and 69.00 % for Empirical Mode Decomposition, Moving Average, Savitzky-Golay and Kalman filters respectively. The REC of the MIDDLE displacements was; 98.65, 81.90, 79.08 and 71.95 % for Empirical Mode Decomposition, Moving Average, Savitzky-Golay and Kalman filters correspondingly. The averages of the COAST displacements were 98.67, 84.88, 85.07 71.94 % for Empirical Mode Decomposition, Moving Average, Savitzky-Golay and Kalman filters respectively. The statistical performance indicators based on Root Mean Square, Percentage Error and Mean Absolute Percentage Error, revealed that the Empirical Mode Decomposition filter was the most efficient comparatively.

Keywords: Moving average filter, Kalman filter, Savitzky-Golay filter, Empirical Mode Decomposition

1. Introduction

Deformation monitoring is of major importance in engineering projects. It is imperative that both natural and man-made edifices are monitored periodically. This is because the earth crust and engineering structures such as buildings, dams, bridges, mining pit walls are subjected to deformation resulting from either natural or man-induced phenomena such as earthquakes, tectonic activities, ground water level changes, tidal phenomena, mining and quarrying (Yakubu et al., 2010). Construction of high-rise buildings and other engineered structures has become more sophisticated over the past decades. The increasing exploitation of both solid and liquid minerals beneath earth surface has given more impetus on the need for studies into crustal movements. Hence, requirements for accuracy of data collected for deformation monitoring has become more significant. In deformation monitoring, practical and scientific reasons exist for the study (Chen, 1983). The spatiotemporal changes of natural or manmade structures, necessitate the need to periodically monitor these structures to ensure their safety. To ensure data integrity and accuracy, the periodic monitoring of the structure requires filtering of the data collected.

In order to minimise the error impact on succeeding analyses, filtering will detect/correct errors in the raw data (Wedin, 2008). Some techniques developed to filter raw data are; Kalman Filter, Moving Average Filter, Savitzky-Golay, Empirical Mode Decomposition (EMD). In this paper, these filtering methods are applied on quantified solid earth tidal effect data from different geographic locations in five regions of Ghana (Yakubu and Kumi-Boateng, 2019). The relatively best filtering method was hybridised with the other filtering method in a bid to have an optimal filtering method(s).

The Kalman filter was developed as a recursive solution to discrete-data linear filtering problem. Based on theory, the Kalman Filter is an estimator for linear-quadratic problem (Kalman and Bucy, 1961). It estimates the instantaneous "state" of a linear dynamic system perturbed by white noise using measurements linearly linked to the state but tainted by white noise. With respect to any quadratic function of estimation error, the resulting estimator is statistically optimised (Mohinder and Angus, 2001). According to Malleswari et al., (2009) stochastic estimation from noisy sensor measurements uses Kalman filtering mathematical toolbox. It is grounded on linear mean square error filtering. Series of measurements observed over a period and contains statistical noise and other inaccuracies uses the Kalman filtering algorithm to denoise the measurement. The uniqueness of the Kalman filter is as a result of its small computational requirement, elegant recursive properties, and its recognition as (one of) the best estimators for one-dimensional linear systems with Gaussian error statistics (Anderson and Moore, 2005). Application areas of the Kalman filter are; smoothing noisy data and making estimates of parameters of interest. Other areas include: Global Positioning System receivers, phase locked loops in radio equipment, smoothing the output from laptop trackpads (Anderson and Moore, 2005). Numerous application areas in technology that stem from navigation, guidance and control of vehicles. Malleswari et al. (2009) applied Kalman filtering in modelling GPS errors affecting GPS signals as they traverse to users on earth from satellites, these errors reduce the precisions of such GPS positions. It was observed after modelling that the accuracies were improved in locating GPS receivers by filtering the range measurement. Differential corrections for refining the precision and reliability of GNSS signals are being developed for use in Correction and Verification (C and V) processors, which implement non-linear Kalman filters (Mohinder et al., 2010). Additionally, Dash et al., (1999) employed Kalman Filtering in the approximation of power system frequency in the occurrence of random noise and distortions from discrete values of 3-phase voltage signals of power system. It was concluded that the state modelled frequency yields unknown power system frequency in estimating near and off-normal power system frequencies. Guvenc et al., (2002) used Kalman filtering in WLAN techniques to improve accuracy. It was observed that the Kalman filters decreased the location errors by reducing sophisticated signals to linear model.

In statistics, a moving average is a technical analysis of data points by generating series of averages of distinct subsets of the full dataset. Box and Pierce (1970) used Integrated Moving Average Time Series models in the distribution of residual autocorrelations in autoregression. The models provided an estimation of the residuals from any moving average or mixed autoregressive-moving average process which was equal as those from a suitable chosen autoregressive process. Said and Dickey (1984), developed a test for unit roots which was based on an estimation of an autoregressive-moving average model by an auto-regression. The objective was testing unit roots in Auto-Regressive Integrated Moving Average (ARIMA) Time Series of unknown order. The Periodic Moving Average filter was also used to remove motion artifacts. As a result, the motion artifacts were removed without the deterioration of the characteristic point (Lee et al., 2007).

The Savitzky-Golay (S-G) filter was developed for smoothing data and calculating the numerical derivatives by Savitzky and Golay (1964). The smoothing points are derived by substituting each data point with the value of its fitted polynomial. The process consists of determining the coefficients of the polynomial which are linear with respect to the data values for fictitious data and using this linear filter over the whole data through a process known as convolution (Schafer, 2011). S-G fits a polynomial of order n in a moving window, requiring that the fitted curve at each point have the same moments as the original data to order n-1 and allows direct computation of the derivatives to be made. Characteristics of this filter are: they are optimal lowpass filters in which case they minimize the noise reduction ratio; their frequency response H (ω) meets predetermined flatness constraints at DC; they optimally suit a set of data points to polynomials of different degrees. Given certain parameters, the Savitzky-Golay filtering offers smoothing without loss of resolution by presuming that the relatively distant data points have some significant redundancy that can be utilized to decrease the level of noise. The exact nature of such presumed redundancy is that the underlying function should be locally well-fitted by a polynomial. When this is right, the Savitzky-Golay filters' performance can be remarkable. However when it is not right, these filters have no outstanding advantage over other classes of smoothing filter coefficients. The Savitzky-Golay filtering method is often used with frequency data or with spectroscopic data. For frequency data, the method is effective at conserving the high-frequency components of the signal. Additionally, the method is effective at conserving higher moments of the peak such as the line width for spectroscopic data. The moving average filter usually filters out a substantial portion of the signal's high-frequency content, and can only preserve the lower moments of a peak such as the centroid as compared to the Savitzky-Golay filtering which is less successful than a moving average filter at rejecting noise (Azami et al., 2012).

EMD is an observational nonlinear analysis tool for interlocking, non-stationary time series which originated from Huang et al., 1998. When combined with Hilbert spectral analysis, it is called Hilbert-Huang Transform (HHT). The technique adjusts and locally decomposes any non-stationary time series in a sum of IMF which zero-mean amplitude and frequency altered components (Keck et al., 2014). An Intrisic Mode Function (IMF) is a function that satisfies two conditions: (1) in the whole dataset, the number of extrema and number of zero crossings must either equal or differ at most by one; and (2) at any point, the mean value of the envelope defined by the local maxima and the envelope defined by the local minima is zero (Huang et al., 1998).

This paper used the four techniques to filter quantified solid earth tidal effect data based on two research conducted on: quantification of geographical variations of solid earth tidal effects for geodetic deformation monitoring in Ghana (Yakubu, and Kumi-Boateng 2019); and the prediction of tidal effect on the earth crust for geodetic deformation monitoring (Yakubu, et al., 2019).

The filtering was further enhanced by hybridisation of the techniques for optimal results. These filtering techniques can be incorporated in deformation studies of structures within the five Regions of Ghana and replicated in other areas. When data for deformation monitoring are filtered it will help in making informed decisions about the actual state of structures.

2. Resources and methods used

The study area is in Ghana which is positioned at the western part of Africa, and share boarders with Togo, Burkina Faso and Ivory Coast. The country lies between latitudes 4º and 12º N and longitude 4º E and 2º W and covers a total land area of 239,460 sq. km. Topographically, it is of low plains with divided plateau in the South-Central area and scattered areas of high relief. The Greenwich Meridian runs through Tema near Accra which makes Ghana geographically contiguous to the center of the world, that is, the speculative point of intersection between the equator and longitude 0˚ located in the Atlantic Ocean is about 614 km from Accra (Mohammed, 2015; Yakubu and Kumi-Boateng 2019).

Currently there are sixteen regions in Ghana. For the purposes of this study, five regions are considered out of the ten in Yakubu and Kumi-Boateng, 2019, were used. They are; Ashanti, Greater Accra, Western, Central and Eastern (Figure 1). Details of the selected regions is published in Yakubu and Kumi-Boateng, (2018). This study applies secondary data obtained from the Survey and Mapping Division in Ghana.

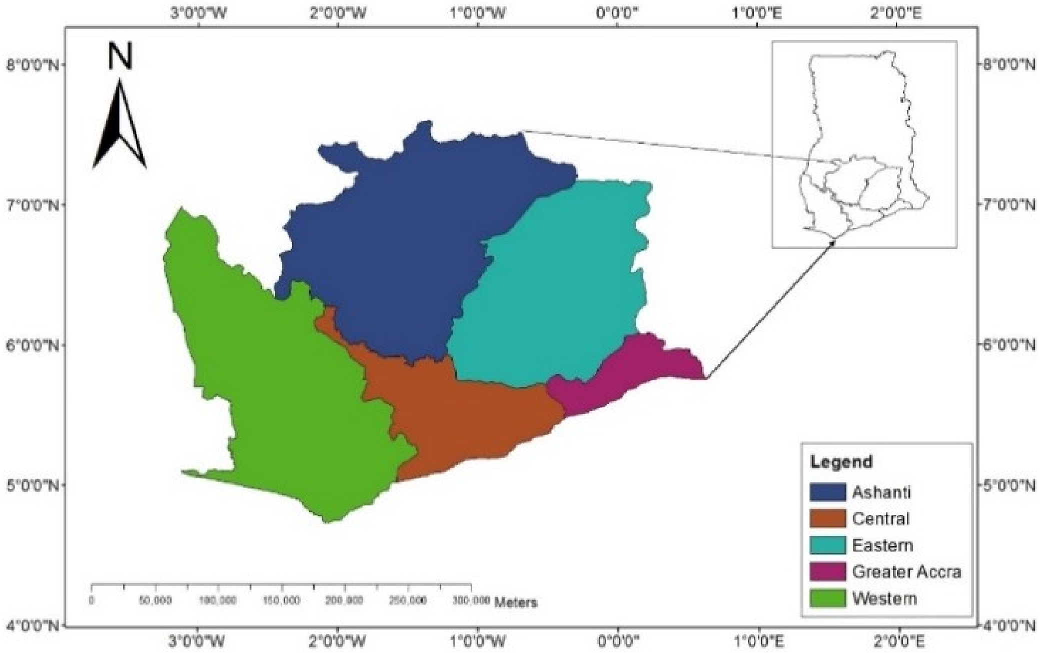

Figure 1: Study Area

Table 1: Statistical description of the datasets

Geographic Extent	Minimum	Maximum	Average	Standard Deviation
Coastal	0.0011	0.0025	0.0019	0.0003
Inland	0.0006	0.0026	0.0018	0.0004
Middle	0.0011	0.0026	0.0019	0.0004

2.1 Methods

2.1.1 Kalman filtering

The Kalman filter model presumes that the state of a system at a time (*t*) evolved from the prior state at time *t-1* according to Equation 1.

$$X_t = F_t X_{t-1} + B_t u_t + w_t \quad (1)$$

Where; X_t is the state vector containing the terms of interest for the system.

F_t is the state transition matrix which applies the effect of each system state at time *t*,

B_t is the control input matrix which applies the effect of each control input parameter in the vector u_t on the state vector and
w_t is the vector containing the process noise terms for each parameter in the state vector.

The process noise is assumed to be drawn from a zero mean multivariate normal distribution with covariance given by the covariance matrix Q_t.

2.1.2 Moving average

Moving average filters the constructed equation is given by the weighted sum of the current input point (X(k)) and some arbitrary number (M-1) of previous input points (X(k-1), X(k-2),…, X(k-n+1)) which equals to a given output (Y(k)) point.

This generalised moving average filter is given in Equation (2). The weighting coefficients b (1) through b (M) is either positive or negative, resulting in "truly" averaging or in differencing type filters. The value of a given coefficient may be 0, meaning that particular input sample will not contribute to the output sample. In general, the more (positive) coefficients are employed, the smoother the output will be (Babu and Reddy, 2014). Given a series of numbers and a fixed subset size, the first element of the moving average is obtained by taking the average of the initial fixed subset of the number series. Then the subset is modified by shifting forward. That is, without the first number of the series and adding the next value in the subset.

Y (k) = b (1) · X (k) + b (2) · X (k-1) + ... + b (M) · X (k-M+1) (2)

2.1.3 Savitzky-Golay filter

The coefficients of a Savitzky-Golay filter, when applied to a signal, perform a polynomial *P* of the degree *k*, is fitted to $N = N_r + N_l + 1$ points of the signal,
Where; N describes window size. N_r and N_l are signal points in the right and signal points in the left of a current signal point respectively. One of the best advantages of this filter is that it tends to keep features of the distribution such as relative with, maxima and minima which are often flattened by other smoothing techniques.
The MATLAB Signal Processing Toolbox has a function *sgolayfilt (x, order, framelen)* for designing and implementing both symmetric and nonsymmetrical S-G filters. There are some important constraints in the utilization of polynomial fitting in general. For example, the number of data points (in this case $2M + 1$) must be strictly greater than the number of undetermined coefficients N + *1* to achieve smoothing by the S-G process. Furthermore, if the order of the polynomial, *N*, is too large, the estimation problem is badly conditioned and the solution will be valueless. Although these factors have significant constraints, a wide range of frequency-domain characteristics can be achieved nevertheless by choosing *M* and *N* appropriately.

2.1.4 Empirical Mode Decomposition filter (EMD)

The reason for the EMD technique is to observationally distinguish intrinsic oscillatory modes by their characteristic time scales in data, and then integrate the data accordingly. Through a process called *sifting,* most of the riding *waves,* i.e. oscillations with no zero crossing between extrema, can be disregarded. The EMD algorithm therefore examines signal oscillations at a very local level and separates the data into locally non-overlapping time scale components. It integrates a signal *x(t)* into its component IMFs obeying two characteristics;

i. An IMF has only one extremum between two subsequent zero crossings, i.e. the number of local minima and maxima differs at most by one.
ii. An IMF has a mean value of zero. Mathematically, EMD is expressed as;

$$x(t) = \sum x_n(t) + r(t) \quad (3)$$

where *x(t) is the signal (t),* $x_n(t)$ *is the number of the decomposed signal t and r(t) is the residual of the signal t.*
EMD is an analytical method and consists of numerical errors that may be involved in the decomposition results. Before giving statistical importance to information content in the IMFs, the IMFs themselves need to be important to the decomposition; to take the calculated IMFs for the EMD, relevant IMFs need to be selected from the resulting IMF, since the IMFs are supposed to be almost unrelated components of the original signal; this presumes that, the irrelevant components would have relatively poor correlation with the original signal (Ayenu and Prah 2010). Therefore, a threshold λ is introduced, which is given as;

$$\lambda = \frac{\max(\mu i)}{10}, \text{ I} = 1, 2, \ldots \text{n} \quad (4)$$

where μi is the correlation coefficient of the ith IMF with the original signal, and n is the total number of IMFs; *max(μ)* is the maximum correlation coefficient observed. The selection criterion for IMFs is given as follows;
If μi >λ, then keep the ith IMF, else eliminate the ith IMF and add it to the residue.

2.1.5 Hybridisation of best filtrating technique with the other techniques

The hybridisation was done by choosing the best filter technique amongst the others. It was observed that, the EMD performed the best filtration amongst the other filtration techniques using relative error correction (REC) for its assessment. The error correction of the filtration techniques was calculated and its percentages (%) were found. It was then hybridized with the best filtration technique per this work which was the EMD to help improve the error correction relativity of the other techniques.

2.1.6 Assessment of performance of techniques

To ascertain the authenticity and correctness of the data and techniques, the following statistical indicators were employed: Relative Error Correction (REC), Root Mean Square Percentage Error and Mean Absolute Percentage Error.
Relative Error Correction was computed using equation (5) which gives the accuracy of the filtered signal with respect to the original signal.

$$\text{REC} = 100 - \left[\frac{1}{N}\sum_{i=1}^{N}\frac{(Oi-Pi)}{Oi}\right] x100 \quad (5)$$

Where *Oi* is the original signal and *Pi* is the filtered signal

Root Mean Squared Percentage Error (RMPS), which gives a sense of the typical size of the value in percentage , was computed using Equation (6):

$$RMPS = \sqrt{\frac{\Sigma(x-\bar{x})^2}{n}}\ x\ 100 \quad (6)$$

The Mean Absolute Percentage Error (MAEPE) measures how closely the data are clustered about the mean. It was computed using Equation (7):

$$MAEPE = \frac{1}{N}\sum_{i=1}^{N}(Oi - Pi) \quad (7)$$

Where *Oi*= Is the original signal
Pi= The filtered signal

3. Results and discussions

The tidal effect on the earth crust was quantified (Figure 2) for various geographic locations in the five (5) Regions of Ghana using the theory of Love for (Yakubu and Kumi-Boateng, 2018). In addition, three mathematical approaches namely Auto-Regressive Integrated Moving Average (ARIMA) Time Series, Non-Linear Auto-Regressive Neural Network (NARNET), and the Hybrid ARIMA and Neural Network model have been used to model and predict the tidal effect on the earth crust for geodetic deformation monitoring for five years (Yakubu et al., 2019). Filtering of the predicted result was carried out using four methods (EMD, Moving Average, Savitzky-Golay and Kalman filters). This is the results of filtering of point with respect to the techniques of assessment categorized under three main groups; those close to the coastline (COAST), those away from the coastline (INLAND) and those in between Coastline and Inland (Middle) (Figures 3, 4 and 5). The relative error correction of the INLAND displacement are; 97.47 %, 76.69 %, 75.47 % and 69.00 % for EMD, Moving Average, Savitzky-Golay and Kalman filters respectively. The relative error correction of the MIDDLE displacement are; 98.65 %, 81.90 %, 79.08 % and 71.95 % for Kalman, Moving Average and Savitzky-Golay filters respectively. The relative error correction of the COAST displacements are 98.67 %, 84.88 %, 85.07 % and 71.94 % for EMD, Moving Average, Savitzky-Golay and Kalman filters respectively. The relative error correction for the above techniques shows that, the EMD incurred lower errors thereby providing a better accuracy of filtering than the other techniques. This also proves to be true after the root mean percentage error was calculated for all the other techniques and it was further noticed the EMD outperformed the other techniques. With respect to that, the EMD was used to hybrid the other techniques which showed a further improvement of the other techniques with respect to the hybridization with the EMD (Figure 6). Analyses of tables 2, 3, 4 confirmed that the EMD technique outperformed the other filtering methods considered in this study. This assertion can additionally be seen from table 1, where the EMD method produced the best REC for INLAND, MIDDLE and COAST, correspondingly. These REC values suggest the extent of the error variations and its correction for accuracy that could be generated when the three methods for filtering were applied on the quantified and predicted tidal data within the study area. These REC results clearly demonstrate the quantitative extent of agreement and precision of the filtered data produced by EMD, Moving Average, Savitzky-Golay Kalman. To further improve on the results, table 3-6, shows an improvement of the other techniques when hybridized with the EMD. Nonetheless, the overall statistical findings suggest that each of the method can confidently be applied to perform denoising in the tidal data.

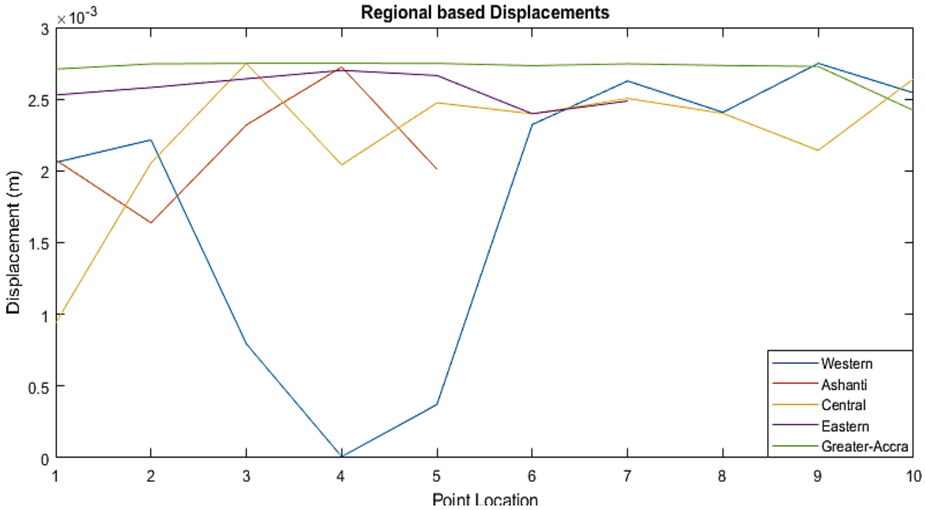

Figure 2: Regional Based Displacement of various Locations

Table 2: Statistical analysis of the filtered results using REC

Filtering Technique	Coast (%)	Middle (%)	Inland (%)
EMD	98.67	98.65	97.47
Moving Average	84.88	81.90	76.69
Savitzky-Golay	85.07	79.08	75.47
Kalman Filtering	71.94	71.95	69.00

Table 3: Statistical analysis of the percentages of error of the other techniques

Technique	Coast (%)	Middle (%)	Inland (%)
Moving Average	15.12	18.10	23.31
Savitzky-Golay	13.95	1.14	9.29
Kalman Filtering	26.04	25.80	20.68

Table 4: Statistical analysis of the hybridisation of EMD with the other techniques

Hybrid Technique	Coast (%)	Middle (%)	Inland (%)
MA-EMD	100.00	100.00	100.00
SG-EMD	99.03	80.22	84.76
KF-EMD	97.97	97.75	89.68

Table 5: Statistical analysis of the filtered results using root mean squared percentage error (units in meters)

Filtering Technique	Coast	Middle	Inland
EMD	0.0338	0.1979	0.1882
Moving Average	0.1890	0.1937	0.1827
Savitzky-Golay	0.1891	0.1937	0.1823
Kalman Filtering	0.1990	0.2044	0.1947

Table 6: Statistical analysis of the filtered results using mean absolute percentage error (units in meters)

Filtering Technique	Coast	Middle	Inland
EMD	1.330E-05	1.437E-05	3.796E-05
Moving Average	0.0010	0.00106	0.00088
Savitzky-Golay	8.446E-05	9.416E-05	3.397E-06
Kalman Filtering	2.226E-05	2.226E-05	2.226E-05

Graphs of the individual filtering techniques (EMD, Moving Average, Savitzky-Golay and Kalman filters) were plotted to illustrate their effectiveness on the data (Figures 3-6).

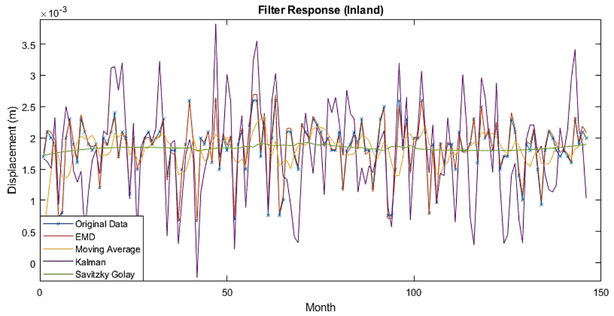

Figure 3: Filter response for the various techniques compared to the original data (Inland)

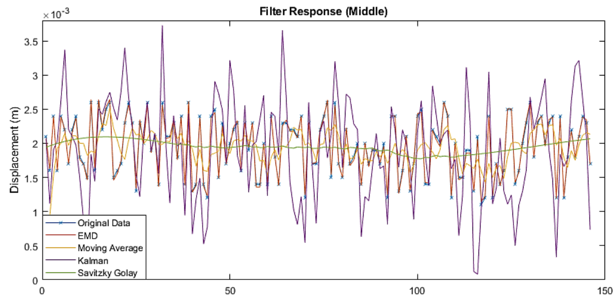

Figure 4: Filter response for the various techniques compared to the original data (Middle)

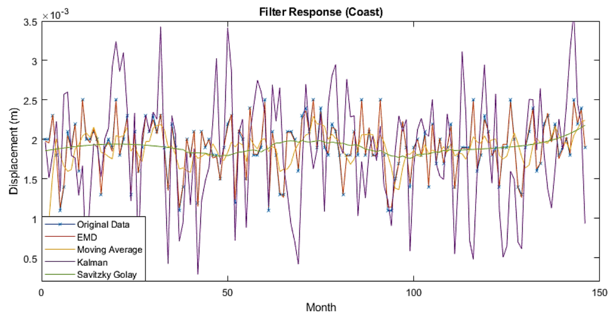

Figure 5: Filter response for the various techniques compared to the original data (Coast)

Results of the EMD filtering techniques hybrid with the other techniques further improved the filtering of the predicted data (Figure 6).

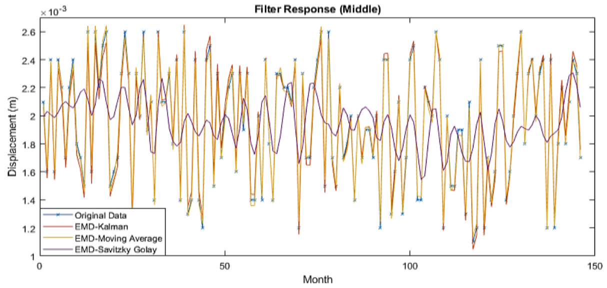

Figure 6: Filter response of EMD hybrid with the various techniques compared to the original data (Middle)

4. Conclusions and recommendations

In deformation monitoring, it is imperative to clearly and carefully identify and understand the sources of errors that are likely to have influence on the results. To significantly remove/reduce sources of errors and their influence on results for high accuracy deformation surveys results and interpretation, the adoption of appropriate method(s) to remove these errors/noise in data is very important, since the interpreted results can have consequences on the lives of people. In view of that, several methods have been developed to filter noise in the data collected. This study utilised and compared four notable filtering techniques namely: Empirical Mode Decomposition, Kalman Filtering, Moving Average and Savitzky-Golay. These methods have been applied to denoise quantified and predicted tidal effect data within the study area.

EMD provided the best filtered results for the predicted future trends of the tidal deformation with high accuracy with respect to REC for all the categories of the data for the future prediction. Comparatively, the EMD also performed better against the other filters in the Root Mean Square Percentage Error and Mean Absolute Percentage Error. The researchers in this study recommends the use of EMD filtering method in the filtering process of the quantified and predicted tidal effect data for the study area other related areas of study. However, Moving Average, Savitzky-Golay and Kalman filtering can as well be used depending on the accuracy required.

Acknowledgements

The authors acknowledge the use of data from the Land Administration Project of the Survey and Mapping Division of the Lands Commission, Ghana. Our sincere gratitude also goes to the anonymous reviewers for their insightful recommendations.

References

Anderson B. D. O. and J.B. Moore (2005). Optimal Filtering, Dover Publications, New York, 368 pp.

Ayenu-Prah A. and N. Attoh-Okine (2010). A criterion for selecting relevant intrinsic mode functions, in Empirical Mode Decomposition. Advances in Adaptive Data Analysis, 2(1), 24.

Azami, H., K. Mohammadi and B. Bozorgtabar (2012). An improved signal segmentation using moving average and Savitzky-Golay filter, Journal of Science and Information Processing, 3, 39-44.

Babu, C.N. and B.E. Reddy (2014). A moving-average filter based hybrid ARIMA–ANN model for forecasting time series data, Applied Soft Computing, 23, 27-38.

Box, G. E. P., and D.A. Pierce (1970). Distribution of residual autocorrelation in autoregressive-integrated moving average time series models. Journal of the American Statistical Association, 65(332), 1509-1526.

Chen, Y (1983). Analysis of Deformation Surveys- A Generalized Method", PhD Thesis, University of New Brunswick, New Brunswick, 281pp.

Dash P.K., A.K. Pradhan and G. Panda (1999). Frequency estimation of distorted power system signals using extended complex Kalman filter, IEEE Transactions on Power Delivery, 14(3), 761-766.

Guvenc I., C.T. Abdallah, R. Jordan and O. Dedeoglu (2002). Enhancements of RSS based indoor tracking system using Kalman filters, International Signal Processing Conference (ISPC) and Global Signal Processing Expo, 13, 12- 15.

Huang N. E., Z. Shen, S. R. Long, M. L. Wu, H. H. Shih, Q. Zheng, N. C. Yen, C. C. Tung, and H. H. Liu. (1998). The empirical mode decomposition and Hilbert spectrum for nonlinear and nonstationary time series analysis, Proceedings of the Royal Society of London, A, 454, 903–995.

Kalman, R. E. and R.S. Bucy (1961). New results in linear filtering and prediction theory, ASME Journal of Basic Engineering, 83, 95-107.

Keck, I.R., A. Zeiler, R. Faltermeier, A.M. Tome, C.G. Puntoret and E.W. Lang (2014). Empirical Mode Decomposition -An Introduction. 9.

Lee, G., J. Lee, H. Lee and W. Jung (2007). Periodic moving average filter for removing motion artifacts from PPG Signals, International Journal of Control, Automation and System, 5(6), 701-706.

Malleswari B.L., I.V. MuraliKrishna, K. Lalkishore, M. Seetha, Nagaratna and P. Hegde (2009). The role of Kalman filters in modelling of GPS Errors, Journal of Theoretical and Applied Information Technology, 2, 2005-2009.

Mohammed, A. S. (2015). Performance Assessment of the Methods used in Transformation from Cartesian Coordinates to Geodetic Coordinates, Unpublished BSc Project Report, University of Mines and Technology, Tarkwa, Ghana, 65.

Mohinder S. G. and P.A. Angus (2010). Applications of Kalman filtering in aerospace 1960 to the present, IEEE Control Systems Magazine, 69-78.

Mohinder, S. G. and P.A. Angus (2001). Kalman Filtering: Theory and Practice using MATLAB, 2nd ed., Wiley and Sons Inc., New York, 401.

Said, E. S., and A.D. Dickey (1984). Testing for unit roots in autoregressive-moving average models of unknown order, Journal of the American Statistical Association. 71(3), 599-607

Savitzky, A. and M.J.E Golay (1964). Smoothing and differentiation of data by simplified least squares procedures, Analytical Chemistry, 36(8), 1627-1639.

Schafer, R. W. (2011). What is a Savitzky-Golay Filtering?, IEEE Processing Magazine, 11, 111-117.

Wedin, O. (2008). Data Filtering Methods, Road Map for Radical Innovations in European Transport Services (ROADIDEA), 42.

Yakubu, I., and B. Kumi-Boateng (2019). Quantification of geographical variations of solid earth tidal effects for geodetic deformation monitoring in Ghana, Ghana Journal of Technology, 3(2), 73 - 81.

Yakubu, I., Y.Y. Ziggah, and K.A. Baafi (2018). Prediction of tidal effect on the earth crust for geodetic deformation monitoring, Ghana Journal of Technology, 2(2), 63 - 69.

Yakubu, I., I. Dadzie and A.A. Mensah (2010). Monitoring levels of deformation within Tarkwa Community: A Multi-GPS receiver network system approach, The XXIV FIG International Congress 2010, Facing the Challenges - Building the Capacity, Sydney, Australia, 11-16.

Evaluation of the simulated data for the kinematic GNSS point positioning and differential techniques

A. Lotfy*, M.A. Abdelfatah and H. Hosny
Construction Engineering & Utilities Department, Faculty of Engineering, Zagazig University, Egypt
*Email: ahmed.lotfy1164@yahoo.com

(Received: Sept. 28, 2019; in final form: July 19, 2020)

Abstract: Scientists and researchers have always been inspired to identify the three-dimensional coordinates of satellite communication. The critical aspect that highly accurate requires is the use of the Global Navigation Satellite Systems (GNSS) in static or semi-static mode. However, it was necessary to study ways of improving the accuracy use of such systems in a dynamic environment, which is of great significance for several applications, because of the substantial improvement of the abilities of satellites and the signaling structure. The objective of this research is to analyze and improve the accuracy of the point positioning technique. The model of the essential positioning point was evaluated. It was proposed to establish a technique of kinematic point positioning. The suggested procedure was tested. A study was carried out. The raw data was extracted from real rover data and simulated databases observed. In order to produce simulated base data, the final products of the International Global Navigation Satellite Network Service (IGS) were used. The results show that using simulated base data, horizontal and vertical accuracy can be increased by 75 % and 72 %, respectively. The Chi-square test is used to evaluate the alternative solution improvement for various cases. The Chi-square test states that two base stations are more accessible to be used during evaluation than one base station.

Keywords: PP, Simulation, GNSS, Kinematic, KPP, SRS

1. Introduction

The Point Positioning (PP) technique presupposes that coherent satellite orbits and clocks worldwide are set or severely constrained and that PP mathematical models are consistent with those used in global network alternatives that estimate orbit/clock products (Kouba et al., 2017). The PP is code and phase measures that are used to accurately determine the receiver position at which the coordinates of the transmitter have been monitored with the known positions of GNSS satellites at an unknown point concerning the reference frame. Also recognized as absolute positioning (Kaartinen et al., 2015). In relative positioning, code and carrier measurements were used to check for receivers' coordinates at an unknown point with respect to a receiver at a known point (El-Rabbany, 2002). The baseline from a known point to an unknown position was determined. Often the term differential positioning was used interchangeably with relative positioning. Moreover, differential positioning has been correlated more commonly with a particular method of relative positioning that applies corrections to unknown measurements at a known location (He et al., 2014). The positioning of GNSS may be classified as either static or kinematic. A GNSS receiver had to be stationary when it is static, while the GNSS data was collected while moving in the kinematic positioning, as shown in figures 1a and 1b. For Kinematic relative positioning, one receiver known as the base was fixed at a known location for the relative kinematic positioning. In contrast, a second receiver known as a rover is moved along the path to be positioned. (Colombo et al., 2004).

Autonomous PP locations are measured at each measurement point in kinematic mode, usually every 1 – 30 s, based on device and consumer dynamics (Chen et al., 2004). When observation intervals are shorter than the sampling of the satellite clock, interpolation of the clock is necessary. As a result of the satellite clock uncertainty, the clock can only be accurately interpolated to the precision level of the cm at a measurement interval of 30s or below. Alternatives for IGS and most IGS Analysis Centers (AC) clocks currently use 30 samples, but more high-rate clock products are available from individual analytical centers for particular applications. (Bock et al., 2009).

Over several years Differential GNSS was created in order to increase the accuracy of positioning. This makes for accurate positioning with the so-called integer ambiguity resolution, also at centimeter rates. The basic concept is to reduce significant error factors, ionosphere and troposphere delays, orbit errors, and satellite clock errors by the collection of satellite data at a known position.

Differential positioning with data from a reference station and rover receiver is used for most scientific and commercial purposes of GNSS kinematic positioning (Furones et al., 2012). The main concern, however, is that the range of residual errors decreases as the distance between the base and the rover receiver decreases. PP is an alternative technique. The accuracy of the PP submeter by centimeter can only be accomplished by one carrier phase GNSS receiver, which ensures that the expense of a GNSS survey is reduced without the use of base stations (Lotfy, 2019). In PP algorithms for processing precisely satellite orbits and clock data instead of broadcasting data, it uses high-resolution carrier and pseudorange observations (Li et al., 2012).

By means of the real-time service available to IGS, accurate orbital and satellite clock corrections can be made more precise in real-time than ultra-rapid (predicted part) products. The products of the RTS have been proven better than the ultra-rapid. Moreover, the RMS solution in comparison with the solution obtained with the expected portion of IGS ultra-rapid products can be increased by around 50 percent with IGS RTS in real-time PPP (Elsobeiey and Al-Harbi, 2015).

Data from different test data sets, including permanent receivers in known points and an installed moving receiver in a van, were used to evaluate PP accuracy. The objectives of this study are therefore improved by using simulated databases, compared to real base data and the performance of the kinematic point positioning technique.

2. Data Collection

In 10th of Ramadan and Enshas city in Egypt, the test areas for this study were. Five routes in the 10th of Ramadan were observed and three routes in Enshas, as shown in figures 2a and 2b. There were two GNSS receivers used for the brand ComNav T300 PLUS, one rover and one base station for the comparison of the results to simulated data, as summarized in table 1, real data performance comparison to simulated data to be obtained. The rover was fixed to a car and derived from observations in table 2.

Only GPS observations have been studied in three different cases. The first case consisted of the analysis of the only rover observed data and was solved as a PP. The second case involved the generation of the basic observations using a simulated reference station (SRS) in the same position as the actual base station. Then the observations by the rover were resolved. As far as the third case is concerned, observations obtained from the rover and real base station have been used and resolved by the Bernese software V.5 with a differencing technique (Diff).

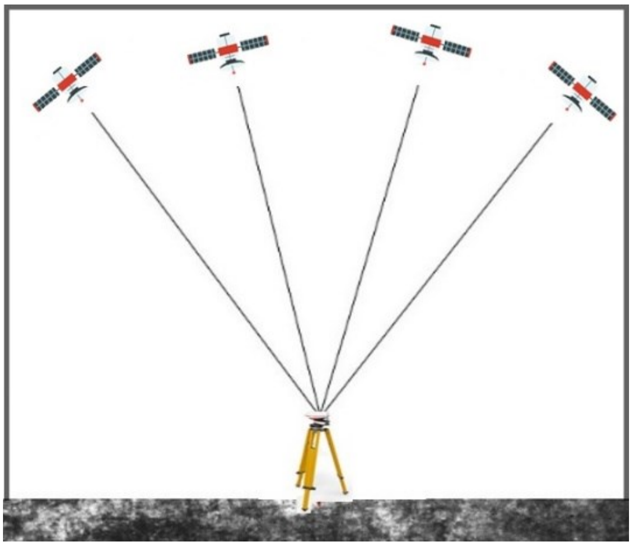

Figure 1a: Static point positioning.

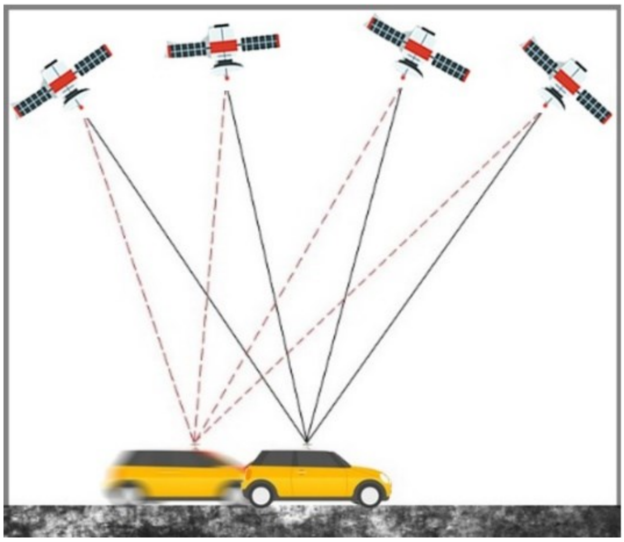

Figure 1b: Kinematic point positioning.

Table 1: The accurate values of stations' coordinates

Station	Code	Latitude (φ)	Longitude (λ)	Height (h)	Receiver Type
10th of Ramadan	ASH	30º17'46.027"	31º44'14.972"	133.83	ComNav T300P
Enshas	ENS	30º20'39.290"	31º26'31.659"	33.65	ComNav T300P

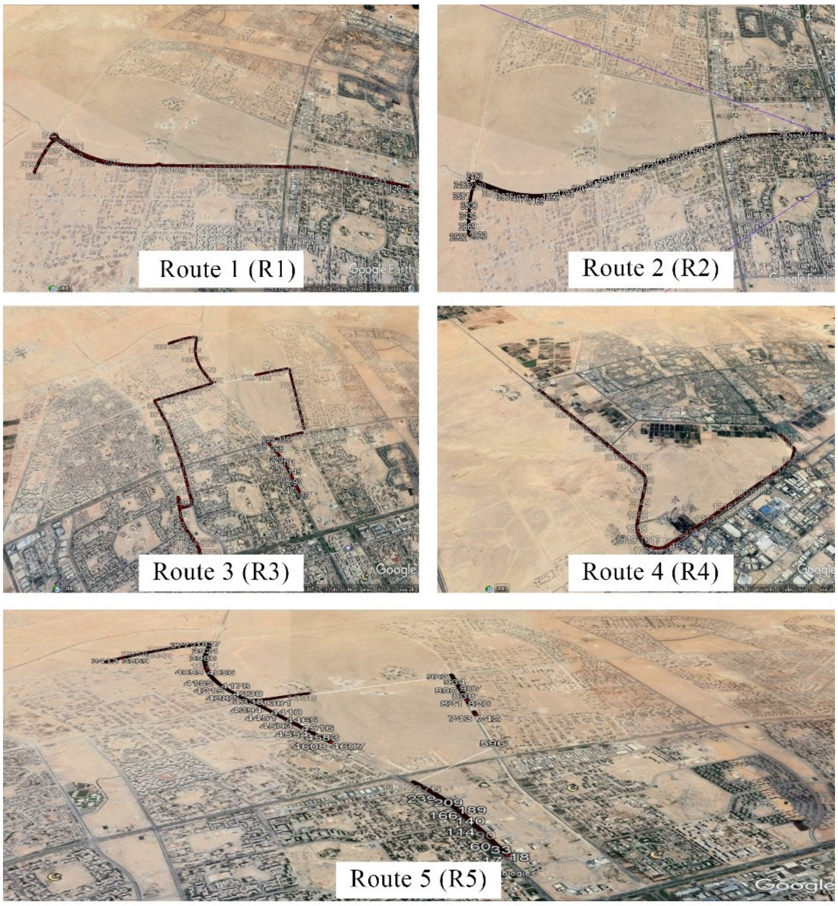

Figure 2a: Map of routes in 10th of Ramadan city.

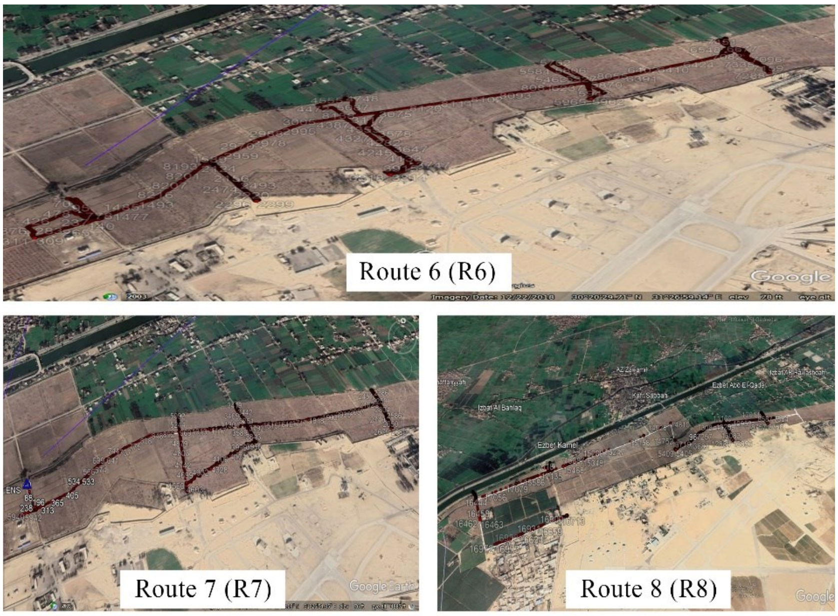

Figure 2b: Map of routes in Enshas city.

Table 2: Number of epochs in each route.

Route no.	Length (km)	No. of epochs	Base stations
R1	15	4190	
R2	10	1915	
R3	10	4719	10th of Ramadan City
R4	12	4144	
R5	12	4609	
R6	4	9376	
R7	7	17643	Enshas
R8	6	12150	

3. Kinematic Positioning Models

3.1 Point Positioning

3.1.1 Code Range Model

The code pseudorange at an epoch t can be modeled by:

$$R_r^s(t) = \varrho_r^s(t) + c\Delta\delta_r^s(t) \quad (1)$$

Where

$R_r^s(t)$ is the pseudorange code measured between the receiver site r and the satellite s.

$\varrho_r^s(t)$ is the geometric distance between the observing point and the satellite.

c is the speed of light.

$\Delta\delta_r^s(t)$ is clock bias representing the combined clock off sets of the receiver and the satellite clock with respect to system time.

Reviewing Eq. (1), the recipient location desired coordinates to be calculated are inferred at the distances $\varrho_r^s(t)$ (Hofmann et al., 2007), which can explicitly be written as:

$$\varrho_{r(t)}^s(t) = \sqrt{(X^s(t) - X_{r(t)})^2 + (Y^s(t) - Y_{r(t)})^2 + (Z^s(t) - Z_{r(t)})^2} \quad (2)$$

Where

$X^s(t), Y^s(t), Z^s(t)$ are components of the satellite's geocentric position vector at epoch t.

$X_{r(t)}, Y_{r(t)}, Z_{r(t)}$ are the three cartesian coordinates of the (stationary) observing receiver site.

3.1.2 Phase Range Model

Pseudoranges can also be taken from measurements of the carrier phase (Hofmann et al., 2007). The mathematical model is given for these measurements by

$$\phi_r^s(t) = \frac{1}{\lambda^s}\varrho_r^s(t) + N_r^s + \frac{c}{\lambda^s}\Delta\delta_r^s(t) \quad (3)$$

Where

$\phi_r^s(t)$ is the measured carrier phase expressed in cycles.

λ^s is the wavelength.

$\varrho_r^s(t)$ is the same as for the code range model.

N_r^s is an integer ambiguity.

C denotes the speed of light.

$\Delta\delta_r^s(t)$ is the combined receiver and satellite clock bias.

Inserting Eq. (1) into Eq. (3) and shifting the (known) satellite clock bias to the left side of the equation yields

$$\phi_r^s(t) + f^s\delta^s(t) = \frac{1}{\lambda^s}\varrho_r^s(t) + N_r^s + f^s\delta_r(t) \quad (4)$$

where the frequency of the satellite carrier $f^s = {}^{c}/_{\lambda^s}$ has been substituted.

3.2 Double Differences Model

Since double differences for a single baseline are already correlated, a correlation for the network must also be expected. The following significantly larger example, however, shows the increasing complexities. Assume three points E, Z, and F as reference bases and R(t) as a rover, for the three baselines E-R(t), Z-R(t), and F-R(t) again. Consider a single epoch t for two satellites, j, and k, where j is taken as the reference satellite for the double-differences (Hofmann et al., 2007).

$$\phi_{*R(t)}^{jk}(t) = \phi_{R(t)}^{k}(t) - \phi_{R(t)}^{j}(t) - \phi_{*}^{k}(t) + \phi_{*}^{j}(t) \quad (5)$$

where (*) referred to E, Z, and F. As in the previous model, a matrix-vector relation is desired. By introducing for the matrix E:

$$\mathrm{E} = \begin{bmatrix} 1 & -1 & 0 & 0 & 0 & 0 & -1 & 1 \\ 0 & 0 & 1 & -1 & 0 & 0 & -1 & 1 \\ 0 & 0 & 0 & 0 & 1 & -1 & -1 & 1 \end{bmatrix}$$

and for the vectors D and Φ:

$$\mathrm{D} = \begin{bmatrix} \phi_{ER(t)}^{jk}(t) \\ \phi_{ZR(t)}^{jk}(t) \\ \phi_{FR(t)}^{jk}(t) \end{bmatrix}, \qquad \Phi = \begin{bmatrix} \phi_{E}^{j}(t) \\ \phi_{E}^{k}(t) \\ \phi_{Z}^{j}(t) \\ \phi_{Z}^{k}(t) \\ \phi_{F}^{j}(t) \\ \phi_{F}^{k}(t) \\ \phi_{R(t)}^{j}(t) \\ \phi_{R(t)}^{k}(t) \end{bmatrix}$$

$$\mathrm{D} = \mathrm{E}\,\Phi \quad (6)$$

The relation in Eq. (6) is valid. The covariance follows by

$$\Sigma_{\mathrm{D}} = \mathrm{E}\,\Sigma_{\Phi}\,\mathrm{E}^{T} \quad (7)$$

which reduces to:

$$\Sigma_{\mathrm{D}} = \sigma^{2}\,\mathrm{E}\,\mathrm{E}^{T} \quad (8)$$

3.3 Simulation PP Model

This model has been designed to obtain the database of simulation. There was established and the distance between the positions of the virtual receiver and satellite. We will express the positioning equation by:

$$P = f(O, E \text{ and } \Delta)$$

Where P is positioning, O is observation, E is ephemeris, and Δ is errors. During the simulation, the inverse of this equation is used:

$$O = f(P, E \text{ and } \Delta)$$

The mathematical model for these measurements is given by:

$$\varrho_r^s(t) = \sqrt{(X^s(t) - X_r)^2 + (Y^s(t) - Y_r)^2 + (Z^s(t) - Z_r)^2} \quad (9)$$

where

$X^s(t), Y^s(t), Z^s(t)$ are components of the satellite's geocentric position vector at epoch t.

X_r, Y_r, Z_r are the three cartesian coordinates of the simulated receiver site.

IGS's final products knew the coordinates of the satellites.

$$\lambda^s \phi_r^s(t) = \varrho_r^s(t) + \lambda^s N_r^s + \Delta\delta_r(t) \quad (10)$$

$$L = AX + V \quad (11)$$

The linearization is performed for $\varrho_r^s(t)$ and known terms are shifted to the left side. Multiplying Eq. 6 by λ and using $c = \lambda f$ yields:

$$\lambda\phi_r^s(t) - \varrho_{r0}^s(t) + c\delta^s(t) = -\frac{X^s(t) - X_{r0}}{\varrho_{r0}^s(t)}\Delta X_r - \frac{Y^s(t) - Y_{r0}}{\varrho_{r0}^s(t)}\Delta Y_r - \frac{Z^s(t) - Z_{r0}}{\varrho_{r0}^s(t)}\Delta Z_r + \lambda N_r^s + c\delta_r(t) \quad (12)$$

Considering four satellites again, the system is given in matrix-vector form $L = AX$ (Hofmann et al., 2007), where

$$L = \begin{bmatrix} \lambda\phi_r^1(t) - \varrho_{r0}^1(t) + c\delta^1(t) \\ \lambda\phi_r^2(t) - \varrho_{r0}^2(t) + c\delta^2(t) \\ \lambda\phi_r^3(t) - \varrho_{r0}^3(t) + c\delta^3(t) \\ \lambda\phi_r^4(t) - \varrho_{r0}^4(t) + c\delta^4(t) \end{bmatrix} \quad (13)$$

$$A = \begin{bmatrix} a_{X_r}^1(t) & a_{Y_r}^1(t) & a_{Z_r}^1(t) & \lambda & 0 & 0 & 0 & c \\ a_{X_r}^2(t) & a_{Y_r}^2(t) & a_{Z_r}^2(t) & 0 & \lambda & 0 & 0 & c \\ a_{X_r}^3(t) & a_{Y_r}^3(t) & a_{Z_r}^3(t) & 0 & 0 & \lambda & 0 & c \\ a_{X_r}^4(t) & a_{Y_r}^4(t) & a_{Z_r}^4(t) & 0 & 0 & 0 & \lambda & c \end{bmatrix} \quad (14)$$

$$X = [\Delta X_r \quad \Delta Y_r \quad \Delta Z_r \quad N_r^1 \quad N_r^2 \quad N_r^3 \quad N_r^4 \quad \delta_r(t)]^T \quad (15)$$

Thus, simulated data can be obtained.

The code observations by

$$\frac{C}{A}\,code = \varrho_1 + \Delta_1 \quad (16)$$

$$p\ code = \varrho_2 + \Delta_2 \quad (17)$$

The phase observations by

$$L_1 = \lambda_1\phi_1 + \Delta_3 \quad (18)$$

$$L_2 = \lambda_2\phi_2 + \Delta_4 \quad (19)$$

The least-squares adjustment is made to create simulated RINEX data, as shown in figure 3 for the solution of this redundant system. The Bernese software V.5 was used to complete these processes.

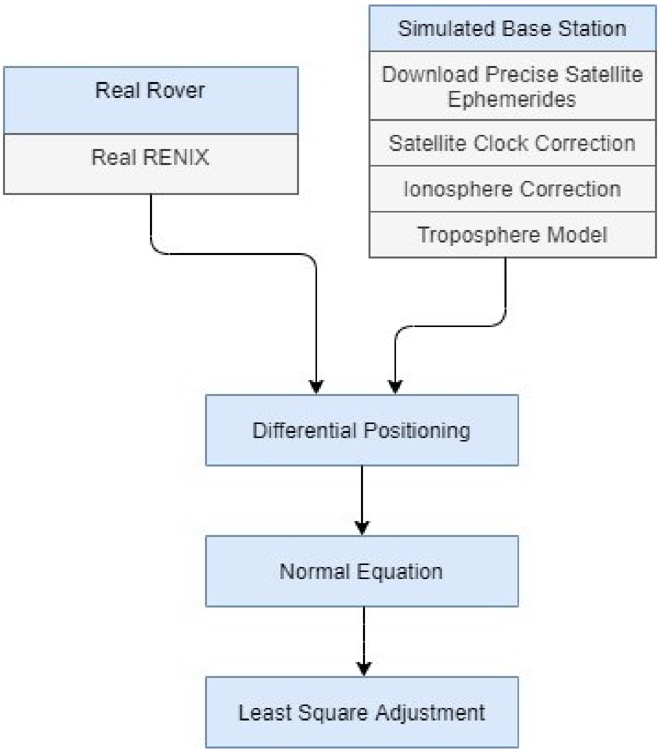

Figure 3: The simulation processes for kinematic point positioning.

4. Results and discussion

Through the Bernese software V.5, data were resolved to analyze the kinematic point positioning for all routes. For all routes, data from the simulated base were generated to increase the reliability of the point positioning technique. The horizontal axis is a millimeter error, and the vertical axis refers to the routes.

4.1. Horizontal accuracy

There are eight routes, five routes in 10th of Ramadan city, and three routes in Enshas to test the model. The easting's error values in millimeters indicated in figure 4. In route 2, the error value was 1267 mm with PP, and the error value was 456 mm with simulated base data. In route 3, the error value was 1609 mm with PP, and the error value was 360 mm when the simulated base station was used. In Route 4, the error value was 476 mm with the use of PP, and the error value was 166 mm with simulated data. In route 5, the error value was 1611 mm with PP, and the error rate was 157 mm when using simulated base results. In route 6, the mistake was 1021 mm when used with PP, and the error was 282 mm when using simulated base data. In Route 7, the error value was 687 mm with PP and 141 mm with simulated base data. In route 8, the error value used for PP was 412 mm, and the error value was 181 mm for the simulated base.

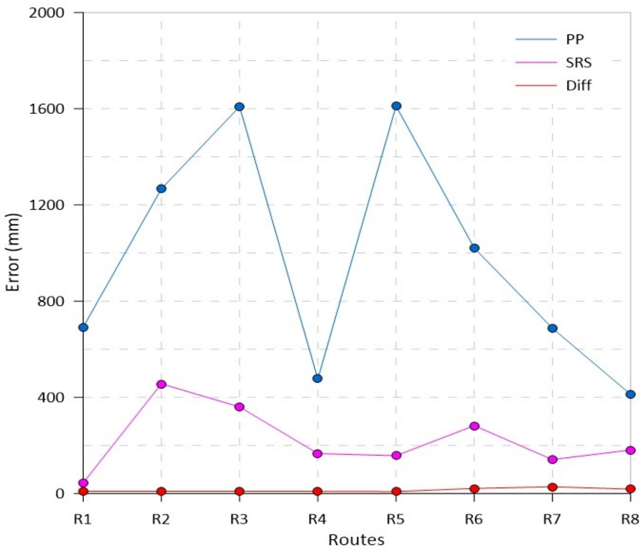

Figure 4: The error of easting for all routes in (mm).

Figure 5 displays the error values of the northern component in millimeters. In route 2, the error value was 3 mm using PP, and the error value was 2 mm with simulated data. The error value in route 3 was 11 mm when PP was used, and the error value was 2 mm in the use of a simulated base. In Route 4, the error value was 3 mm using PP, and the error value was 1 mm when the data were simulated. The error value in route 5 was 12 mm by using PP and 1 mm by using a simulated base. In route 6, the error value was 7 mm with PP, and the error value was 3 mm with simulated base data. In Route 7, the error value was 2 mm with the evaluation of PP, and the error value was 3 mm with the simulated data. In route 8, the error value was 3 mm with PP, and the error value was 1 mm with the simulated base results. In previous charts, the percentage changed for horizontal elements using simulated base data was 75%. Due to the use of the differencing technique with one actual rover, the errors in the IGS simulation results are reduced.

As shown, the distance and number of epochs greatly influence the accuracy of the observation. As the distance is increased at low speed, the number of epochs increases, and hence accuracy is improved. Apart from the effect of the observer, 10th of Ramadan City is an urban area that has a clear view of the sky without obstacles or large buildings nearby, so the accuracy of the observations is high. However, the number of epochs is less than Enshas because the area is non-urban, and it has high constructions, obstacles, and narrower sightings about the view of the antenna. Being aware that in all cases the GDOP had been fixed.

4.2. Vertical accuracy

Figure 6 of the chart shows error values for height in millimeters. In route 2, the error value was 924 mm with PP, and the error value was 244 mm when simulated base data were used. The error value of route 3 with PP was 922 mm, and the error value of 272 mm with the simulated base data. In Route 4, the error value used by PP was 648 mm, and the error value was 253 mm when simulated bases were used. In route 5, the error value was 830 mm with PP, and the error value was 212 mm with simulated base data. The error value was 902 mm in route 6 using PP, and the error value was 294 mm when the simulated base data was used. In route 7, the error value was 915 mm with PP, and the error value was 278 mm with simulated data. In route 8, the error value was 912 mm with PP, and the error value 276 mm when using simulated data. The previous charts show that the percentage of improvement for a vertical component using simulated base data was 72%.

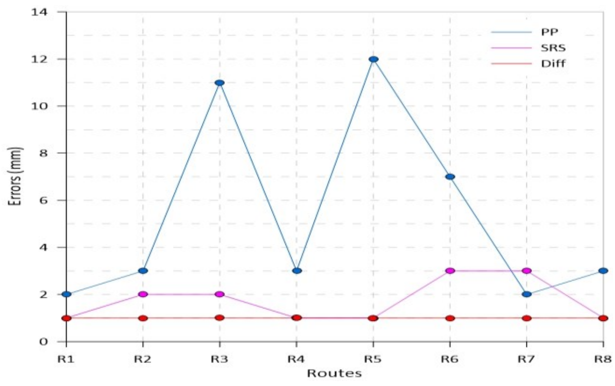

Figure 5: The error of northing for all routes in (mm)

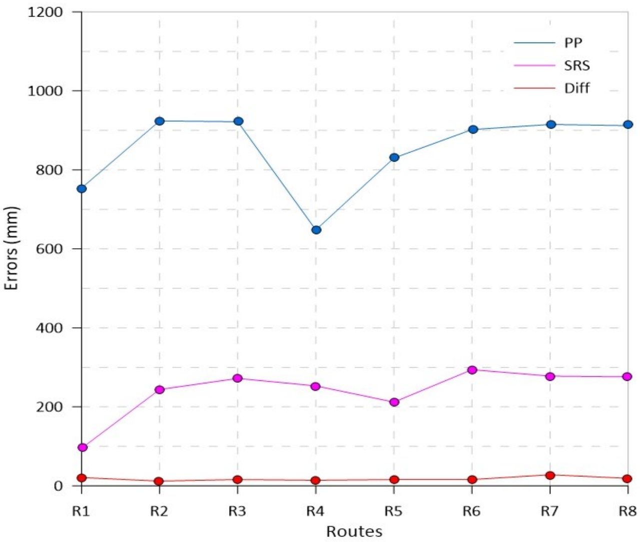

Figure 6: The error of height for all routes in (mm)

4.3. Statistical tests

One of the most useful statistics for testing hypotheses is the Chi-square test (also known as the Pearson Chi-square test, or just the Chi-square). In comparison to most statistics, Chi-square (χ^2) not only provides information about the significance of observed differences but also provides detailed information about which groups precisely are responsible for any differences found. Therefore, the volume and specificity of this data will make it a particularly valuable resource in a variety of analytical methods accessible to researchers.

The test statistic is

$$\chi^2 = \sum_{i=1}^{K} \frac{(O_i - E_i)^2}{E_i} \tag{16}$$

where O_i and E_i represent for each K class, respectively, the observed and theoretical frequencies. This statistic is compared with a value obtained from χ^2 tables with v degrees of freedom. In general, $v = K - 1$. Even if the theoretical distribution includes m parameters to be computed from the data observed, then v becomes $K - 1 - m$. If χ^2 is greater than the critical value, we reject the null hypothesis that the observed and theoretical distributions agree.

Journal of Geomatics Vol. 14, No. 2, October 2020

The Chi-square test values for the easting component are displayed in table 3. The Chi-square is applied using the differential method (Diff.) for all cases, point positioning (PP), and simulation (SRS). The tablet value of chi-square is 1591.22, which is 95 %. The values for the chi-square test are accepted below the tabulated value and above the tabulated value.

The values of the chi-square test for the north component are shown in table 4. The Chi-square is applied using the differential method (Diff.) for all cases, point positioning (PP), and simulation (SRS). The tabulated value of chi-square is 15.51 at 95 % confidence. The values in the chi-square method are recognized smaller than the tabulated are accepted value and more significant than the tabulated value are rejected.

The Chi-square test values for the height are displayed in table 5. The Chi-square is applied using the differential method (Diff.) for all cases, point positioning (PP), and simulation (SRS). The table value of chi-square is 1591.22, which is 95 %. The values for the chi-square test are accepted below the tabulated value and above the tabulated value.

Table 3: Chi-square test for different cases in easting

Case	**PP**		**SRS**	
	T-test	**Status**	**T-test**	**Status**
Route 1 (R1)	4026.71	rejected	23.51	accepted
Route 2 (R2)	15392.54	rejected	1488.4	accepted
Route 3 (R3)	22770.81	rejected	676	accepted
Route 4 (R4)	1655.51	rejected	64.18	accepted
Route 5 (R5)	29299.51	rejected	74.11	accepted
Route 6 (R6)	3132.01	rejected	24.69	accepted
Route 7 (R7)	591.6	accepted	69.01	accepted
Route 8 (R8)	299.02	accepted	0.01	accepted

Table 4: Chi-square test for different cases in northing

Case	**PP**		**SRS**	
	T-test	**Status**	**T-test**	**Status**
Route 1 (R1)	1	accepted	0.001	accepted
Route 2 (R2)	4	accepted	1	accepted
Route 3 (R3)	100	rejected	1	accepted
Route 4 (R4)	4	accepted	0.001	accepted
Route 5 (R5)	121	rejected	0.001	accepted
Route 6 (R6)	36	rejected	4	accepted
Route 7 (R7)	1	accepted	4	accepted
Route 8 (R8)	4	accepted	0.001	accepted

Table 5: Chi-square test for different cases in height

Case	PP		SRS	
	T-test	Status	T-test	Status
Route 1 (R1)	1409.22	accepted	62.98	accepted
Route 2 (R2)	5386.8	rejected	128.13	accepted
Route 3 (R3)	3629.03	rejected	78.4	accepted
Route 4 (R4)	1843.31	rejected	91.21	accepted
Route 5 (R5)	2805.63	rejected	16.9	accepted
Route 6 (R6)	1412.74	accepted	2381.4	rejected
Route 7 (R7)	1440.09	accepted	0.014	accepted
Route 8 (R8)	2743.6	rejected	38.93	accepted

5. Conclusions

During kinematic positioning applications, high accuracy can be achieved conveniently by the availability of the IGS services. The following conclusions can be inferred on the analysis of results for previous kinematic point positioning and simulated base station: The accuracy of kinematic point positioning was 972 mm in the horizontal component and 223 mm with an improvement of a percentage of 77 % in the simulated base technique proposed. The accuracy of kinematic point positioning was 851 mm, and 250 mm was used to increase the percentage of 72 % in a vertical component. In view of the influence of the length of the route, the number of epochs, and the location of observation, because by increasing the number of epochs and observed in urban areas, accuracy increases. As it is clear from the previous conclusions, this technique, Simulated Reference Station (SRS), has a significant positive impact on improving the Point Positioning (PP) technique

References

Bock, H., R. Dach, A. Jäggi and G. Beutler (2009). High rate GPS clock corrections from CODE: Support of 1 Hz applications, Journal of Geodesy, 83(11), 1083.

Chen, W., C. Hu, Z. Li, Y. Chen, X. Ding, S. Gao and S. Ji (2004). Kinematic GPS precise point positioning for sea level monitoring with GPS buoy, Journal of Global Positioning Systems, 3(1-2), 302-307.

Colombo, S.A.W. and A.G. Evans (2004). Evaluation of precise kinematic GPS point positioning, In Proceedings of ION GNSS 17th International Technical Meeting of the Satellite Division, Long Beach, California (1423-1430).

El-Rabbany, A. (2002). Introduction to GPS: The Global Positioning System. Artech House, ISBN 1-58053-183-0.

Elsobeiey, M., and S. Al-Harbi (2015). Performance of real-time precise point positioning using IGS real-time service, GPS solutions, 20(3), 565-571.

Furones, M., A. Esteban, A.B. Anquela, V. Berné and M. Sanmartín (2012). Kinematic GNSS-PPP results from various software packages and raw data configurations, Scientific Research and Essays, 7(3), 419-431.

He, H., J. Li, Y. Yang, J. Xu, H. Guo, and A. Wang (2014). Performance assessment of single and dual frequency BeiDou/GPS single epoch kinematic positioning, GPS solutions, 18(3), 393-403.

Hofmann-Wellenhof B., H. Lichtenegger and E. Wasle (2007). GNSS Global Navigation Satellite Systems: GPS, GLONASS, Galileo, and More. Springer Science and Business Media, ISBN 978-3-211-73012-6.

Kaartinen, H., J. Hyyppä, M. Vastaranta, A. Kukko, A. Jaakkola, X. Yu and R. Kaijaluoto (2015). Accuracy of kinematic positioning using global satellite navigation systems under forest canopies, Forests, 6(9), 3218-3236.

Kouba, J., F. Lahaye and P. Tétreault (2017). Precise Point Positioning". In: Teunissen P.J., Montenbruck O. (eds) Springer Handbook of Global Navigation Satellite Systems. Springer Handbooks. Springer, Cham. ISBN: 978-3-319-42926-7.

Li, B., Y. Shen and X. Zhang (2012). Three frequency GNSS navigation prospect demonstrated with semi-simulated data, Advances in Space Research, 51(7), 1175-1185.

Lotfy, A. (2019). Optimization analysis for improving the performance of regional kinematic GNSS networks. Master thesis, Faculty of Engineering, Zagazig University, Egypt.

Lotfy, A., M. A. Abdelfatah and H. Hosny (2019). Quality control of kinematic GNSS networks: A case study of regional network at Sharqia Governorate in Egypt. Civil Engineering Research Magazine (CERM), Al Azhar University, Egypt, 41(3: 359-368).

Journal of Geomatics Vol. 14, No. 2, October 2020

The integration of Analytical Hierarchy Process (AHP), Fuzzy Analytical Hierarchy Process (FAHP), and Bayesian Belief Network (BBN) for flood-prone areas identification – A Case study of the Greater Accra region, Ghana

B. Kumi-Boateng*, M.S. Peprah and E.K. Larbi
Department of Geomatic Engineering, University of Mines and Technology, Tarkwa, Ghana
*Email: kumi@umat.edu.gh

(Received: June 24, 2019; in final form: July 21, 2020)

Abstract: Flood has become a destructive natural disaster in the world, which seriously threatens the safety of human and properties. This has drawn the attention of numerous researchers with the need to study the increasing incidences of flooding in Sub Saharan African countries including Ghana. Conversely, this is a result of increasing climate change, urbanization growth, improper sanitation practice and the increased occurrences of high intensity rainfall. This study used Greater Accra Region as a case study, which involves a quantitative and qualitative analysis and review of relevant literature. The quantitative approach involves the utilization of soft computing techniques such as fuzzy logics and Bayesian theorem and qualitative analysis such as Analytical Hierarchy Process. In this study, the geo-environmental causative factors that were used in the flood susceptibility mapping included; slope, land use and land cover, precipitation, soil types and lithology, water bodies, aspect and Digital Elevation Model (DEM) of the study area. The integrated Bayesian Model was used to assign the conditional weights to the various cost criteria. Both Fuzzy AHP and AHP were used to form the posterior and prior probabilities respectively. The achieved result is much better and reliable because more than one modelling technique and contributing factors were considered and analyzed at the same time. Also, weights were assigned to these contributing factors before overlaying them to produce the final map. The previously occurred flood places were all found in the zones of high possibilities of flooding. The flood hazard prone map indicates that almost the whole area of Accra and Greater Accra Region has a possibility of flooding. However, the riskiest areas are Lolonya, Lakpleku, Dawa and Kpantsedor areas.

Keywords: Geographic Information System, Hazard Risk, Land Cover Changes**,** Multicriteria Decision Analysis, Soft Computing Techniques, Spatial Modelling, Susceptibility Mapping

1. Introduction

Flood occurrences within the recent and past decades have become a global pandemic. It is one of the most common and catastrophic geo-hazards that are poorly understood due to the rapid change of demographic growth, urbanization trends and climate change (Wang et al., 2020; Tehrany et al., 2014a). The severe impact of floods has become a major problem on the world's natural ecosystems and human activities have greatly affected economic and social sustainability (Mensah and Ahadzie, 2020). Floods can have devastating impacts which may cause major disruption to agriculture, power energy, potable quality water, communication, and transportation. In addition to, it interferes with public and private services, natural environment, cultural heritage, environmental pollution, severe changes to habitats, illegal migration and many other aspects of urban infrastructure. Hence, flood control and prevention measures are urgently required (Tehrany et al., 2014b; Asumadu-Sarkodie et al., 2015a). Moreover, floods can bring pathogens into urban environments and can cause lingering damp and microbial development in buildings and outbreak of diseases such as diarrhoea, cholera, dysentery and many others (Tehrany et al., 2014a; Abu and Codjoe, 2018). Early warnings and emergency responses to floods are needed so that governmental agencies and planners can prevent as much damage as possible (Rahmati et al., 2015; Gyekye, 2011). Therefore, it is essential to identify flood prone zones to prevent or mitigate adverse effects of flooding. In the republic of Ghana, flood occurs every year, which adversely affects livelihoods, property infrastructure, lives and renders many citizens homeless (Mensah and Ahadzie, 2020). Flooding as a natural disaster cannot be eradicated in the world however, its effect can be minimized by undertaking the integrated flood management and developmental approach that can promote the coordinated management and development of water, land and related resources (Asumadu-Sarkodie et al., 2015a). The supposed and actual causes of flood hazards in the cities of sub-Saharan African countries have come under tremendous debate (Amoako and Boamah, 2014). In Accra, the capital of Ghana, flooding has been the key source of human vulnerability and numerous studies have been carried out in the city giving varied attributions to their frequent occurrences (Amoako and Boamah, 2014; Karley, 2009). The conventional techniques for flood studies in Ghana included identifying watermarks on structures, media reports and aerial photographs interpretation (Nyarko, 2000). These classical methods used by the agencies are woefully inadequate, because there are always new areas that periodically experience floods. Therefore, there was a need to explore novel techniques in identifying and mapping flood hazards zones that will help in planning and managing the problem in spatial context.

According to Mensah and Ahadzie, (2020) the causes of urban floods in Ghana are poor urban planning and development, poor and inadequate drainage facilities, poor environmental attitude and extreme rainfall. The authors concluded from their study that, the most reported coping strategies were relocation and protection of properties and construction of drains. The first step in flood management is the development of hazard maps. Flood hazard mapping forms the foundation of the decision-making process by providing information which is essential to the understanding of the nature, risk and characteristics of flooding to the community or city that could be affected by the flood (Kwang and Osei Jnr, 2017). Also, it can serve as an important source of information by assisting decision makers, engineers and planners in making the right decisions and in taking the appropriate steps in dealing with flood related issues and controlling. Moreover, it plays an important role when it comes to land use management and planning. This can be achieved either through a quantitative approach or qualitative techniques. The prediction of flood susceptibility can decrease the flood associated fatalities and economic losses. Modelling of flood sensitive areas is a strategic component in any flood mitigation strategy (Sarhadi et al., 2012; Chapi et al., 2017). A major contribution and understanding of flood susceptibility and planning is derived from the information made available by the use of remote sensing technologies and its integration with geographical information systems (GIS). In recent years, hazard mapping and flood susceptibility analyses through remote sensing and GIS tools are done by many researchers which provided considerable good accuracy as recorded in the following literatures (Pradhan et al., 2009; Bates, 2012; Rahmati et al., 2016a, 2016b; Wanders et al., 2014; Fekete, 2009; Nikoo et al., 2016). In the past recent years, numerous mathematical models and soft computing techniques methods have been successfully applied in flood susceptibility modelling. Mathematical methods are mainly based on the assumption that, historical flood events are closely related to flood predisposing factors (Wang et al., 2020). Notably among the mathematical models are frequency ratio (Ullah and Zhang, 2020; Rahmati et al., 2016a; Tehrany et al., 2015a; Pradhan, 2010; Kornejady et al., 2014, Kornejady et al., 2015; Lee et al., 2012), logistic regression (Tehrany et al., 2014a; Youssef et al., 2015), weight of evidence (Rahmati et al., 2015; Tehrany et al., 2014b; Rahmati et al., 2016a), analytical hierarchy process (Meshram et al., 2019; Das, 2019; Costache et al., 2020a; 2020b Dano et al., 2019; Das, 2018; Chen et al., 2011; Kazakis et al., 2015; Rahmati et al., 2016b), and multiple criteria decision analysis (Liu et al., 2018; Santos et al., 2019; Wang et al., 2019a, 2019b). Based on these models, flood susceptibility mapping and prediction were achieved at a good precision. Recently, soft computing techniques have been applied for flood prediction. Notably among the soft computing techniques include fuzzy logic (Chapi et al, 2017; Bui et al., 2020; Bui et al., 2019; Meshram et al., 2019; Pierdicca et al., 2010; Zou et al., 2013), artificial neural networks (Janizadeh et al., 2019; Costache et al., 2020; Bui et al., 2019; Kia et al., 2012), support vector machines (Wang et al., 2020; Choubin et al., 2019;Tehrany et al., 2015b), adaptive neuro-fuzzy inference system (ANFIS) (Bui et al., 2018a, 2018b), biogeography based optimization and BAT algorithms (Ahmadlou et al., 2019), reduced error pruning trees (Khosravi et al., 2018), multivariate adaptive regression splines (Moghadam et al., 2018), convolutional neural network (Wang et al., 2020), decision tree (Janizadeh et al., 2019; Choubin et al., 2019; Khosravi et al., 2018; Tehrany et al., 2013), and random forest (Tang et al., 2020a; Tang et al., 2020b; Rizeei et al., 2018) are used. The authors concluded from the studies that; the models predicted the flood hazards at a better precision with much accuracy. Moreover, no conclusion has been made for the selection of the best model for flood susceptibility studies (Wang et al., 2020). However, other machine learning algorithms such as decision tree, radial basis function, generalized regression neural network, group method of handling data, game theory, least square support vector machines, random forest algorithms, genetic algorithms, monte Carlo simulation, multivariate adaptive regression splines, box Jenkins, extreme learning machines, gaussian approach, wavelet transform model, ARIMA, particle swarm optimization and many others that were not considered in this study can be used in the future research.

The main objective of the study was to generate static flood hazard map in Greater Accra region using geo-environmental factors such as land use and land cover, soil types and lithology, precipitation data, slope, water bodies, aspect and Digital Elevation Model (DEM) of the area. The utilization of soft computing techniques such as Fuzzy AHP and Bayesian Belief network were adopted. The frequent annual occurrences of flood and the effectiveness of soft computing techniques as recommended by numerous researchers demonstrated an optimistic strategy for flood prioritization. Therefore, the current study is devoted to prioritize flood hazard of Accra based on the geo-environmental parameters. The modeling procedure is established using the aforementioned soft computing methods. Moreover, the present study provides a reliable methodology for flood prioritization at the Greater Accra region, contributing to multiple flood occurrences, hazard risks, and water resource engineering disciplines. This is highly essential for such a region where the reliable flooding management and sustainability is very much needed.

2. Study area

The study area (Figure 1) is the capital city of the Republic of Ghana. The area hosts majority of the Ministerial institutions, governmental and non-governmental agencies, public and private companies, which makes it one of the most populated urban cities in Ghana but most often the city is faced with several annual flooding issues (Okyere et al., 2013). The area and its surrounding communities are situated in low land topographic areas with average altitude of about 100 m above mean sea level (Nyarko, 2000). Geographically, the area is found within longitude 0° 03′ and 0° 25′ West and latitude 5° 30′ and 5° 53′ North (Kwang and Osei Jnr, 2017). Accra covers a land mass of about 3533 km^2 and it stretches from Botianor to Sakumo, and James Town to Oyarifa. Tema bounds it on the East, on the South by the sea, West by the Weija Dam, and North by the Akwapim Hills (Asumadu-Sarkodie et al., 2015a). According to Asumadu-Sarkodie et al., (2015b) characteristics of Accra are lowlands, and hilly areas that makes easily movement of running waters into the sea as a result of rain from the city. The intensity of rainfall events occurs in the eight drainage basins in Accra namely; Kpeshie, Korle, Densu, Sakumo, Lafa, Osu, Songo, Mokwe and Chemu (Asumadu-Sarkodie et al., 2015a). The area is drained through by natural streams and valley network and artificial drains. Most of the streams like Odaw, Sakumo, Mahahuma, Lador, and Dzorwulu, take their source from the Akwapim range. The artificial drainage is mostly built-up structures that enable quick discharge of waste and storm water. (Okyere et al., 2013). The area falls within the anomalous dry equatorial climate region and experiences double maxima rainfall and a prolonged dry season with occasional dry harmattan condition being experienced. The hottest months are February and March, just before the rainy season, with mean monthly temperatures of 27°C, whilst the coolest months are June – August. During this period temperature are around 21°C. Rainfall in this area has two periods in May to August and October to November, with an annual amount between 780 mm and 120 mm. There are two main vegetation types within the area, namely the coastal scrub and grasslands, and mangrove forest. The mangrove forests are found in the coastal lagoon areas where the soil is waterlogged and salty (Nyarko, 2000). The flooding of Accra normally occurs between June and July and the history of Accra flood is tabulated in (Kwang and Osei Jnr, 2017). Accra metropolitan area consists of many sub-metropolitan areas which include; Kpeshie, Osu-Clottey, Central Ayawaso, East Ayawaso, West Ayawaso, Ashiedu-Keteke, Okai-Koi North, Okai-Koi South, Ablekuma South and Ablekuma North (Asumadu-Sarkodie et al., 2015a).

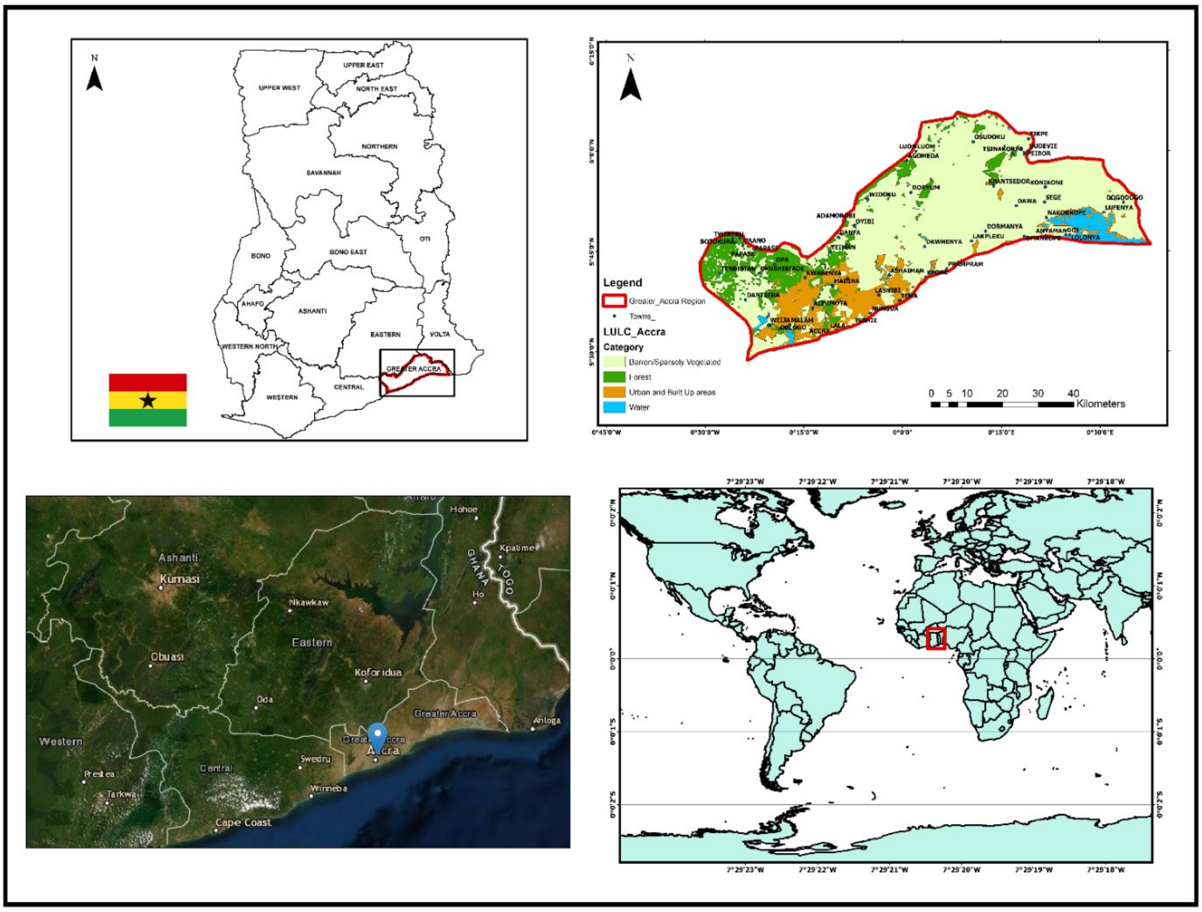

Figure 1: Location map of study area

3. Resources and methods

3.1 Resources
The geo-environmental variables that were used as a triggering causative factors for generating static flood hazard map of Greater Accra Region was obtained from the Survey and Mapping Division of the Lands Commission of Ghana which includes: Soil types and lithology, land use and land cover, water bodies, slope and slope aspect. The precipitation data downloaded from the World Climate website, (https://www.worldclim.org/data/index.html). These variables were used as flood causative factors.

3.2 Methods
3.2.1 Model generation
The Integrated Bayesian model was used to assign the conditional weights to the various cost criteria. Both Fuzzy AHP and AHP formed the Posterior and Prior probabilities respectively. First, a consistency check was carried out to determine the consistency of the selected criteria. The calculated Consistency ratio, C_r for the cost criteria using AHP was 0.10, this implies the calculated weights were consistent. The consistent set criteria were then fed into the fuzzy AHP using the triangular fuzzy membership function. The obtained Triangular fuzzy weights were defuzzied to obtain the crisp weights using the center of area method before it was finally normalized to obtain the required posterior weights. The flood susceptibility model was generated in the ArcGIS environment as given by Equation (1) (Peprah *et al.*, 2018) as:

$$F = \sum_{i=1}^{n} W_i C_i \prod_{j=1}^{n} r_j \quad (1)$$

where; F = Flood Model; W_i = weight of variables; C_i =Model variables; r_j = Restrictions. This model equation was adopted for generating flood hazard prone areas in Accra because several factors such as suitability criteria, weights criteria, and restriction criteria are all factored in the modelling process (Peprah *et al.*, 2018).

3.2.2 Bayesian Belief Network (BBN)
In this study, the Bayesian Network Model was used to assign probabilistic weights to the various geo-environmental criteria. The essence is to verify the interdependencies of the variables employed in flood identification using joint probability networks (Kabanda, 2019; Tang *et al*, 2020). The nodes and directed links in the model signify system variables and their causal dependencies, the prior nodes are expressed as P [Y (i)] = (Y_1, Y_2, Y_3…. Y_8) (Wu *et al*, 2019; Sedki *et al*, 2015; Requejo-Castro *et al*, 2019). From Figure 2a, the prior weights given by each rectangular box were obtained from Analytical Hierarchy Process to represent the root nodes of the Bayesian Network. Eight (8) collectively exhaustive parental nodes were employed as the set criteria. The introduction of a conditional set, which is represented as B links all the independent variables as observed in Figure 2a. Set B was introduced based on the triangular fuzzy membership function, Figure 2a and 2b represent a graph of the Bayesian Belief Network and flowchart of the methodology respectively.

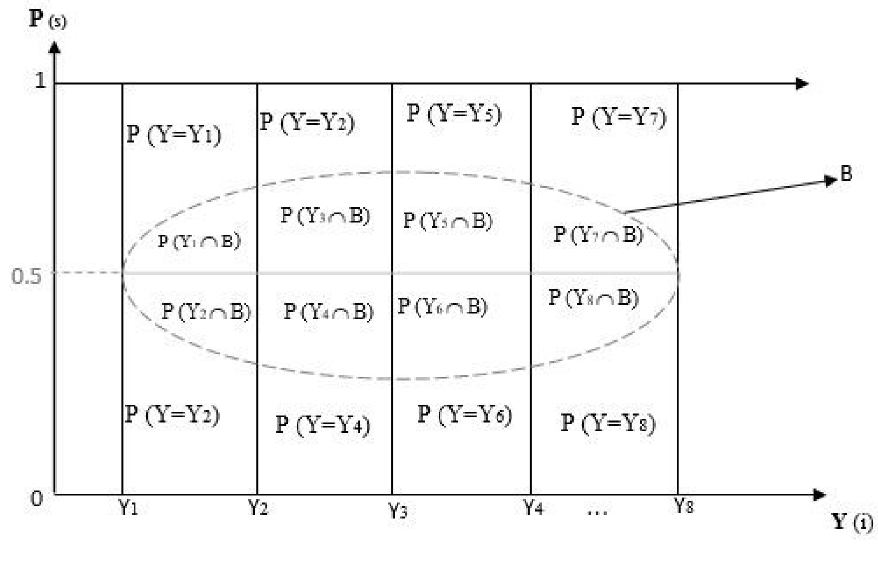

Figure 2a: Bayesian belief network model

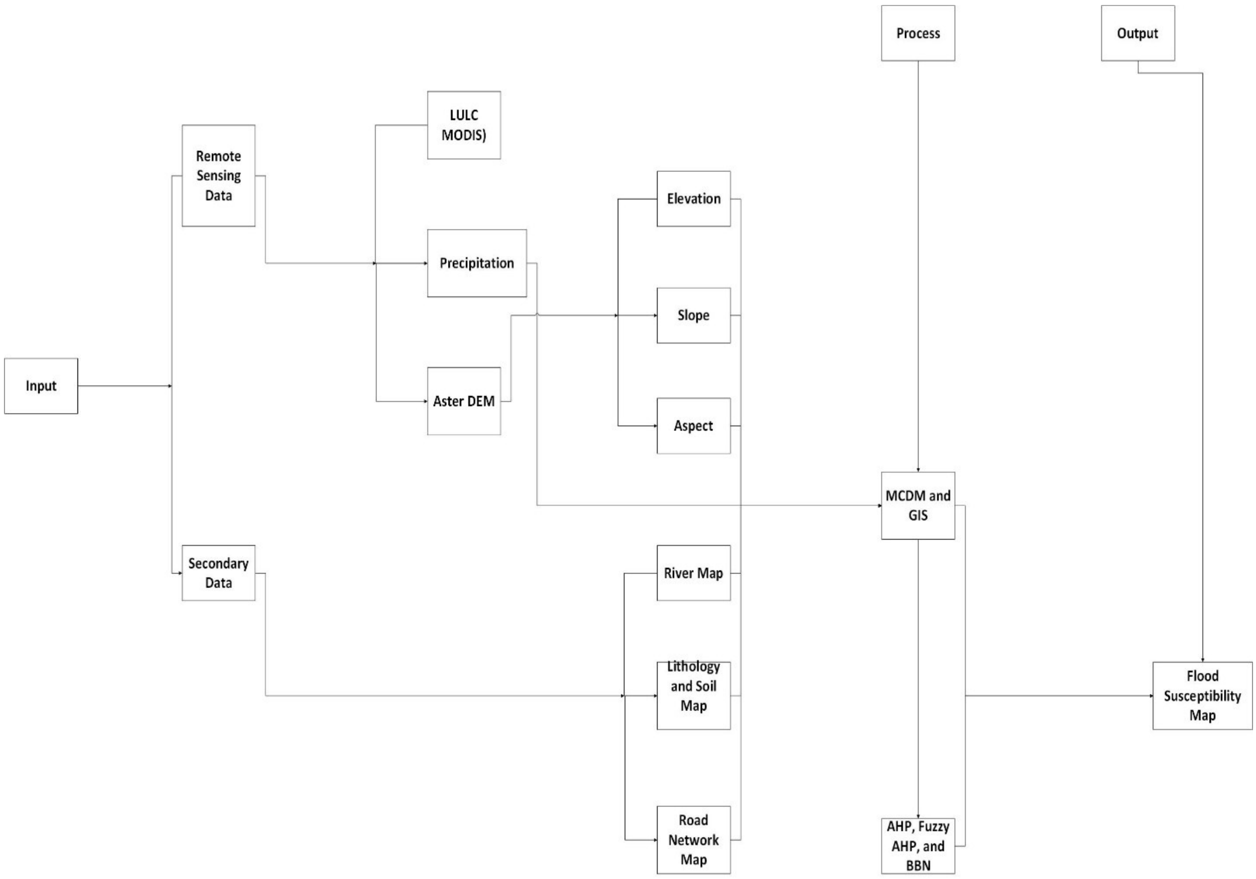

Figure 2b: Flowchart of the methodology

The Posterior probability is given by Equation (2) as:

$$P(B|Y_i)=\frac{P(Y_i \cap B)}{P(Y_i)} \tag{2}$$

Equation 3 represents the conditional probability introduced by the Fuzzy set B as:

$$P(Y_i|B)=\frac{P(Y_i \cap B)}{P(B)} \tag{3}$$

Re-arranging Equation (2) and Equation (3) gives Equation (4) denoted as:

$$P(Y_i \cap B) = P(B|Y_i)[P(Y_i)] = P(Y_i|B)[P(B)] \tag{4}$$

From Equation (4), Equation (3) can be re-written as;

$$P(Y_i|B)=\frac{P(B|Y_i)[P(Y_i)]}{P(B)} \tag{5}$$

From Figure 2, Set B can be expressed as:

$$P(B) = P(Y_1 \cap B)+P(Y_2 \cap B)+P(Y_3 \cap B)\cdots P(Y_8 \cap B) \tag{6}$$

Applying Equation (4) to Equation (6) results into Equation (7) given as:

$$P(B)= P(B|Y_1)[P(Y_1)]+P(B|Y_2)[P(Y_2)]+P(B|Y_3)[P(Y_3)]\cdots P(B|Y_8)[P(Y_8)] \tag{7}$$

Hence, The Generalized Bayesian Formula is thus given by Equation (8) as:

$$P(Y_i|B)=\left[\frac{P(B|Y_i)[P(Y_i)]}{\sum_{i=1}^{n} P(B|Y_i)[P(Y_i)]}\right] \tag{8}$$

3.2.3 Fuzzy AHP (FAHP)

FAHP was used to generate the posterior weights of the variables. The reason is to deal with the uncertainties and the unbalanced scale of judgement experienced in the traditional AHP (Ozdagoglu, 2007; Fazlollahtabar *et al*, 2009). The fuzzy members are represented in the form $\tilde{q}_i = (e_{ij}, f_{ij}, g_{ij})$ and in geometric space as shown in Figure 3 (Firoozi *et al.*, 2017). Equation (9) denotes the fuzzy judgement matrix, formed based on the respondents and experts' advice (Kim *et al*, 2019).:

$$\begin{bmatrix} (1,1,1) & (e_{12}, f_{12}, g_{12}) & \dots & (e_{1n}, f_{1n}, g_{1n}) \\ (e_{21}, f_{21}, g_{21}) & (1,1,1) & \dots & (e_{2n}, f_{2n}, g_{2n}) \\ (e_{n1}, f_{n1}, g_{n1}) & (e_{n2}, f_{n2}, g_{n2}) & \dots & (1,1,1) \end{bmatrix} \tag{9}$$

The Geometric mean is calculated along each row according to Equation (10) (Firoozi *et al.*, 2017):

$$\tilde{\sigma}_i = \left(\Pi_{j-1}^{n} \tilde{q}_{ij}\right)^{\frac{1}{n}} \tag{10}$$

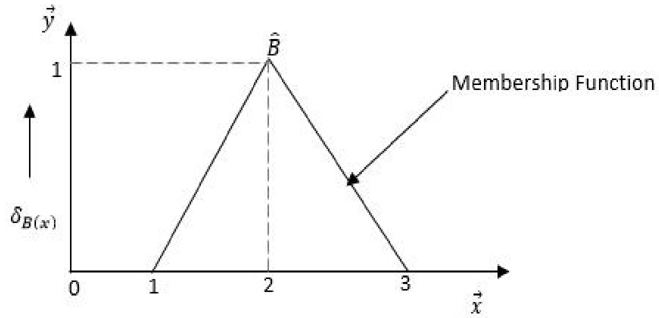

Figure 3: Triangular Fuzzy Membership

where; $\tilde{\sigma}_i$ = Geometric mean values, $\tilde{q}_{ij}$ = Triangular Fuzzy Members, n = number of criteria. The Fuzzy Geometric Mean is obtained by the column summation of the Geometric Mean of each criterion according to Equation (11) given as:

$$\sum_{i=1}^{n} \tilde{\sigma}i = \tilde{\sigma}1 + \tilde{\sigma}2 + \tilde{\sigma}3 \cdots \tilde{\sigma}n \tag{11}$$

The Fuzzy weights are obtained by normalization according to Equation (12) as:

$$\tilde{r}_{ij} = \tilde{w}_{ij} = \frac{\tilde{\sigma}i}{\sum_{i=1}^{n} \tilde{\sigma}i} \tag{12}$$

where; $\tilde{r}_{ij}$ = normalized weights of the secondary variables (option i weight than criterion j), $\tilde{w}_{ij}$ = weights of the main variable or criteria. The final weights, $\tilde{U}_i$ are thus obtained in Equation (13) given as:

$$\tilde{U}_i = \sum_{i=1}^{n} \tilde{w}_{ij}\, \tilde{r}_{ij} \tag{13}$$

3.2.4 Analytical Hierarchy Process (AHP)

The prior weights representing the root nodes of the integrated model was generated using AHP. The purpose is to prioritize in hierarchical order the various alternatives used in the multi-criteria decision-making process (Meshram et al., 2019). A decision matrix was formed using Saaty's scale and factor attributes as seen in table 1 (Larbi et al., 2018). The relative weights of the criteria were determined by forming a pairwise matrix for comparing the relative importance of the variables based on experts' advice (Aschilean et al., 2016).

Table 1: The relative importance values (Akay and Yilmaz, 2017)

Scale	Definition of Scale
1	Equal Importance
3	Moderately Important
5	Strongly Importance
7	Demonstrated Importance
9	Absolute Importance
2,4,6,8	Intermediate values between the two adjacent judgements

3.2.5 Consistency check

A consistency check was carried out on the geo-environmental variables. The consistency ratio was used to check whether the threshold value proposed by Sir Saaty's was not exceeded (Larbi *et al.*, 2018). For consistency, the consistency ratio should not exceed $0.10 (c_r < 0.10)$. The consistency ratio is obtained by dividing the calculated consistency index by its corresponding criteria Random Index. First, the weighted sum is multiplied by the criteria matrix given by Equation (14) as:

$$W_s = \begin{bmatrix} w_1 \\ w_2 \\ w_3 \\ w_4 \end{bmatrix} \tag{14}$$

where; W_s = weighted sum vector. The Eigen Vector is calculated by division of the weighted sum vector by the criteria weights given by Equation (15) as:

$$e_i = \frac{1}{\tilde{w}_{ij}} (w_s) \tag{15}$$

where; e_i = Eigen vectors; $\tilde{W}_{ij}$ = weights of the main variable. The average eigen vectors is calculated by Equation (16) given as:

$$\lambda_{\max} = \frac{\sum_{i=1}^{n} e_i}{n} \tag{16}$$

where; $\lambda_{\max}$ = Average of the Eigen vectors; n = number of criteria. The Consistency Index, C_i is calculated by Equation (17) as:

$$C_i = \frac{\lambda_{\max} - n}{n-1} \tag{17}$$

The Consistency ratio is computed by Equation (18) as:

$$C_r = \frac{C_i}{R_i} \tag{18}$$

where; C_r= Consistency ratio, and Ri = Random Index

3.2.6 Cost Criteria

The Cost Friction surface is a raster dataset represented by grid cells. This is based on a set of defined criteria. Various thematic maps according to the defined cost criteria were generated in the ArcGIS environment to assist in identifying flood prone areas in intensifying degrees. In this study, eight (8) main cost factors were selected and used for the flood studies based on the experts' advice. The factors were classified and weighted using both the AHP and fuzzy AHP. The final conditional weights were obtained using the Bayesian Belief Network (BBN). Table1 is the classification of the flood cost factors.

Precipitation

Precipitation is the major natural agent to consider in flood prediction studies. Flood disaster occurs due to extreme rainfall and the inability of disaster bearers to mediate or adapt to the environmental challenges (Wu *et al*, 2019). The lack of proper drainage facilities such as gutters and drains especially in the urban areas coupled with its numerous impervious layers results in flooding of those areas. Poor layout systems, slums, rampant dumping of refuse and littering forms blockades for run off waters by choking drains and gutters. In the event of rainfall, the waters overflow their banks and results in flooding of the urban areas. In this research, the monthly average precipitation data (TRMM) for the year (2012 to 2018) was downloaded from the World Climate website, (https://www.worldclim.org/data/index.html) in a raster format. The downloaded data had a resolution of 30 seconds (~1km^2). The particular precipitation covering the entire study area was extracted using the boundary shape file. The study area has a monthly average precipitation of 200mm. Figure 4 shows the precipitation data of the study area.

Topographic characteristics

Topography plays an important role in flood occurrence and redistribution. It encompasses elevation and slope data, which are the influencing agents of terrain in flood disaster. Slope is the measure of the average rate of change of altitude in a given area. Elevation is the vertical distance from a specified surface to a reference datum. The Elevation data was an Aster DEM downloaded from the USGS website, http:// lpdaac.usgs.gov/products/astgtmv003/. The downloaded has a resolution of 30m. The Slope data was generated from the DEM in the ArcGIS environment and latter classified as seen in table 2. Figure 5 and Figure 6 represents the topographic characteristics of the study area.

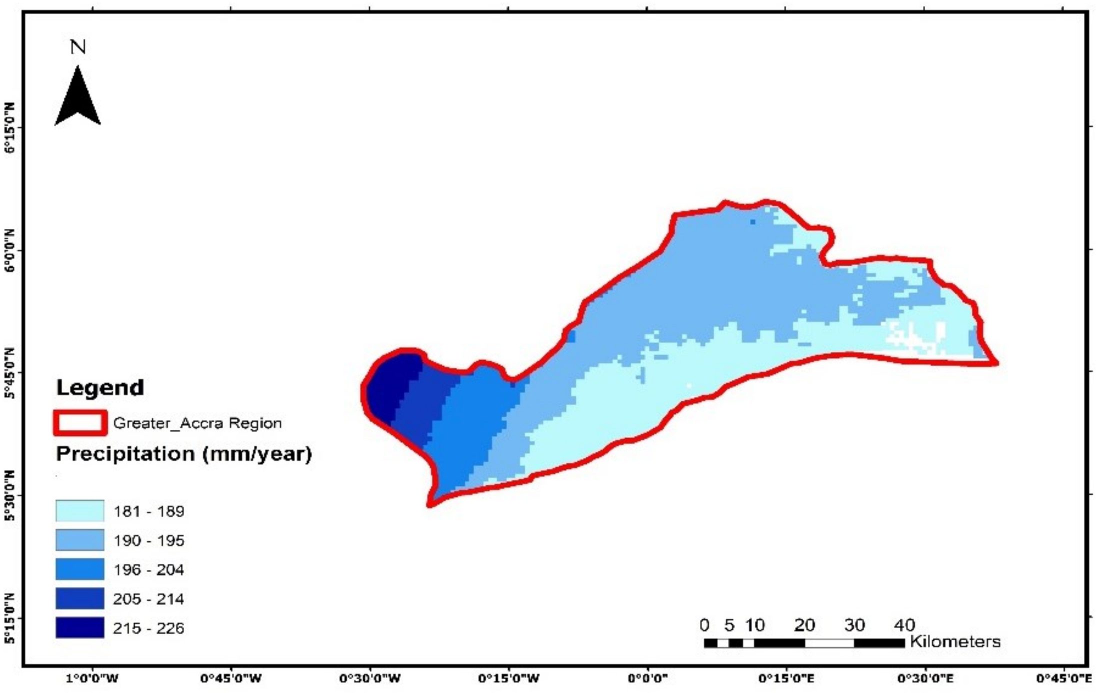

Figure 4: Precipitation Map

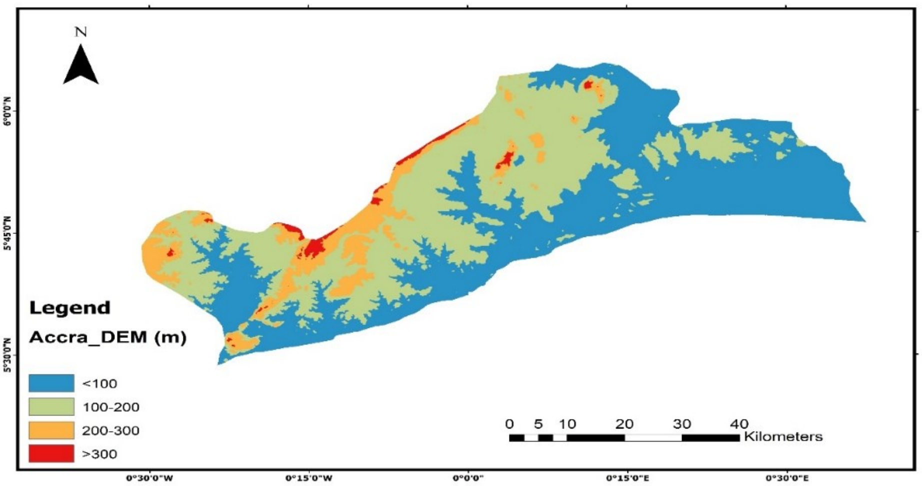

Figure 5: Digital Elevation Model

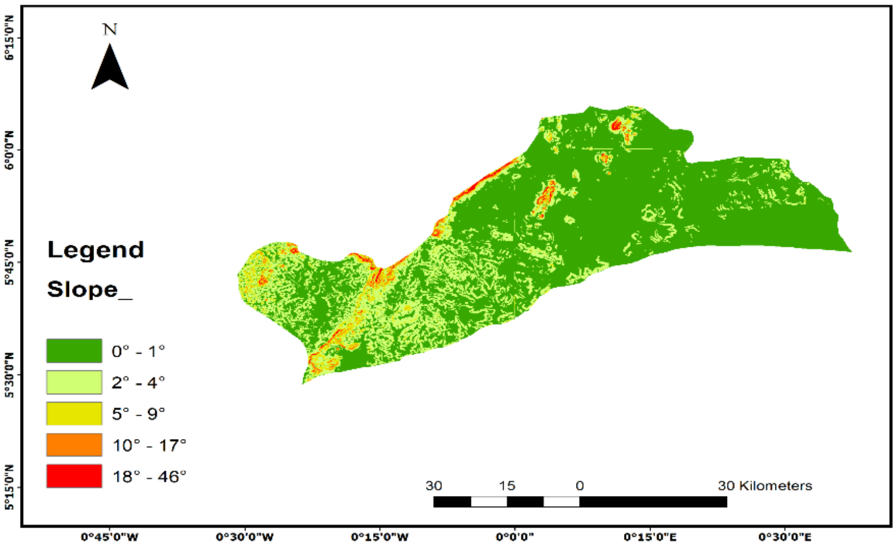

Figure 6: Slope Map of study area

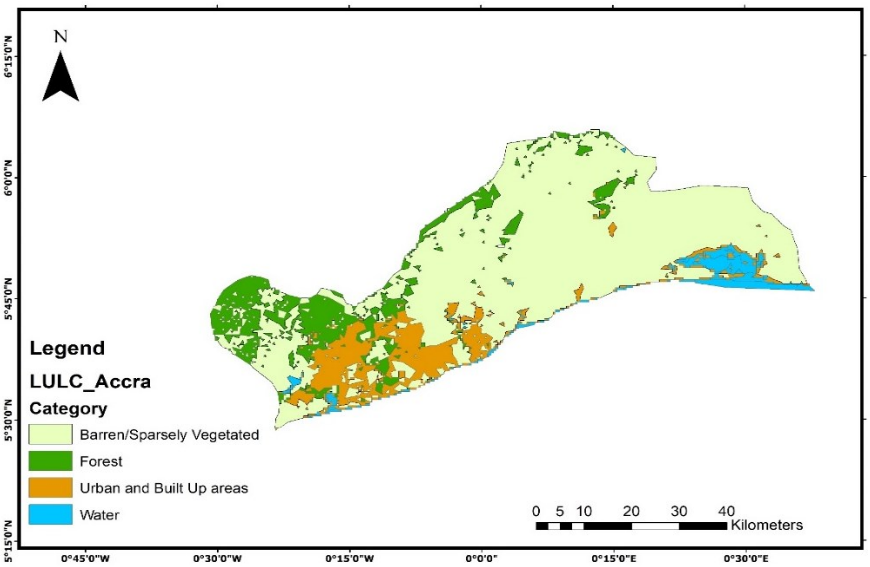

Figure 7: Land Use-Land cover Map

Land Use-Land Cover (LULC)

The LULC comprises of both the pervious and the impervious areas. The pervious areas are the areas that allow the seepage of water into the depths of the land. The impervious areas block the passage of water hence results in more run offs through built drains, gutters and roofing materials (Mojaddadi *et al*, 2017). The pervious areas include forests areas, soil, farmlands and fields whiles the impervious areas consist of the paved surfaces such as roads, built up areas and buildings. The LULC data was obtained from MODIS satellite imagery data and classified using the IGBP classification scheme, https://earthexplorer.usgs.gov. Table 2 is a description of the MODIS LULC classification. Figure 7 is the Land Use-Land cover data of Greater Accra Region.

River Network

The distribution of river network plays a crucial role in flood disaster especially the river network density of the water and the distance to the river. Hence, the river density and river proximity analysis as proposed by the town and country planning of Ghana was carried out to account for the flood formation. River density refers to the length of the river per unit area, which was obtained from the Line Density Function at 250 m radius. The River proximity sets a restriction on the closest distance, one can erect a structure close to the river without it not being prone to flood. This was performed using the multiple buffer operator. Greater Region (study area), comprises of a lot of coastal areas boarded to the south by the Gulf of Guinea, it is characterized by a well distribution of river networks which easily overflow their banks in the event of rainfall. The river network data was obtained from the Ghana Survey and Mapping Division of the Ghana Lands Commission. Figure 8 gives the drainage distribution of the study area

Road Network

A Line Density Function and road proximity analysis was performed on the road to determine the ratio of the impervious areas to the total area and also the buffered proximity distance of building along roads. The buffer road proximity distance was carried at a 100 m radius. This is important as paved surfaces are one of the major contributors to flood disasters. The road network was obtained from the Survey and Mapping Division. The distribution of roads is shown in Figure 9.

Aspect

Aspect data plays a significant role in assessing the slope stability of a local terrain based on the type of slope face (Mojaddadi *et al*, 2017). The Aspect was generated from the slope data using ArcGIS 10.4 software, which was later grouped into ten (10) classes. The Aspect Map is as shown in Figure 10.

Table 2: Description of Land Use Land Cover Classes (IGBP Classification Scheme) (Dugarsuren *et al*, 2011)

LULC Classes (Level 1)	Description
Barren/Sparsely Vegetated	Lands with exposed soil, sand and rocks with more than (>10%) vegetated cover during any time of the year.
Forest	Land dominated by tree canopy with a percent cover (> 60%) and height exceeding 2m. Consist of tree communities with interspersed mixtures or mosaics of other forest types. Has an intra-annual cycle of leaf -on and leaf-off periods.
Urban and Built up areas	Rural and Urban settlements.
Water	Land with permanent water.

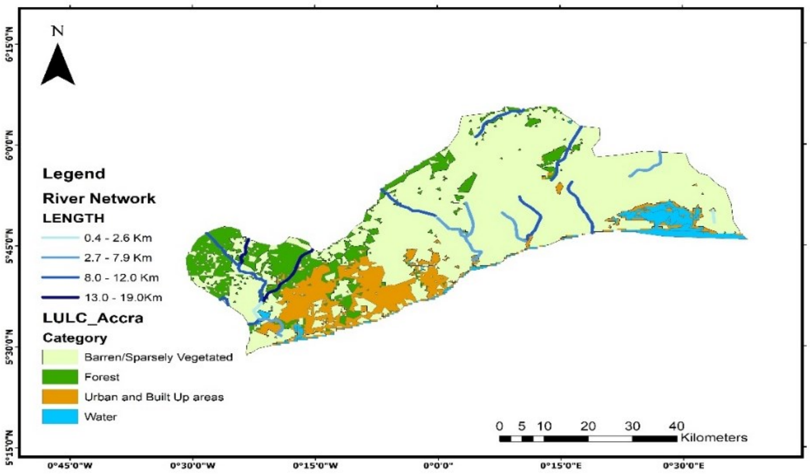

Figure 8: River Network

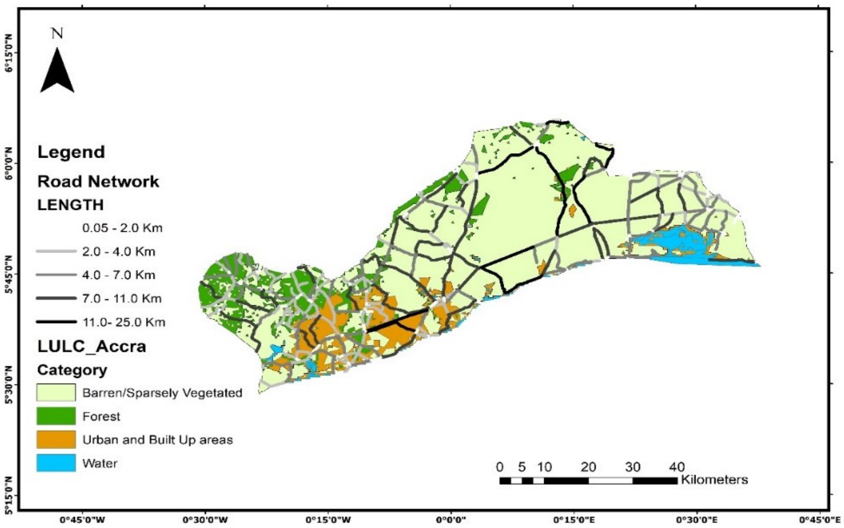

Figure 9: Road Network

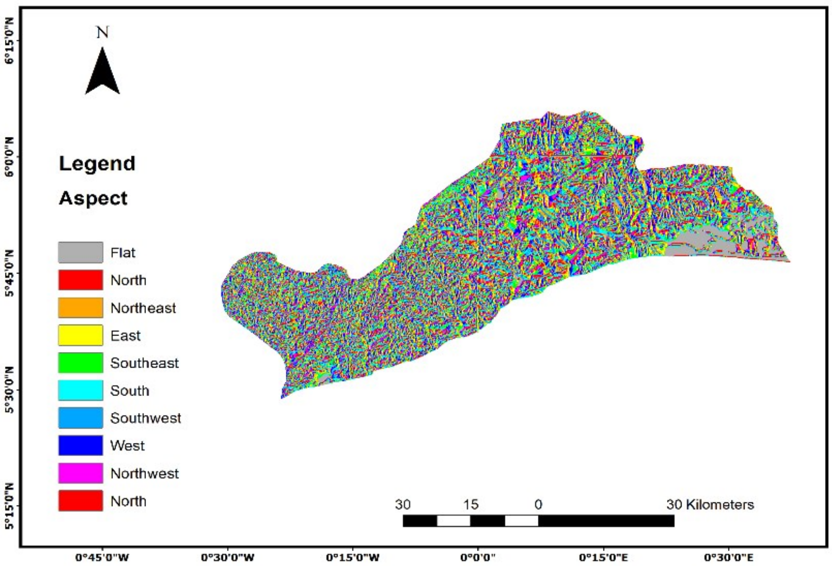

Figure 10: Aspect Map

Lithological and Soil Type

Lithology and soil types are essential parameters in locating sensitive areas prone to flooding. Soil type affects the water seepage process due to properties such as texture, aggregates, porosity and permeability degree (Mojaddadi *et al*, 2017). The study area is characterized by soil types. Lithology regarding rock permeability is also required in flood hazard assessment. Figure 11 represents the Lithology of the study area. The western side of the study area is covered by basic lithological formations whereas the eastern side are marked by acidic lithological layers. Data was obtained from the Geological and Mineral Department of Ghana.

Index Value Scoring

Index Value Scoring is very essential because various variables can be evaluated based on their relative importance using their respective weights, observed values can also be scored or grouped into classes and scored based on their sensitivity to flood (Sharma *et al*., 2012). The Index Value Scoring was carried out using the weighted overlay tool in the ArcGIS environment. Table 3 describes the assigned values used in scoring the various variable classes and Table 4 shows the classification of flood cost factors.

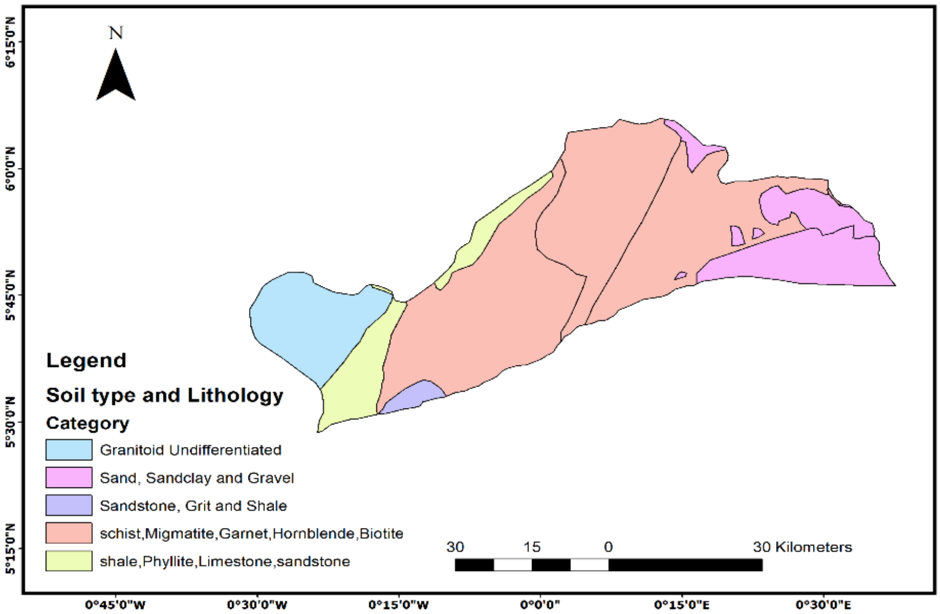

Figure 11: Soil Types and Lithology

Table 3: Index Value Scoring (Sharma *et al.*, 2012)

Index Value	Description
1	Very Low
2	Low
3	Moderate
4	Moderate High
5	High
6	Very High

Table 4: Classification of Flood Cost Factors

Variables	Classes	Index Values	Description
Precipitation (mm)	181-189	1	Very Low
	189-195	2	Low
	195-204	4	Moderate High
	204-214	5	High
	214-226	6	Very High
Rivers (km)	0.4-2.6	2	Low
	2.7-7.9	3	Moderate
	8.0-12.0	4	Moderate High
	13.0-19.0	6	Very High
Road (km)	0.05-2.0	1	Very Low
	2.0-4.0	2	Low
	4.0-7.0	3	Moderate
	7.0-11.0	4	Moderate high
	11.0-25.0	6	Very High
Landuse-Landcover (LULC)	Barren/Sparsely vegetated	3	Moderate
	Forest	2	Low
	Urban and Built up areas	5	High
	Water	6	Very High
Slope	0°-1°	6	Very High
	2°-4°	4	Moderate High
	5°-9°	3	Moderate
	10°-17°	2	Low
	18°-46°	1	Very Low
Elevation (m)	<100	6	Very High
	100-200	5	High
	200-300	3	Moderate
	>300	2	Low
Aspect	Flat	1	Very Low
	North	2	Low
	Northeast	3	Moderate
	East	4	Moderate High
	Southeast	5	High
	South	6	Very High
	Southwest	4	Moderate High
	West	3	Moderate
	Northwest	3	Moderate
	North	5	High
Soil type and Lithology	Granitoid Undifferentiated	2	Very Low
	Sand, Sand clay And Gravel	3	Moderate
	Sandstone, Grit and Shale	4	Moderate High
	Schist, Migmatite, Garnet, Hornblende	5	High
	Shale, Phyllite, Limestone, Sandstone	6	Very High

3.2.7 Proximity analysis and line density function

Buffer Distance Analysis was carried out on the drainage features (rivers) and paved surfaces (roads) in the study area. This was done to determine the ideal distance to build houses or erect other structures close to the rivers or the roads so as to guard against flooding. This was carried out to assess the compliance to the set standards by the Town and Country Planning, Ministry of Lands and Administration and the Survey and Mapping Division. An analysis buffer of 200 m was used for the rivers whiles 60 m buffer zone was considered for the roads. Figure 12 is a map of the road buffer zones whereas figure 13 shows the buffer areas of the river. The Line Density Function was also employed in this study to determine the degree of concentration of the linear features in a particular area so as to clarify its contributing factor to the flood occurrence. Figure 14 represents a map of the road density. A map of the river density of the study area is shown in figure 15. This was achieved using the ArcGIS 10.4 software. The detailed buffer analysis and Line density functions is tabulated in table 5.

Table 5: Buffer analysis and line density functions

Restriction Source	Minimum Buffer Distances(m)	Maximum Buffer Distance(m)	Analysis Buffer Distance(m)	Line Density Buffer Radius(km)
River	100	300	200	8
Roads	30	90	60	5

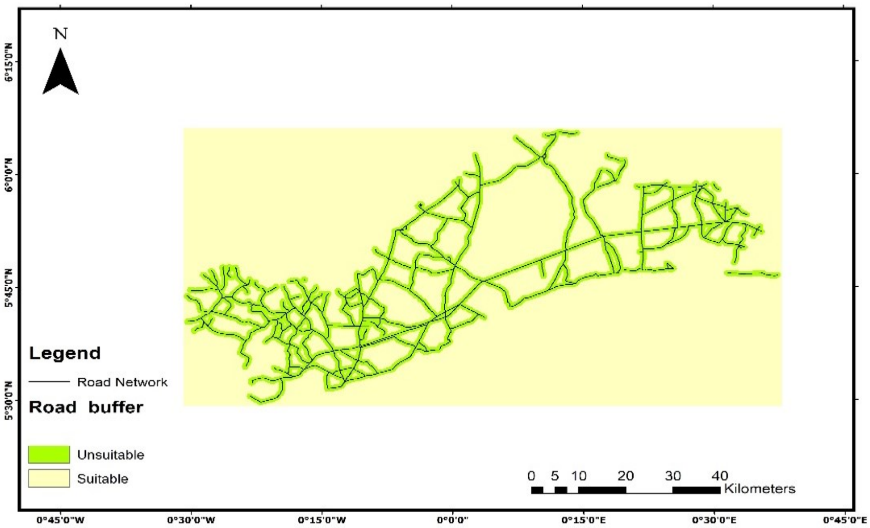

Figure 12: Road Buffer

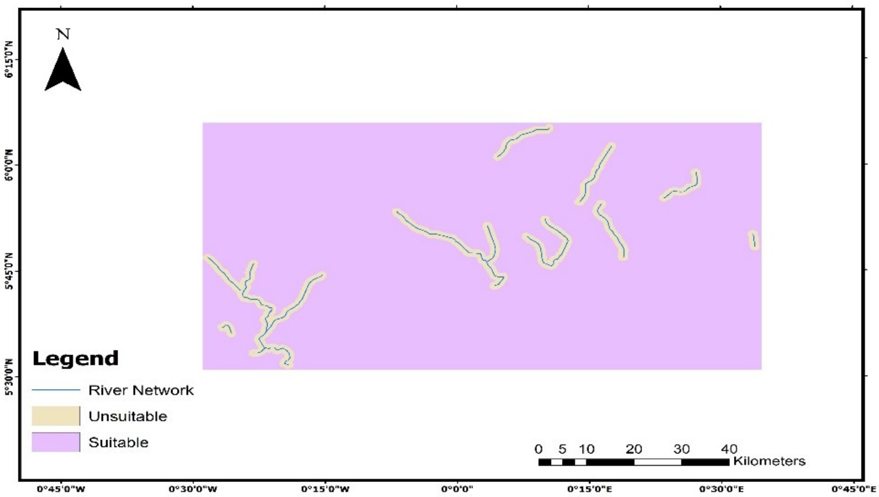

Figure 13: River Buffer

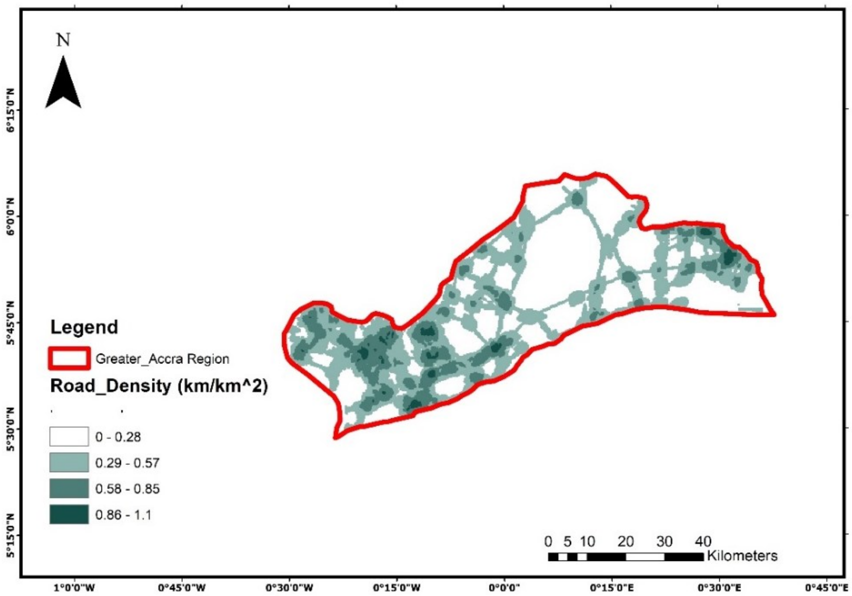

Figure 14: Road Density

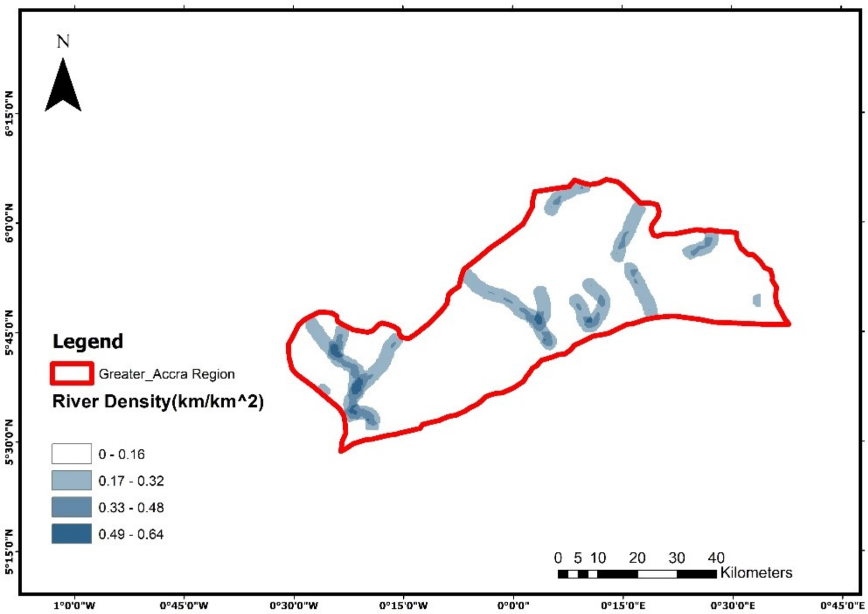

Figure 15: River Density

4. Results and discussion

The paper aims at the identification of flood prone areas in the Greater Accra Region of Ghana through the integration of three mathematical models, namely the AHP, Fuzzy AHP and the Bayesian Belief Network Model (BBN). This was achieved using the joint probability idea as seen in Figure 2a and 2b. The Flood Identification Model consists of the weights, selected criteria and the restriction source as shown in Equation 1. First, weights were generated using AHP as seen in Equation 14, this was used to form the parental nodes of the joint probability network. A consistency check was carried to validate the trustworthiness of the decision matrix using the linguistic variables (Table 1) given by Equation 18. The Consistency ratio was 0.1, which implies the weighted criteria was consistent. A triangular fuzzy member function (Figure 3) was applied on the pairwise matrix of the AHP to generate the fuzzy set as seen in Equation 9, this generated the posterior probabilities of the joint probability network. Applying the Bayes Conditional set theory as seen in Equation 11, the integration of both AHP and the Fuzzy AHP were made possible. This enables the factoring in of the interdependencies between the various criteria in the course of the weight calculation as proposed by the Flood Identification model. The Cost criteria for this study comprises of secondary data obtained from the Survey and Mapping Division of Ghana during the national photogrammetry exercise and the downloaded secondary data from online services. All maps of the weighted criteria were generated using ArcGIS 10.4 software.

Table 6: AHP Pairwise matrix

Criteria (n)	P	W	R	LULC	S	El	A	S_o
P	1	1	1	2	2	2	2	2
W	**1**	1	1	1	2	2	2	2
R	**1**	**1**	1	1	1	2	2	2
LULC	**0.5**	**1**	**1**	1	1	2	2	2
S	**0.5**	**0.5**	**1**	**1**	1	1	1	2
El	**0.5**	**0.5**	**0.5**	**0.5**	**1**	1	1	2
A	**0.5**	**0.5**	**0.5**	**0.5**	**1**	**1**	1	1
S_o	**0.5**	**0.5**	**0.5**	**0.5**	**0.5**	**0.5**	**1**	1

Table 7: Normalized matrix and weights

n	P	W	R	LULC	S	El	A	S_o	**Weights**
P	0.18181	0.16667	0.15385	0.266667	0.21053	0.17391	0.16667	0.14286	*0.18287*
W	0.18181	0.16667	0.15385	0.13333	0.21053	0.17391	0.16667	0.14286	*0.16620*
R	0.18181	0.16667	0.15385	0.13333	0.10526	0.17391	0.16667	0.14286	*0.15305*
LULC	0.09090	0.16667	0.15385	0.13333	0.10526	0.17391	0.16667	0.14286	*0.14168*
S	0.09090	0.16667	0.15385	0.13333	0.10526	0.08696	0.08333	0.14286	*0.10998*
El	0.09090	0.08333	0.07692	0.06667	0.10526	0.08696	0.08333	0.14286	*0.09203*
A	0.09090	0.08333	0.07692	0.06667	0.10526	0.08696	0.08333	0.07143	*0.08310*
S_o	0.09090	0.08333	0.07692	0.06667	0.05263	0.04348	0.08333	0.07143	*0.07109*

where; P = Precipitation; *W*= Water bodies; *R* = Roads; *LULC* = Land use-Landcover; *S*= Slope; *El*= Elevation; *A*=Aspect and S_o= Soil type and Lithology.

$$\begin{array}{c|cccccccc}
n & P & W & R & LULC & S & El & A & S \\
\hline
P & (1,1,1) & (1,1,1) & (1,1,1) & (1,2,3) & (1,2,3) & (1,2,3) & (1,2,3) & (1,2,3) \\
W & (1,1,1) & (1,1,1) & (1,1,1) & (1,1,1) & (1,2,3) & (1,2,3) & (1,2,3) & (1,2,3) \\
R & (1,1,1) & (1,1,1) & (1,1,1) & (1,1,1) & (1,1,1) & (1,2,3) & (1,2,3) & (1,2,3) \\
LULC & \left(\frac{1}{3},\frac{1}{2},1\right) & (1,1,1) & (1,1,1) & (1,1,1) & (1,1,1) & (1,2,3) & (1,2,3) & (1,2,3) \\
S & \left(\frac{1}{3},\frac{1}{2},1\right) & \left(\frac{1}{3},\frac{1}{2},1\right) & (1,1,1) & (1,1,1) & (1,1,1) & (1,1,1) & (1,1,1) & (1,2,3) \\
El & \left(\frac{1}{3},\frac{1}{2},1\right) & \left(\frac{1}{3},\frac{1}{2},1\right) & \left(\frac{1}{3},\frac{1}{2},1\right) & \left(\frac{1}{3},\frac{1}{2},1\right) & (1,1,1) & (1,1,1) & (1,1,1) & (1,2,3) \\
A & \left(\frac{1}{3},\frac{1}{2},1\right) & \left(\frac{1}{3},\frac{1}{2},1\right) & \left(\frac{1}{3},\frac{1}{2},1\right) & \left(\frac{1}{3},\frac{1}{2},1\right) & (1,1,1) & (1,1,1) & (1,1,1) & (1,1,1) \\
S & \left(\frac{1}{3},\frac{1}{2},1\right) & \left(\frac{1}{3},\frac{1}{2},1\right) & \left(\frac{1}{3},\frac{1}{2},1\right) & \left(\frac{1}{3},\frac{1}{2},1\right) & \left(\frac{1}{3},\frac{1}{2},1\right) & \left(\frac{1}{3},\frac{1}{2},1\right) & (1,1,1) & (1,1,1)
\end{array} \tag{19}$$

$$\begin{array}{c|cccc}
n & U & M & L & Weights \\
\hline
P & 0.091 & 0.183 & 0.319 & 0.198 \\
W & 0.091 & 0.168 & 0.278 & 0.179 \\
R & 0.091 & 0.154 & 0.243 & 0.162 \\
LULC & 0.079 & 0.141 & 0.243 & 0.154 \\
S & 0.069 & 0.109 & 0.184 & 0.121 \\
El & 0.052 & 0.091 & 0.184 & 0.109 \\
A & 0.052 & 0.084 & 0.161 & 0.099 \\
S_o & 0.040 & 0.071 & 0.161 & 0.090
\end{array} \tag{20}$$

where; *n* = criteria; *U*=Upper Values; *M* = Middle values; *L*= Lower values

Table 8: Integrated AHP, Fuzzy AHP and BBN for weight calculation

AHP			Fuzzy AHP	Bayes		
Variables	Prior	P(Yi)	P(B|Yi)	P(Yi)[P(B|Yi)]	P(Y_i|B)	Weights (%)
P	Y_1	0.1828	0.198	0.036	0.24048828	24
W	Y_2	0.1662	0.179	0.030	0.1976681	20
R	Y_3	0.153	0.162	0.025	0.16468687	16
LULC	Y_4	0.1417	0.154	0.022	0.14499169	15
S	Y_5	0.1099	0.121	0.013	0.08835591	9
EL	Y_6	0.092	0.109	0.010	0.06662955	7
A	Y_7	0.0831	0.099	0.008	0.05466241	5
S_o	Y_8	0.0711	0.090	0.006	0.0425172	4

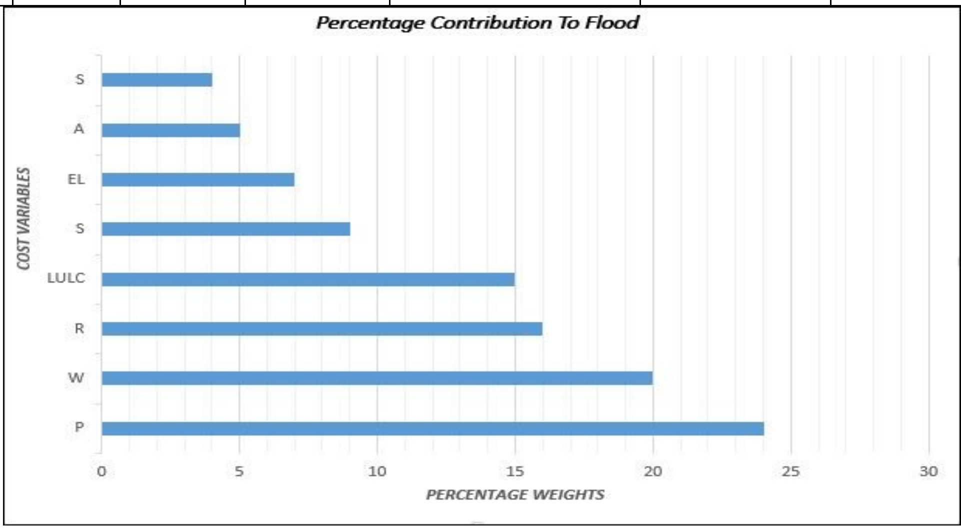

Figure 16: Bar graph showing the percentage contribution of criteria to flood

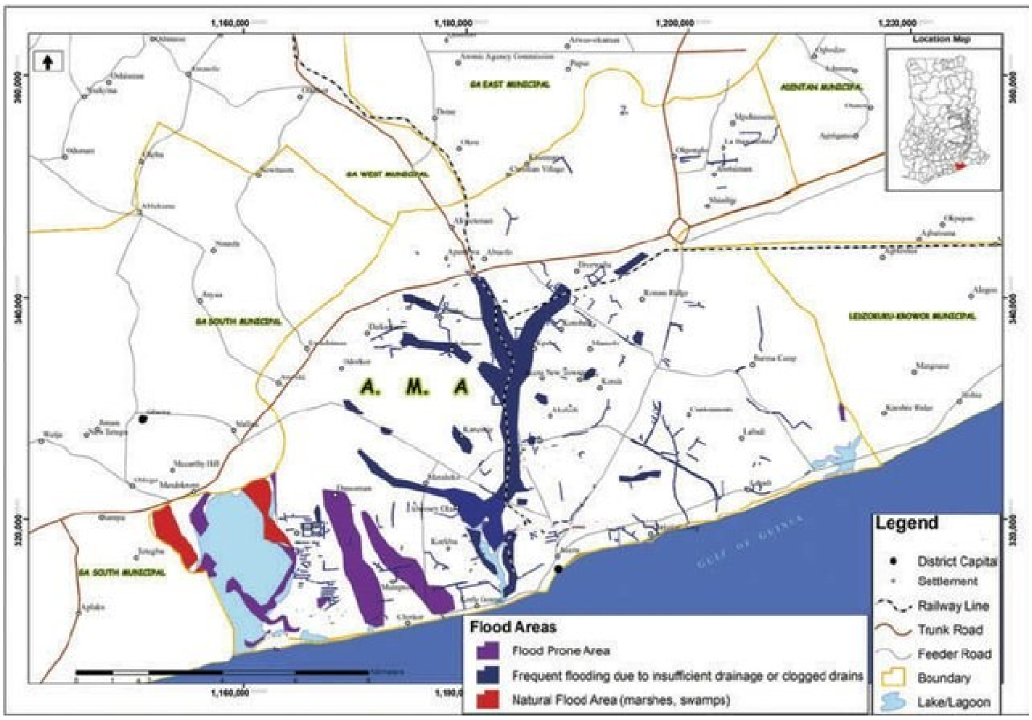

Figure 17: Flood Extent Map of the Metropolitan Section of the study area (Amoako and Boamah, 2014)

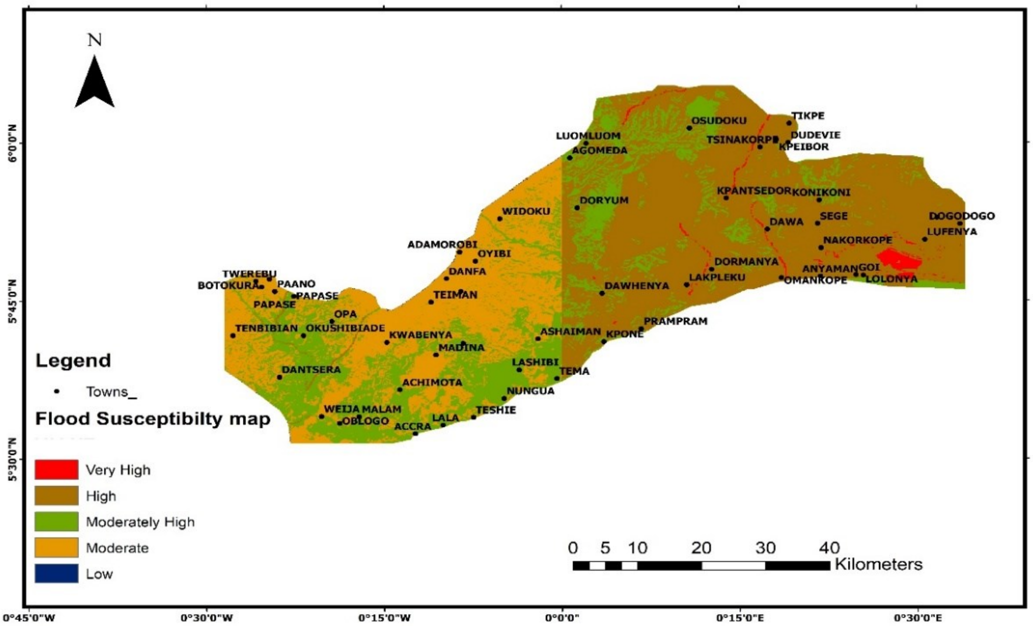

Figure 18: Flood susceptibility map

Table 9: Area and percentage coverage of the flood map

	Description	Area (km^2)	Coverage (%)
Flood Prone Areas	Very High	145.519	4.12
	High	2498.291	70.7
	Moderately High	426.136	12.06
	Moderate	460.517	13.03
	Low	3.517	0.1
	Total	**3533.98**	100

Figure 4 is the monthly precipitation data of the study area in the year 2018 downloaded from the world climate website, https://www.worldclim.org/data/index.html. The intensity of the rainfall increases from the west to east side of the study area. Figure 5 is the elevation data of the study area; the lowest elevation areas are those below the 100m contour. Figure 6 is the slope map generated from the DEM of the area. The classified land-use and land-cover data is shown in Figure 7. The land use - land cover map was classified into four groups using the MODIS IGBP classification scheme, https://yceo.yale.edu/modis-land-cover-product-mod12q/. Table 2 gives the description of the different LULC classes. Figure 8 and figure 9 shows the River and Road Network respectively. The linear features (rivers and roads) were classified based on their respective lengths in km. This was to enable the calculation of both the river and road density as seen in figures14 and 15 respectively, which is the length (km) of the linear features per the area (km^2) under studies. The reason is to find out how its concentration contributes to the formation of flood in the respective areas. The Aspect map is shown in figure 10. The Aspect map helped in assessing the slope stability of the terrain. The Soil types and lithology is shown in figure 11. The dominant lithology class was schist, migmatite, garnet, hornblende and biotite. The various classes of the criteria was scored using the index values scoring scheme as shown in table 3. The reason is to account for their different levels of sensitivity to flood aside the general weights of the major criteria. The classification of the flood cost factors is given in table 4. Table 5 presents the proximity and Line density analysis carried out on the linear features. This is to set a restriction buffer zone by classifying areas into suitable and unsuitable areas as seen in figure 13 and river figure 14. An analysis buffer of 200m was employed in the river buffer whiles that of the road was 60m. The radius for the river line density was 8km whereas that of the roads were 5km. These were chosen based on experts' advice and opinion. Table 6 shows the results for the pairwise comparison of the AHP. The reason was to arrange in order of priority the various multi-criteria decisions. The normalized decision matrix is given in table 7. This was done to calculate the corresponding weights of the criteria. The Fuzzy membership matrix is shown in equation 19. The Fuzzy set was formed from the pairwise AHP matrix using the triangular membership function. This was to enable a balanced scale of judgement in the generation of the weights of the criteria as an advantage over the traditional AHP as given in equation 20. The Fuzzy weights formed the posterior nodes of the joint probability network. Table 8 shows the calculated integration results of the AHP and Fuzzy AHP using the Bayesian Belief Network. This was made possible using the Generalized Bayesian conditional formula given in equation 11. The purpose is to verify the interdependencies between the multi-criteria decisions for a more accurate model result. Most methods used such as the stand alone AHP or Fuzzy AHP produces a mutually exclusive results and fails to factor in the interdependencies between the set criteria, should in case they are mutually dependent. The results will be far from accurate. The weights obtained from the BBN was graphically shown using Bar graphs to give a clear view on each criteria's sensitivity to flood as seen in figure 16. Figure 17 is a flood extent map showing the real recorded cases of flood in the Accra Metropolitan Assembly, a section of the study area with reported cases of flood. Flood occurrence in the metropolis was a result of improper waste disposal, clogged gutters and poor drainage facilities in the urban area (Amoako and Boamah, 2014). The purpose of the flood extent map was to provide a comparative reference to the final flood susceptibility map produced in this study as shown in figure 18. Figure 18 is a Flood Identification map of the entire region. Floodable areas recorded in the flood extent map were also identified as flood prone areas in the final flood susceptibility map. These areas include Kaneshie, Tesano, Kokomlemle, Alajo, Madiina, James Town and Accra. These were as a result of poor drainage facilities, clogged drains and gutters in the urban area. Other flood prone areas further identified as seen in figure 18 includes Dawhenya, Kpone, Achimota, Weija, Kwabenya, Lakpleku, Teshie. The eastern side of the flood susceptibility map was found to be more prone to flood because of its accompanied lower elevation compared to the western area. The reported cases recorded in the western side was mainly due to the poor layout of the urban areas, slums and its associated poor waste disposal. Table 9 is the area and percentage coverage of the flood susceptibility map. These were put into five (5) classes namely Very High, High, Moderately High, Moderate and Low susceptibility to flood. The purpose is to be able to analyse the risk severity of the area as far as flood occurrence is concerned. Upon analysis, it was found that the entire region has about 86% chance of flood occurrence (very high, high and moderately high). This is more than half of the entire area. The region is also a coastal zone borded to the south by the Gulf of Guinea. Figure 19 displays a pie chart of the flood condition in Accra. This is to give a graphical and statitical clarity on the flood condition of the study area. According to history, most of the flooding in Accra occurs between June and July. Kwang and Osei Jnr (2017) carried out a research on the flood history of Accra from 1959 to 2016. As a form of validation of results, areas with numerous records of flooding in Accra were researched on. These flood prone areas were also seen in the high floodable areas, these include Tema, Accra, Teshie, Kpone, Awushi, Ashaiman, Mallam, Achimota, Madina, sections of Ga West and Ga South areas.

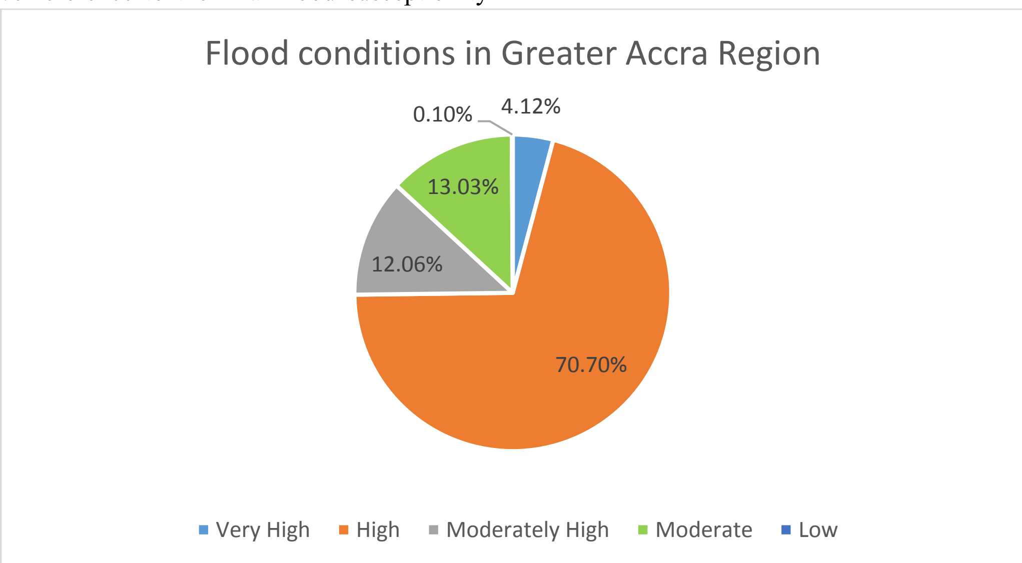

Figure 19: A pie chart illustration of the flood conditions in Greater Accra region

5. Conclusions and recommendations

Whilst heavy rainfalls and increased intensity of rainfall may result in flooding, the fundamental problem is that, flood prone cities are being blocked as a result of human activities such as building houses on river beds and across water courses, the lack of adequate and the right drainage infrastructure and the siltation of limited drainage systems. Thus, it is essential to have a holistic approach towards resolving the flooding problem and at the same time devising approaches necessary to mitigate the specific problems of affected communities. To determine flood risk zones in Accra and its environs, a flood hazard risk map was integrated into the GIS platform, by utilizing soft computing methods such as Fuzzy AHP and Bayesian Belief Network and conventional methods such as AHP. The results show that the delineated areas however experience same rainfall intensity of about 200 mm yet the flood intensities of the areas differ. For instance, the high flood risk zone covers 37% of the study area, whiles the low risk zone covers 5%. The result of the research showed that potential areas likely to experience periodic floods with a given input of rainfall are mostly below the 100 m contour. It was also noted that, the flood experienced by an area is mostly dependent on rainfall intensity no matter the catchment area. However other factors such as inadequate drains, choked gutters as a result of poor sanitation habits by the habitants, land use were identified as contributing factors to flooding in the study area. It was also observed that about 95% of the study areas fall within flood risk zone. In search for a method to determine flood risk zones, the use of soft computing techniques models within a geographic information system model is very effective if only the appropriate decision rule was defined. Geographic Information Systems (GIS) and Remote Sensing (RS) techniques are some of the techniques used recently in solving problems concerning the environment. GIS and RS have also proven to be useful in making decisions. GIS can be combined with soft computing techniques and multi-criteria decision analysis (MCDA) tools such (AHP, Fuzzy AHP and BBN to produce the best result. In this research work, the capabilities of GIS, Soft computing and MCDA were illustrated through the production of the flood prone map of Accra. The result obtained was more accurate as compared to the previous works done on Accra flood studies. This is because more than one technique and contributing factor were considered and at the same time weights were assigned to these contributing factors before overlaying them to produce the final map. The previously occurred flood places were all found in the high possibilities flooding zones. The flood prone map indicates that almost the whole area of Accra and Greater Accra Region has a possibility of flooding. However, the most risk areas are Accra Metropolitan, Nungua, Achimota, Tema, Teshie, Kpone, Awushi, Ashaiman, Mallam, Madina, sections of Ga West and Ga south respectively. An enforcement of building regulations that prevents people from building in flood prone areas and flood plains will help to reduce flood frequencies in Accra. Employing the integrated flood management mix options into already existing strategies will help curb the frequent menace of flood in Accra. We recommend public education that can reduces the risk of exposure to flood and outbreak of diseases through flood mitigation measures, including the construction of drains in communities and educating communities on good sanitation. Thus, this method is recommended for use in hydrological studies, and disaster management. The proposed method can be considered as a robust method for flood susceptibility mapping and the produced map aid planners, decision makers and governmental agencies engaged in flood management and planning in the study area.

The outcome of the present study can be used in taking mitigation measures to minimize the loss in agricultural production, lives and properties, game and wild animals' reserves, and economic cost to the nation. The results also provide information which will be instrumented for governmental agencies to optimally allocate drains. It is recommended that; the Town and Country Planning department should use this map for future redevelopment of the study area. Moreover, the Geological Survey Department, Survey and Mapping Division of Lands Commission, and Meteorological Department of the country should produce an up to date rainfall map, aspect map, flood hazard maps, and geomorphological map of the study area for further studies to review the affected areas and help give relevant solutions to mitigate the menace to prevent loss of lives and properties.

Conversely, the application of soft computing techniques methods to solve a particular problem, feature engineering is a critical step that obtains an appropriate feature representation from the raw data (e.g pixel values of the image) prior to data modelling. Furthermore, the performance of soft computing methods depends to a large extent on the representation of the raw data. In this sense, soft computing methods cannot directly uncover instructive representations from the raw data, nor can they obtain new insights from the representatives, this further improving predictive capability (Wang et al., 2020). More recently, deep learning is one of the most popular techniques that has been receiving attention worldwide by numerous researchers such as convolutional neural network (CNN), Shuffled Frog Leaping Algorithm (SFLA), Particle Swarm Optimization (PSO), Brain Inspired Emotional Neural Network, Group Method of Data Handling, Support Vector Machine, Backpropagation Neural Network, Fuzzy logics, Adaptive Neuro-Fuzzy Interference System, Gaussian Process Regression, Decision Trees, Principal Component Analysis, Group Analysis, Population-based Evolutionary Algorithms, Invasive Weed Optimization, Differential Evolution, Firefly, Bees algorithms, Radial Basis Function Neural Network, Generalized Regression Neural Network, k-Nearest Neighbor, Elephant Herding Optimization

Evolutionary techniques. Other conventional techniques such as, Contour banking, backfilling methods, phytoremediation techniques, water erosion prediction project (WEPP) model, revised universal soil loss equation (RUSLE), Siberia model, geoflu natural regrade design, that were not considered in this present study should be given attention in the future studies. Using soft computing to generate static flood hazard map is a good methodology that results in good response, but it is necessary to be cautious with the chosen of the causative criteria. In this study, the adopted soft computing techniques could generate static flood hazard map with much better accuracy, but did not recognize with great accuracy points with low risks thus; the direction of the flow of the waters. Nevertheless, with good repeatability, testing other optimization methods, as well as executing the sensitivity analysis of the flood conditioning factors, are good subjects for future studies, which probably will result in achieving more reliable results. Future repeatedly studies should include more static variables, such as NDVI images and distances to roads and settlement areas. Also, it would be very interesting studying for a longer period, to see seasonal changes in meteorological variables. Location of drains along the prone areas is highly recommend and education of habitants about proper sanitation procedures in avoidances of floods.

Acknowledgements

The authors would like to appreciate the anonymous reviewers for their helpful comments, time and effort that made this piece of knowledge a better paper. Our sincere appreciation also goes to the Survey and Mapping Division of Lands Commission and Geological Survey Department of Ghana for providing us with the necessary data used in the investigation of the research findings.

References

Abu, M., and S.N.A. Codjoe (2018). Experience and future perceived risk of floods and diarrheal disease in urban poor communities in Accra, Ghana, International Journal of Environmental Research and Public Health, 15, 1-16.

Ahmadlou, M., M. Karimi, S. Alizadeh, A. Shirzadi, D. Parvinnejhad, H. Shahabi, and M. Panahi (2019). Flood susceptibility assessment using integration of Adaptive Network based Fuzzy Inference System (ANFIS) and Biogeography-Based Optimization (BBO) and BAT algorithms (BA), Geocarto International, 34(11), 1252-1272. DOI: 10.1080/10106049.2018.1474276

Amoako, C. and E.F. Boamah (2014). The three-dimensional causes of flooding in Accra, Ghana, International Journal of Urban Sustainable Development, http://dx.doi.org/10.1080/19463138.2014.984720, 1-22.

Asumadu-Sarkodie, S., P.A. Owusu, and H.M.P.C. Jayaweera (2015a). Flood risk management in Ghana: A case study in Accra, Advances in Applied Science Research, 6(4), 196-201.

Asumadu-Sarkodie, S., P.A. Owusu, and P. Rufangura (2015b). Impact analysis of flood in Accra, Ghana, Advances in Applied Science Research, 6(9), 53-78.

Bates, P. D., (2012). Integrating remote sensing data with flood inundation models: how far have we got?, Hydrological Processes, 26(16), 2515–2521.

Bui, D.T., N.D. Hoang, F. Martínez-Álvarez, P.T.T. Ngo, P.V. Hoa, T.D. Pham, P. Samui, P., and R. Costache (2020). A novel deep learning neural network approach for predicting flash flood susceptibility: A case study at a high frequency tropical storm area. Science of The Total Environment 701, 134413.

Bui, D.T., M. Panahi, H. Shahabi, V.P. Singh, A. Shirzadi, K. Chapi, K. Khosravi, W. Chen, S. Panahi, S. Li, and B.B. Ahmad (2018a). Novel hybrid evolutionary algorithms for spatial prediction of floods, Scientific Reports, 8(1), 15364, 1-14.

Bui, D.T., K. Khosravi, S. Li, H. Shahabi, M. Panahi, V. Singh, K. Chapi, A. Shirzadi, S. Panahi, W. Chen, and B. Bin Ahmad (2018b). New hybrids of ANFIS with several optimization algorithms for flood susceptibility modeling, Water, 10(9), 1210.

Bui, D.T., P. Tsangaratos, P.T.T. Ngo, T.D. Pham, and B.T. Pham (2019). Flash flood susceptibility modeling using an optimized fuzzy rule-based feature selection technique and tree-based ensemble methods, Science of the Total Environment, 668, 1038-1054.

Chapi, K., V.P. Singh, A. Shirzadi, H. Shahabi, D.T. Bui, B.T. Pham, and K. Khosravi (2017). A novel hybrid artificial intelligence approach for flood susceptibility assessment, Environmental Modelling & Software, 95, 229-245.

Chen, Y.R., C.H. Yeh, and B. Yu (2011). Integrated application of the analytic hierarchy process and the geographic information system for flood risk assessment and flood plain management in Taiwan, Natural Hazards, 59(3), 1261–1276.

Choubin, B., Ehsan Moradi, Mohammad Golshan, Jan Adamowski, Farzaneh Sajedi-Hosseini and Amir Mosavi (2019). An ensemble prediction of flood susceptibility using multivariate discriminant analysis, classification and regression trees, and support vector machines, Science of The Total Environment, 651, Part 2, 2087-2096.

Costache, R., Q.B. Pham, E. Corodescu-Rosca, C. Cimpianu, H. Hong, N.T.T. Linh, C.M. Fai, A.N. Ahmed, M. Vojtek, S.M. Pandhiani, G. Minea, N. Ciobotaru, M.C. Popa, D.C. Diaconu, and B.T. Pham (2020a). Using GIS, remote sensing, and machine learning to highlight the correlation between the land-use/land-cover changes and flash-flood potential, Remote Sensing, 12(1422), 1-31.

Costache, R., Q.B. Pham, E. Sharifi, N.T.T. Linh, S.I. Abba, M. Vojtek, J. Vojtekova, P.T.T. Nhi, and D.N. Khoi

(2020b). Flash-flood susceptibility assessment using multi-criteria decision making and machine learning supported by remote sensing and GIS techniques, Remote Sensing, 12(106), 1-27.

Dano, U.L., A.L. Balogun, A.N. Matori, K.W. Yusouf, I.R. Abubakar, M.A.S. Mohamed, Y.A. Aina, and B. Pradhan (2019). Flood susceptibility mapping using GIS-based analytic network process: A case study of Perlis, Malaysia, Water, 11(615), 1-28.

Das, S. (2018). Geographic Information System and AHP-based flood hazard zonation of Vaitarna basin, Maharashtra, India, Arabian Journal of Geosciences, 11(19), 1-13.

Das, S. (2019). Geospatial mapping of flood susceptibility and hydro-geomorphic response to the floods in Ulhas basin, India, Remote Sensing Applications: Society and Environment, 14, 60–74.

Dugarsuren, N., C. Lin, and K. Tsogt (2011). Landcover change detection in Mongolia in last decade using MODIS imagery, 32nd Asian Conference on Remote Sensing 2011, ACRS 2011. 4.

Fazlollahtabar, H., H. Eslami, and H. Salmani (2009). Designing a fuzzy expert system to evaluate alternatives in fuzzy analytic hierarchy process, Journal of Software Engineering and Applications, 3, 409-418, doi:10.4236/jsea.2010.34046

Fekete, A. (2009). Validation of a social vulnerability index in context to river-floods in Germany, Natural Hazards and Earth System Sciences, 9(2), 393–403.

Firoozi, M.A., M. Goodarzi, and R. Shirali (2017). Assessment and potential survey of lands in Khuzestan Province using the Buckley Geometric Mean Model and Geographic Information System (GIS), Open Journal of Geology, 7, 234-241.

Gyekye, K. A. (2011). Geomorphic assessment of flood within the Urban Environment of Gbawe-Mallam, Accra, Ghana Journal of Geography, 3, 199-229.

Janizadeh, S., M. Avand, A. Jaafari, T.V. Phong, M. Bayat, E. Ahmadisharaf, I. Prakash, B.T. Pham, and S. Lee (2019). Prediction success of machine learning methods for flash flood susceptibility mapping in the Tafresh Watershed, Iran, Sustainability, 11(5426), 1-19.

Kabanda, G., (2019). A Bayesian network model for a Zimbabwean cyber security system, Oriental Journal of Computer Science and Technology, 12(3), 27-30.

Karley, N.K. (2009). Flooding and physical planning in urban areas in West Africa: Situational analysis of Accra, Ghana, Theoretical and Empirical Researches in Urban Management, 3(13), 25-41.

Kazakis, N., I. Kougias and T. Patsialis (2015). Assessment of flood hazard areas at a regional scale using an index-based approach and Analytical Hierarchy Process: application in Rhodope-Evros region, Greece, Science of The Total Environment, 538, 555–563.

Khosravi, K., B.T. Pham, K. Chapi, A. Shirzadi, H. Shahabi, I. Revhaug, I. Prakash, and D.T. Bui (2018). A comparative assessment of decision trees algorithms for flash flood susceptibility modeling at Haraz watershed, northern Iran, Science of The Total Environment, 627, 744–755.

Kia, M.B., S. Pirasteh, B. Pradhan, A.R. Mahmud, W.N.A. Sulaiman, and A. Moradi (2012). An artificial neural network model for flood simulation using GIS: Johor River Basin, Malaysia, Environmental Earth Sciences, 67(1), 251–264.

Kim, S., H. Lee, and Y. Lin (2019). Geometric mean block matrices, Linear Algebra and its Applications, 575, 299-313, https://doi.org/10.1016/j.laa.2019.04.008.

Kornejady, A., K. Heidari, and M. Nakhavali (2015). Assessment of landslide susceptibility, semi-quantitative risk and management in the Ilam dam basin, Ilam, Iran, Environmental Resources Research, 3(1), 85–109.

Kornejady, A., H. Kohzad, M. Sarparast, G. Khosravi, and M. Mombeini (2014). Performance assessment of two “LNRF” and “AHP-area density” models in landslide susceptibility zonation, Journal of Life Science and Biomedicine, 4(3), 169–176.

Kwang, C., and E.M. Osei Jnr (2017). Accra flood modelling through application of Geographic Information Systems (GIS), remote sensing techniques and analytical hierarchy process, Journal of Remote Sensing & GIS, 6(1), 1-6.

Larbi, E.K., C.B. Boye, and M.S. Peprah (2018). A GIS approach in optimal route selection in the mining communities using the analytical hierarchy process and the least cost path analysis, 5th UMaT Biennial International Mining and Mineral Conference, pp. GLM 50-62.

Lee M.J., J.E. Kang and S. Jeon (2012). Application of frequency ratio model and validation for predictive flooded area susceptibility mapping using GIS, In: IEEE International Geoscience and Remote Sensing Symposium (IGARSS), Munich, pp. 895–898.

Liu, F., G. Aiwu, V. Lukovac and M. Vukic (2018). A multicriteria model for the selection of the transport service provider: a single valued neutrosophic DEMATEL multicriteria model. Decision Making: Applications in Management and Engineering, 1, 121–130.

Mensah, H., and D.K. Ahadzie (2020). Causes, impacts and coping strategies of floods in Ghana: A systematic review, SN Applied Sciences, A Springer Nature Journal, 2(792), 1-13.

Meshram, S.G., E. Alvandi, V.P. Singh, and C. Meshram (2019). Comparison of AHP and Fuzzy AHP models for prioritization of watersheds, Soft Computing, 23, 13615–13625.

Moghadam, S.H., R. Valavi, H. Shahabi, K. Chapi, and A. Shirzadi (2018). Novel forecasting approaches using combination of machine learning and statistical models for flood susceptibility mapping, Journal of Environmental Management, 217, 1–11.

Mojaddadi, H., B. Pradhan, H. Nampak, N. Ahmad, and A. Halim bin Ghazali (2017). Ensemble machine –learning based geospatial approach for flood risk assessment using multi-sensor remote sensing data and GIS, Geomatics, Natural Hazards and Risk. doi: https://dx.doi.org/10.1080/19475705.2017.1294113.

Nikoo, M., F. Ramezani, M. Hadzima-Nyarko, E.K. Nyarko, and M. Nikoo (2016). Flood routing modeling with neural network optimized by social-based algorithm, Natural Hazards, 82(1), 1–24.

Nyarko, B.K. (2000). Flood risk zoning of Ghana: Accra experience, International Archives of Photogrammetry and Remote Sensing, XXXIII(B7), 1039-1050.

Okyere, C.Y., Y. Yacouba, and D. Gilgenbach (2013). The problem of annual occurrences of floods in Accra: An integration of hydrological, economic, and political perspectives, Theoretical and Empirical Researches in Urban Management, 8(2), 45-79.

Ozdagoglu, A., and G. Ozdagoglu (2007). Comparison of AHP and Fuzzy AHP for the multi-criteria decision-making processes with linguistic evaluations, Istanbul Ticaret Universitesi, 6(1), 65-85.

Peprah, M.S., C.B. Boye, E.K. Larbi, and P. Opoku Appau (2018). Suitability analysis for siting oil and gas filling stations using multi-criteria decision analysis and GIS approach – A case study in Tarkwa and its environs, Journal of Geomatics, 12(2), 158-166.

Pierdicca N., L. Pulvirenti, M. Chini, L. Guerriero and P. Ferrazzoli (2010). A fuzzy-logic-based approach for flood detection from Cosmo-Sky Med data, In: Geoscience and Remote Sensing Symposium (IGARSS), 2010 IEEE International, pp. 4796–4798.

Pradhan, B. (2009). Flood susceptible mapping and risk area delineation using logistic regression, GIS and remote sensing, Journal of Spatial Hydrology, 9(2), 1–18.

Rahmati, O., H.R. Pourghasemi, and H. Zeinivand (2015). Flood Susceptibility Mapping Using Frequency Ratio and Weights-of-Evidence Models in the Golastan Province, Iran, Geocarto International, DOI: 10.1080/10106049.2015.1041559, 1-46.

Rahmati, O., H.R. Pourghasemi, and H. Zeinivand (2016a). Flood susceptibility mapping using frequency ratio and weights-of-evidence models in the Golestan Province, Iran, Geocarto International, 31(1), 42–70.

Rahmati, O., H. Zeinivand, and M. Besharat (2016b). Flood hazard zoning in Yasooj region, Iran, using GIS and multi-criteria decision analysis, Geomatics, Natural Hazards and Risk, 7(3), 1000–1017.

Requejo-Castro, D., R. Gine-Garriga, and A. Perez-Foguet (2019). Bayesian network modelling of hierarchical composite indicators, Science of The Total Environment, 668, 936-946. https://doi.org/10.1016/j.scitotenv.2019.02.282

Rizeei, H.M., B. Pradhan, and M.A. Saharkhiz (2018). An integrated fluvial and flash pluvial model using 2D high-resolution sub-grid and particle swarm optimization-based random forest approaches in GIS, Complex and Intelligent Systems, 5, 283-302.

Santos, P.P., E. Reis, S. Pereira, and M. Santos (2019). A flood susceptibility model at the national scale based on multicriteria analysis, Science of The Total Environment, 667, 325–337.

Sarhadi, A., S. Soltani, and R. Modarres (2012). Probabilistic flood inundation mapping of ungauged rivers: linking GIS techniques and frequency analysis, Journal of Hydrology, 458, 68–86.

Sedki, K., V. Delcroix, F. Lepoutre, E. Adam, A. Maquinghen-Godillon, and I. Ville (2015). Bayesian network model for decision problems, Intelligent Information Systems, 5, 285-298.

Sharma, L.K., S. Kanga, S. Nathawat, S. Sinha, and P.C. Pandey (2012). Fuzzy Ahp for forest fire risk modelling, Disaster Prevention and Management, 21(2), 160-171. doi: 10.1108/09653661211219964

Tang, X., J. Li, M. Liu, W. Liu, and H. Hong, H. (2020a). Flood susceptibility assessment based on a novel random naïve bayes method: A comparison between different factor discretization methods, Catena, 190(104536), 1-15.

Tang, X., J. Li, W. Liu, and H. Hong (2020b). Flood susceptibility assessment based on a novel random naïve bayes method: A comparison between different factor discretization methods, National Foundation Science of China doi: 10.1016/.catena.2020.104536

Tehrany, M.S., B. Pradhan, and M.N. Jebur (2013). Spatial prediction of flood susceptible areas using rule-based Decision Tree (DT) and a novel ensemble bivariate and multivariate statistical models in GIS, Journal of Hydrology, 504, 69–79.

Tehrany, M.S., M.J. Lee, B. Pradhan, M.N. Jebur, and S. Lee (2014a). Flood susceptibility mapping using integrated bivariate and multivariate statistical models, Environmental Earth Sciences, 72, 4001–4015.

Tehrany, M.S., B. Pradhan, and M.N. Jebur (2014b). Flood susceptibility mapping using a novel ensemble weights-of-evidence and support vector machine models in GIS, Journal of Hydrology, 512, 332–343.

Tehrany, M.S., B. Pradhan, and M.N. Jebur (2015a). Flood susceptibility analysis and its verification using a novel ensemble support vector machine and frequency ratio method, Stochastic Environmental Research and Risk Assessment, 29, 1149–1165.

Tehrany, M.S., B. Pradhan, S. Mansor, and N. Ahmad (2015b). Flood susceptibility assessment using GIS-based support vector machine model with diff erent kernel types, Catena, 125, 91–101.

Ullah, K., and J. Zhang (2020). GIS-based flood hazard mapping using relative frequency ratio method: A case study of Panjkora river basin, Eastern Hindu Kush, Pakistan, PLoS ONE, 15(3), 1-18.

Wanders, N., D. Karssenberg, A.D. Roo, S. De Jong, and M. Bierkens (2014). The suitability of remotely sensed soil moisture for improving operational flood forecasting, Hydrology and Earth System Sciences Discussions, 18(6), 2343–2357.

Wang, Y., Z. Fang, and H. Hong (2019a). Comparison of convolutional neural networks for landslide susceptibility mapping in Yanshan County China, Science of The Total Environment, 666, 975-993.

Wang, Y., Hong, Haoyuan, Chen, Wei, Li, Shaojun, Pamucar, Dragan, Gigovic, Ljubomir, Drobnjak, Siniša, Tien Bui, D. and Duan, Hexiang (2019b). A hybrid GIS multi-criteria decision-making method for flood susceptibility mapping at Shangyou, China, Remote Sensing, 11. 62. 10.3390/rs11010062.

Wang, Y., Z. Fang, H. Hong, and L. Peng (2020). Flood susceptibility mapping using convolution neural network frameworks, Journal of Hydrology, 582(124482), 1-16.

Wu, Z., H. Wang, and M. Wu (2019). Assessing urban flood disaster risk using Bayesian network model and GIS applications, Geomatics, Natural Hazards and Risk, 10(1), 2163-2184, doi: 10.1080/19475705.2019.1685010.

Youssef, A. M., B. Pradhan, M.N. Jebur, and H.M. El-Harbi (2015). Landslide susceptibility mapping using ensemble bivariate and multivariate statistical models in Fayfa area, Saudi Arabia, Environ. Earth Sci., 73, 3745–3761.

Zou, Q., J. Zhou, C. Zhou, L. Song, and J. Guo (2013). Comprehensive flood risk assessment based on set pair analysis-variable fuzzy sets model and fuzzy AHP, Stoch. Env Res Risk Assess, 27(2), 525–546.

Cotton crop production estimation using Sentinel 2A MSI data

P.P. Nageswara Rao*, I. Nisarga, P. Srikanth and D. K Prabhuraj
Karnataka State Remote Sensing Applications Centre,
Doora Samvedi Bhavana, Major Sandeep Unnikrishnan Road,
Doddabettahalli, Bengaluru-560097, India
*Email: ppn1953@gmail.com

(Received: May 26, 2020; in final form: August 04, 2020)

Abstract: The study is an attempt to estimate the cotton crop production, at the taluk level, using data from Multi-Spectral Instrument (MSI) onboard Sentinel-2A satellite. The study was carried out in Raichur *taluk*, Raichur district, in the Indian state of Karnataka during the cotton growing season 2018-19. Spectral signatures and temporal profiles of vegetation indices have helped the identification of cotton crop grown under irrigated and rainfed conditions. Supervised digital image classification of MSI data, acquired at the time of flowering and boll development stage (November 2018) of cotton crop, gave an overall classification accuracy of 88.28 % (kappa coefficient 0.878) with MSI band combination of blue (490 nm), green (560 nm), red (665 nm) and near-infrared (842 nm), having 10 meter spatial resolution. An overall accuracy of 89.93 % (kappa 0.894) was obtained using the principal components 1, 2 and 3. The estimated area under irrigated cotton was within 5% relative deviation (RD) and that of rainfed cotton within 3% RD. The temporal profiles of Normalized Difference Vegetation Index (NDVI), Normalized Difference Red Edge (NDRE) index and Red Edge Position (REP) plotted from September 2018 till February 2019 gave sufficient information on the in-season condition of cotton crop. The NDVI and NDRE profiles of irrigated cotton were higher than that of rainfed cotton, indicating their yield potential and crop duration. The REP profile of irrigated cotton moved from shorter wavelengths (730 nm) to longer wavelengths (737nm) as the crop reached flowering stage and then moved towards shorter wavelengths (723 nm) as maturity progressed. While the REP profile of rainfed cotton moved from 727 nm to 730 nm and then shifted towards shorter wavelength (724 nm), as the crop experienced water stress and maturity. Seed cotton yield prediction of irrigated crop was estimated using season's peak NDVI ($NDVI_{max}$) and NDVI accumulated during flower bud formation to boll filling ($NDVI_{sum}$), REP and Simplified Canopy Chlorophyll Index (SCCI). Seed cotton yield estimation of rainfed crop was accomplished using the season's $NDVI_{max}$, maximum Normalized Difference Moisture Index ($NDMI_{max}$) and Growing Degree Days (GDDs). Cotton crop yield map, prepared for the study area, showed cotton yields varying from 500 to 1100 kilograms per hectare (kg/ha) of rainfed cotton and 600 to 1600 kg/ha of irrigated cotton.

Keywords: Cotton crop production, Raichur taluk, Sentinel-2A-Multispectral Instrument, Vegetation index profiles, Red edge position, Seed cotton yield rate map.

1. Introduction

Cotton is an important fiber and cash crop of India. It plays a major role in the economy of India by providing basic raw material to cotton textile industry. Cotton crop provides 200 man-days per hectare of employment. As per India Brand Equity Foundation (IBEF), cotton-related industry is the second-largest employer in India after agriculture, providing employment to over 52 million people directly and 68 million indirectly, including unskilled women. In the state of Karnataka, area and production of cotton are experiencing fluctuating trend over the years (Reddy et al., 2013). They analyzed the spatial and temporal variations in cotton yields at district level. Siva Sankar and Naidu (2016) have reported that the frequent droughts and unreliable irrigation water supply are threating cotton production in Karnataka state, where the coefficient of variation (CV) is as high as 20% in area, 47% in production and 35% in productivity. These studies clearly show that for taking appropriate decisions related to farmers' welfare like crop insurance, credit and subsidy that are dependent on crop area and yield estimates, a better information system than the conventional method of condition assessment and production estimation of cotton crop is needed. Another major worry for the cotton growers is the serious pest infestation by pink boll worm and white fly. One of the methods of controlling the cotton crop pests is to cut off the food supply to the larval population of the insect pests by terminating the crop by December or at least by January. This calls for scientific methods of determining spatial and temporal distribution and continuous monitoring of changing scenarios of cotton crop to ensure that the farmers comply with the advisory services.

Estimates of cotton crop production are needed much before harvest to decide the exportable surplus and for advising the cotton growers on the choice of crop types every season. Such information can benefit several stakeholders including farmers and officials of the government dealing with policies and support services. Information on cotton cultivation is also needed by India's National Programme for Organic Production (NPOP). At the national level, Cotton Advisory Board (CAB), Ministry of Textiles prepares the cotton supply and demand scenarios. Cotton Association of India (CAI) provides several services to entire value chain in the cotton trade and textile industry.

At the state level in Karnataka, cotton crop production estimates are generated by the Karnataka State Department of Agriculture (KSDA) and the Directorate of Economics and Statistics (DES). Notwithstanding the several innovations brought in by these organizations, the system is suffering from delays and inaccuracies in the estimation of area, yield and production of cotton crop. In order to overcome such conditions, the governments have initiated several schemes to improve the quality of information by adapting new technologies, improved sampling and data processing techniques. One such major innovation is the applications of geomatics in which satellite remote sensing is one of the major components.

A comprehensive review of development and applications of remote sensing for crop inventory in India is given by Navalgund et al (1991). One of the earliest attempts of using satellite remote sensing for cotton crop acreage estimation has been made by Ajai (1992). This experimental study on cotton crop showed that the data from Linear Imaging Self-Scanning System (LISS)-1 of Indian Remote Sensing Satellite (IRS)-1A can be successfully used for cotton acreage estimation provided the selection of date of satellite pass is optimally chosen. Identification of major crops, including cotton was accomplished using ERS-1 Synthetic Aperture Radar (SAR) data in some parts of Guntur district of Andhra Pradesh (Premlatha and Nageswara Rao, 1994). The change in backscattering coefficient over the growing period of crops was used to identify the crops. Cotton production estimation at district level was attempted by Ray et al (1994, 1999) using a linear time series trend and actual evapo-transpiration (AET)-based model for irrigated cotton and an empirical model relating AET and yield for unirrigated cotton. They had also used the area under NDVI spectral profiles drawn from IRS-1A LISS-1 sensor data for yield estimation.

Several researchers have reported the use of REP as an indicator of crop type, chlorophyll content, severity of stress and stage of maturity (Collins et al 1978., Horler et al. 1983., Curran et al., 1990., Tarpley et al., 2000., Dash and Curran, 2004). Raper and Varco (2015) found strongest wavelength correlations with nitrogen concentration and cotton lint yield near 700 nanometer (nm) spectral band. Ballester et al. (2017) have used the NDRE index and SCCI for assessing the cotton nitrogen status and lint yield prediction using data collected by an unmanned aerial system. Their study shows that NDVI is more sensitive to leaf internal structure and green biomass, whereas NDRE is sensitive to physiological processes like chlorophyll content and Nitrogen uptake.

Recently, Ray et al. (2019) reported that the Mahalanobis National Crop Forecast Centre (MNCFC) in collaboration with Karnataka State Remote Sensing Applications Centre (KSRSAC) and KSDA, has been generating crop estimates for major crops, including cotton, at the district level, for the state of Karnataka under a project called **F**orecasting **A**gricultural output using **S**pace, **A**grometeorology and **L**and-based observations (FASAL). However, these studies have not adequately met the requirements of the Pradhan Mantri Fasal Bima Yojana (PMBFY), wherein the basic insurance unit (IU) is the village panchayat. The revised guidelines of the PMFBY suggested rationalization of the number of crop cutting experiments (CCEs) based on in-season crop condition assessment and pre-harvest yield estimation at taluk / hobli level (sub-district-level administrative units). Unlike other crops, the farmers harvest cotton through several pickings depending on its growth condition. Hence, there is a need for evaluating the utility of better spatial, spectral and temporal resolution remotely-sensed data in generating estimates of cotton crop area, in-season health assessment and yield mapping much before its harvest, at the sub-district level, so that the information thus generated could form the basis for rationalizing the number of CCEs and adjudicating the crop insurance claims.

It is in the above-mentioned context that the present study was taken up. Additional work that has been carried out, over and above that was accomplished in the FASAL project, consists i) *taluk*-level estimation of area and production of irrigated and rainfed cotton before harvest, ii) use of the REP and NDRE indices, in addition to NDVI, for monitoring the growth of irrigated and rainfed cotton, iii) use of new spectral indices like SCCI, NDMI, REP for yield modelling and iv) preparation of cotton yield rate map, at *taluk* / *hobli* level.

2. Materials and methods

2.1 Study area

Raichur *taluk* is one of the five taluks of Raichur district, in the northeastern part of the Karnataka state. It is located at 15^0 33'- $16^0$34' northern latitudes and 76^0 14'- 77^0 36' eastern longitudes. Its total geographical area is 1,56,585 ha. The taluk is bounded by the Krishna river on the north and the Tungabhadra on the south. It has six hoblies (Figure 1). It has medium to deep black soils in the west and red sandy soils in the eastern part of the taluk. As per DES, the net sown area (NSA) is 95,275 ha in which different crops are grown including Paddy (rice) Cotton, Jowar, Maize, Tur, etc. Cotton crop is sown during 1st week of May to 3rd week of July and harvested during December to April. Mainly hybrids and high yielding varieties of cotton are cultivated. Irrigated cotton is grown in the medium to deep black soils and rainfed cotton in the red clay-loam soils. About 45% of cotton grown area in the taluk is irrigated. During the cotton growing period, the average temperature varies between 30° C in June and 23°C in December while the average rainfall ranges from 86 mm in June to 165 mm in September and 13mm in November.

2.2 Data used

Level-1C products of Sentinal-2A MSI data acquired from September 2018 until February 2019 were used in the analysis. These products contain per-pixel level radiometric measurements of top of atmosphere (TOA) reflectance. More details on MSI sensor characteristics can be found online in the Sentinel-2 User Guide at the European Space Agency (ESA) web site. The data from this sensor is freely available and has better spatial and spectral resolution in the visible, near-infrared and shortwave infrared region of the electromagnetic spectrum. The 5-day revisit time of MSI offers better opportunities to acquire cloud-free images for monitoring in-season crop condition and production forecasting well before harvest even during Kharif season.

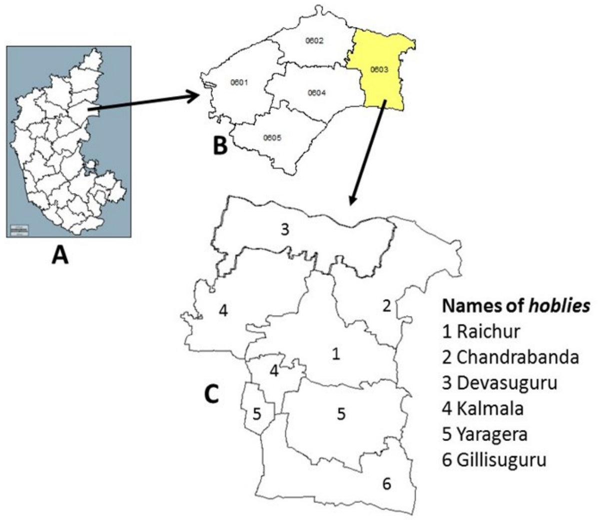

Figure 1: Study area. Karnataka state (A), Raichur district (B), Raichur taluk (C) with hoblies labelled as 1,2,3,4,5,6

Required "ground truth" was collected in December 2018 and February 2019. Another visit was made in April 2019 to meet the farmers and seek their yield reports. Google images of the study area were also used in selecting the sites for "ground truth" collection. These sites were located at the intersection of roads with canals, roads or railway lines. The sites chosen had fairly large fields of cotton at least one-hectare (ha) size, so that they are easy to locate on the ground. Total 74 points were collected, of which 34 from irrigated and 40 from rainfed cotton cultivated areas. Field photographs were also taken using geotagging camera application. Cotton yield (seed cotton) data was collected from several farmers through personal interviews (more details given in section 2.5). The booklets entitled "District at a Glance" were also collected from the Office of the District Statistical Officer, Raichur. Shape files of administrative boundaries of Raichur taluk and its hoblies were collected from KSRSAC, Bengaluru.

2.3 Cotton crop identification and area estimation

At the outset, layer stacking of MSI spectral bands was done in Hexagon Geospatial's ERDAS® IMAGINE environment. Radiometric corrections viz., haze removal and noise reduction, were carried out. The digital images were subjected to geometric correction and transformed to Universal Transverse Mercator (UTM) projection so as to overlay the boundaries of Raichur taluk and its *hoblies* (shape file) and for clipping corresponding images from MSI digital data. The steps involved in cotton crop area estimation are illustrated in figure 2.

All spectral bands of MSI have12 bit radiometric resolution providing greater quantization levels and better information content. Coefficient of variation (CV) expressed in percent was calculated for all the spectral bands to know the measures of dispersion about the mean and the distribution of features / land cover types in the study area (Table 1). The MSI spectral bands having higher CV values were chosen for subsequent image processing and classification. In addition, since the MSI has several spectral bands and some of them are highly correlated, Principal Components Analysis (PCA) was carried out to reduce the redundancy as well as for feature selection based on amount of variance explained by each component (PC). The newly-created PCA images that account for the most variance were then used as inputs, instead of original raw bands, into the digital classification. We strongly believe that the PCA in effect performs feature selection and reduces the dimensionality of the dataset.

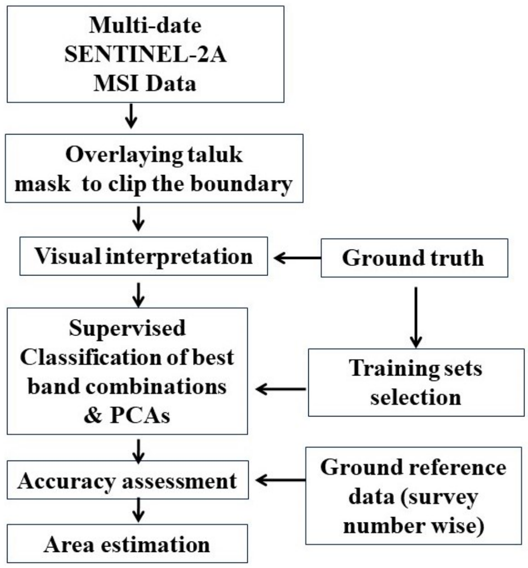

Figure 2: Sequence of steps followed in cotton crop area estimation

Table 1: Coefficient of variation (CV) observed in all the spectral bands of Sentinel-2A MSI Data of the study area

MSI Spectral Bands		Spatial Resolution (meters)	CV (%)
1	443 nm Coastal aerosol	60	83.73
2	490 nm Blue	10	84.71
3	560 nm Green	10	86.83
4	665 nm Red	10	93.42
5	705 nm VRE 1	20	92.25
6	740 nm VRE 2	20	91.53
7	783 nm VRE 3	20	91.94
8	842 nm NIR	10	91.95
8A	865 nm VRE4	20	91.60
9	945 nm WV	60	89.74
10	1375 nm SWIR- cirrus	60	87.20
11	1610 nm SWIR-1	20	95.40
12	2190 nm SWIR-2	20	98.9

As a first step, identification of the cotton crop was attempted through visual interpretation based on tonal and textural changes, spatial patterns, shape, size and association observed on the standard false colour composites (FCCs) of different dates. Changes in spectral reflectance (average values of several samples) of cotton and associated crops in the month of November (Figure 3) and that of irrigated and rainfed cotton during September to February 2018 were also studied (as discussed later in section 3.1, figure 6) to understand the subtle differences in their growth.

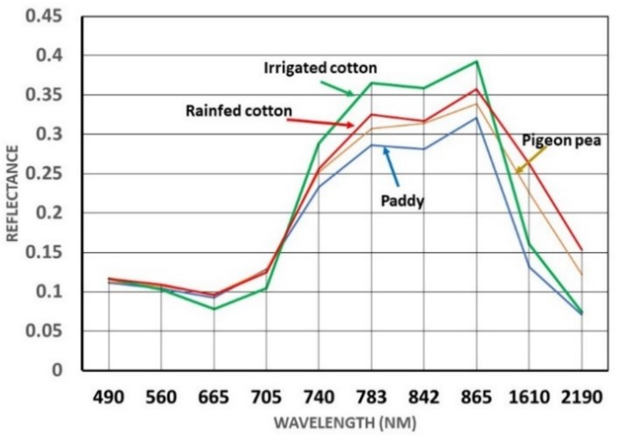

Figure 3: Spectral reflectance of cotton and two associated crops in the study area in the month of November 2018

In addition, we calculated many spectral indices as shown below and the NDVI change over time graphically presented was also used to identify the nature of crop cover types.

NDVI = (MSI 8 – MSI 4) / (MSI 8+ MSI 4)

Where, MSI 8 refers to DN values of Near Infrared (842 nm) and MSI 4 is DN values of red band (665nm).

NDRE= (MSI 8 – MSI 5) / (MSI 8+MSI 5)

Where, MSI 5 represents the DN values of vegetation red edge band (705 nm).

NDMI = (MSI 8 – MSI 11) / MSI 8 + MSI 11)

Where, MSI 11 is the DN values of shortwave infrared band (1610 nm).

$REP = 700 + 40 (\rho_{(red\ edge)} - \rho_{(705\ nm)}) / \rho_{(740\ nm)} - \rho_{(705\ nm)}$

Where, $\rho_{(red\ edge)} = \rho_{(665\ nm)} + \rho_{(783\ nm)} / 2$

The symbol ρ represent the DN values observed in the respective wavelengths given in the formula.

SCCI = NDRE / NDVI

Where, NDRE is the Normalized Difference Red Edge index and NDVI is the Normalized Difference Vegetation Index.

This was followed by digital image analysis using the best set of spectral band combinations and PCs as input to the supervised image classification adopting maximum likelihood algorithm. Irrigated and rainfed cotton crop areas were estimated by multiplying the number of pixels classified as cotton with the size of the pixel (10*10 meter) and expressed in hectares (ha).

2.4 Cotton crop growth monitoring

The procedure followed for cotton crop growth monitoring is presented in figure 4. NDVI and NDRE profile parameters like height of the profile, date on which the profile reached the maximum and width of the profiles of both irrigated and rainfed cotton were recorded for monitoring the condition of cotton crop and for yield prediction (discussed subsequently). In addition, REP was generated as per the methodology reviewed by Framton et al (2013) and SCCI as per Raper and Varco (2015).

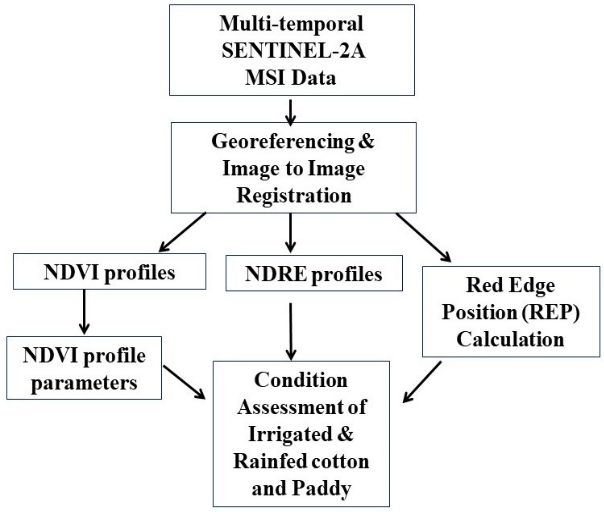

Figure 4: Sequence of steps followed in cotton crop growth monitoring

2.5 Seed cotton yield estimation

The procedure followed for estimating seed cotton yield (locally called Kapas) is schematically shown in figure 5. The NDVI statistics, viz., $NDVI_{max}$, $NDVI_{sum}$ extracted from the NDVI temporal profiles, REP index and SCCI were used in irrigated cotton crop yield modeling.

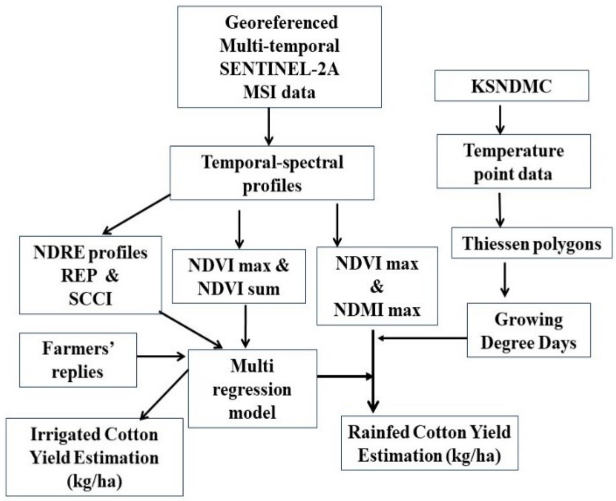

Figure 5: Sequence of steps followed in cotton crop yield estimation

For rainfed cotton yield estimation, $NDMI_{max}$ and $NDVI_{max}$ values were used. In addition, GDDs have been used for assessing the growth of only rainfed cotton, but not irrigated cotton. For calculating GDD, daily temperature point data collected from Karnataka State Natural Disasters Monitoring Centre (KSNDMC) was interpolated using. Thiessen polygons technique in ArcGIS environment so that the point temperature data relates to cotton field polygons. Using this interpolated daily temperature data, GDDs were generated as the accumulation of daily average temperature above a 15.6° C threshold for the period mid July 2018 to end February 2019. Simple regression and correlation were carried out between cotton yields reported by farmers and remotely-sensed indices and GDDs.

Collection of famers' reported yield data: There are about 17000 farmers cultivating cotton in the taluk. We have chosen 10% of them (1700) as our sample to seek their replies, of which 600 are irrigated cotton farmers and the rest 1100 are rainfed cotton growers. Survey numbers of the large cotton fields (at least not less than one-hectare), their GPS coordinates, survey numbers and names of farmers were noted in the spread sheets (MS Excel). This criterion of field size reduced the sample to less than 1% of the total cotton-cultivating farmers. Personal interviews were conducted by visiting the farmers' houses. The farmers reported their seed cotton harvested by them in quintals from their respective farm sizes. Their reports have been normalized to kg/ha. Necessary corrections were applied to the yield figures (seed cotton) reported by farmers to adjust for dried bur, leaf bits and moisture. Thus, the weight of cleaned and dry seed cotton is only 60% of the yield reported by the farmers.

2.6 Seed cotton yield rate map preparation

Cotton crop yield rate map was prepared for the study area by reclassifying the entire classified output pixels by giving 1 to cotton and 0 for all other crops. Then value of vegetation indices of each pixel of cotton was replaced with predicted yield value using spatial analyst and raster calculator tool in ARC MAP. The map thus prepared showed seed cotton yield in kg/ha.

2.7 Accuracy assessment

Identification accuracy of crop pixels labelled as cotton through digital classification was carried out with the help of ground truth samples collected at 74 specific x, y locations of cotton crop (mostly road and canal intersections) using a smart phone with an inbuilt Global Positioning System (GPS), three times during the growth cycle of cotton., twice before and once after the classification. These samples were divided into 39 training and 35 test samples. An error matrix was created between the digital classified output and ground reference data (test samples). The diagonal of the matrix gave the number of pixels that were assigned to the correct class. The sub-routine available in ERDAS® IMAGINE was used to know how well the image was classified, to characterize errors, and the accuracy of estimates derived from it. Overall classification accuracy (OCA) expressed in percentage and Kappa coefficient were generated as per Congalton and Green (1999). The Kappa coefficient is measure of agreement between the two sources of data. Relative deviation (RD), of area and production estimates generated using November 2018 data, from that of Karnataka State DES statistics for the year 2018-19, was also calculated at only taluk level, because DES estimates at hobli-level were not available by then.

3. Results and discussion

3.1 Cotton crop area estimation at taluk level

The best spectral bands, having CV greater than 90%, were found out to be red, vegetation red edge 1, 2, 3, near infrared (NIR), vegetation red edge 4 and SWIR-1 and SWIR-2 (refer again table 1). *G*raphical representation of spectral reflectance plotted against the spectral bands of MSI (see figure 3 above) showed that there is a fairly good separability of the cover types in red (band 4), vegetation red edge (bands 5, 6, 7) and near-infrared (band 8) and better separability in vegetation red edge-4 (band 8A). It is interesting to see good separability in the short-wave-infrared (SWIR) bands (1610 and 2190 nm). It is very clear that the reflectance from cotton crop types is higher than paddy and Pigeon pea in the near-infrared and vegetation red edge-4 regions (bands 8 and 8A) indicating more above ground green biomass. Whereas in the SWIR region, the reflectance from irrigated cotton and paddy is much less than Pigeon pea and rainfed cotton indicating that these latter crops have less leaf water content. Spectral reflectance of irrigated and rain fed cotton crops (Figure 6) during the study period showed distinct reflectance in the month of November. Irrigated cotton clearly showed the pigment absorption in the visible region, i.e., in the spectral bands 2, 3, 4 and 5 of MSI, followed by dramatic rise in reflectance in the red edge and near-infrared regions (bands 6,7, 8 and 8A).

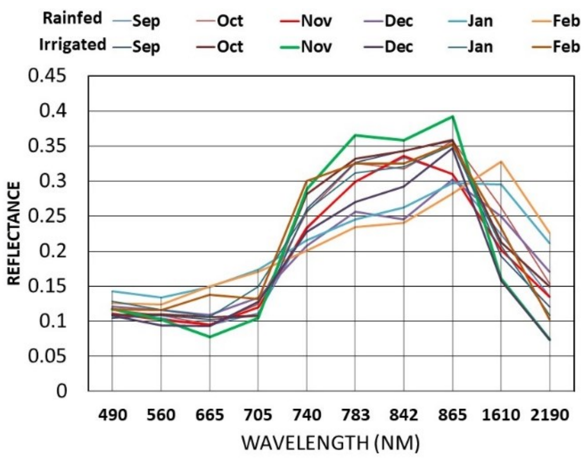

Figure 6: Change in spectral response of irrigated and rainfed cotton during September 2018 till February 2019

Irrigated cotton showed very clear dip indicating leaf-water absorption at 1610 and 2190 nm. Irrigated cotton canopy reflectance reached its peak in November 2018 in the 8A band (865 nm) and maximum absorption in red band 4 (665 nm). Canopy reflectance of rainfed cotton also showed more or less similar spectral response, but with noticeable differences in the pigment absorption, red edge, NIR reflectance and leaf water absorption in the SWIR band. As the crop season was advancing from September to February, the rainfed cotton showed reduction in pigment absorption at 665 and 705 nm, NIR reflectance (783 nm) and leaf water absorption at 1610 and 2190 nm especially during January and February months of the year 2019.

Rainfed cotton showed peak reflectance in the 7th band (783 nm) in October 2018 followed by another peak in November 2018 in 8A band (865 nm). It is interesting to see a subtle dip in the reflectance at 842 nm (MSI 8 band), a near-infrared band, as a result of flowering and boll opening occurring in both irrigated and rainfed cotton crops. Significant rise in the SWIR-1 (1610 nm) band reflectance from rainfed crop in January and February is indicative of drying of the crop. It is this phenomenon that encouraged us to use NDMI as one of the variables for yield modeling of rainfed cotton.

Careful examination of the statistics (refer table 1 again) show that spectral bands 4 (red), 5 (vegetation red edge), 8 (NIR), 11(SWIR-1) and 12 (SWIR-2) have higher CV% than other bands, indicating more information content. The six sets of band combinations chosen for running the supervised image classification, the OCA and kappa coefficient are given in table 2.

Table 2: Overall classification accuracy (OCA) and Kappa coefficient (K) obtained with different best band combinations of Sentinel-2A MSI Data

Combinations of MSI best Spectral Bands				OCA (%)	K
B	G	R	NIR	88.28	0.878
G	R	NIR	RE4	85.14	0.842
R	RE2	NIR	SW-1	76.33	0.753
RE3	NIR	SW-1	SW-2	74.68	0.738
R	RE1	NIR	SW-1	77.5	0.765
R	RE3	NIR	SW-2	80.08	0.792

It may be seen that a band combination using blue (B), green (G), red (R), and NIR all having 10 m spatial resolution gave maximum overall accuracy of 88.28 % at kappa coefficient (K) 0.878. The second-best band combination (G, R, NIR, and vegetation red edge 4 (RE-4)) gave an overall accuracy of 85.14 at K 0.842. The accuracy obtained using the third-best band combination with R, vegetation red edge 3, NIR and short-wave infrared band (SW-2) is 80.08% at K 0.792. These results are in agreement with Immitzer et al (2016) who reported their first experience with Sentinel-2 data in classifying the crop and tree species in Central Europe.

The combination of PCs 1, 2, 3 gave better accuracy of 89.93% at K 0.894 than other PC combinations (Table 3). Area estimates and relative deviation (RD) of irrigated and rainfed cotton crop for Raichur taluk are given in table 4. It may be seen that the RD values between cotton area estimates made with MSI and that of DES are within 5%. This may be due to the optimal spatial and spectral resolution of the MSI sensor that are adequate for the cotton crop field sizes and associated cover types in the study area. It is also well known that during the recent years, the crop statistics generated by primary workers and aggregated at district level by Karnataka state DES have better reliability because of several innovations brought into their data collection, compilation and reporting. Area estimates at hobli-level are presented in table 5. Comparison of MSI-data based estimates with the DES statistics at hobli-level was not done because of unavailability of data from the conventional system by that time. Several attempts made subsequently seeking data from DES went in vain.

Table 3: Overall classification accuracy (OCA) and Kappa coefficient (K) obtained with different combination of Principal Components (PC) generated with MSI Data

Components	OCA (%)	K
PC 123	89.93	0.894
PC 234	79.75	0.789
PC 124	87.77	0.872

Table 4: Comparison of cotton crop area estimates made at Taluk level using MSI best band combination and PC 1,2, and 3 with DES statistics

Cotton types	Estimated Cotton Area (Ha)					
	MSI	DES	RD	PC	DES	RD
Irrigated	1235	1176	4.7	1223	1176	3.83
Rainfed	1444	1406	2.6	1403	1406	0.23
Total	2679	2582	3.6	2626	2582	1.66

RD % = {(MSI-DES) / MSI)} x 100

Table 5: Hobli wise area estimates under irrigated and rainfed cotton in Raichur taluk using MSI best band combination and PC 1, 2, & 3 composites

Hoblie Names	Estimated Cotton Area (Ha)			
	MSI best band combination		PC 1, 2, & 3	
	Irrigated	Rainfed	Irrigated	Rainfed
C. banda	175.57	408.65	198.77	395.48
Devasugur	288.85	432.12	296.87	415.97
Gillisuguru	232.30	267.13	208.37	262.18
Kalmala	237.72	43.77	198.66	52.98
Raichur	147.26	166.56	135.55	156.06
Yaragera	154.20	125.77	186.70	120.06

3.2 Cotton crop growth assessment at taluk level

The NDVI profiles (Figure 7) irrigated cotton reached its NDVI maximum (0.7) in the month of November and rainfed cotton attained its maximum NDVI (0.62) in October 2018. The NDVI profile of paddy crop reached its maximum (0.6) in October. There is an overlap of NDVI maximum values of rainfed cotton and paddy in October but rapid decline of paddy crop NDVI in subsequent months made its identification easy. It is very clear that the irrigated cotton NDVI profile is higher than that of rainfed cotton, indicating their yield potential and crop duration.

The NDRE profiles of cotton and paddy crops are shown in figure 8. The NDRE profile of irrigated cotton was maximum (0.65) in November and reduced gradually., that of rainfed cotton reached its maximum (0.61) in October and remained lower than irrigated cotton most of the time. The profile of paddy reached its maximum (0.68) in

October and gradually reducing as the crop matured, reaching lowest value of 0.2 in December. Its profile started rising then onwards showing the presence of second crop.

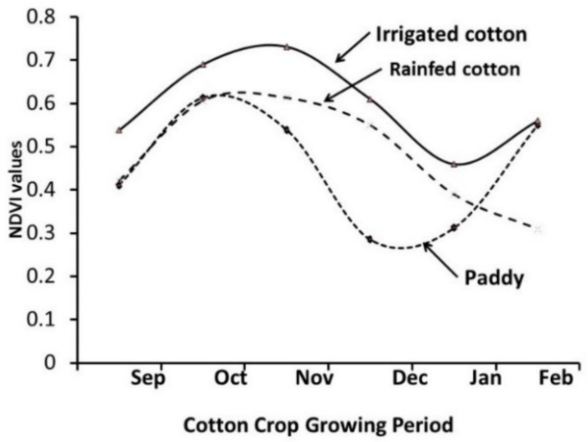

Figure 7: Spectral-temporal profiles of Normalized Difference Vegetation Index (NDVI) of cotton and paddy crops

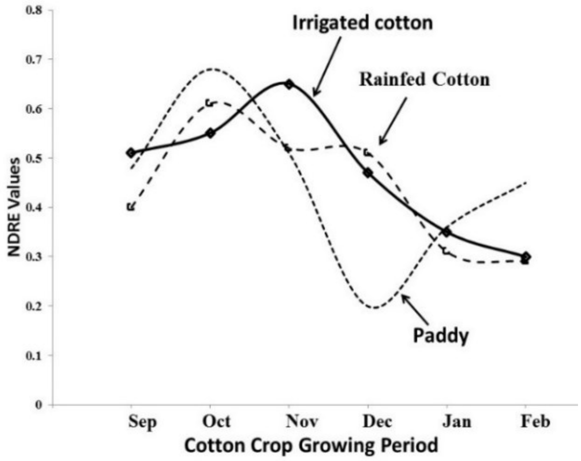

Figure 8: Spectral-temporal profiles of Normalized Difference Red Edge (NDRE) of cotton and paddy crops

The study showed that the NDVI and NDRE indices are highly correlated. The observed coefficient of determination (r^2) between NDVI and NDRE of irrigated cotton was 0.7019 and that of between NDVI and NDRE of rainfed cotton 0.7004. However, the temporal variability shown by NDRE profiles of rainfed cotton is more dynamic than NDVI owing to its better sensitivity to crop growth during later stages of maturity. The REP profiles of irrigated and rainfed cotton crops are very distinct (Figure 9). The REP profile of irrigated cotton moved from shorter wavelengths (730 nm) to longer wavelengths (737nm) as the crop reached flowering stage and then moved towards shorter wavelengths (723 nm) as maturity progressed. While the REP profile of rainfed cotton moved from 727 nm to 730 nm and then shifted towards shorter wavelength (724 nm), as the crop experienced water stress and senescence. These observations are in agreement with several researchers who reported that in comparison to broad band reflectance, the red edge measurements are very valuable for assessment of crop condition and early stress detection (Gao, 1996., Schlemmer et al, 2005., Immitzer et al, 2016., Song et al, 2017., Zheng et al, 2018).

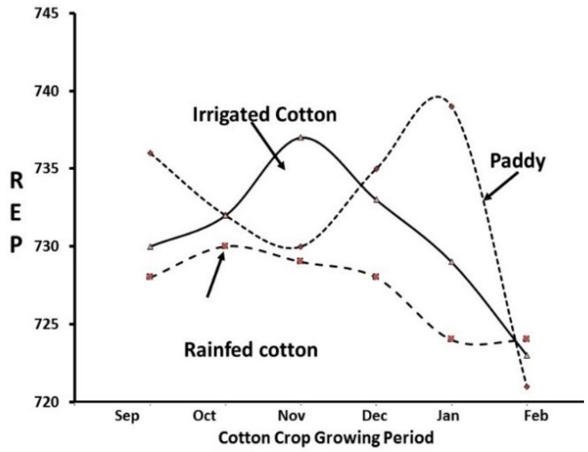

Figure 9: Change in red edge position (REP) of cotton and paddy crops during September 2018 through February 2019

3.3 Cotton crop yield estimation

The study showed that there is a positive correlation between spectral indices and cotton crop yields, as indicated by coefficient of determination (r^2) and F values shown in table 6. It is clear that the relation between rainfed cotton yield and NDMI $_{max}$ is better than that of NDVI $_{max}$ because NDMI responds to crop water stress better than NDVI (Mutanga and Skidmore, 1999). The relation between rainfed cotton yields and GDDs is not as good as the spectral indices. The relationships between irrigated cotton yield with NDVI $_{max}$ is better than NDVI $_{sum}$ and SCCI.

Table 6: Correlation between spectral indices and cotton crop yields

Cotton type	Indices	r^2 values	RMSE (kg/ha)
Rainfed Cotton	NDVI max	0.612	14.00
	NDMI max	0.650	13.90
	SCCI	0.603	18.77
	GDD	0.641	32.70
Irrigated Cotton	NDVI max	0.692	21.32
	NDVI sum	0.586	24.98
	SCCI	0.633	19.88

The scatter plot between observed and predicted yields of irrigated cotton obtained using maximum NDVI is shown in figure 10 and that of rainfed cotton using maximum NDMI in figure 11. It may be noted that the r-squared (r^2) values and root mean square error (RMSE) are confirming that these two spectral indices are fairly good predictors of cotton crop yields.

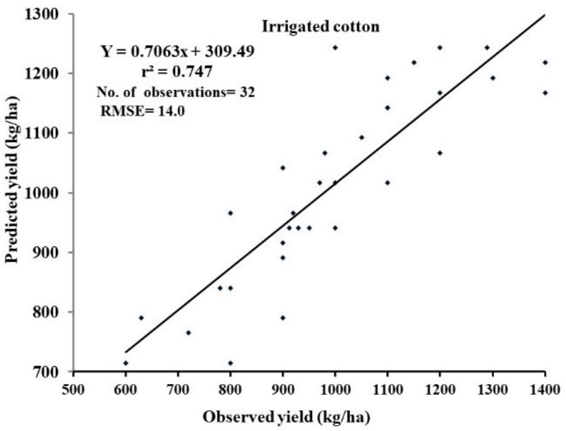

Figure 10: Relationship between observed and predicted yields of irrigated cotton crop using NDVI max

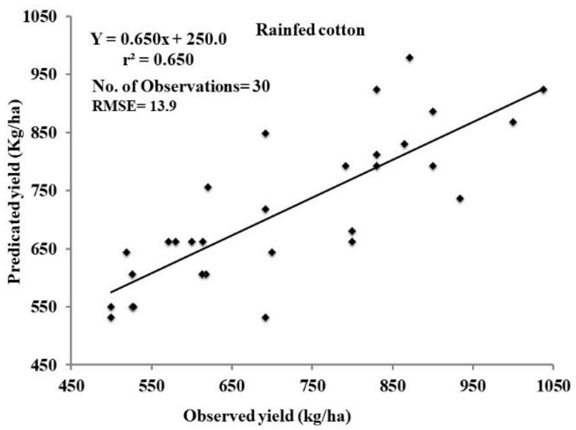

Figure 11: Relationship between observed and predicted yields of rainfed cotton crop using NDMI max

3.4 Cotton yield rate map

Yield rate (kg/ha) map of entire Raichur taluk was prepared, but for want of space, the yield rate map of Gillisuguru hobli only, is shown in figure 12. It was found that in the study area, rainfed cotton yield rates varied from 500 to 1100 kg/ha of seed cotton and 600 to 1600 kg/ha in case of irrigated areas. These variations are expected because of differences in crop management inputs. This spatial yield variability map could be used for identifying the cotton fields that require additional inputs, advising the farmers to practice precision farming and adjudicating the crop insurance claims by them. Cotton crop production estimates made at taluk-level with MSI data and that of DES are shown in table 7 and hobli-wise production estimates are in table 8. It is common to express cotton production in bales when it is in fiber (lint) form. Since our estimates are seed cotton, it is expressed in tons.

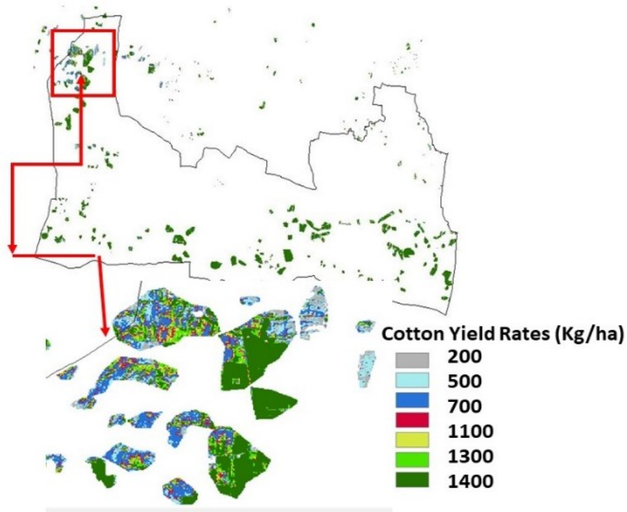

Figure 12: Seed cotton (kapas) yield rate map of Gillisuguru hobli in 2018-19

Table 7: Comparison of cotton crop production estimates at taluk level using best band combinations of MSI and PC 1,2, & 3 with the DES statistics

Cotton type	Estimated Production (Tons)					
	Best band combination			PC 1, 2, & 3		
	MSI	DES	RD	MSI	DES	RD
Irrigated	1308	1245	4.81	1295	1245	3.83
Rainfed	1047	1019	2.62	1017	1019	(-) 0.26
Total	2355	2264	3.84	2312	2264	2.04

Table 8: Hobli wise production estimates under irrigated and rainfed cotton in Raichur taluk using MSI best band combination and PC 1, 2, & 3 composites

Hoblie Names	Estimated cotton production (Tons)			
	Irrigated	Rainfed	Irrigated	Rainfed
C. banda	186	296	210	286
Devasugur	306	313	314	301
Gillisuguru	246	193	221	190
Kalmala	252	317	210	384
Raichur	156	120	143	113
Yaragera	163	911	198	870

4. Conclusions

The study clearly demonstrated that the Sentinel-2A MSI is useful for estimating production of irrigated and rainfed cotton at the taluk and *hobli*-level. The methodology can be extended to major cotton growing areas after understanding the cropping patterns. The yield variability maps have to be carried out at Village Panchayat-level so that the remotely sensed estimates are useful for adjudicating the crop insurance claims. The research at the KSRSAC is progressing towards this goal in collaboration with MNCFC, New Delhi.

Acknowledgements

The authors sincerely thank Director, KSRSAC for providing the laboratory facilities for data processing and for sparing the shape files of the administrative boundaries. Thanks, are also due to Director, KSNDMC for weather data. The help rendered by Shri G N Naveen, Sr. Project Scientist, KSRSAC during data analysis is worth mention here. The cooperation extended by several farmers at many *hoblies* of Raichur taluk, for truthfully stating their seed cotton yields and permitting entry into their fields is thankfully acknowledged. We thank the Copernicus Open Access Hub for allowing free downloading of Sentinel-2A MSI data. Thanks, are also due to two anonymous reviewers for their valuable suggestions.

References

Ajai (1992). Cotton Acreage Estimation and Condition Assessment, in Natural Resource Management – A New Perspective. (R. L. Karale: Editor), Indian Space Research Organisation, Government of India, Bangalore, pp. 267-273.

Ballester, C., J. Hornbuckle, J. Brinkhoff, J. Smith, and W. Quayle (2017). Assessment of In-season Cotton Nitrogen Status and Lint Yield Prediction from Unmanned Aerial System Imagery, Remote Sensing, 9, 1149, doi: 10.3390/rs 111149.

Collins, W (1978). Remote Sensing of Crop Type and Maturity, Photogrammetric Engineering & Remote Sensing, 44 (1), 43-55.

Congalton, R.G. and K. Green (1999). Assessing the Accuracy of Remotely Sensed Data: Principles and Practices. Lewis Publishers, Boca Raton, London and New York.

Curran, P.J., D.L. Dungan and H.L. Gholz (1990). Exploring the relationship between reflectance red edge and chlorophyll content in slash pine, Tree Physiology, 7, 33-48.

Dash, J. and P.J. Curran (2004). The MERIS Terrestrial Chlorophyll Index, International Journal of Remote Sensing, 25 (23), 5403-5413.

Framton, W.J., J.Dash, G. Watmough, and E.J. Milton (2013). Evaluating the capabilities of Sentinel-2 for quantitative estimation of biophysical variables in vegetation. ISPRS Journal of Photogrammetry and Remote Sensing, 82, 83-92.

Gao, B.-C. (1996). NDWI- a normalized difference water index for remote sensing of vegetation liquid water from space. Remote Sensing of Environment, 58 (3), 257-266.

Horler, D.N.H., M. Dockray, J. Barber and A.R. Barringer (1983). Red Edge Measurements for Remotely Sensing Plant Chlorophyll Content, Advances in Space Research, 3, 273-277.

Immitzer, M., F. Vuolo and C. Atzberger (2016). First Experience with Sentinel-2 Data for crop and tree species classification in Central Europe, Remote Sensing, 8, 166, doi:10.3390/rs 8030166.

Mutanga, O. and A. K. Skidmore (1999). Narrow band vegetation indices overcome the saturation problems in biomass estimation, International Journal of Remote Sensing, 25 (19), 3999-4014.

Navalgund R.R., J. S. Parihar, Ajai and P.P. Nageswara Rao (1991). Crop inventory using remotely sensed data. Current Science, 61, 162–171.

Premlatha M and P.P. Nageswara Rao (1994). Crop Acreage Estimation Using ERS-1 SAR data. Journal of Indian Society of Remote Sensing, 22 (3), 39-47.

Raper, T.B. and J.J. Varco (2015). Canopy-scale Wavelength and Vegetation Index Sensitive to Cotton Growth Parameters and Nitrogen Status, Precision Agriculture, 16, 62-76.

Ray, S.S., S.S. Pokharna and Ajai (1994). Cotton Production Estimation using IRS-1B and Meteorological Data, International Journal of Remote Sensing, 15 (5), 1085-1090.

Ray, S.S., S.S. Pokharana and Ajai (1999). Cotton Yield Estimation Using Agrometerological Model and Satellite-Derived Spectral Profile. International Journal of Remote Sensing, 20 (14), 2693-2702.

Ray, S.S., Neethu and S. Mamatha (2019). Cutting-edge technology for crop estimation. Smart Agri Post, 6 (6),16-20.

Reddy, A.R., S. M. Yelekar and I. Agarwal (2013). Cotton Productivity variation in India: An Assessment, Cotton Research Journal, 5 (2), 86-193.

Schlemmer, M.R., D. D. Francis, J.F. Shanahan and J.S. Schepers (2005). Remotely Measuring Chlorophyll Content in Corn Leaves with Differing Nitrogen levels and Relative Water Content, Agronomy J. 97, 106-112.

Siva Sankar, A. and V.B. Naidu (2016). Growth and Instability of Cotton Crop in Major Cotton Growing States in India, Int. J. Advanced Educational Research, 1(5), 15-19.

Song, X., C. Yang, M. Wu, C. Zhao, G. Yang, W.C. Hoffmann and W. Huang (2017). Evaluation of Sentinel-2A Satellite Imagery for Mapping Cotton Root Rot, Remote Sensing, 9 (9), 906, http:// doi.org/10.3390/ rs 9090906.

Tarpley, L., K.R. Reddy and G.F. Sessenrath-Cole (2000). Reflectance Indices with Precision and Accuracy in Predicting Cotton Leaf Nitrogen Concentration, Crop Science, 40, 1814-1819.

Zheng, Q., W. Huang, X. Cui, Y. Shi and L. Liu (2018). New Spectral Index for Detecting Wheat Yellow Rust Using Sentinel-2 Multispectral Imagery, Sensors, 18, 868, doi: 103390/ s 18030868.

Journal of Geomatics Vol. 14, No. 2, October 2020

Study of the dynamics of Manas-Beki river for assessment of erosion in upper Assam using geospatial techniques

Phuntsho Dorji[1*], Dechen Wangmo[1], Ugyen Tshering[1], Gopal Sharma[2] and P.L.N. Raju[2]
[1]University of Petroleum and Energy Studies (UPES), Dehradun- 248001
[2]North Eastern Space Applications Centre (NESAC), Umian-793103
*Email: dphuntsho69@gmail.com

(Received: April 03, 2020; in final form: Oct 14, 2020)

Abstract: The bank line erosion of Manas-Beki river has become a major problem especially for Barpeta and Baksa districts of Assam as the river is characterized by rapid changes in its morphological dynamics. About 75km stretch of Manas-Beki river starting from the foothills of Bhutan has been studied using geospatial techniques. Digital IRS LISS-III data of time frame 2008-2015 has been analysed in GIS environment for identifying erosional and depositional areas along the bank of Manas-Beki river. Sinuosity index, channel length, channel width and plan form index have been studied to understand the erosion and deposition processes that took place over seven years. It is observed that a total area of 22.57 km^2 was eroded and 10.03 km^2 was deposited, indicating dominance of erosion processes with an average of 3.22 km^2/year. Although heavy rainfall, associated flooding, landslides in upper reaches, excessive siltation and braiding channel are primary causes, another possible reason could be sudden flooding due to water release from Kurichu dam in Bhutan during this period. Results of this study provides important information on river dynamics and erosional activity along the bank of Manas-Beki river, which can be utilised for designing and implementation of drainage development programmes and erosion control schemes.

Keywords: Bank line erosion, river dynamics, IRS, LISS-III, GIS, Manas-Beki River

1. Introduction

River bank erosion associated with channel migration is one of the major geological hazard in north-east India causing loss of adjoining valuable land, which could be either agricultural land, forest land, tea plantations or human settlements or associated infrastructure. It is reported that total land loss per year due to erosion of Brahmaputra river is around 80 km^2 /year and bank erosion has wiped out more than 2500 villages and 18 towns including sites of cultural heritage and tea gardens affecting lives of 500,000 people, who are forced to migrate and relocate themselves and are deprived of their basic livelihood (Phukan et al., 2012; Das et al., 2014). Property worth around Rs. 182.24 Crore was damaged as a result of bank erosion (Das et al., 2014; Sayanangshu Modak and Nirmalya Choudhury, 2017). According to Das et al. (2014) "It is observed that after forced human migration due to bank erosion, displaced people face economic insecurity due to loss of agricultural land and become unemployed. The victims also suffer from social insecurity due to deprivation of civic rights, health insecurity due to lack of basic infrastructure, etc. All these insecurities caused by forced displacement lead to deprivation, destitute, fragility and increased vulnerability of the families". Study of erosion-deposition processes around Majuli island, Assam based on study of Survey of India (SOI) topo sheets and Indian Remote Sensing (IRS) satellite imagery spanning the period from 1966-1975 to 2008 in a Geographical Information System (GIS) environment revealed average annual rate of erosion and deposition to be 8.76 km^2/year and 1.87 km^2/year respectively, indicating significant rate of erosion than the deposition (Dutta et al., 2010). Analysis of temporal Landsat data for time frame 1989 to 2017 of the Subansiri river in its highly dynamic and unstable lower 100 km stretch, lying in Assam revealed that about 103 km^2 land area got eroded with an average of 3.68 km^2/year (Bordoloi et al., 2020). Many other previous studies in north-east region of India and parts of Bangladesh have attempted to study bank line erosion (Goswami et al., 1999; Kotoky et al., 2003; Sankhua et al., 2005; Das et al., 2007; Islam, 2009; Sharma et al., 2010; Sarma and Acharjee, 2012; Sarkar et al., 2012; Sinha and Ghosh, 2012; Talukdar, 2012; Khan, 2012; Gogoi and Goswami, 2013; Gogoi and Goswami, 2014; Chakraborty and Mukhopadhyay, 2015; Deka and Talukdar, 2016; Sarmah and Sarma, 2017).

The bank line erosion of Manas-Beki river has become a major problem especially for Barpeta and Baksa districts of Assam as the river is characterized by rapid changes in its morphological dynamics. According to Sayanangshu Modak and Nirmalya Choudhury (2017), "In 2007, alone around 440 hectares of land was eroded and around 76 villages and some 2500 families were affected from the river bank erosion. The total loss of property was around Rs. 33 million". In order to estimate changes subsequent to 2007, the present paper describes the study of Manas-Beki river during the time frame 2008 to 2015. It describes dynamics of river system and channel configuration leading to erosion and deposition. Sinuosity index, channel length, channel width and plan form index have been studied to understand the erosion and deposition processes.

2. Study area

Study area is shown in figure 1. Manas-Beki river (Kurichhu in Bhutan) originates from a Himalayan glacier and the main river and its tributary channels flow south through the plains of Assam (through Baksa and Barpeta districts in north-west, Assam) for about 85km, drain an area of 26,243 square kilometers approximately and meets the Brahmaputra river. Erosion and the recurring floods of characteristically high magnitude by Beki river have been heavily affecting the agricultural lands, crops, cattle and people of Barpeta district of Assam (Deka and Talukdar, 2016). Barpeta district of Assam is mostly affected by erosion and flood, 80 villages are fully affected and some others are partially affected in the district (Khan, 2012). The river channel changes its course due to changes in rainfall pattern, heavy landslide in catchment area causing sudden rise in the silt load, beheading of the one river into another, impact of seismic activity in bed slope etc. Every year very high magnitude flood also causes channel widening, river bank erosion and changes in channel pattern and the changes in the river system bring episodes of changed geomorphic scenario. Temporal change in the behavior of Manas-Beki river system and continuous changing braided behavior of river Brahmaputra cause dynamic changes in the sandbars (Sarmah and Sarma, 2017). Manas-Beki river system dynamics is in terms of bank line, alteration of direction of flow due to neck cut off, widening of channel and progressive shifting of meander bends. Changes in bank line are prevalent throughout the study period but with an increased severity during the last decade (Purkait, 2004).

The river crosses through Barpeta and Baksa districts of north-west Assam in India. The climate is extremely varied, ranging from hot and humid subtropical conditions in the south to cold and dry alpine conditions in the north, heavy rainfall and frequent floods in the region (Goyal, 2014; Jain, 2006).

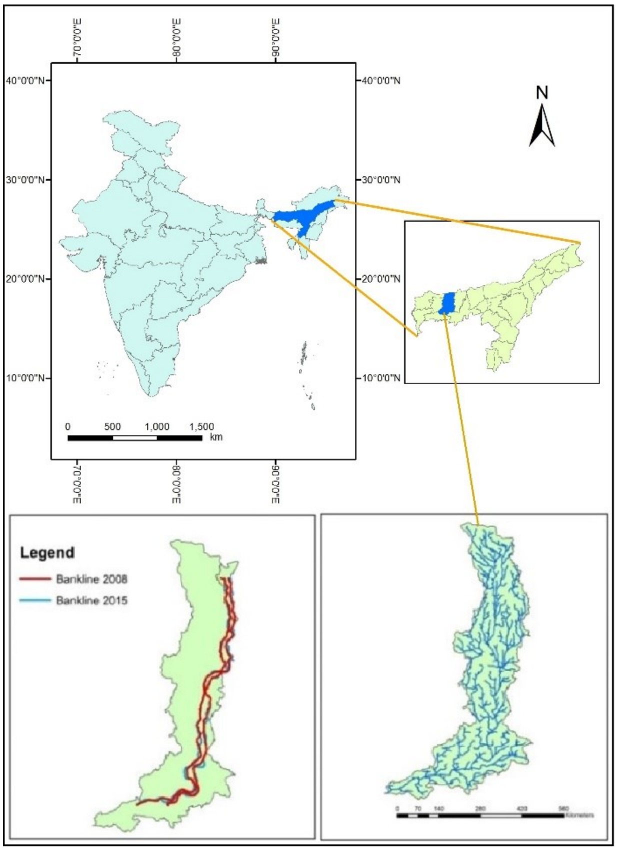

Figure 1: Location map of the study area

3 Material and methods

3.1 Data used

Digital images of the Indian Remote Sensing Satellite (IRS), LISS III sensor, comprising of scenes for the years 2008 (16 October) and 2015 (27 December) were used. The LISS III images are precisely ortho-rectified with the following parameters: Sensor: LISS-III Path: 109 Row: 053 Date of pass: 16Oct08/27Dec15. The other data used in the present study includes Digital Elevation Model (DEM) of Cartosat.

3.2 Bankline erosion

To identify bankline erosion, after due co-registration of LISS-III images, the right and left banks of the river were visually interpreted on screen at 1:25, 000 scale in GIS environment using ERDAS Imagine and ArcMap image processing and GIS software available at NESAC. After overlaying the bank lines of both years, bank lines were visually compared to identify the erosion and deposition sites. To quantitatively calculate the amount of erosion and deposition, the study area was divided into seven reaches. The total area covered by erosion and deposition was calculated using the polygon estimation tool available in GIS, the total area covered by erosion and deposition was calculated. When erosion and deposition occurs, they are accompanied by changes in the width of the channel (Islam, 2009). The shifting of the bank lines indicates the occurrence of erosion and deposition (Clerici and Perego, 2016). The study area was divided into seven equal sections and changes observed along the river banks during the seven years were studied (Figure 2 and Figure 3).

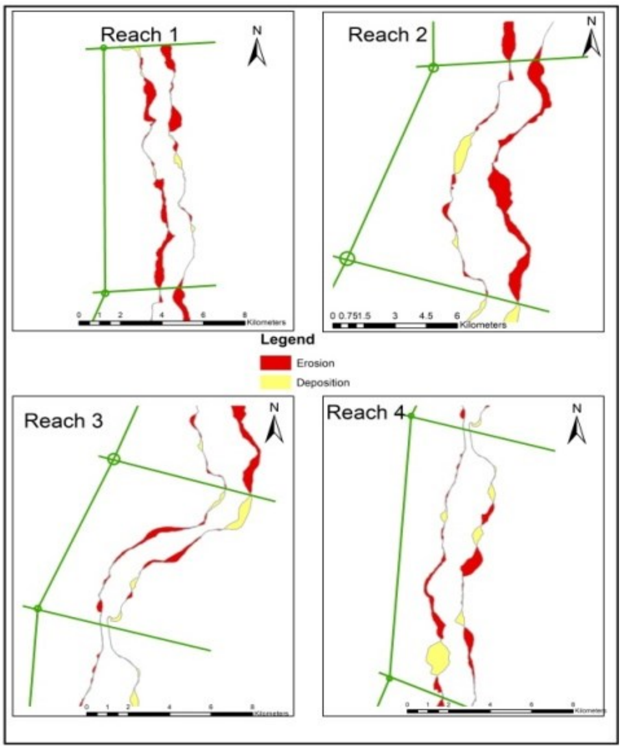

Figure 2: Erosion/deposition (Reach 1 to Reach 4) in various reaches of Manas-Beki River over a period of 7 years (2008-2015)

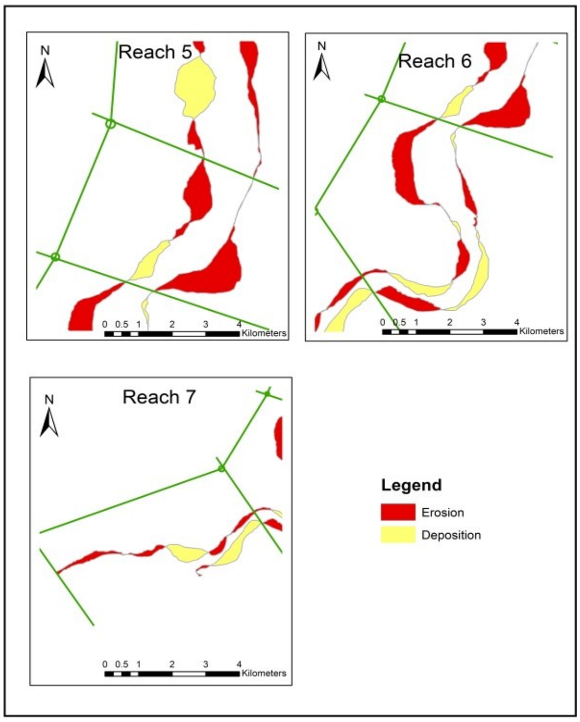

Figure 3: Erosion/deposition (Reach 5 to Reach 7) in various reaches of Manas-Beki River over a period of 7 years (2008-2015)

3.3 Sinuosity index

The curvilinear distance and straight line distance was measured (Sapkale et al., 2016). A python script tool which calculates the ratio between the two was used to find the sinuosity index. Sinuosity index of each reach were calculated and the average indices of the different years (2008 and 2015) were compared.

3.4 Channel Length

The channel lengths were measured using measurement tool available in ARCMAP. Variations observed within the seven years have been quantified.

3.5 Plan Form Index

Plan form index (PFI) reflects the fluvial landform disposition with respect to a given water level and its lower value is indicative of higher degree of braiding was utilized (Figure 4). The expression is formulated as; PFI= (T*100)/(B*N) (Pande and Moharir, 2017). Where, T= Flow top width B= overall width of the river section N= Number of braided channel. For providing a broad range of classification of the braiding phenomenon, the following threshold values for PFI were proposed, highly braided: PFI<4 moderately braided: 19>PFI>4 Low braided: PFI>19

4. Results and discussion

The total amounts of erosion/deposition that took place within seven years in the right and left bank are shown reach wise in table 1. The maximum erosion of 4181050 m^2 took in reach 1 and minimum erosion 1487251m^2 took place in reach 3 as shown in figure 5.

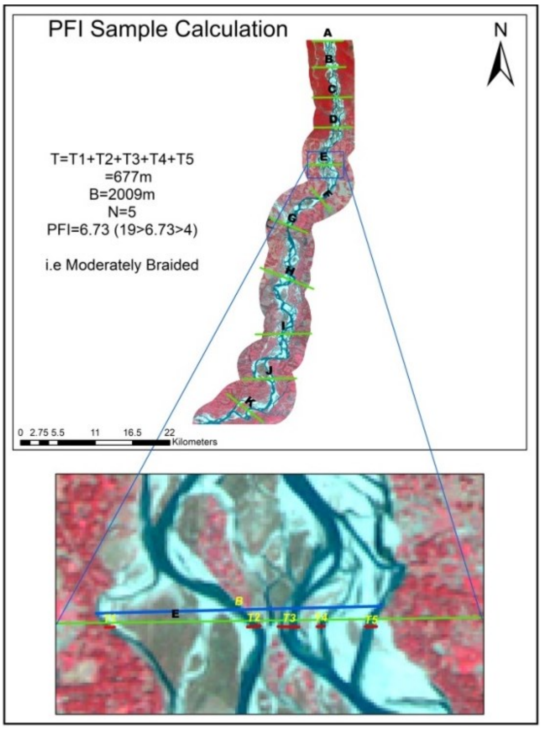

Figure 4: PFI sample calculation

Table 1: Total amount of erosion in left and right bank (2008-2015)

Reach	Left bank erosion(m^2)	Right bank erosion(m^2)	Total Erosion(m^2)
1	2661690	1519360	4181050
2	470142	2957830	3427972
3	918109	569142	1487251
4	1682980	2200210	3883190
5	1156170	1999660	3155830
6	2754500	1360160	4114660
7	2199590	123560	2323150

Likewise, as shown in table 2 maximum deposition of 3139510m^2 took place in reach 7 and minimum deposition of 493815.6 m^2 took place in reach 5. From the year 2008 to 2015 Manas-Beki River has experienced more erosion compared to deposition as clearly seen in figure 5.

Table 2: Total amount of deposition in left and right bank (2008-2015)

Reach	Left bank deposition (m^2)	Right bank deposition (m^2)	Total Deposition (m^2)
1	235573	282409	517982
2	561565	499.676	562064.676
3	153352	837094	990446
4	1783890	867122	2651012
5	490703	3112.6	493815.6
6	747851	932942	1680793
7	1412810	1726700	3139510

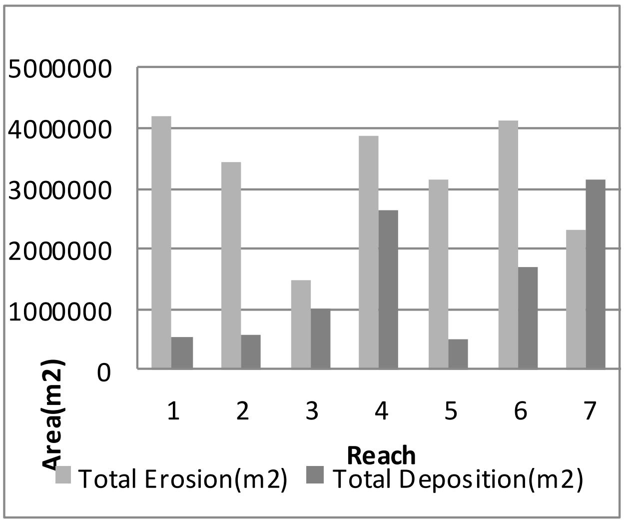

Figure 5: Total erosion and deposition (m^2)

A total area of 22573103m^2 was eroded and 10035623.276m^2 was deposited. The difference given by the erosion and deposition will give the weathered material. Hence, an area of 12537479.724m^2 has been weathered out. Therefore, this amount of weathering has been contributing in flooding in the state of Assam.

Reach one has undergone maximum erosion (table 1) and forested areas. One of the reasons for maximum erosion could be high slope due to which increases velocity of the river flow eroding the material along the river bank (Sarma and Acharjee, 2018). In case of Reach two erosions occurs is found to be higher on right bank as compare to left bank. In this case, the river enters the flat plain from the high elevation, meandering occurs and maximum erosion occurs at the cut bank (Florsheim et al., 2008). Udmari, Jaria and Sawpur are a place which falls in Reach five, here agriculture land and settlement comprising of almost 2 km^2 were eroded within seven years. The River has changed its course after entering this reach, flow direction changed from South to South west. Second highest erosion took place in Reach six, good amount of erosion has occurred in both sides of the bank. The eroded land mostly consists of agricultural land and settlement. Titapani, Bankabhanga and Balikuri N.C are some settlements which are near Reach six. Erosion and deposition is accompanied by variation in the channel width (Sapkale et al., 2016). In the present study area, channel width has increased indicating the occurrence of erosion within seven years. Table 3 shows the variation in the channel width within seven years.

Sinuosity index can be explained as the deviations from a path defined by the direction of maximum downslope (Sapkale et al., 2016). For this reason, bedrock streams that flow directly downslope have a sinuosity index of 1, and meandering streams have a sinuosity index that is greater than 1. Sinuosity index of year 2008 and 2015 is shown in Table 3 as well as the length of the channel. The sinuosity index decreased from 1.178 to 1.169 from 2008 to 2015. Correspondingly the channel length has also been decreased from 71.175km to 70.582km from the 2008 to 2015. This decrease in both the sinuosity index and channel length indicates the occurrence of erosion.

Table 3: Channel width section

Section	Width (m) 2008	Width (m) 2015
A	1920	1565
B	639	1399
C	666	921
D	650	1177
E	1912	2253
F	391	463
G	870	913
H	1221	2032
I	1443	1857
J	1587	2517
K	638	474

After applying the expression formulated by Sharma et al. (2010), the calculated PFI value of each section for the year 2008 and 2015 were shown in Table 4(a) and Table 4(b). Section 1,2,3,5 and 6 falls under moderately braided class(19>PFI>4) and section 4, 7 and 8 falls under low braided class(PFI>19) in the year 2008. Section 1,2,3,5 and 6 falls under moderately braided class(19>PFI>4) and section 4,7 and 8 falls under low braided class((PFI>19) in the year 2015.

Table 4(a). Plan Form Index (2008)

PFI of 2008				
Section	*N(m)*	*B(m)*	*T(m)*	*PFI(08)*
1	3	1172	365	10.38111
2	2	673	217	16.12184
3	6	1325	495	6.226415
4	4	882	704	19.95465
5	4	1969	843	10.7034
6	2	1236	466	18.85113
7	2	962	520	27.02703
8	3	806	694	28.70141

Table 4(b). Plan Form Index (2015)

PFI of 2015				
Section	*N(m)*	*B(m)*	*T(m)*	*PFI(15)*
1	4	1502	344	5.725699
2	4	1034	219	5.294971
3	3	1025	288	9.365854
4	3	1116	841	25.11947
5	4	2009	677	8.424589
6	2	1279	276	10.78968
7	2	979	691	35.29111
8	2	571	541	47.37303

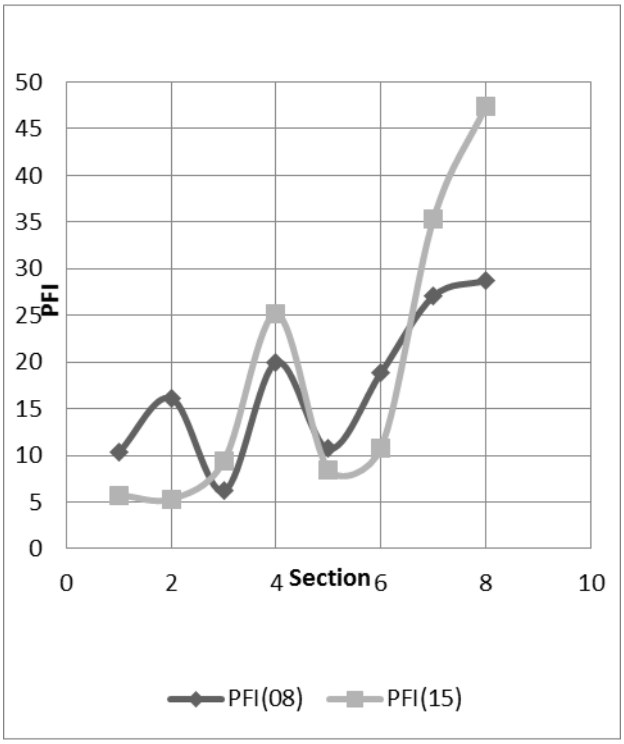

Figure 6: PFI comparison plot

Figure 6 shows how the PFI value has varied between 2008 and 2015. PFI value in section 1 and 2 has deceased tremendously from 2008 to 2015 indicating highly braided and increased in the PFI value in section 7 and 8 indicating low braided. The PFI value has varied throughout the sections indicating the occurrence of erosion and deposition (Sharma et al., 2010).

5. Conclusion

The present study of using the integrated approach of remote sensing and geographic information system has revealed the amount of erosion and deposition within seven years (2008-2015) along with the change in the river morphology. It is observed that the river has experienced erosional activity more in both banks than depositional activity. The change in the channel width, decrease in the sinuosity index and channel length all indicates the occurrence of erosional activities (Elliott, 2011).

The present work using multi-temporal spatio satellite data has exhibit a useful application of remote sensing and Geographic information system, allowing the synoptic viewing of the large regions, assessing the river dynamics and erosional/depositional activity. The information generated from this study can be in cooperated with other studies like climate change, flood control measures and can be helpful to take flood/erosion protection measures in Manas-Beki River.

From the present study, it can be concluded that more erosion has occurred where the river course is more prominent. A total area of 22573103m^2 was eroded and 10035623.276m^2 was deposited. Also reach one proved to be the most critical area having erosion of 4181050m^2 which is also evidently shown in the PFI plot.12537479.724m^2 of materials are weathered at the downstream area of Assam during the study period (2008-2015). Planning and extension of settlement and agricultural activities around this area should be avoided. River enhancement protection structures and methods should be given first priority around the areas where change in course is more drastic (Basiago, 1998).

One of the reasons for erosion in Manas-Beki River is due to the sudden water release from Kurichu dam in Bhutan, which affected thousands of people in Barpeta District and Baksa District. Kurichu is a 60MW hydropower project involving a 55m high concrete gravity and discharge capacity of 12,200m^3/second which can have massive downstream impacts if the downstream area is already facing rainfall and floods (Mahanta, 2010). Central water commission's flood forecasting site reported on oct14,2014 that Beki River at Beki NHC crossing was flowing at 45.25m, above the warning level of 44.1m, danger level of 45.1m (Purkait, 2004). Bhutan must inform central warning system about the release of water from the dam and avoid releasing the water without any information.

Acknowledgements

Authors are thankful to Department of Space, Government of India for providing necessary facilities at North Eastern Space Application Centre, Umiam Meghalaya to carry out the work. Authors also thank anonymous reviewers for their valuable suggestions and comments which improved the present study many fold.

References

Basiago, A.D. (1998). Economic, social, and environmental sustainability in development theory and urban planning practice, Environmentalist, 19(2), 145-161.

Bordoloi, K., B.R. Nikam, S.K. Srivastav and D. Sahaariah (2020). Assessment of riverbank erosion and erosion probability using geospatial approach: a case study of the Subansiri River, Assam, India, Applied Geomatics, https://doi.org/10.1007/s12518-019-00296-1.

Chakraborty, S. and S. Mukhopadhyay (2015). River bank erosion and channel width adjustments across a meandering channel of North Bengal, India, Earth Science India, 8(3).

Clerici, A. and S. Perego (2016). A set of GRASS GIS-based Shell scripts for the calculation and graphical display of the main morphometric parameters of a river channel, International Journal of Geosciences, 7(2), 135-143.

Das, J.D., T. Dutta and A.K. Saraf (2007). Remote sensing and GIS application in change detectionof the Barak river channel, N.E. India, Journal of Indian Society of Remote Sensing, 35(4), 301-312.

Das, T.K., S.K. Haldar, I.D. Gupta and Sayanti Sen (2014). River bank erosion induced human displacement and its consequences, Living Rev. Landscape Res. 8, 3.

http://www.livingreviews.org/lrlr-2014-3, doi:10.12942/lrlr-2014-3.

Deka, M. and B. Talukdar (2016). A study of an erosion-affected reach of the River Beki using mathematical modeling, World Environmental and Water Resources Congress, 334-342.

Dutta, M.K., S. Barman and S.P. Aggarwal (2010). A study of erosion-deposition processes around Majuli island, Assam, Earth Science India, 3(4), 206-216.

Florsheim, J.L., J.F. Mount and A. Chin (2008). Bank erosion as a desirable attribute of rivers, BioScience, 58(6), 519-529.

Gogoi, C. and D.C. Goswami (2013). A study on bank erosion and bank line migration pattern of the Subansiri River in Assam using remote sensing and GIS technology, The International Journal of Engineering and Science, 2(9), 1-6.

Gogoi, C. and D.C. Goswami (2014). A study on channel migration pattern of the Subansiri River in Assam using remote sensing and GIS technology, Current Science, 106(8), 113-1120.

Goswami, U., J.N. Sarma and A.D. Patgiri (1999). River channel changes of the Subansiri in Assam, India, Geomorphology, 30(3), 227-244.

Goyal, M. K. (2014). Statistical analysis of long term trends of rainfall during 1901–2002 at Assam, India, Water Resources Management, 28(6), 1501-1515.

Islam, M. T. (2009). Bank erosion and movement of river channel: A study of Padma and Jamuna Rivers in Bangladesh using remote sensing and GIS. Division of Geoinformatics, Royal Institute of Technology, Stockholm, Sweden.

Jain, S. K., A.K. Saraf, A. Goswami and T. Ahmad (2006). Flood inundation mapping using NOAA AVHRR data. Water Resources Management, 20(6), 949-959.

Khan, M. H. (2012). River erosion and its socio-economic impact in Barpeta District with special reference to Mandia Dev. Block of Assam. International Journal of Engineering and Science, 1(2), 177-183.

Kotaky, P., D. Bezbaruah, J. Baruah and J. Sarma (2003). Erosion activity in Majuli –The largest river island in the world, Current Science, 84(7), 929-932.

Mahanta, A. (2010). The Case of Kurichu in the Indo-Bhutan Context – Transboundary Hydropower Projects and Downstream Flooding. indiawaterportal.org/sites/indiawaterportal.org/files/kurichu.pdf

Pande, C.B. and K. Moharir (2017). GIS based quantitative morphometric analysis and its consequences: a case study from Shanur river basin, Maharashtra, India, Applied Water Science, 7(2), 861-871.

Phukan, A., R. Goswami, D. Borah, A. Nath and C. Mohanta (2012). River bank erosion and Restoration in the Brahmaputra River in India, Clarion, 1(1), http://clarion.ind.in/index.php/clarion/article/view/17.

Purkait, B. (2004). Hydrometeorology, In The Brahmaputra Basin Water Resources, Springer, Dordrecht, 24-34.

Sayanangshu Modak and Nirmalya Choudhury (2017). villagesquare.in/2017/09/06/river bank-erosion-no-less-disaster-assam-floods/

Sankhua, R.N., N. Sharma, P.K. Garg and A.D. Pandey (2005). Use of remote sensing and ANN in assessing of erosion activities in Majuli, the world's largest river island, International Journal of Remote Sensing, 26(20), 4445-4454.

Sapkale, J.B., Y.U. Kadam, I.A., Jadhav and S.S. Kamble (2016). River in planform and variation in sinuosity index: A study of Dhamni River, Kolhapur (Maharashtra), India, Int. J. Sci. Eng. Res, 7, 863-867.

Sarma, J.N. and S. Acharjee (2012). A GIS based study on bank erosion by the river Brahmaputra around Kaziranga National Park, Assam, India, Earth System Dynamics Discussions, 3(2), 1085-1106.

Sarkar, A., R.D. Garg and N. Sharma (2012). RS-GIS based assessment of river dynamics of Brahmaputra river in India, J. Water Resour. Prot., 04(02), 63-72.

Sarma, J.N. and S. Acharjee (2018). A study on variation in channel width and braiding intensity of the Brahmaputra River in Assam, India. Geosciences, 8(9), 343.

Sarmah, R.K. and U. Sarma (2017). Temporal changes of fluvio-morphological scenario and its impact on settlement: A GIS based study for Mandia block, Barpeta District, Assam, ADBU Journal of Engineering Technology, 6(2).

Sharma, N., Amoako Johnson, F., W Hutton, C., & Clark, M. (2010). Hazard, vulnerability and risk on the Brahmaputra basin: a case study of river bank erosion. The Open Hydrology Journal, 4(1).

Sinha, R. and S. Ghosh (2012). Understanding dynamics of large rivers aided by satellite remote sensing: a case study from Lower Ganga plains, India, Geocarto International, 27(3), 207-219.

Talukdar, B. (2012). "River Bank Erosion – A Perspective, Conference Paper. http://www.iitg.ernet.in/coeiitg/31.pdf.

Journal of Geomatics Vol. 14, No. 2, October 2020

Integrating Analytical Hierarchy process (AHP) and Grey Relativity Analysis (GRA) in suitable landfill site selection – A case study in Tarkwa and its environs

B. Kumi-Boateng*, M. S. Peprah, E. K. Larbi
University of Mines and Technology, Tarkwa, Ghana
*Email: kumi@.umat.edu.gh

(Received: June 27, 2020; in final form: Oct. 29, 2020)

Abstract: The rapid increase in human population growth of developing countries including Ghana in the past few decades and its resulting accelerated urbanization phenomenon demand development of environmentally sustainable and efficient waste management systems and policies. Landfill studies constitutes one of the core primary methods of municipal solid waste disposal. Waste management in Tarkwa and its environs is mainly by open space dumping which can results into contamination of both surface and underground water around these open dumps' areas. The siting of suitable landfill areas should meet both the economic and environmental requirements of a landfill site. Optimized siting decision making process have gained considerable importance to ensure minimum damage to the various environmental sub-components as well as to reduce the stigma associated with the residents living in the study area, thereby enhancing the overall sustainability associated with the life cycle of a landfill. Present study addresses the issues of siting a new suitable landfill area utilizing Multi-criteria Decision Analysis (MCDA) and Geographic Information System (GIS) approach. Several geo-environmental factors such as land use and land cover, water bodies, slope, Digital Elevation Model (DEM), railroads, roads and geology of the study area obtained from the Survey and Mapping Division Department of the Lands Commission of Ghana were extracted and used in the suitable siting process. Analytical Hierarchy Process (AHP) was integrated with Grey Relativity Analysis (GRA)in assigning weights to each criterion depending upon their relative importance and ratings in accordance with the siting process. Spatial analysis was carried out in ArcGIS environment to show areas suitable or unsuitable for siting a landfill site. The results showed different classes of the study area with regards to their suitability in siting a landfill site with11% of the area highly suitable (in compliance with the set rules and regulations), 59%of the area less suitable (not in compliance with the set rules and regulations) and 30% not suitable. Atuabo, Anyinakrom, and Atoboareasare highly recommended for construction of engineering landfill sites according to the results achieved in this study. Additionally, it is situated within the Birimian system with low potential of contaminating ground waters and possess good geophysical and geotechnical properties as highlighted in previous studies of the area. Integrating GIS and MCDA techniques have proven to be an effective tool for selecting suitable sites for landfill site selection and very useful in determining places of suitable and unsuitable for future planning and redevelopment of the study area. The proposed raster map can be used by decision makers for future siting of suitable landfill areas within the study area. Moreover, it is recommended that, soil chemical test, detailed geomorphological studies, and socio-economic impact assessment of the selected areas should be evaluated. In addition, the authorities should put measures in place to combine education and enforcement of laws to prosecute offenders who are found throwing solid wastes at unsuitable areas to bring sanity to the environment.

Keywords: Analytical Hierarchy Process, Geographic Information System, Grey Relativity Analysis Landfill Site Selection, Multi-Criteria Decision Analysis, Solid Waste Management

1. Introduction

Suitable landfill site selection studies which happens to be one of the major environmental problem in recent years have become necessary, receiving much attention from numerous researchers in the fields of waste management and environmental sciences in developing countries including Ghana (Abujayyab et al., 2017; Aksoy and San, 2016; Sener et al., 2010). This is as a result of the highly rapid increase in human population growth and its associated anthropogenic activities which is one of the main causes of human waste and needs a proper solid waste management (Mat et al., 2017). Improper solid waste management can cause environmental pollution, land degradation, and hot climatic conditions (Sumathi et al., 2008). Additionally, it can cause deterioration of industrial areas, future land use, the tourism industry and properties (Abujayyab et al., 2017). Landfill which has become the most commonly method in solid waste management can minimize environmental hazards, minimize risks to public health and safety. Hence, there is a need to select a suitable landfill for solid waste management.

Solid waste management has become one of the major problems in Tarkwa and its environs due to very low waste collection (roughly about 10%) (Kwesi et al., 2020) and has giving rise to open dumping at inappropriate locations (Kwesi et al., 2018). This is because there is an existence of only one open dump site at Aboso to accommodate a large amount of waste generated daily in Tarkwa and its surrounding communities (Asante-Annor et al., 2018; Aboziah, 2016). The annual waste estimate of the area for 2015 using time series approach was 151469 tonnes (Ademola et al., 2012). Akyen et al., (2016) and (2017) used time series analysis (ARIMA and Time value of Money mathematical models) to forecast the upcoming years annual solid waste until 2031 with a mean, minimum and maximum value to be 22780.75 tonnes, 18120 tonnes, and 27735 tonnes respectively. The composition of the solid waste in the study area mostly comprise of the household waste, yard trimmings, agricultural and industrial wastes (Aboziah, 2016). Conversely, a greater proportion of the household waste is made up of organic and inorganic material substances. The Tarkwa Nsuaem Municipal Assembly is responsible for the efficient and safe collection and management of all municipal solid waste within its catchment area, nearby and surrounding communities. Due to constraints in logistics and human resources, the Municipal Assembly has contracted Zoomlion Ghana Company to do the daily collection and disposal of wastematerials (Aboziah, 2016). The waste is transported to the final disposal site at Aboso which is about 10 km from Tarkwa and 14 km from Huni-Valley respectively. Solid waste collection is mainly by either house-to-house or central container collection and the waste collected is finally disposed of at the landfill site located at Aboso (Ademola et al., 2012). There are other several private waste management companies that operate within the municipality but are not contracted by the Municipal Assembly. They either collect solid waste generated by the mining companies or individual households and dispose of at the dump site. This has become very necessary because of the logistics and financial constraints affecting the Assembly in collecting and disposing of waste promptly (Aboziah, 2016).

Moreover, most urban landscapes found within the study are characterized by mountains of uncollected garbage, gutters choked with waste, open reservoirs that appear to be a little more than toxic pools of liquid, beaches, drains and stream with plastic garbage, abandoned quarries and valleys filled with garbage (Asante-Annor et al., 2018; Aboziah, 2016). According to Aboziah, (2016) the Aboso open waste dump site which is about 24 acres in size has been in operation since 2004. It is currently serving as the main dumping site for the municipality and operating above its capacity due to lack of an alternative landfill site. A study made by Asante-Annor et al., (2018) revealed that, the existing landfill site at Aboso is not suitable for the construction of an engineered landfill due to high water table, leachate runoff to nearby stream, presence of structural deformation and proximity to built-up areas. Furthermore, the dump site is closer to residential areas and is not equipped with appropriate lining to prevent the contamination of underground water by leachate and spread of infections through run offs during rains (Aboziah, 2016). In order to control this menace, the government of Ghana has put in policy measures requiring all authorities to phase out open dumping and replace them with engineered landfill sites and many other improved systems of solid waste disposal methods (Kwesi et al., 2020). It is in line with this implementation of policy that, this present study seek to site a suitable landfill sites for disposal of refuse especially in mining areas where surface water bodies are polluted and many residents depends other sources of water for domestic and other activities (Joe-Asare et al., 2018; Ewusi and Kuma, 2014).

Conversely, selecting a suitable site for landfill involves several factors such as environment, social as well as technical factors (Akyen et al., 2017). These factors are very important and when not properly evaluated may result in health implications to humans and other living organisms (Akyen et al., 2017). Moreover, other factors such as economical and infrastructure constraints, including unavailability of land for safe waste disposal and lack of public awareness and fear at all levels restrain progress resulting in inefficient and unsafe urban solid waste management which may contaminate both surface and groundwater, contaminate soils and affect plants, animals and microorganisms (Asante-Annor et al., 2018). Furthermore, other factors such as special purpose engineering, geological and hydro-geological studies be conducted in other to assess the groundwater quality assessment, soil properties, geophysical and geotechnical nature of the area (Aboziah, 2016). Additionally, before the commencement of a suitable landfill site, certain criteria need to be carefully analyzed and studied to select an appropriate site that would have minimum environmental and economic impact, that would be accepted by the public, and that would comply with regulations as well (Kao andLin, 1996). Site selection and analysis can be improved by using Geographic Information System (GIS) and Multi-criteria Decision Analysis (MCDA). The ability to manage large amounts of spatial data in different formats from diverse sources using GIS techniques makes it useful for site selection studies (Aboziah, 2016). GIS can process large amounts of spatial data by saving time, energy and resources during landfill site selection. With GIS techniques, data are efficiently stored and retrieved, analyzed and results displayed according to the decision makers preference or user specification (Daneshvar et al., 2005).

Municipal solid waste disposal and management has become one of the threats to global environmental health. Developing and maintaining an effective and efficient solid waste management system in the Tarkwa Nsuaem Municipality, requires the establishment and enforcement of legislation, by-laws and implementation of proper waste management practices that are specific enough to address the sanitation issues in the municipality (Aboziah, 2016). Due to the presence of numerous mining companies in the Tarkwa Nsuaem Municipality, there are a lot of commercial activities and increase in population growth due to rural-urban migration yielding large amounts of waste generated daily. The cost associated with the collection, haulage and proper disposal of wastes puts a huge financial strain on the coffers of the assembly and residents of the study area as well. Also, the volume of waste generated exceeds the capacity of the only open dumping site available, and management of the waste collected becomes a problem for the assembly, which could result in various environmental and public health issues (Aboziah, 2016). The availability of land and selecting the most environmentally and economically suitable site for the construction of a landfill site to receive the large amounts of waste generated is a major step towards solving the problem of solid waste management in the municipality. Currently, there is no engineered landfill site in the study area at the moment and numerous researchers have suggested alternative ways for siting a suitable landfill for Tarkwa and its surrounding communities (Asante-Annor et al., 2018; Aboziah, 2016).

Siting a suitable landfill area requires an extensive evaluation process in order to identify the best disposal location available. The selected location must comply with the requirements of governmental set rules and regulations, environmental conditions, health factors, geological parameters such as ground water quality assessment, soil properties and depth to groundwater (Spigolon et al., 2018; Bilgilioglu and Bilgilioglu, 2017). In addition to that, the suitability siting must involve processing and analyzing a large amount of spatial data, standard rules and acceptance criteria. In the recent years, the modern technique for suitable and non-suitable landfill site selection involves the use of GIS and MCDA methods which enables spatial data display and facilitates the selection process (Djokanovic et al. 2016).

GIS has emerged as a very important tool for land use suitability analysis. GIS can recognize, correlate, and analyze the spatial relationship mapped phenomena, thereby enabling policy makers to link disparate sources of information, perform sophisticated analysis, visualize trends, project outcomes and strategize long-term planning goals (Malczewski, 2004). MCDA methods have been developed to assist decision makers in either ranking a known set of alternatives for a problem or making a choice among this set while considering the conflicting criteria. Also, it has evolved as a major tool to assist decision makers in analyzing and solving multiple criteria decision problems. Conversely, the alternatives are compared against each other based on how they perform relative to each criterion. Ideally, some methods require comparison of the criteria to arrive at the relative importance of each criteria. MCDA methods utilize this information to assign ranks to the alternatives. Some of the applications of GIS and MCDA in suitable landfill site selection are present in the various literatures (Kwesi et al., 2020; Asante-Annor et al., 2018; Sumathi et al., 2008; Malczewski, 2004; Djokanovic et al., 2016; Lokhande et al., 2017; Mat et al., 2017; Yal and Akgun, 2013; Abujayyab et al., 2017; Sener et al., 2010; Aksoy and San, 2016). The integrating of these techniques for landfill site selection is a difficult process because it requires knowledge about many criteria parameters and regulations.

Upon carefully reviewing of existing literatures for the study area concerning suitable landfill site selection, the MCDA techniques that have been applied in suitable landfill site selection for the study area include DRASTIC method (Kwesi et al., 2020), AHP (Asante-Asantor et al., 2018; Aboziah, 2016) and time series analysis (Akyen et al., 2017; Akyen et al., 2016; Ademola et al., 2012). The utilization of other techniques is yet to evaluated in suitable landfill site selection at the moment. The assessing of the efficacy of a Hybridized Grey Relativity Analysis (HGRA) was adopted in suitable landfill site selection for the study area. The aim of this present study is to find the best location for landfill site that will minimize hazards to the environment utilizing MCDA, HGRA and GIS techniques. This is because a proper selection of the disposed sites is probably the most important step in the development of solid waste management. Moreover, these techniques provide a means of decomposing the problem into a hierarchy of sub-problems that can be more easily comprehended and subjectively evaluated. The subjective evaluations are converted into numerical values that are ranked on a numerical scale. Furthermore, MCDA and GIS are one of the well-known for landfill suitability analysis. These techniques were integrated for getting more reliable and accurate results and decisions. The obtained results will be validated with previous works done concerning the area of study. The geophysical and geotechnical investigations were not considered since it was beyond the scope of the work due to unavailability of geophysical tools during the investigation of the research findings. This research will provide additional information for the Town and Country Planning Department, Municipal Environmental Department, other researchers, policy makers, organizations and institutions that intend to make interventions to develop the administrative and the infrastructure aspects of sustainable waste management system in the Tarkwa Nsuaem Municipality to improve the environment and public health.

2. Study area

The study area (Figure 1a and Figure 1b) is situated at the mid-southern part of the Western Region of the Republic of Ghana with geographical location between longitude 001°45′ 00″ W to 002°15′ 00″ W and latitude 005°00′ 00″ N to 005°30′ 00″ N with an average topographic altitude of about 78 m above mean sea level (MSL) (Kumi-Boateng and Peprah, 2020; Peprah et al., 2017; Peprah and Mensah, 2017). Geographically, the land is generally undulating with steep slopes parallel to each other and to the strike of the rocks in the north-south direction (Joe-Asare et al., 2018). The area lies within the main gold belt of the Republic of Ghana that stretches from Axim in the south-west direction to Konongo in the north-east direction (Kortatsi, 2004). The town is well noted for mining precious minerals such as gold and manganese which contribute significantly to the economic development of the country (Boye et al., 2018). The study area is found within the rainforest of Ghana. The mean rainfall is approximately 1500 mm with peaks of more than 1700 mm in June and October. Between November and February, the rainfall pattern decreases to between 20 mm to 90 mm (Peprah and Mensah, 2017).

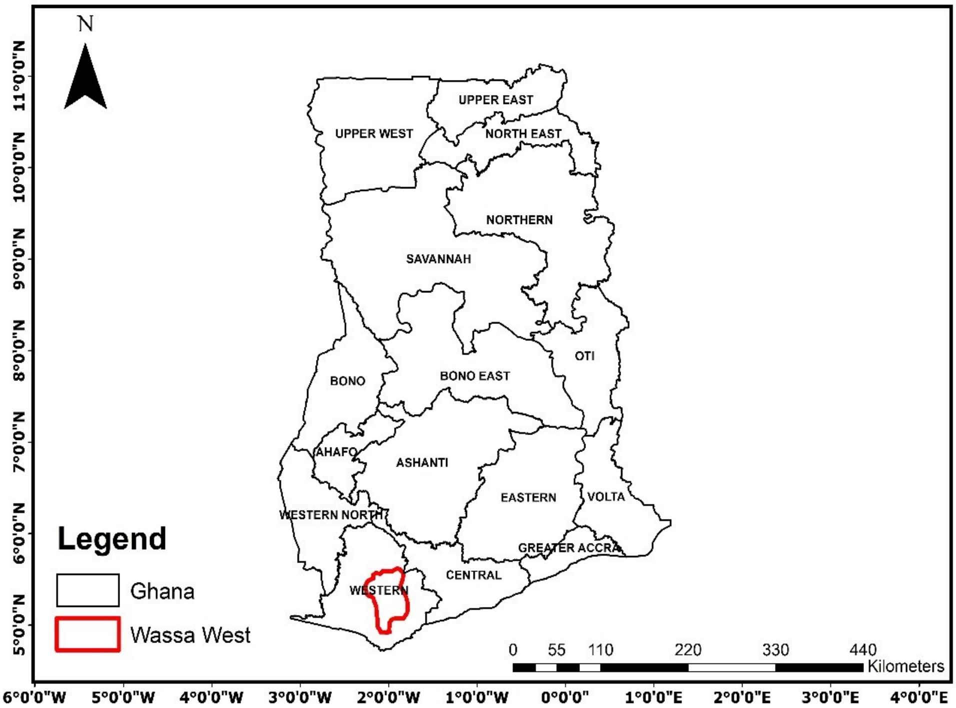

Figure 1a: Location map of Study Area

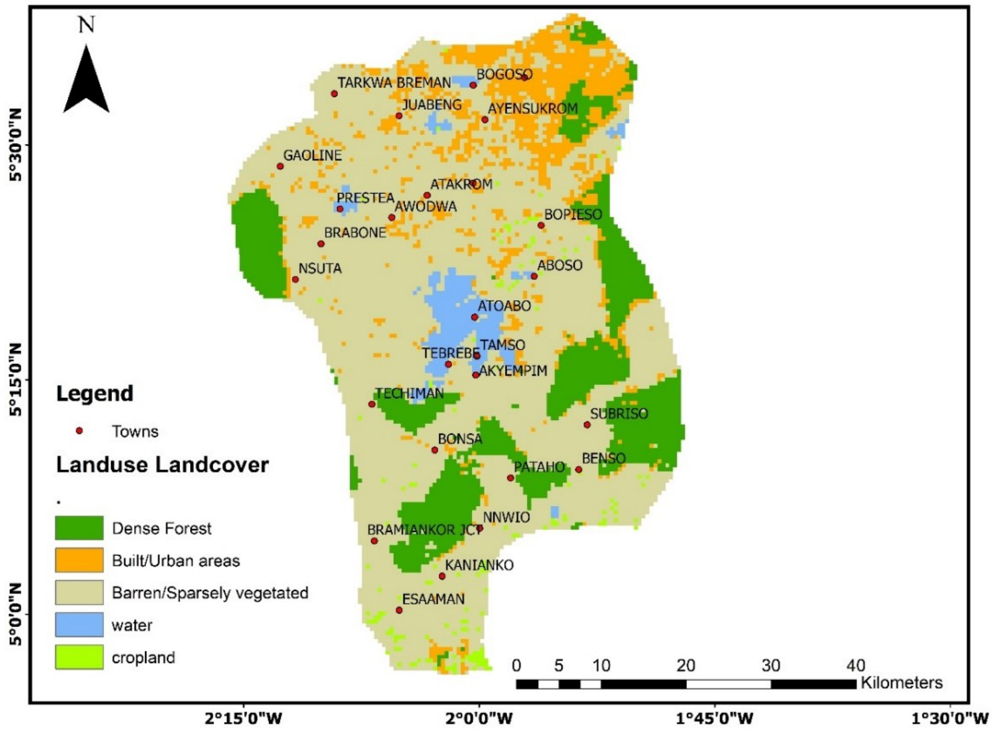

Figure 1b: Map of the Study area

3. Resources and methods used

3.1 Resources

The data used for the study comprise of a secondary data obtained from the Survey and Mapping Division Department of the Lands Commission of Ghana. The data consist of topographical and soil maps from which features such as land use and land cover, roads, railroads lithology and geology, slope, elevation and water bodies of the study area were extracted and used.

3.2 Methods used

3.2.1 Proximity Analysis

Proximity analysis was carried out to determine the spatial relationship between the suitable selected areas and their neigbouring features with regards to distances (Peprah et al., 2018; Sara et al., 2011). In addition to that, it also allowed the spatial features to be reclassified based on distances that meet the standard set criteria (Njoku and Alagbe, 2015; Tah, 2017; Aslani and Alesheikh, 2011). Buffer analyses of the suitable selected areas to road, railroads, water bodies and settlement areas were performed to assess the proximity of suitable areas to roads, railroads. Populated areas and water bodies. Buffer analysis of suitable areas to roads, railroads, distance to water bodies and settlement areas were done in ArcGIS environment. This was done to assess the areas compliance to suitable set standards. Areas that fell within the specified buffer distances complied with the set standards and are likely to pose less hazard to the environment while those that fell outside the buffer zone are expected to pose hazards to the environment. A buffer zone of maximum distance 1000 m, 500 m and minimum distance of 300 m were generated in ArcGIS environment for land use and land cover, roads, railroads, and water bodies to assess the level of compliance.

3.2.2 Landfill Suitability Modelling

The suitable landfill sites were selected based on spatial analyses of the following dataset: slope, elevation, lithology and geology, land use and land cover, roads, railroads and water bodies. The various datasets are of varying relative importance and therefore the Analytical Hierarchy Process (AHP) based on pairwise comparisons was used to generate weights for each criterion. The relative importance between two criteria was measured based on a numerical scale of 1 to 9 (Wind and Saaty, 1980; Saaty, 1980). Figure 2 shows the flowchart of the MCDA process. The AHP, which was modified by Saaty (1977) but first developed by Myers and Alpert (1968) was used because the technique assess a set of evaluation criteria and search for the optimal solution among a set of alternatives options (Larbi et al., 2018; Peprah et al., 2018; Akay and Erdogan, 2017; Akay and Yilmaz, 2017). In the solution process of the AHP, the study area was classified as suitable, less suitableand not suitable. The suitability and restriction model were created in ArcGIS environment according to Equation 1 given as (Peprah et al., 2018):

$$\int = \sum_{i=1}^{n} \omega_i * \varsigma_i \prod_{j=1}^{m} \gamma_j \qquad (1)$$

Where $\int$ is the suitable landfill area, ω_i is the weight for each criterion, ς_i is the criterion for suitability, and γ_j is the restriction. In creating a restriction model will require a minimum and maximum buffer distances for suitable site selection. Table 1 is the standards set for suitability selection by the Environmental Protection Agency (EPA) 2002 in Ghana, and table 2 is the adopted set standards used in ArcGIS environment. Table 3 is the relative importance values. The following procedure was adopted for creating the final raster map:

- Creating a buffer around the major selected criteria (land use and land cover, slope, roads, railroads, and water bodies);
- Converting all the vector layers to raster layers;
- Creating a restricting model using the null tool to depict the viable areas for suitable landfill site selection;
- Combination of the various restrictions to obtained the final restriction model; and
- The restriction model and the suitability model are combined to give the final suitability of locations appropriate for siting the landfill suitable areas.

Table 1: Criteria for the Selection of a Suitable Landfill Site (Asante-Annor et al., 2018; EPA, 2002)

Criterion	Buffer Zone (m)	Buffer Zone Significance
Wetlands	500	This is to prevent the creation of breeding grounds for insects such as mosquitoes, house flies, etc.
Roads	300	This is to minimize the cost of constructing connecting roads to the suitable landfill site.
Railway	300	This is to prevent train accidents as a result of dumping of waste by the inhabitants of the area.
Built-up-Areas	300	This is to minimize the health hazards and environmental pollution caused by solid and liquid waste.
Surface Water	300	This is to minimize leachate seeping into the surface and ground waters that can caused the water pollution.

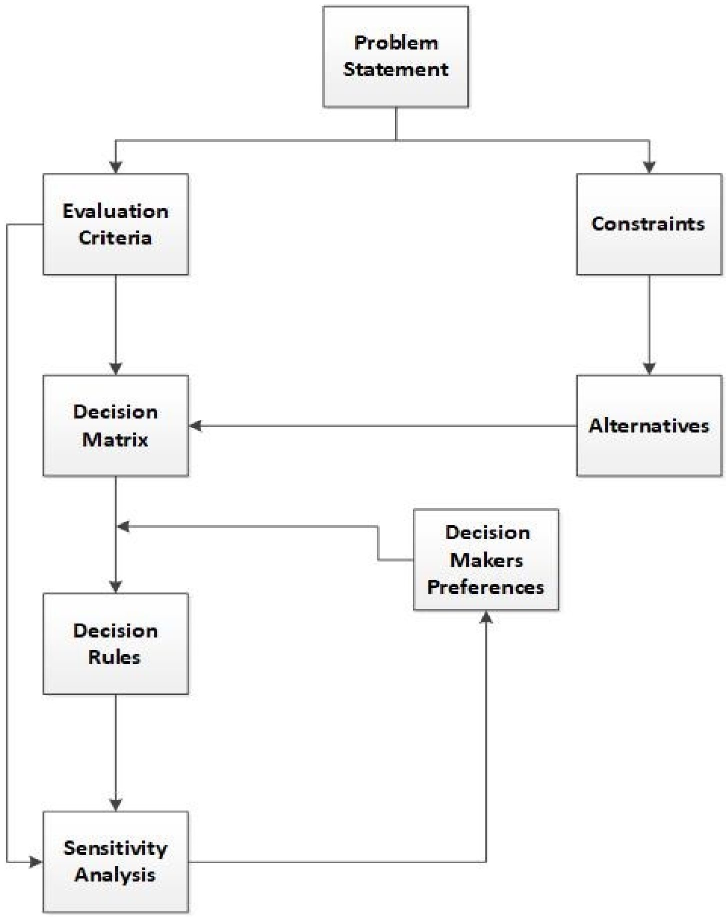

Figure 2: Flowchart of the MCDA Process (Source: Yakubu et al**., 2015; Malczewski, 1999)**

Table 2: Restrictions Standards for Suitability Landfill Site Selection

Restriction Source	Minimum Buffer Distance/Degree	Maximum Buffer Distance/Degree	Analysis Buffer Distance/Degree
Slope	0°	20°	≤ 20°
Land use and Land Cover	500 m	1000 m	500 m
Roads	300 m	500 m	300 m
Railroads	300 m	500 m	300 m
Water bodies	300 m	500 m	300 m

Figure 3 shows the suitability and restrictions model generated respectively for the suitable site selection. The combined model for the final output raster map is shown by figure 5.

From table 3, the values assigned to the sub-criteria were evaluated with regards to suitable site selection. Higher score was given when the criterion was more important (Larbi et al., 2018; Peprah et al., 2018; Akay and Erdogan, 2017; Akay and Yilmaz, 2017). The derived matrix was normalized to obtain the eigen vectors (weights) which were assigned to the selection criteria.

3.2.3 Mathematical Concept of the Analytical Hierarchy Process (AHP)

The AHP method provides a structural basis for quantifying the comparison of decision elements and criteria in pairwise fashion, making decision making less difficult, and providing a means of decomposing the problem statement at hand into a hierarchy of sub problems which can be more easily be understood and subjectively evaluated (Larbi et al., 2018). The subjective evaluations are then converted into numerical values and processed into ranks each alternative on a numerical scale (Saaty, 1980). The AHP was used to produce surface grids of each criterion and combine them into a single surface grid for engineering, environmental, and planning purposes.

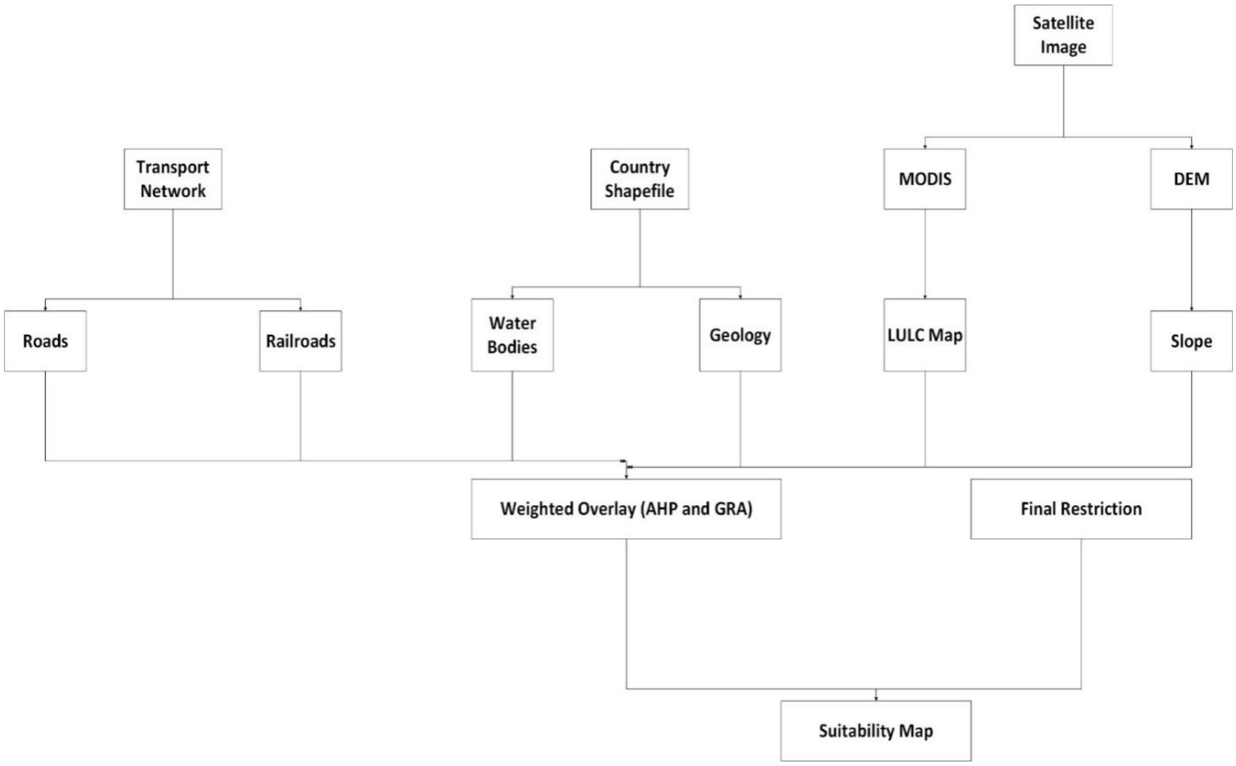

Figure 3: Flow Chart of the Suitability Model

Table 3: The 9-Points Scale Used in Typical Analytic Hierarchy Studies (Wind and Saaty, 1980)

Intensity of Importance	Definition	Explanation
1	Equal Importance	Two activities contribute equally to the objective
3	Weak importance of one over another	Experience and judgement slightly favour one activity over another
5	Essential or strong importance	Experience and judgement strongly favour one activity over another
7	Demonstrated importance	An activity is strongly favoured and its dominance is demonstrated in practice
9	Absolute importance	The evidence favouring one activity over another is of the highest possible order of affirmation
2,4,6,8	Intermediate values	When a compromise is needed
Reciprocals	If activity i has one of the above nonzero numbers assigned to it, when compared with activity j, the activity j has the reciprocal value when compared with i	

Defining the Criterion Used for the Suitable Landfill Site Selection

The suitability analysis relies on a major relevant dataset, which are raster datasets. The value of each cell represents the per unit distance of crossing that cell. The suitable site selection was based on a set of defined criteria such as slope, land use and land cover, roads, railroads, water bodies, and lithology and geology.

- Topography: Slope and Elevation is one of the most important criteria in suitable landfill selection decision making process. Areas of mild slope are very suitable as compared to areas of steep slope. This factor was considered because places of higher relief are not suitable for siting landfill sites since extensive downpour of rains can wash solid waste to lowlands; The Digital Elevation data was obtained from the Survey and Mapping Division of Ghana. It has a resolution of (30 x 30 m).

- Land use and Land cover: Land use and land cover encompasses of industrious areas, green lands, and human settlement areas. The suitable sites must be far from human settlement in order to minimize environmental pollution. This criterion is a crucial factor, hence higher score was assigned to it. Ideally, there is no human settlement in the green land areas, but the decompose solid waste would help enrich the soil and serve as food for other living organisms;
- Transport Network: Roads and Railroads were considered as the main transport network in this present studies. Roads helps in transporting the solid waste to the damped sites. In selecting a suitable landfill sites, it should be easily accessible and better routes must be designed to help in the transportation of the solid wastes; Old Rail freight trains could alternatively be used to convey community waste to the right disposal sites hence the need to also consider rail roads in suitable landfill analysis.
- Water bodies: Water bodies comprise of streams, dams, and rivers. The suitable sites must be far from water bodies to prevent the toxics and other harmful substance from human solid and liquid waste getting into water bodies. This is because the water bodies serve as an alternative potable drinking water to some communities due to the irregular supply of water from the Ghana water company (Joe-Asare et al., 2018; Seidu and Ewusi, 2018); and
- Geology: Soil types and geology of the area were considered and evaluated to see whether their physical and chemical properties will be suitable in selection of a landfill area.

Standardization of each Criterion maps

Standardization of each attribute was performed in ArcGIS environment. The spatial analyst tool was used for the reclassification module. Also, a linear transformation was adopted to transform the criterion attribute into a scale that ranges from 1 to 9, where the value of 1 is the least importance and 9 is the highest important as tabulated and explain in table 2.

Computation of Criterion Weight

The relative weight of each criterion ς_{ij} is obtained by comparing the criteria in pairs. The scale of differential scoring presumes that the row criterion is of equal or greater importance than the column criterion. The reciprocal values have been used where the row criterion is less important than the column criterion. A decision matrix was created by Saaty's preference scale (Saaty, 1980) and factor attributes are compared pairwise in terms of their relative importance of each criterion/decision element to that of the next level. Once the pairwise matrix is made, Saaty's method of eigen vectors/relative weights are computed as tabulated in table 4.

Table 4: A Pairwise matrix

ς_{11}	ς_{12}	ς_{13}
ς_{21}	ς_{22}	ς_{23}
ς_{31}	ς_{32}	ς_{33}

Where ς_{ij} is the pairwise matrix. The values in each column of the pairwise matrix is sum and each element in the matrix is divided by its column total to generate a normalized pairwise matrix according to Equation 2 given as:

$$\chi_{ij} = \frac{\varsigma_{ij}}{\sum_{j=1}^{n} \varsigma_{ij}} \tag{2}$$

Where χ_{ij} is the normalized matrix and n is the number of criteria tabulated in table 5.

Table 5: Normalized Matrix

χ_{11}	χ_{12}	χ_{13}
χ_{21}	χ_{22}	χ_{23}
χ_{31}	χ_{32}	χ_{33}

The normalized column of the matrix was divided by the number of criteria to generate a weights matrix according to Equation 3 given as:

$$\omega_{ij} = \frac{\sum_{j=1}^{n} \chi_{ij}}{n} \tag{3}$$

The weighted sum vector was calculated by multiplying the weighted matrix by the criteria matrix according to Equation 4 denoted as:

$$\omega_{ij} \times \varsigma_{ij} = W_s \tag{4}$$

where W_s is the weighted sum vector. The consistency vector was computed by dividing the row sum of the weighted sum vector by the criterion weight as according to Equation 5 given as:

$$W_S \times \frac{1}{\omega ij} = C_V \tag{5}$$

where C_V is the consistency vector. Conversely, once the consistency vector is calculated, $\lambda_{\max}$ is computed by dividing the column sum of the consistency vector by the number of criteria used according to Equation 6 given as:

$$\lambda_{\max} = \frac{\sum_{i=1}^{n} C_v}{n} \tag{6}$$

The Consistency Index, CI was then calculated according to Equation 7:

$$CI = \frac{\lambda_{\max} - n}{n-1} \quad (7)$$

The Consistency index reveals the measure of deviation from consistency, $\lambda_{\max}$ is the maximum eigen value and n is the number of criteria used. Consistency ratio CR should be achieved such that $CR < 0.10$ and it was calculated by dividing the consistency index by the random Index according to Equation 8 given as:

$$CR = CI/RI \quad (8)$$

3.2.4 Grey Relativity Analysis (GRA)

Grey Relational Analysis is a prioritization technique for generating optimal results of a selected criteria (Thapa and Engelken, 2020). GRA wasused in conjunction with AHP for the optimal weighting of the selected variables to be used in the landfill suitability The quality characteristics for the "higher the better" was used for the normalization sequence of the Transport network criteria whereas the "lower is better" criteria were used for normalizing the slope, landuse and landcover (LULC), geology and the water bodies. If the target value of the original sequence is infinite, the original sequence is normalized as given by Equation 9 given as (Ramanan and Dhas, 2017):

$$x_i^*(k) = \frac{x_i(k) - \min x_i(k)}{\max x_i(k) - \min x_i(k)} \quad (9)$$

where; $x_i^*(k)$ is the normalized value of the k^{th} performance characteristic in the i^{th} experiment; and $x_i^*(k)$ is the original k^{th} performance value in the i^{th} experiment. If the target value is "lower the better", the original sequence is normalized as according to Equation 10 given as (Ramanan and Dhas, 2017):

$$x_i^*(k) = \frac{\max x_i(k) - x_i(k)}{\max x_i(k) - \min x_i(k)} \quad (10)$$

The deviation sequence is determined using Equation 11 given as (Zhao and Liang, 2008):

$$\Delta_{oi} = \left| x_o^*(k) - x_i^*(k) \right| \quad (11)$$

where; Δ_{oi} = Deviationsequence; $x_o^*(k)$ = Reference sequence or idealseries; and $x_i^*(k)$ = Comparability sequence. The Grey Relational Coefficient is then calculated using Equation 12 given as (Zhao and Liang, 2008):

$$\xi_i(k) = \frac{\Delta\min + \zeta\,\Delta\max}{\Delta_{oi}(k) + \zeta\,\Delta\max} \quad (12)$$

where; $\xi_i(k)$ = Grey relational co-efficient, ζ = Distinguishing co-efficient, $\Delta_{\min}$ = the smallest value of $\Delta_{oi}(k)$ whereas $\Delta_{\max}$ = the largest value of $\Delta_{oi}(k)$. The Grey Relational Grade is calculated by Equation 13 given as (Thapa and Engelken, 2020):

$$\gamma_i = \frac{1}{n}\sum_{k=1}^{n} w_k(k)\,\xi_i(k) \quad (13)$$

where; γ_i = Grey Relational Grade (GRG), $w_k(k) = 1$, n = number of criteria used. The GRG values are expressed as the optimized percentage weights and assigned to the corresponding criteria.

4. Results and discussions

The study aims at identifying areas suitable for siting landfill in the Wassa West district of Ghana by integrating AHP and GRA mathematical models. Equation 1 represents the mathematical model used in the suitability studies. The model has two (2) components thus, the weighting component and the restriction component. Five (5) set criteria were used in this study (Transport network, slope, geology, water bodies and land use land cover). The outcome of the buffer analyses is presented by figure 4 (the restriction surfaces). The buffer maps serve as a constraint maps that restrain unsuitable areas (areas that will cause environmental pollution) from suitable areas (areas that will cause less environmental pollution). The restriction model gave two colour code results for each map generated. These colour codes were grouped into suitable and unsuitable area. AHP is mostly used to prioritize in hierarchical order the various alternatives used in the MCDA process (Meshram et al., 2019). In this study, the main purpose of the AHP was to verify whether the pairwise comparison matrix to be normalised using the GRA normalization sequence was consistent. Equation 2 was used in the normalisation of the pairwise matrix to generate weights as seen in Equation 3 for the AHP. To check for consistency, the weighted sum matrix was formed according to Equation 4 by multiplying the weights by the pairwise matrix. The weighted sum was then divided by the criteria weights to obtain the consistency vectors according to Equation 5. The average of the column sum of the consistency vectors is given in Equation 6 known as $\lambda_{\max}$. This helps in the calculation of the CI as given in Equation 7. The CR is obtained according to Equation 8 by dividing the CI by the RI. The CR obtained for this study was 0.09, which implies the scores assigned are not biased. GRA was used in this study for the optimization of weights for the maximum prioritization of the selected criteria. This was carried out to assist the identification of the best areas for landfill site selection in the Wassa West district. Equation 9 and Equation 10 represents the normalization sequence for the higher the better and lower the better characteristic respectively. Based on the hierarchical order of the AHP, the higher the better was chosen for the Transport network whereas lower the better normalization sequence was used on the other variables (slope, geology, water bodies, land use and land cover). Table 6 represents the pairwise matrix used in the GRA. The maximum and minimum values were selected from the respective columns of the criteria. This was later used in the normalization sequence shown in table 7 as given by Equation 9 and Equation 10. The deviation sequence is calculated from the absolute of the difference between the minimum value of the normalization sequence and the comparability sequence that is each value in the normalization sequence matrix. The obtained values were the same as the normalization sequence table since the minimum value of the normalization sequence table was 0 and the absolute of the difference was also required in its calculation. This is observed in table 7 and table 8. The Grey Relational Coefficient is thus calculated according to Equation 12 using the absolute deviation sequence values in table 8 from Equation 11 along with the maximum and minimum values of the absolute deviation table. The Grey Relational Coefficients can be observed in table 9. The Grey Relational Grade (GRG) which is used for the optimal ranking of the selected criteria was computed from Equation 13. GRG is computed by dividing the row sum of the Grey relational coefficients by the number of criteria (n). The GRG was then expressed in terms of percentage by finding the column total and dividing each corresponding grade by the column total and then the results was multiplied by 100. Figure 5 is the Geology map of the study area. The northwestern areas are characterized by Kawere conglomerates, south eastern areas are noted with banket rocks whiles the middle belt are lined with quartzites, phyllites and Sandstones.The lithology and geology of the study area were considered in siting a suitable landfill site. Some properties of the soil help in the decaying process of the waste materials while some does not and not suitable for siting engineered landfill sites (Asante-Annor et al., 2018; Aboziah, 2016; Aysen, 2003; Budhu, 2011; Frost and Frost, 2014). According to Kwesi et al., (2020), the groundwater vulnerability model created for Tarkwa and its environs reveals that, the northern of Tarkwa and its surrounding communities are within the Tarkwaian system and has high to very high potential of contaminating surface and ground waters. Hence, not recommended for siting engineering landfills. Moreover, the southern of the area is found within the Birimian system and would have low potential of contaminating the aquifers.

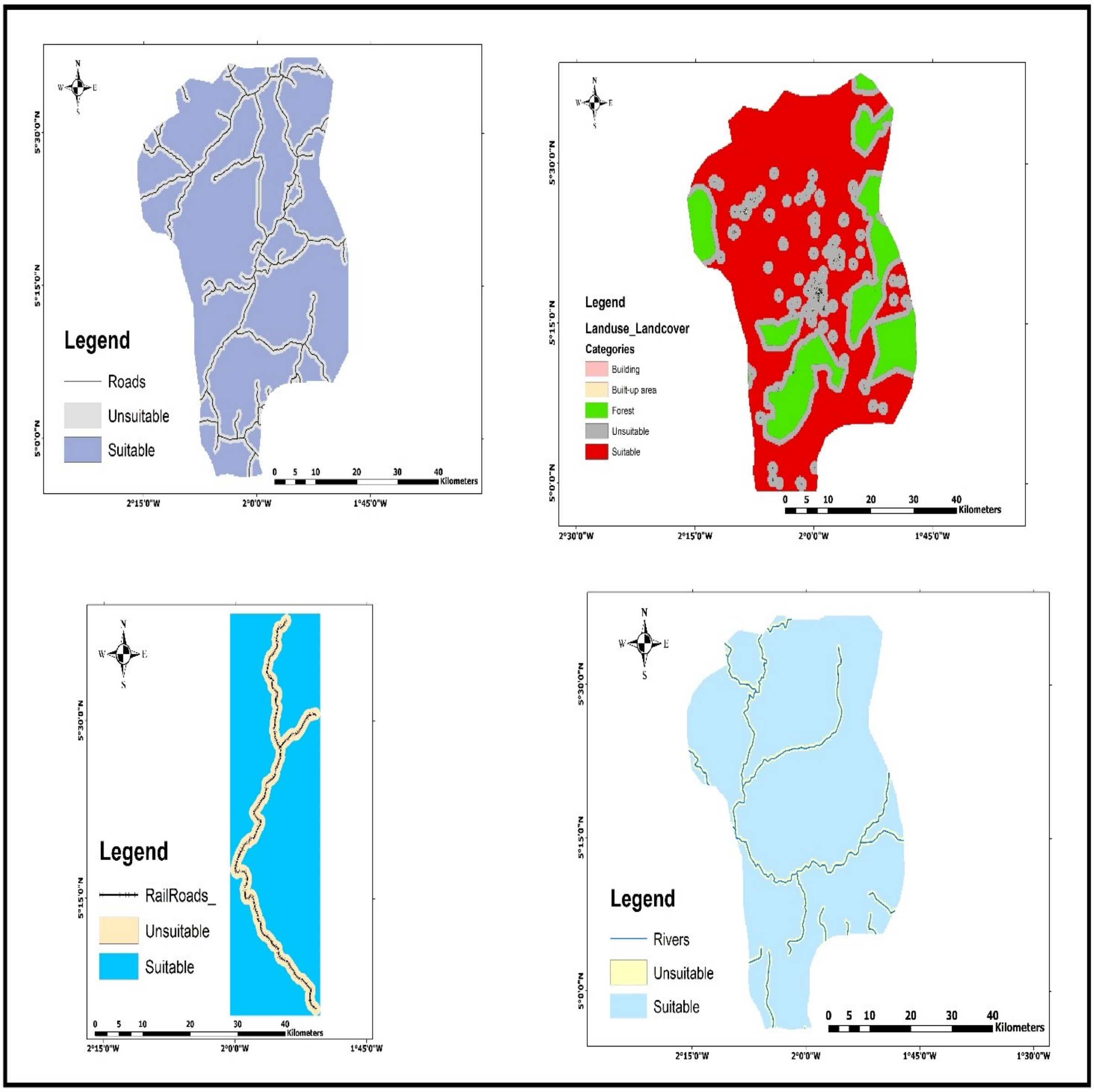

Figure 4: Restriction maps (roads, railroads, rivers, land use and land cover)

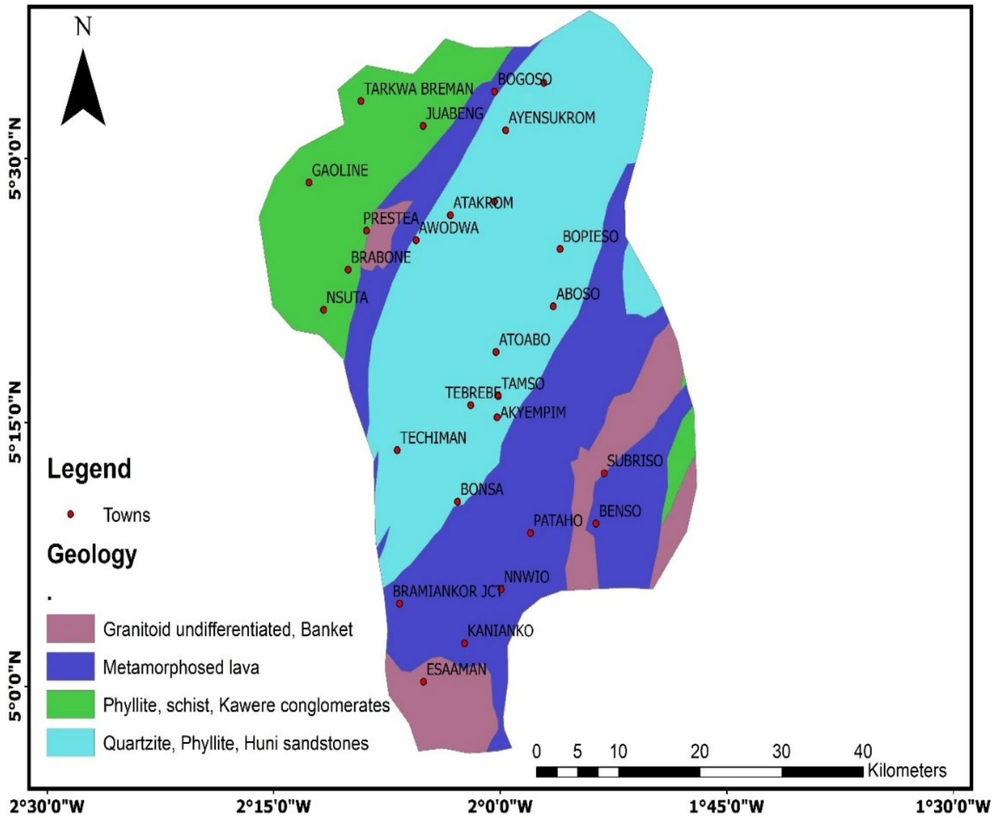

Figure 5: Geology map of the area

Table 6: A Pairwise Comparison Matrix of AHP in GRA

Criteria(n)	Transport Network	LULC	Slope	Geology	Waterbodies
Transport Network	1	1	2	2	2
LULC	**1**	1	1	2	2
Slope	**0.5**	**1**	1	1	2
Geology	**0.5**	**0.5**	**1**	1	1
Waterbodies	**0.5**	**0.5**	**0.5**	**1**	1
Max	**1**	**1**	**2**	**2**	**2**
Min	**0.5**	**0.5**	**0.5**	**1**	**1**

Table 7: Normalization Sequence Using GRA

Criteria(n)	Transport Network	LULC	Slope	Geology	Waterbodies
Transport Network	1	0	0	0	0
LULC	1	0	0.666667	0	0
Slope	0	0	0.666667	0.666667	0
Geology	0	1	0.666667	0.666667	0.666667
Waterbodies	0	1	1	0.666667	0.666667
Max	**1**	**1**	**1**	**0.666667**	**0.666667**
Min	**0**	**0**	**0**	**0**	**0**

Table 8: Absolute Deviation Sequence

Criteria(n)	Transport Network	LULC	Slope	Geology	Waterbodies
Transport Network	1	0	0	0	0
LULC	1	0	0.666667	0	0
Slope	0	0	0.666667	0.666667	0
Geology	0	1	0.666667	0.666667	0.666667
Waterbodies	0	1	1	0.666667	0.666667
max	**1**	**1**	**1**	**0.666667**	**0.666667**
min	**0**	**0**	**0**	**0**	**0**

Table 9: The Grey Relational Coefficients

Criteria(n)	Transport Network	LULC	Slope	Geology	Water bodies	GRG	**Weight (%)**	**Rank**
Transport Network	0.3333	1	1	1	1	0.867	26	1
LULC	0.3333	1	0.4286	1	1	0.7521	22	3
Slope	1	1	0.4286	0.3333	1	0.7524	23	2
Geology	1	0.3333	0.4286	0.3333	0.3333	0.4857	15	4
Water bodies	1	0.3333	0.3333	0.3333	0.3333	0.4667	14	5

Table 10: Landfill classes and Areas

Description	Area (Km^2)	Area (%)
Very Suitable	15	1
Suitable	247	10
Less Suitable	1486	59
Unsuitable	728	29
Very Unsuitable	19	1

The Digital Elevation Model is given by figure 6. Figure 7 is the slope map of the study area, ranging from 0° to 2.53°. The slope map was categorized into five (5) classes. Higher slope angles were found between 0.48° to 2.53° and the low to moderate angles were from 0° to 0.47°. Finally, the landfill suitability map was generated from the weight overlay of the various cost maps and the restriction surfaces based on the assigned optimal weights in the ArcGIS environment, represented in figure 8. The landfill suitability map was categorized into five (5) classes namely Very suitable, suitable, less suitable, unsuitable and very unsuitable areas for landfill site selection. Atuabo, Animakrom and Aboso were locations identified as very suitable for landfill sites. Suitable areas include Tarkwa, Atakrom and Awodwa. Less suitable areas comprise of Bonsa, Presta, Bogoso, Damang and Tamso. Subriso, Ningo, Nsuta, Huni Valley and Bopieso were among the unsuitable areas. Benso, Esikuma, Gaoline, Wassa Nkran are very unsuitable areas for landfill site selection. Table 10 represents the various classes and areas of the landfill suitability sites. The optimal areas for the landfill sites have a total area mass of 262 km^2 forming 11% of the total land mass. The less suitable zones recorded the highest area size of 1486 km^2 which is 59% of the study area. The Unsuitable zones recorded an area value of 747 km^2forming 30% of the total land mass. The evaluation and assessment of a new solid waste disposal site is a very complicated process as it requires considerable expertise in diverse social and environmental fields. This present study was based upon a set of key criteria such as slope, elevation, water bodies, land use and land cover, geology, transport network (railroads and roads) which were selected based upon thorough review of relevant literature and upon the already available knowledge from experts in the field of study. The development of a municipal solid waste landfill requires the acquisition of large tracts of land in its suitable siting of the landfill. Water bodies is one the major factor considered in siting a landfill area. The waste management observed by most of the residents in the study area is burning which can make the air unsafe for human breathing or by disposal into water bodies which can kill aquatic organism and making streams/rivers unsuitable potable drinking water since some waste contains toxic and heavy metals. This can also lead to an outburst of chronic diseases such as diarrhea, cholera, typhoid, dysentery, and many others. There is no human settlement around the green land areas, but some of the waste products are biodegradable products which can decompose and serve as organic materials which can enriched the soil and enhance plant growth. Excessive downpour of rainfall can lead to washing away solid waste to choked gutters which results in flooding and breeding grounds for mosquitoes. The road and railroads were considered to aid the collection and transportation of the solid waste. From the research findings of Asante et al., (2020), the proposed areas based on the geophysical and geotechnical investigations is suitable for the construction of engineered landfills as confirmed in this study.

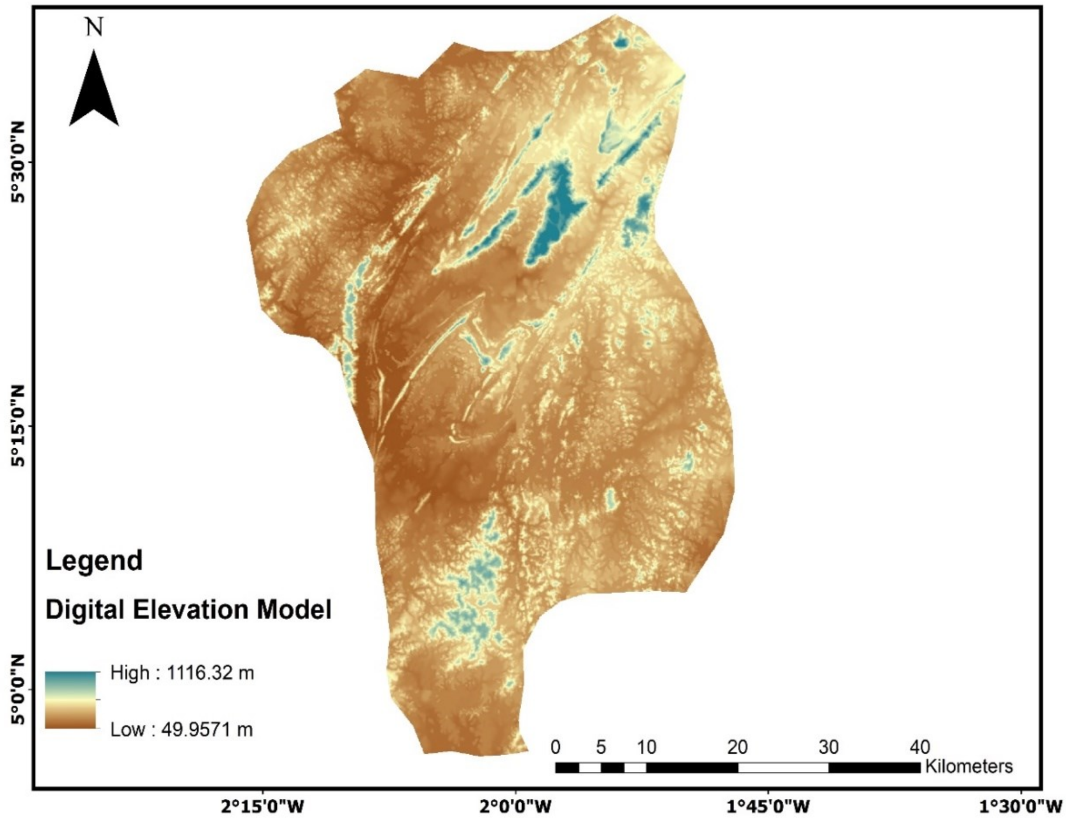

Figure 6: Digital Elevation Model of the area

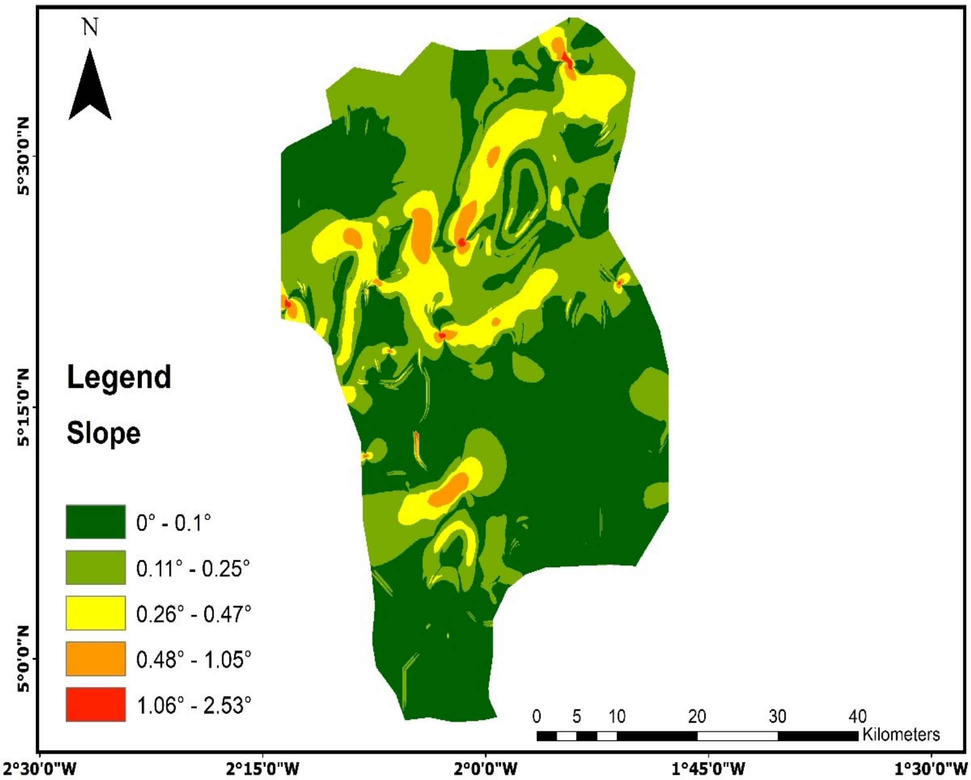

Figure 7: Slope map

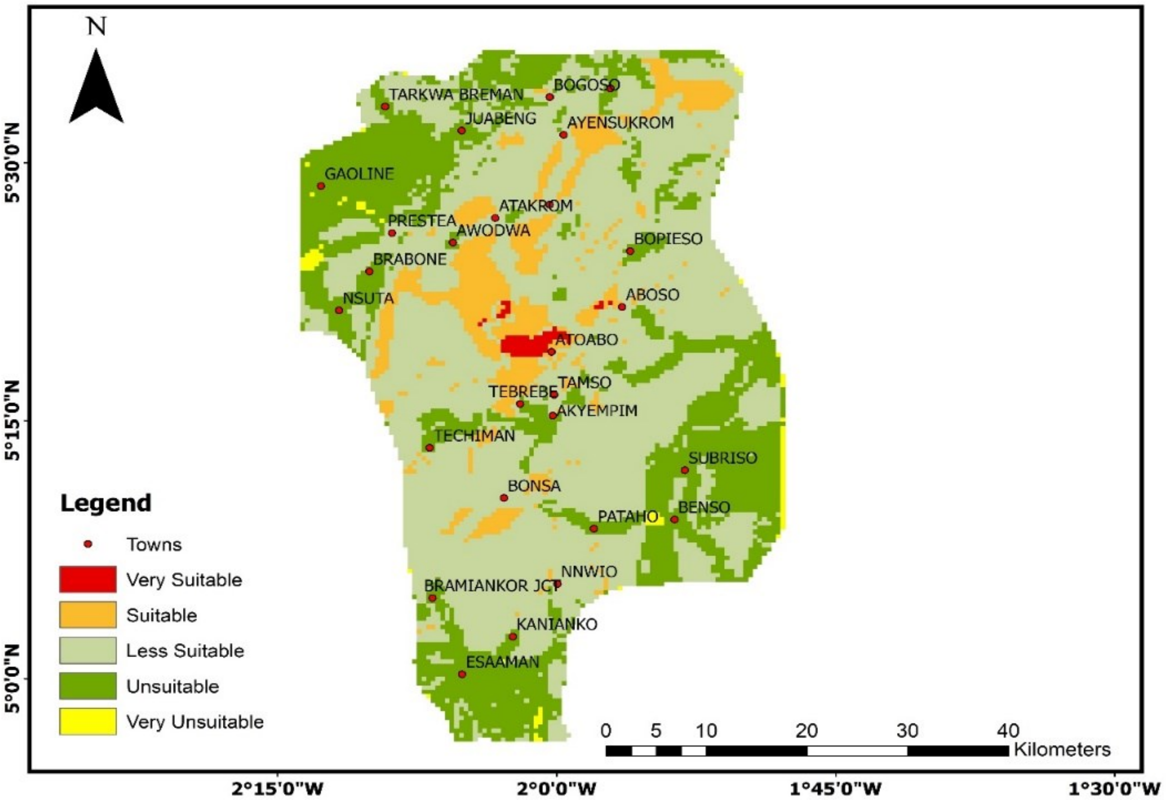

Figure 8: Landfill Suitability map

5. Conclusions and recommendations

Selecting a suitable landfill site is a very complicated process since it requires thorough knowledge about many criteria, set rules and standards, parameters and regulations. The objective of this present study was to select a suitable site for solid waste management for future planning and redevelopment of the study area. To determine the best suitable site for the study area, GIS and MCDA approach were adopted. Five criteria are discussed, compared and evaluated. The final optimal map was obtained by overlaying analysis and is reclassified into five (5) classes very suitable, suitable, less suitable, unsuitable and very unsuitable. The analysis revealed factors such as Transport Network, land use and land cover, geology, and slope are more important. This is because improper waste management and throwing of solid waste into water bodies can kill aquatic living organisms and small fingerlings in the water bodies. Also, it will make the water unpotable drinking water since some communities depend on these water bodies for drinking, farming and other domestic activities. Moreover, this can lead to outbreak of contagious diseases such as diarrhea, malaria, cholera, dysentery, typhoid fever, fellow fever, and many others. From the present study, it has been found that, some parts of the study area are suitable (about 11%) for siting landfill site and will produce less hazards to the environment, 59% were less suitable and 30% was not suitable. Aboso, Atuabo and Animakrom community was chosen as the best areas for construction of engineering landfill site with regards to drawing conclusion of previous studies at the moment. The study has revealed the spatial distribution for siting landfill in the study area for future planning purposes. The proximity analyses point to the fact that, some portions of the landfill areas are sited in an uncongenial environment and will therefore poses threat to the lives and water bodies within their vicinity. The study has again demonstrated the usefulness of MCDA, AHP, GRA and GIS tools in solving spatially related pertinent problem.

It is recommended that the suitability map produced for the study area should be used and further environment impact assessment should be carried out by the authorities to assess the significant impacts the sited areas have on the environment. It is also recommended that site suitability analyses be incorporated in the Town and Country Department's planning scheme for future development and policy formulation. Measures should be put in place to enforce the set standards and prosecute offenders to bring sanity to the environment. Also, it is recommended that this study should be replicated in other parts of the country or be adopted for future redevelopment of the study area. Moreover, for future studies groundwater quality map assessment, soil chemical testing, socio economic impact of the proposed selected area, aspects and drainage information, geomorphological map and hydrogeological map be produced by the Geological and Survey Department of Ghana for the study area. This will help in analyzing and evaluating the groundwater quality heavy metals analysis because of disposing solid and liquid waste to unsuitable areas.

Acknowledgements

The authors would like to recognize the anonymous reviewers for their helpful comments that made this piece of knowledge a better one. We also thank the Survey and Mapping Division Department of the Lands Commission of Ghana for providing us with data that was used in the investigation of the research findings.

References

Aboziah, R. A. (2016). Landfill Site Selection for Solid Waste Disposal Using Geographical Information System (GIS) and Multi-Criteria Approach in the Tarkwa Nsuaem Municipality, Ghana. Published MSc Thesis, Department of Environmental Science, College of Science, Kwame Nkrumah University of Science and Technology, Kumasi, Ghana, 1-93.

Abujayyab, S. K. M., M.S.S. Ahamad, A.S. Yahya, S.Z. Ahmad, and H.A. Aziz (2017). Automating an integrated spatial data-mining model for landfill site selection, Proceedings of the International Conference of Global Network for Innovative Technology and AWAM International Conference in Civil Engineering, Malaysia, 130001-130009.

Ademola, S.A., K.A. Stephen, and M.K. Charles (2012). Assessment of solid waste management in Tarkwa Municipality Ghana: Time series approach, Journal of Environment and Earth Science, 2(10), 135-147.

Akay, A. E., and A. Erdogan (2017). GIS-based multi-criteria decision analysis for forest fire risk mapping, ISPRS Annals of the Photogrammetry, Remote Sensing and Spatial Information Sciences, Vol. IV-4/WA, 2017 4th International GeoAdvances Workshop, 14-15 October 2014, Safranboln, Karabuk, Turkey, 25-30.

Akay, A. E., and B. Yilmaz (2017). Using GIS and AHP for planning primer transportation of forest products, ISPRS Annals of the Photogrammetry, Remote Sensing and Spatial Information Sciences, Vol. IV-4/WA, 2017 4th International GeoAdvances Workshop, 14-15 October 2014, Safranboln, Karabuk, Turkey, 19-24.

Aksoy, E., and B.T. San (2016). Using MCDA and GIS for landfill site selection: Central districts of Antalya Province, The International Archives of the Photogrammetry, Remote Sensing and Spatial Information Sciences, Volume XLI-B2, 2016 XXIII ISPRS Congress, 12-19 July 2016, Prague, Czech Republic, 151-157.

Akyen, T., C.B. Boye, and Y.Y. Ziggah (2016). Municipal solid waste estimation and landfill lifespan prediction, 4th UMaT Biennial International Mining and Mineral Conference, Tarkwa, Ghana, GG127-133.

Asante-Annor, A., S.A. Konadu, and E. Ansah (2018). Determination of potential landfill site in Tarkwa area using multi-criteria GIS, geophysical and geotechnical evaluation, Journal of Geoscience and Environment Protection, 6, 1-27.

Aslani, M., and A.A. Alesheikh (2011). Site selection for small gas stations using GIS, Scientific Research and Essays, 6(15), 3161-3171.

Aysen, A. (2003). Problem Solving in Soil Mechanics. A. A. Balkema Publishers, Lisse, Abingdom, Exton (PA), Tokyo, Japan, 1-77.

Bilgilioglu, S. S., and B.B. Bilgilioglu (2017). Selection of suitable site for municipal solid waste disposal sites for the Aksaray, (Turkey) using AHP and GIS Methods, Journal of Scientific and Engineering Research, 4(11), 36-45.

Boye, C. B., M.S. Peprah, and N.K. Kodie (2018). Geographic assessment of telecommunication signals in a mining community: A case study of Tarkwa and Its Environs, Ghana Journal of Technology, 2(2), 41-49.

Budhu, M. (2011). Soil Mechanics and Foundations. 3rd Edition, John Wiley and Sonc, Inc., USA, pp. 1-43.

Daneshvar, R., L. Fernandes, M. Warith, and B. Daneshfar (2005). Customizing ArcMap interface to generate a user-friendly landfill site selection GIS tool, Journal of Solid Waste Technology and Management, 31(1), 1-12.

Djokanovic, S., B. Abolmasov, and D. Jevremovic (2016). GIS application for landfill site selection: A case study in Pancevo, Serbia, Bulletin of Engineering Geology and the Environment, 75, 1273-1299. https://doi.org/10.1007/s10064-016-0888-0.

Environmental Protection Agency (EPA) (2002). Ghana Landfill Guidelines, Environmental Protection Agency Unit, Accra, Ghana, 1-81.

Ewusi, A., and J.S.Y. Kuma (2014). Groundwater assessment for current and future water demand in the Daka Catchment, Northern Region, Ghana, Natural Resources Research, 23, 355-365.

Frost, B. R., and C.D. Frost (2014). Essentials of Igneous and Metamorphic Petrology. Cambridge University Press, UK, 1-40.

Joe-Asare, T., M.S. Peprah, and M.M. Opoku (2018). Assessment of the potability of underground water from a small-scale underground mine: A case stud, Ghana Mining Journal, 18(2), 61-67.

Kao, J.J. and H.Y. Lin (1996). Multifactor spatial analysis for landfill siting, Journal of Environmental Engineering, 122(10), 902-908.

Kortatsi, B. K. (2004). Hydrochemistry of Groundwater in the Mining Area of TarkwaPrestea, Ghana. Published PhD Thesis, University of Ghana, Legon-Accra, Ghana, 1-45.

Kumi-Boateng, B., and M.S. Peprah (2020). Modelling local geometric geoid using soft computing and classical techniques: a case study of the university of mines and technology (UMaT) local geodetic reference network, International Journal of Earth Sciences and Knowledge Applications, 2(3), 166-177.

Kwesi, E.A.A., K.N. Asamoah, F.A. Arthur, and J.A. Kwofie (2020). Mapping of ground water vulnerability for landfill site selection assessment at the district level – a case study at the Tarkwa Nsuaem Municipality of Ghana, Ghana Journal of Technology, 4(2), 57 - 65.

Kwesi, E.A.A., L.C. Horror and J.K. Annan (2018). Provision of sanitation maps for improving waste management and sanitation at the district level: case study in the Tarkwa Nsuaem Municipality of Ghana, Conference Proceedings, 5th UMaT Biennial International Mining and Mineral Conference, 1st – 4th August, 2018, UMaT, Tarkwa, Ghana, 15- 20.

Larbi, E. K., C.B. Boye, and M.S. Peprah (2018). A GIS approach in optimal route selection in the mining communities using the analytical hierarchy process and the least cost path analysis, 5th UMaT Biennial International Mining and Mineral Conference, GLM 50-62.

Lokhande, T.I., S.J. Mane, and S.T. Mali (2017). Landfill site selection using GIS and MCDA methods: A review, International Journal of Research in Engineering Science and Technology (IJRESTS), 3(3), 25-30.

Malczewski, J. (1999). GIS and Multicriteria Decision Analysis. John Wiley and Sons, New York, 1-40.

Malczewski, J. (2004). GIS-based Land-use Suitability Analysis: A Critical Overview. Progress in Planning, 62(1), 3-65.

Mat, N.A., A.M. Benjamin, and S. Abdul-Rahman (2017). a review on criteria and decision-making techniques in solving landfill site selection problems, Journal of Advanced Review on Scientific Research, 37(1), 14-32.

Meshram, S.G., E. Alvandi, V.P. Singh, and C. Meshram (2019). Comparison of AHP and Fuzzy AHP models for prioritization of watersheds, Soft Computing,1-12.

Myers, J. H., and M.I. Alpert (1968). Determinant buying attitudes: meaning and measurement, Journal of Marketing, 32, 13-20.

Njoku, C.G., and A.O. Alagbe (2015). Site suitability Assessment of Petrol Filling Stations (PFSs) in Oyo Town, Oyo State, Nigeria: A Geographic Information Systems (GIS) approach. IOSR Journal of Environmental Science, Toxicology and Food Technology (IOSR-JESTFT), 9(12), 8-19.

Peprah, M. S., and I.O. Mensah (2017). Performance evaluation of the Ordinary Least Square (OLS) and Total Least Square (TLS) in adjusting field data: an empirical study on a DGPS data, South African Journal of Geomatics, 6(1), 73-89.

Peprah, M.S., C.B. Boye, E.K. Larbi, E. K., and P. Opoku Appau (2018). Suitability analysis for siting oil and gas filling stations using multi-criteria decision analysis and GIS approach – A case study in Tarkwa and its Environs, Journal of Geomatics, 12(2), 158-166.

Peprah, M.S., Y.Y. Ziggah, and I. Yakubu (2017). Performance evaluation of the Earth Gravitational Model (EGM2008) – A case study, South African Journal of Geomatics, 6(1), 47-72.

Ramanan, G., and E.R.J. Dhas (2017). Response surface modelling and grey relative analysis to optimize the wire edm machining parameters with multiple response characteristics, International Journal of Control Theory and Applications, ISSN:0974-5572, 27(10).

Saaty, T. L. (1977). A scaling method for priorities in hierarchical structures, Journal of Mathematical Psychology, 15, 234-281.

Saaty, T. L. (1980). The Analytic Hierarchy Process: Planning, Priority Setting, Resource Allocation. McGraw-Hill, New York, USA, 641-658.

Sara, R.G., C. Christine, G. Donn, and J. Brad (2011). The Benefits of Using Geographic Information Systems as a Community Assessment Tool. Public Health Reports, 126(2), 298-303.

Seidu, J., and A. Ewusi (2018). Assessment of groundwater quality using hydrogeochemical indices and statistical analysis in the Tarkwa Mining area of Ghana, Journal of Environmental Hydrology, 26, 1-15.

Sener, S., E. Sener, B. Nas, and R. Karaguzel (2010). Combining AHP with GIS for landfill site selection: a case study in the lake Beysehir catchment area (Konya, Turkey), Waste Management, 30, 2037-2046.

Spigolon, L.M.G., M. Giannotti, A.P. Larocca, M.A.T. Russo, and N.D.C. Souza (2018). landfill siting based on optimisation, multiple decision analysis, and geographic information system analysis, Waste Management & Research, 36(7), 606-615. https://doi.org/10.1177/0734242X18773538.

Sumathi, V.R., U. Natesan, and C. Sarkar (2008). GIS-based approach for optimized siting of municipal solid waste landfill, Waste Management, 28, 2146-2160.

Tah, D.S. (2017). GIS-based locational analysis of petrol filling stations in Kaduna Metropolis, Science World Journal, 12(2), 8-13.

Thapa, S. and R. Engelken (2020). Optimization of pelleting parameters for producing composite pellets using agricultural and agro-processing wastes by taguchi grey relational analysis, Carbon Resources Conversion, doi: https://doi.org/10.1016/j.crcon.2020.05.001.

Wind, Y., and T.L. Saaty (1980). Marketing applications of the analytic hierarchy process, Management Science, 26(7), 641-658.

Yakubu, I., D. Mireku-Gyimah, and A.A. Duker (2015). Review of methods for modelling forest fire risk and hazard, African Journal of Environmental Science and Technology, 9(3), 155-165.

Yal, G. P., and H. Akgun (2013). Landfill site selection and landfill liner design for Ankara, Turkey, Environmental Earth Sciences, 70, 2729-2752.

Zhao, X., and T. Liang (2008). The supplier evaluation model based on the analytic hierarchy process and grey relative analysis process, International Conference on Automation and Logistics, doi:10.1109/1CAL.2008.4636531

Landslide susceptibility hazard prone areas identification using Multi-Criteria Decision Analysis (MCDA) and GIS techniques: A case study of Tarkwa and its environs

B. Kumi-Boateng*, M. S. Peprah, E. K. Larbi
University of Mines and Technology, Tarkwa, Ghana
*Email: kumi@umat.edu.gh

(Received: June 27, 2020; in final form: Oct. 29, 2020)

Abstract: Landslide susceptibility hazard areas identification have become very necessary with regards to the assessment of landslide hazards and risks, preventing loss of lives and properties, casualties and economic cost to the nation. Landslide management is one of the key components in hazard and risk assessment, crisis management and land use planning. In the past and recent years, numerous studies have utilized Geographic Information System (GIS) and Remote Sensing (RS) techniques as an effective tool for landslide disaster mapping and mitigation. The objective of the present study is to generate a landslide hazard prone area map for the study area through a Multi-Criteria Decision Analysis (MCDA) and GIS approach. The geo-environmental causative factors used in this study is a secondary data obtained from the Survey and Mapping Division Department of the Lands Commission of Ghana which comprise of a topographical and soil maps from which geology, slope, land use and land cover, water bodies, and roads were extracted and used in the research investigation analysis. The precipitation data used in this study was downloaded from the World climate website (https://www.worldclim.org/data/index.html), which happens to be a six-year annual data (from 2012 to 2018) with a resolution of 1km^2. ESRI ArcGIS software (ArcMap) was used for processing and analyzing the data to delineate the area into various hazard classes based on their degree of susceptibility to slope failures. The data analysis involves an improved quantitative and qualitative method of weightages and overlaying techniques. In this study, the Analytical Hierarchy Process (AHP) mathematical procedure was adopted to assign rankings and weights for ArcGIS analysis. Rankings and weightages were assigned based on experts' knowledge and review of relevant literature. The computed consistency ratio was 0.10, which implies the assigned weights were consistent. The results achieved in this study revealed that, the highly susceptible areas were found to be in Atoabo, Awodwa Nkwanta, Bonsa, Prestea, Aboso, Bogoso, Animakrom, Tarkwa, Teberebe and Akyempim These areas requires much attention to prevent any future landslides. This study has provided a proposed optimal raster map for future redevelopment and planning of the study area. It is recommended that; the Geological and Survey Mapping Division, Survey and Mapping Department, and Meteorological Department of Ghana produce a detailed geomorphological map, aspect map, and rainfall map of the various high-risk areas that will help in future studies in reviewing more relevant information to help mitigate future landslides.

Keywords: Analytical Hierarchy Process; Geographic Information System; Geomorphology; Hazard Mapping; Landslide Susceptibility

1. Introduction

Landslide studies have become obligatory, drawing the attention of many researchers globally mainly due to increasing community awareness of its socio-economic impacts and also increasing pressure of urbanization in mountainous environments (Chaturvedi and Dutt, 2018; Kanungo et al., 2006). It has high potential hazard of natural blockages such as mountainous lakes, dams, rivers caused by earth tremors, earthquakes, flooding and anthropogenic activities (Tanyas, 2019; Strom, 2010). Additionally, landslides cause extensive damages to economic properties, agriculture, transportation, land use, life, and economic cost to the nation (Chaturvedi and Dutt, 2018). Landslide is the second most frequent natural catastrophic occurring geological events after hydro meteorological event occurrences (Kouli et al., 2014). Hence, identification of landslide prone areas plays an important role in preventing and minimizing their impacts on the environment.

Landslide hazard assessment and risk reduction can be achieved by providing risk managers, governmental agencies and community people with easily accessible, continuous, and accurate information about their occurrence in spatial and nonspatial context. Thus, an accurate susceptibility mapping can be the key information for a large variety of users such as from both private and public sectors, from governmental and non-governmental departments and the geoscientific community (Kouli et al., 2014). Several physical factors such as ground slope, soil depth, rainfall, land development and other man-made anthropogenic activities may lead to the occurrence of extreme natural events like landslides (Chaturvedi and Dutt, 2018).

The study area is situated within the main tropical rainforest of Ghana that records the highest rainfall in Ghana with average annual precipitation of 1696 mm (Larbi et al., 2018) and few dry seasons. Upon carefully reviewing of existing literatures concerning the study area, there is no existing studies on landslides for the area at the moment and this motivated the researchers to embark on this study. Hence, the prioritization and assessment of landslide for the area under study is a crucial step towards the mitigation of menace and for proper future planning by decision makers and planners.

The geophysical and geotechnical investigational analysis were not considered due to unavailability of geophysical tools and seismic data for the study area. The study area host several large scale, medium scale and small scale mining operations with few reports of falling rocks during their operations but these mining activities contribute significantly to the national income of the country (Boye et al., 2018).There is a good network of water bodies such as rivers and streams, notable among them are river Bonsa, Tano and Ankobra. There are two main rainfall regimes: thus; March to July and September to early December and the dry season starts from October to February. The interplay of heavy rainfall and soil types find expression in the vegetation cover. The semi deciduous forest is found in the northern part while the tropical rainforest is to the south where rainfall is heaviest (Larbi et al., 2018). Geographically, the lands are generally undulating with steep slopes parallel to each other and to the strike of the rocks in the North south direction with several hills making farming and other developmental activities a bit stressful (Joe-Asare et al., 2018; Kortatsi, 2004). The area is found within the main gold belt of the Republic of Ghana that stretches from Axim in the Southwest direction, to Konongo in the Northeast direction (Kortatsi, 2004; Asklunel and Eldvall, 2005). The average annual temperature is 26˚C with small daily temperature variations. Relative humidity varies from 61 % in January to a maximum of 80 % in August and September (Peprah and Mensah, 2017). A detailed geology of the place can be found in the work of (Asante-Annor et al., 2018).

Assessment of landslide hazard therefore requires knowledge about a large series of data, ranging from geological structure to land use. Many studies have proposed various techniques in landslides assessment as presented in the works of (Samia et al., 2018; Kouli et al., 2014; Umar et al., 2014; Westen et al., 1999). In this present study, a probabilistic approach based on the observed relationships between each conditioning factor and the distribution of landslide was adopted. Hazard map will depict areas likely to have landslides in the future by correlating some of the principal factors that may contribute to landslides. Geographic Information System (GIS) is an efficient technique for landslide modelling and are also capable of identifying suitable and unsuitable areas for developmental projects (Umar et al. 2014). GIS techniques have allowed numerous researchers to come up with different empirical models for landslide susceptibility modelling and prediction (Samia et al., 2018) and have been applied in landslide mapping as presented in the following literatures (Umar et al., 2014; Shahabi et al., 2012; Kanungo et al., 2006; Westen et al., 2000; Westen et al., 1999). In addition, direct geomorphological mapping, heuristic approaches and quantitative statistical models have all been applied in landslide susceptibility modelling and prediction.

A Multi-Criteria Decision Analysis (MCDA) and GIS techniques were adopted in landslide susceptibility hazard prone areas mapping in spatial context using geo-environmental causative factors such as land use and land cover, geology, slope, roads, precipitation and water bodies data. MCDA and GIS are very relevant tool for solving problems which have a hierarchy process in spatial context (Peprah et al., 2018) because various decision variables can be evaluated and weighted according to their relative importance to achieve the final optimal solution (Broekhuizen et al., 2015; Kihoro et al., 2013). In addition, MCDA has the ability to judge qualitative criteria along with quantitative criteria (Boroushaki and Malczewski, 2008). Moreover, it is simple to understand, easy to implement, modify and suitable for problems which have a hierarchical framework (Aslani and Alesheikh, 2011). Furthermore, a proposed hazard risk map of the study has been produced for showing areas suitable and unsuitable for developmental projects and human settlement.

2. Study area

The study area (Figure 1a to 1c) is located at the mid-southern part of the Western Region of the Republic of Ghana with geographical location between longitude 001° 50′ 00″ W to 002° 20′ 00″ W and latitude 005° 00′ 00″ N to 005° 40′ 00″ N. The area has average topographic altitude of about 78 m above mean sea level (MSL) (Peprah et al., 2017). The type of coordinate system used in the study area is the Ghana projected grid derived from the Transverse Mercator 001° North West (NW) and the World Geodetic System 1984 (WGS84) (Universal Transverse Mercator (UTM) Zone 30 North (N)) (Kumi-Boateng and Peprah, 2020; Yakubu et al., 2018). The horizontal geodetic datum of the study area is the War Office 1926 ellipsoid, and the vertical datum is the MSL which approximate the geoid (Kumi-Boateng and Peprah, 2020; Peprah et al., 2017). Figure 1a to 1c show the study area maps respectively.

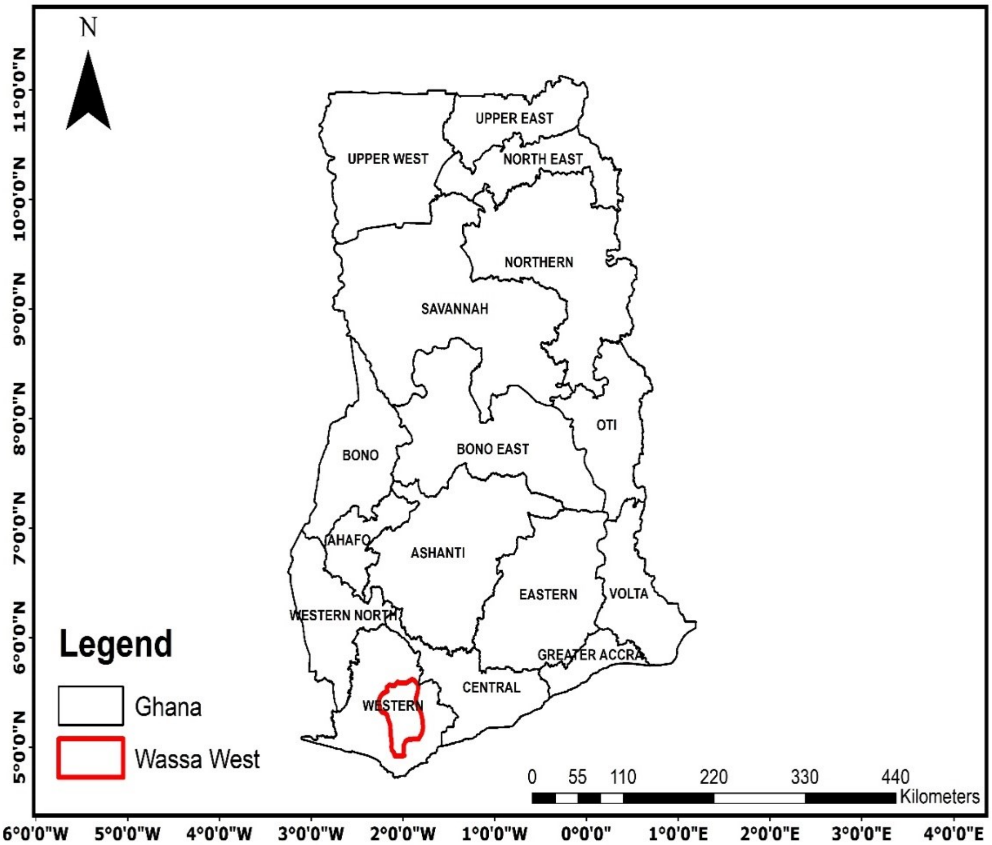

Figure 1a: Regional Map of Ghana showing the study area

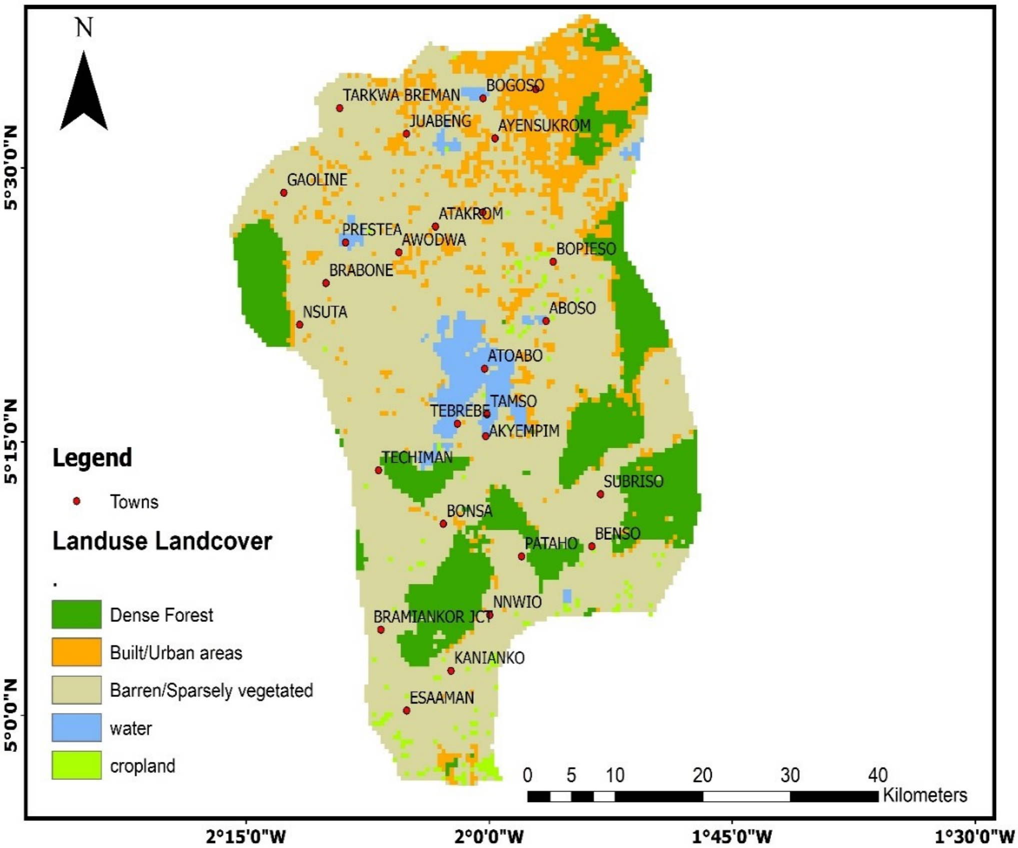

Figure 1b: Map of study area

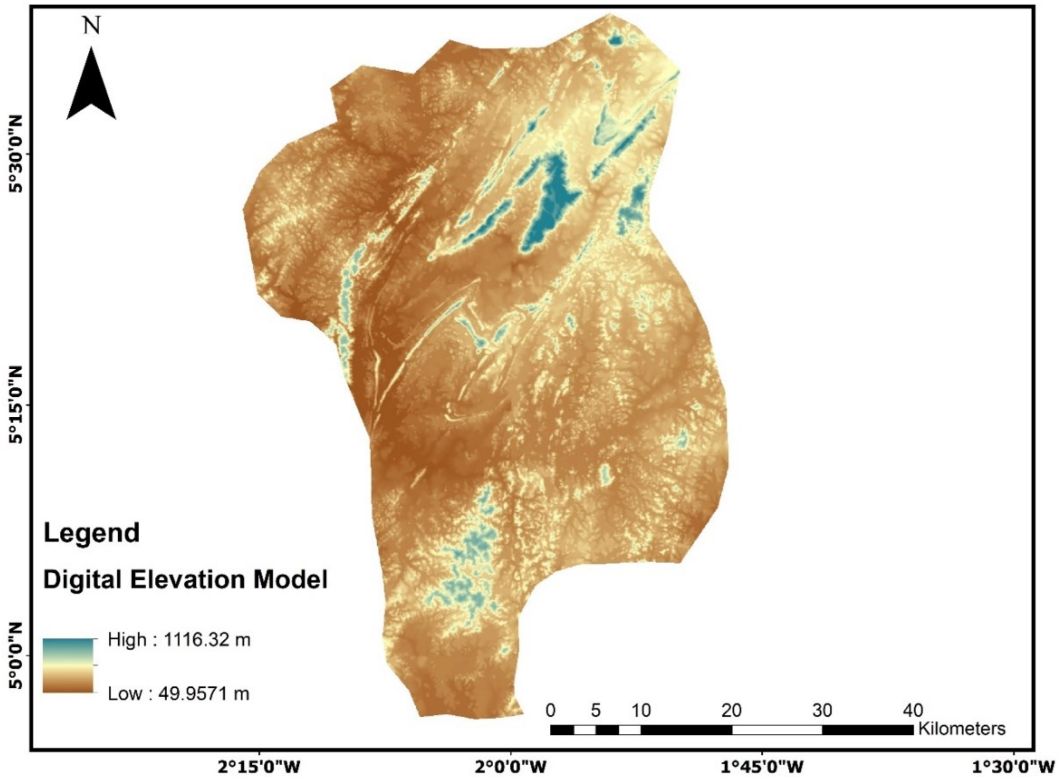

Figure 1c: Digital Elevation Model of the study area

3. Resources and methods used

3.1 Resources

The data used for the study comprise of a secondary data obtained from the Survey and Mapping Division Department of the Lands Commission of Ghana. The data consist of topographical and soil maps from which geo-environmental features such as land use and land cover, roads, geology, slope, and water bodies of the study area were extracted and used in the research investigation analysis. The precipitation data was downloaded from the Worldclimate website, https://www.worldclim.org/data/index.html.

3.1.1 Defining the relative importance of each causative factor considered

In the current study, six different causative factors defined in Section 3.1 were used. Different thematic maps of the factors considered were generated in ArcGIS environment to produce the final optimal susceptibility map.

Road factor

Road plays a vital role in landslide studies as a triggering factor for landslides occurrences. Conversely, road construction involves extensive excavations of load materials which leads to static and dynamic loads, vegetation removal, and many others along natural and engineered slopes (Kouli et al., 2014). This disturbs the natural channel which increase anthropological instability (Khadka et al., 2018). This factor was considered in the design of the landslide susceptibility map by creating a road network buffer zones to show areas more suitable and less suitable. Minimum buffer distance of 300 m and maximum buffer distance of 500 m were created in ArcGIS environment to produce different classes. The road was considered for the susceptibility as it influences to cause landslide. Since, the major occupation in the study area is mining and farming, there is huge pressure on the existing road. This is because, the railroads which serves as alternative means of route for transporting haul materials and foodstuffs have been broken down (Larbi et al., 2018) creating pressure on the existing road and gets damaged in no time. This cause for repairing, patching, and creating alternate routes to ease pressure on the existing roads. The construction process involves the removal and excavations of raw materials that can lead to landslide occurrences.

Slope

Slope is one of the most important factors to be considered in landslide susceptibility mapping and a fundamental part of hazard assessment model creation (Kouli et al., 2014). Per the reports from previous studies, slope with angles $> 20^o$ has high influence in the landslide susceptibility mapping (Khadka et al., 2018). The slope of the study area was reclassified into various classes as fair slope, moderate slope, steep slope, and very steep slope. Also, is very useful to reclassify the relief of the study area and locating minimum and maximum heights within terrains which may have direct or indirect relationships to cause the landslide and weathering phenomena which is the factor of sliding closely in relation to the altitude (Khadka et al, 2018). The general topography of the study area is undulating with steep slopes which makes some areas very unsuitable and prone to landslide hazards. There is a growing recognition that an understanding of geomorphology can greatly improve environmental outcomes particularly for areas that have been subjected to large-scale earth movement (Hancock et al., 2019).

Geomorphology of the area is an important factor for hazard assessment and in mountainous areas since it plays an important role in the analytical analysis and assessment (Cellek, 2018; Mountjoy and Micallef, 2018). Most rock types also have the properties to undergo physical and chemical weathering (Aysen, 2003; Budhu, 2011; Frost and Frost, 2014).

Geology
Geology and Soil types are one of the strong causative factors that influences the occurrences of landslides. Geographically, the study area environs lie within the mountainous regions covered by thick forest and interjected by undulating terrain with few scarps (Boye et al., 2018). The topography is generally described as series of ridges and valleys. The ridges are formed by the Banket and Tarkwa Phyllites whereas upper Quartzite and Huni Sandstones are present in the valleys (Peprah and Mensah, 2017). Surface gradients of the ridges are generally very close to the Banket and Tarkwa Phyllites (Peprah et al., 2017). The study area is within regions where geologically some parts are strong, and others are weak and fragile. A detailed review of the geological information is presented in the work of (Asante-Annor et al., 2018).

Precipitation data
High precipitation is the main causative factor constituting the triggering of landslides occurrences. In this study, precipitation data (Tropical Rainfall Measuring Mission) over a period of 6 years (2012 to 2018) from the Worldclimate website (https://www.worldclim.org/data/index.html) was downloaded in raster format. The downloaded data had a resolution of 1 km^2 which was later resampled to 150m by 150m resolution in the ArcGIS environment. The particular precipitation data covering the entire study area was extracted and used for the research analysis. The average annual precipitation of the study area is 1200 mm.

Water bodies
Water bodies are also one of the major causative factors of landslides. Fluvial erosion as a result of flooding caused by excessive intensive rainfall is one of the most common triggering conditioning factors of the landslides and usually affects the slope toe (Kouli et al., 2014). In this current study, proximity analysis of the water bodies was done by creating buffer zones around the water bodies with a minimum and maximum distance of 300 m and 500 m respectively. The water bodies were considered since intensive erosion cause by the waves of the water bodies and severe rainfall can cuts the toe of the slopes in hilly terrains and involves in landslides (Cellek, 2018; Khadka et al., 2018). Previous studies reveal that, most landslides occurring worldwide follow periods of rainfall with much concern about the effects the climate change in some mountainous areas of which the study area happens to be a mountainous area (Sidle et al., 2019).

Land use and Land cover
This factor is one of the most important factor to be considered in decision making process since is the most commonly used human induced factor responsible for the occurrence of landslide (Silva and Sooriya, 2018). Land use and land cover data obtained from the Survey and Mapping Division Department consist of human settlement areas such as schools, market areas, hospitals, industries, banks, green lands, and many others. Vegetation is also related with the occurrence of landslides. The strong root system of the woody vegetation provides both hydrological and mechanical effects that stabilize soil slopes (Kouli et al., 2014). Moreover, landslides events occurring in woodlands are much less than those occurring in unvegetated or irrigated cultivated areas.

3.2 Methods used

3.2.1 Proximity analyses
Proximity analyses was carried out in ArcGIS environment to determine the spatial relationship of the major selective causative factors to their neighbouring features with respect to distances (Peprah et al., 2018; Sara et al., 2011). Moreover, proximity analyses allowed the selected features to be reclassified based on distance that meet the set criteria or standards (Aslani and Alesheikh, 2011; Njoku and Alagbe, 2015). Buffer analysis of roads and water bodies were done in ArcGIS environment to assess the study area which will be suitable or unsuitable for developmental projects.

3.2.2 Landslide susceptibility modelling
The hazard prone areas were obtained based on spatial analyses of the following dataset; slope, land use and land cover, roads, geology, precipitation data and water bodies. Each dataset is of varying importance in determining the hazard prone areas. Hence, the Analytical Hierarchy Process (AHP) based on pairwise comparisons was used to compute weights for each criterion. AHP is a multi-criteria decision approach and was first developed by Myers and Alpert (1968) and modified by Saaty (1977). The AHP which has proven to be a useful method for decision making analysis (Saaty, 1980), was used because this technique assess a set of evaluation criteria and search for the optimal solution among a set of alternative options (Politis et al., 2010; Sumi, 2010). The relative importance between two criteria was measured based on a numerical scale from 1 to 9 (Saaty, 1983). Figure 2 shows the flowchart of the MCDA. Figure 3 and 4 show the suitability and restriction model generated respectively for the landslide susceptibility map.

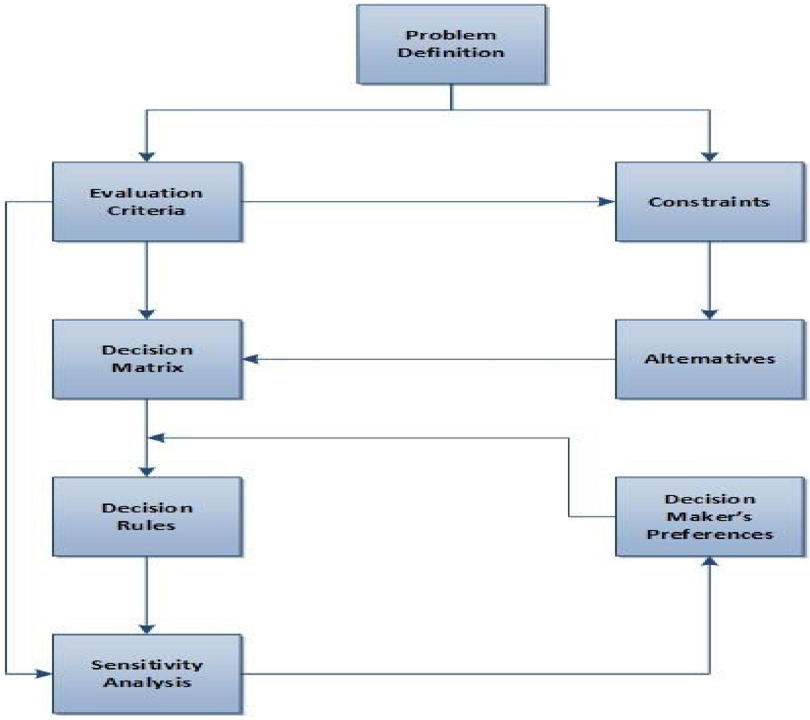

Figure 2: Flowchart of the MCA Process (Source: Yakubu et al., 2015; Malczewski, 1999)

3.2.3 Model generation

The varying degree of landslide susceptibility was generated in the ArcGIS environment according to Equation 1 given as (Peprah et al., 2018):

$$\beta = \sum_{i=1}^{n} w_i \times c_i \prod_{j=1}^{m} r_j \qquad (1)$$

where β is the susceptibility model; w_i is the calculated weight for each criterion; c_i is criteria set employed in the study; and r_j is the restriction factors. Table 1 is the AHP scale for pairwise comparison, table 2 is the random indices as proposed by Saaty, (1980) and table 3 is the restriction standards set for landslide susceptibility mapping.

Table 1: AHP Scale for Pairwise Comparison (Saaty, 1983)

Intensity of Importance	Definition	Explanation
1	Equal Importance	Two activities contribute equally to the objective
3	Weak importance of one over another	Experience and judgement slightly favour one activity over another
5	Essential or strong importance	Experience and judgement strongly favour one activity over another
7	Demonstrated importance	An activity is strongly favoured and its dominance is demonstrated in practice
9	Absolute importance	The evidence favouring one activity over another is of the highest possible order of affirmation
2,4,6,8	Intermediate values	When a compromise is needed
Reciprocals	If activity i has one of the above nonzero numbers assigned to it, when compared with activity j, the activity j has the reciprocal value when compared with i	

Table 2: Random Indices (Saaty, 1980)

Criteria (N)	1	2	3	4	5	6	7	8	9	10
Random Index (RI)	0	0	0.58	0.9	1.12	1.24	1.32	1.41	1.46	1.49

Table 3: Restriction standards for landslide susceptibility mapping

Restriction Source	Minimum Buffer Distance/Degree	Maximum Buffer Distance/Degree	Analysis Buffer Distance/Degree
Contours	0°	20°	≤ 20°
Roads	300 m	500 m	300 m
Water bodies	300 m	500 m	300 m

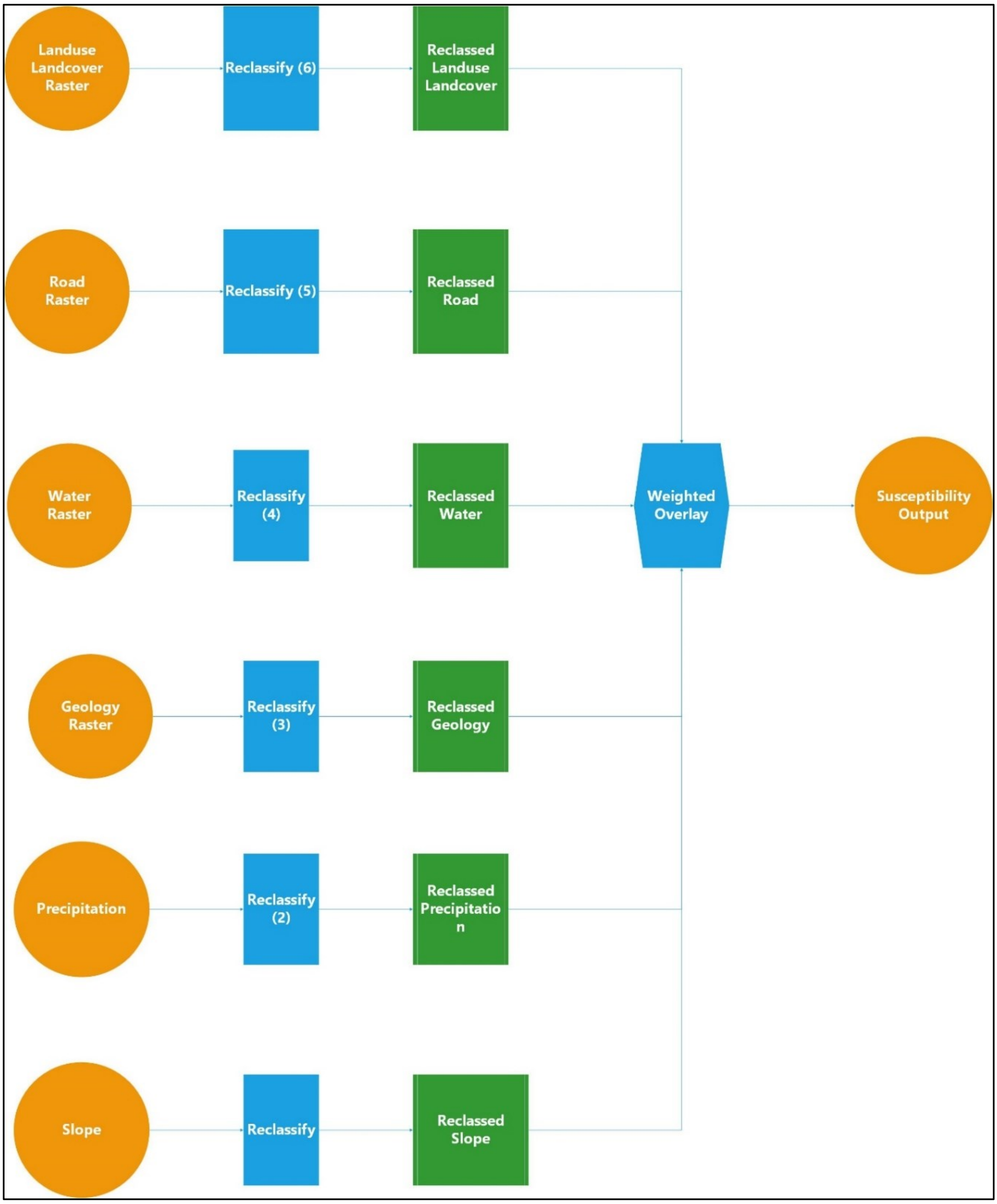

Figure 3: Susceptibility model

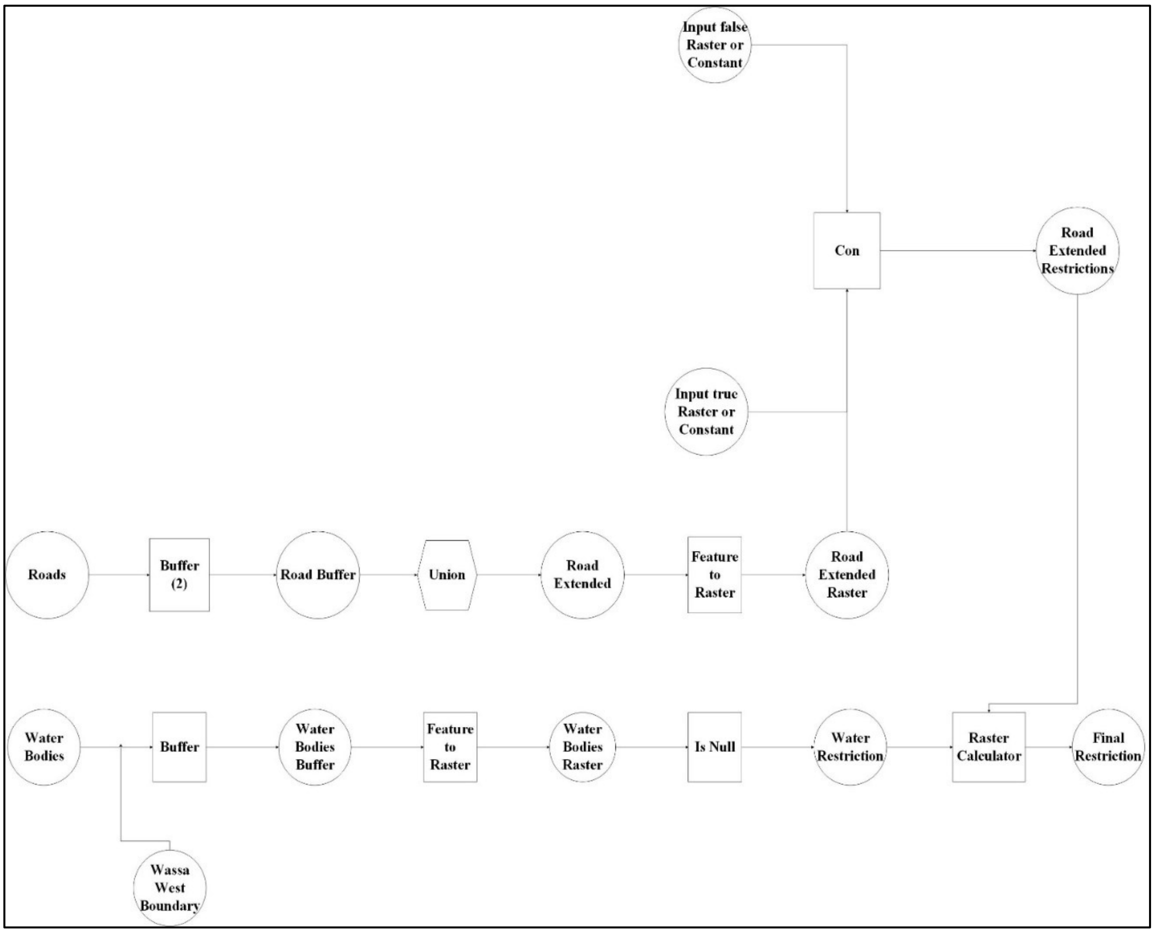

Figure 4: Restriction model

3.2.4 Analytical Hierarchy Process (AHP)

The weights of the selected geo-environmental variables were generated using the AHP. The purpose is to prioritize in hierarchical order the various alternatives used in the MCDA process (Meshram et al., 2019). From table 1, the scores were assigned to the linguistic variables using the pairwise comparison of the AHP according to their relative importance as shown in table 4. Higher scores are normally given when the criterion is of much importance than the other (Peprah et al., 2018; Akay and Yilmaz, 2017; Akay and Erdogan, 2017). The scores are then normalised to obtain their respective weights using their column sum as represented by Table 5.

3.2.5 Consistency check

A consistency check was carried out on the geo-environmental variables. This was to verify whether the threshold value as proposed by Saaty was not exceeded (Larbi et al., 2018). For consistency, the consistency ratio should not exceed $(CR \leq 0.10)$. The Consistency Ratio (CR) is obtained by dividing the calculated Consistency Index (CI) by its corresponding criteria Random Index (RI). First, the column weights are multiplied by the pairwise matrix to generate the weighted sum matrix given by Equation (2) as:

$$W_s = \begin{bmatrix} w_{11} & \cdots & w_{1n} \\ \vdots & \ddots & \vdots \\ w_{m1} & \cdots & w_{mn} \end{bmatrix} \tag{2}$$

where; W_s is the weighted sum matrix. The Consistency vector is calculated by dividing the weighted sum matrix by the criteria weights given by Equation (3) as:

$$C_v = \frac{1}{W_{ij}}(W_s) \tag{3}$$

where; C_v is the Consistency vectors; W_{ij} is the weights of the main variable. $\lambda_{\max}$ which is the average of the consistency vectors is calculated by Equation (4) given as:

$$\lambda_{\max} = \frac{\sum_{i=1}^{n} C_v}{n} \tag{4}$$

where; $\lambda_{\max}$ is the Average of the consistency vectors; n is the number of criteria. CI is calculated by Equation (5) as;

$$CI = \frac{\lambda_{\max} - n}{n-1} \tag{5}$$

CR which is the consistency ratio was then finally computed to know the consistency of the evaluations made for the pairwise comparison matrices. The smaller the value of this ratio, the better the assigned weights (Kihoro et al., 2013; Broekhuizen et al., 2015). This was calculated to prevent bias through criteria weighting according to Equation (6) given as:

$$CR = CI/RI \tag{6}$$

4. Results and discussion

The study aims at the identification of areas susceptible to landslide in the Wassa West district of Ghana using the AHP model. Six (6) set criteria were used in this study with its corresponding RI of 1.24. Table 4 displays the pairwise scores of the selected criteria of the AHP. These values were then normalised using their column sum to obtain the respective weights of the linguistic variables tabulated in Table 5. From Table 5, slope has the highest score of 24% whiles land use land cover recorded the least score of 12%. The scores of the criteria can be observed in decreasing order as; slope>geology> precipitation> water bodies> roads> land use land cover. In order for these weights to become optimal for its utilization, it must be consistent. For consistency to be achieved, the calculated CR should not exceed 0.10 thus, $(CR \leq 0.10)$. To check for consistency, the weighted sum matrix was formed according to Equation (2) by multiplying the weights by the pairwise matrix. The weighted sum was then divided by the criteria weights to obtain the consistency vectors according to Equation (3) and table 6. Therefore, CI is calculated according to Equation (5). The CR is obtained according to Equation (6) by dividing the CI by the RI. The CR obtained for this study was 0.09, which implies the scores assigned are not biased. Proximity Analysis was also performed by creating buffer zones around the various unsuitable areas as given in table 3. The buffer maps serve as a constraint maps that restrain unsuitable areas (hazard prone areas) from suitable areas (less hazard prone areas). The minimum and maximum buffer distances used for the study analysis can be seen in table 3 and were based on experts' advice. The analysis buffer distances for both roads and rivers were 300m. The suitable areas are those which are beyond the set distances and the unsuitable areas are those below the set distances. Figure 5 represents the Geology map of the study area. The northwestern areas are characterized by Kawere conglomerates, south eastern areas are noted with banket rocks whiles the middle belt are lined with quartzites, phyllites and Sandstones. The Land use and Land cover map of the study area is depicted by figure 6. Land use and land cover play important role with regards to instability of slopes and occurrences of landslides as recommended in available literatures (Silva and Sorriya, 2018; Kouli et al., 2014). The restriction map for the water bodies and roads is represented by figure 7 and figure 8 respectively. The study area is well known for mining activities such as small-scale mining, medium scale mining, and large-scale mining. These mining operations involves the removal of the top most soil, blasting, and drenching deep into the inner core to mine precious minerals. These can cause motion movement within the earth crust under the influence of gravity, as well as the operations by human activities and can result in landslides (Cadraku and Bejta, 2018). Majority of the land cover areas in the study area is covered by mining industries, forestland, and human settlement. Figure 9 is the slope map of the study area, ranging from 0° to 2.53°. The slope map was categorized into five (5) classes. Some of the slope angles were found between (0.48° to 2.53°) and were most vulnerable to cause landslides such as Bonsa, Atoabo, Tamso and Briamiankor JCT. Figure 10 represents the annual average precipitation map of the study area, ranging between 1598.28 mm to 923.224 mm within a period of six (6) years (2012 to 2018). Areas in the southern belt experiences more rainfall than those in the northern sectors of the study area.

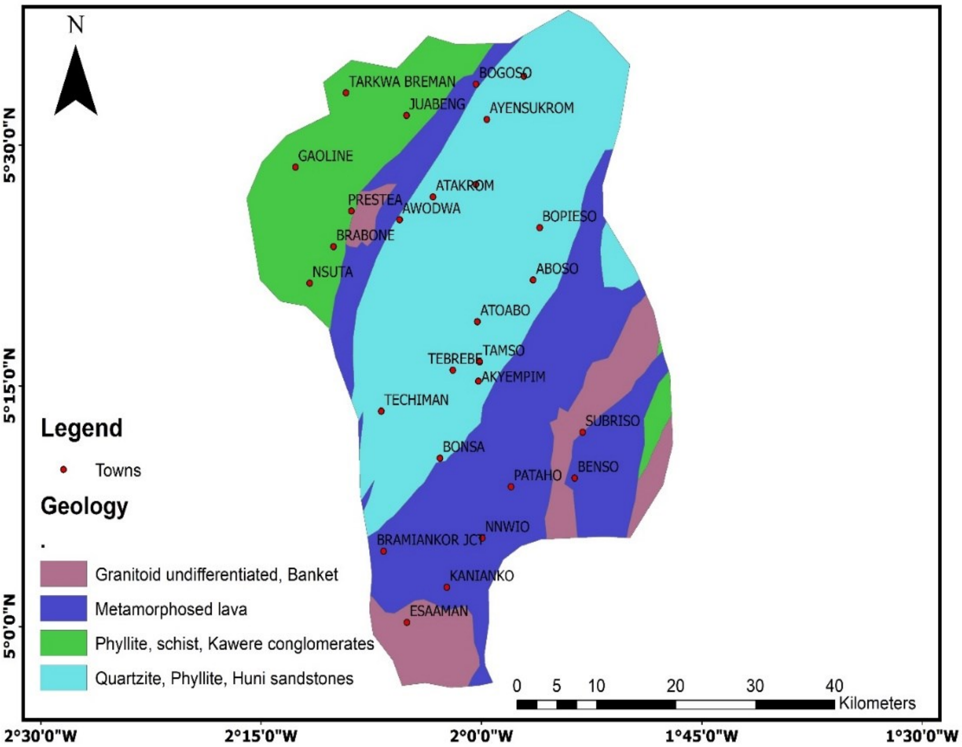

Figure 5: Geology map

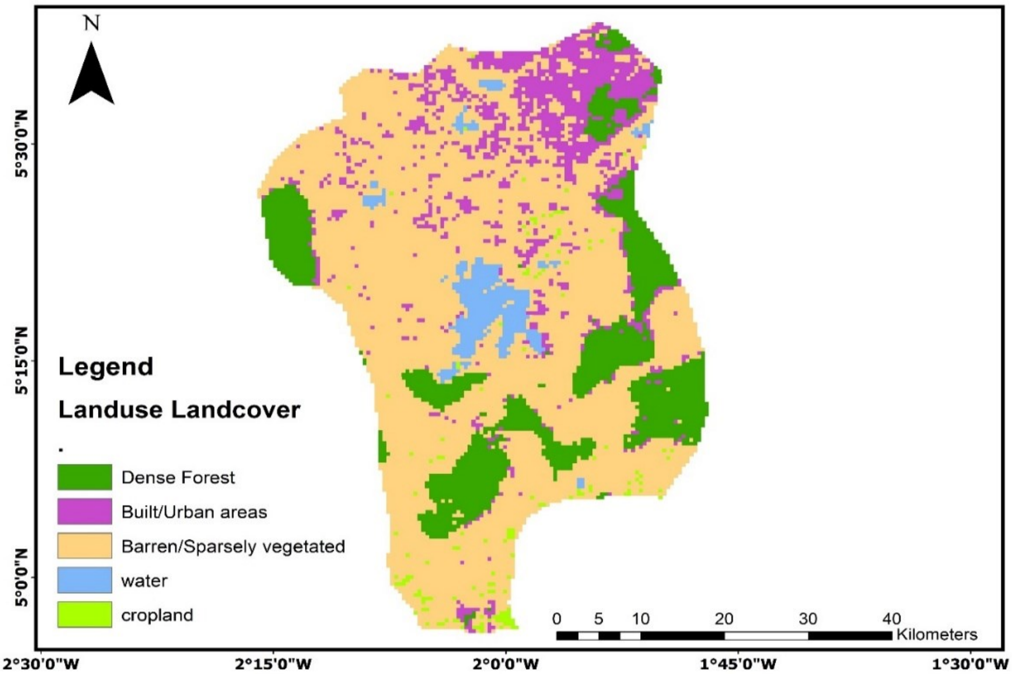

Figure 6: Land use and Land Cover map

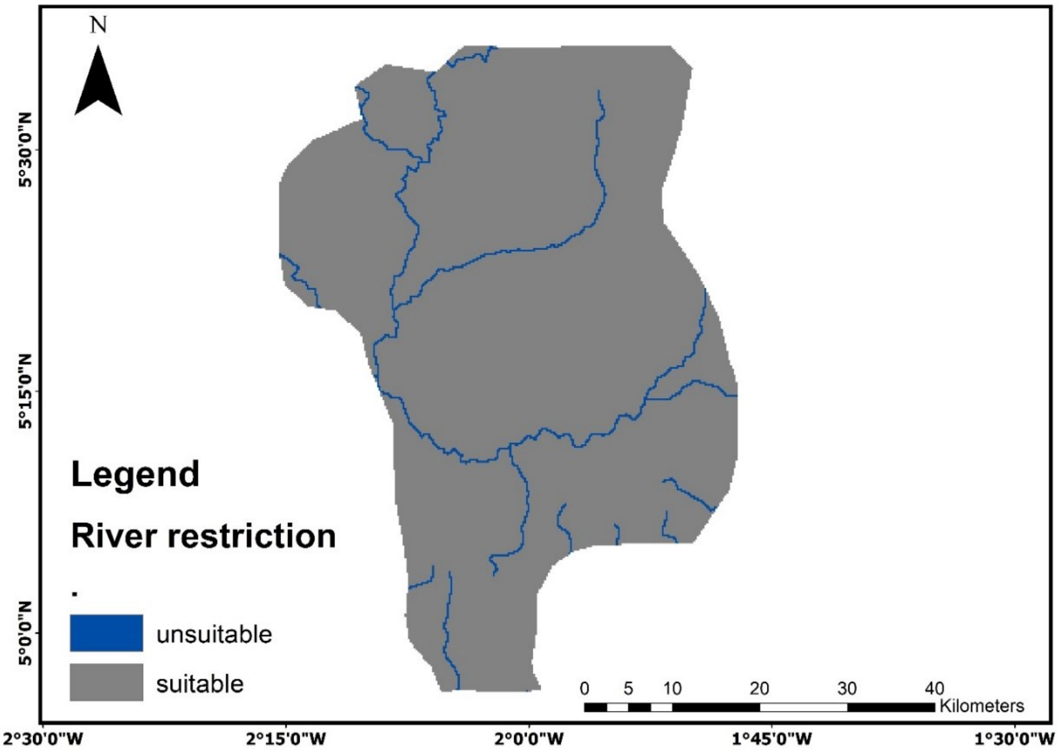

Figure 7: River restriction

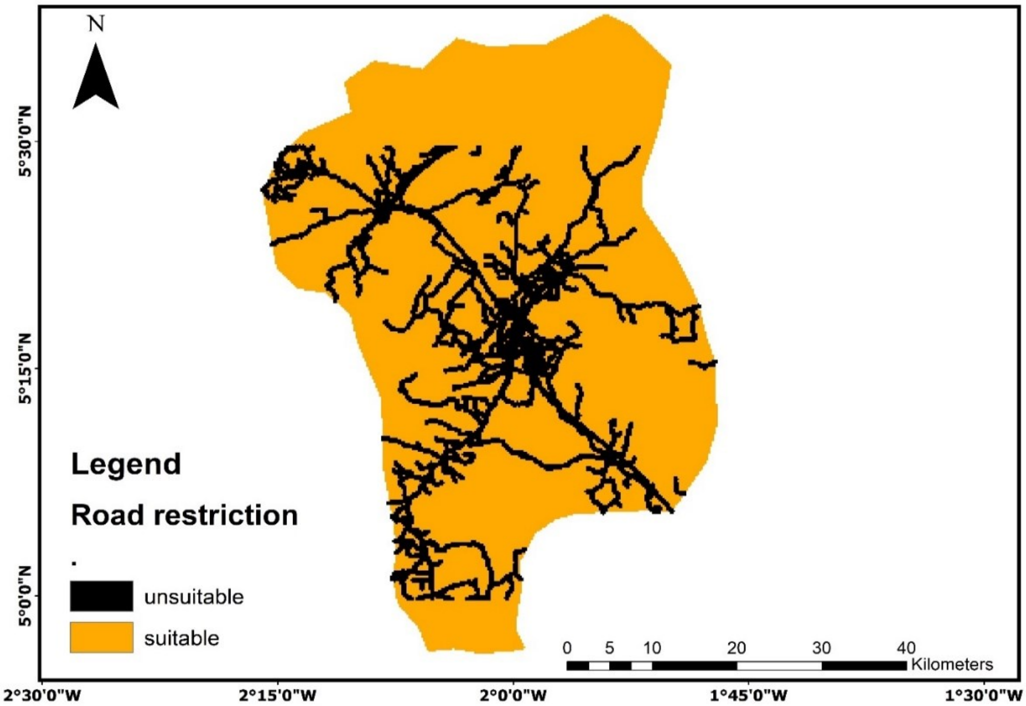

Figure 8: Road restriction

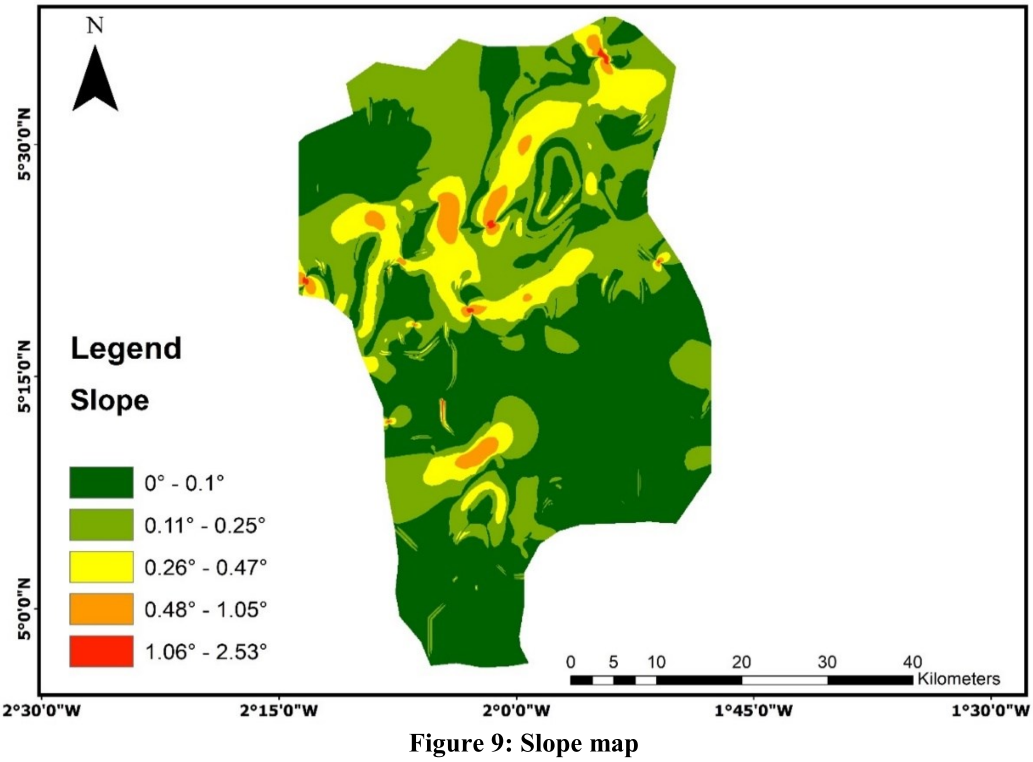

Figure 9: Slope map

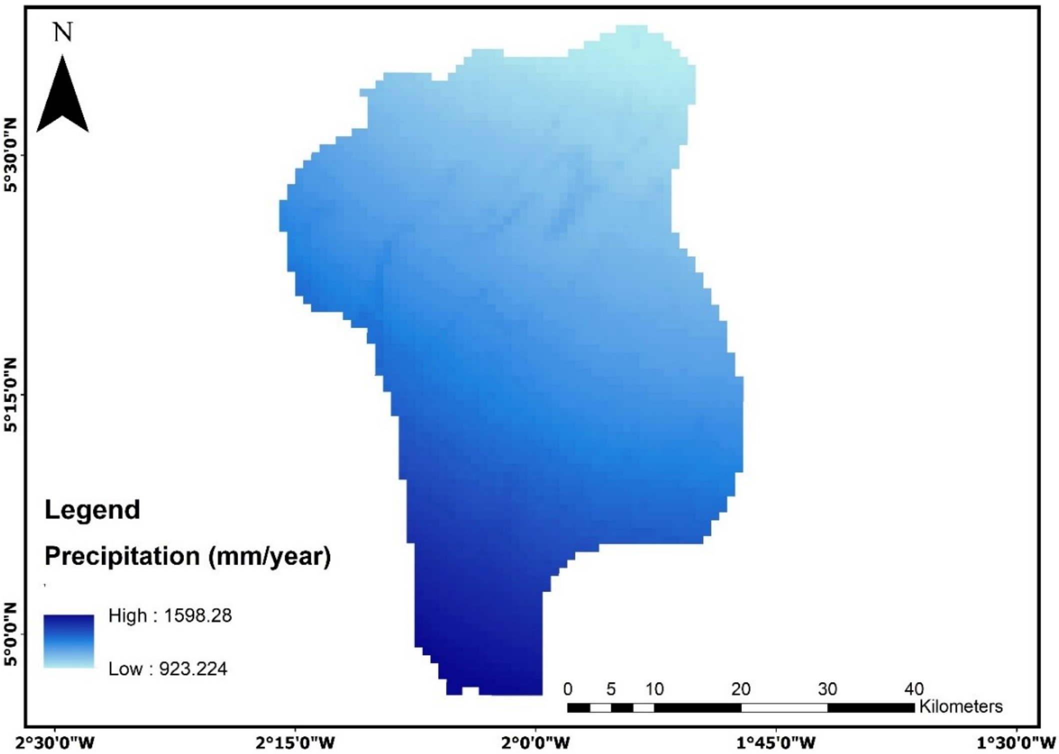

Figure 10: Precipitation map

Table 4: A Pairwise comparison

Criteria (n)	Slope	Geology	Precipitation	Water bodies	Road	LULC
Slope	1	2	2	2	1	2
Geology	1	1	1	1	1	2
Precipitation	1	2	1	2	0.5	1
Water bodies	1	1	1	2	0.5	1
Road	1	1	0.5	1	0.5	1
LULC	0.5	1	1	1	0.5	1
Sum	5.5	8	6.5	9	4	8

Table 5: Normalised data with weights

Criteria (n)	Slope	Geology	Precipitation	Waterbodies	Road	LULC	Weights (%)
Slope	0.1818	0.2500	0.3077	0.2222	0.2500	0.2500	24
Geology	0.1818	0.1250	0.1538	0.1111	0.2500	0.2500	18
Precipitation	0.1818	0.1250	0.0769	0.1111	0.1250	0.1250	17
Waterbodies	0.1818	0.1250	0.1538	0.2222	0.1250	0.1250	16
Road	0.1818	0.1250	0.0769	0.1111	0.1250	0.1250	13
LULC	0.0909	0.1250	0.1538	0.1111	0.1250	0.1250	12

Table 6: Calculation of the consistency vectors

Criteria (n)	Slope	Geology	Precipitation	Waterbodies	Road	LULC	Consistency Vectors
Slope	0.2436	0.4872	0.4872	0.4872	0.2436	0.4872	10
Geology	0.1786	0.1786	0.1786	0.1786	0.1786	0.3573	7
Precipitation	0.1763	0.3526	0.3526	0.3526	0.0882	0.1763	7.5
Waterbodies	0.1555	0.1555	0.1555	0.3110	0.0777	0.1555	6.5
Road	0.1241	0.1241	0.0621	0.1241	0.0621	0.1241	5
LULC	0.0609	0.1218	0.1218	0.1218	0.0609	0.1218	5

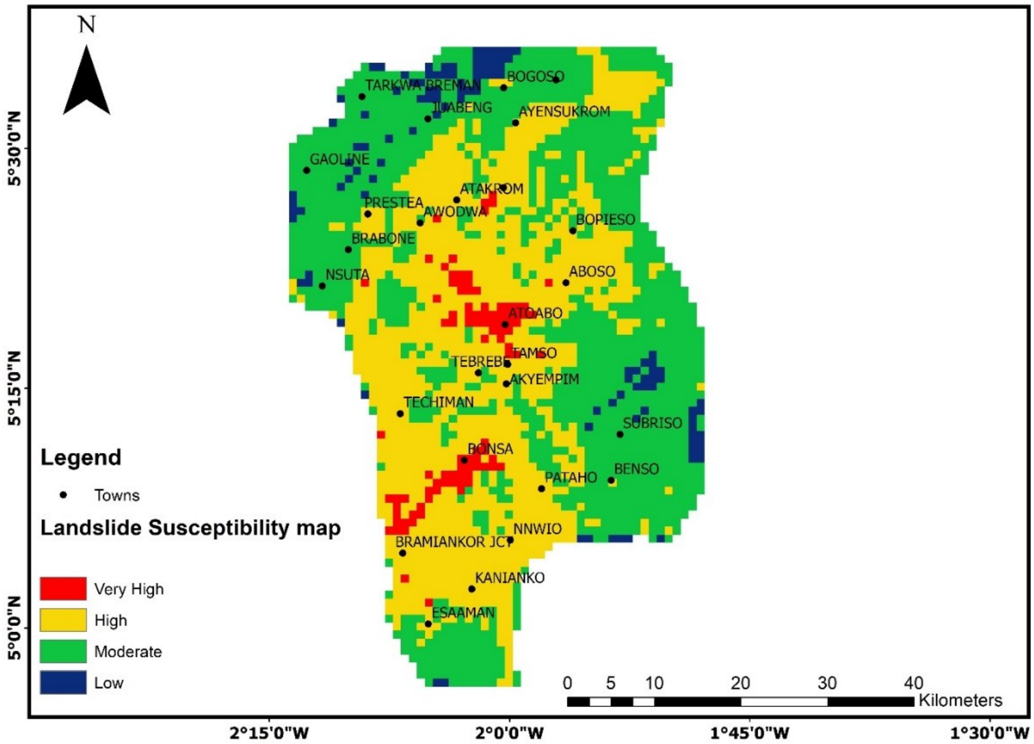

Figure 11: Landslide susceptibility map

Finally, a weighted overlay operation was carried out to sum up the weighted criteria together according to their relative importance to produce a weighted overlay map. The following procedure was adopted in creating the optimal land susceptibility map: Creating buffer zones around the major causative factors (Roads, Water bodies, Slope); Conversion of all the vectors layers to raster layers; Creating a restriction model using the null tool to depicts areas viable or unviable for land use planning; Combination of the various restriction models to attain the final model; and Combination of the final restriction model and suitability model to obtain the final optimal land susceptibility map of the study area. The Landslide susceptibility map is represented by figure 11. The susceptibility zones are grouped into four (4) classes namely; Very High, High, Moderate and Low susceptibility zones with Red, Yellow, Green and Blue colors depicting each zone respectively. The very highly susceptible areas are; Atoabo, Bonsa, Awodwa Nkwanta and Animakrom. The highly prone areas include; Prestea, Aboso, Bogoso, Tarkwa, Tebrebe, and Akyempim. The Moderately prone areas comprise; Nsuta, Bopieso, Subriso, Gaoline, Anyinase, Wassa Nkran, and Huni Valley. Areas that are least susceptible to landslides are Eshireso, Juabeng and Memawoamo. Landslide mapping using GIS and MCDA have shown a great deal of importance and depicting areas suitable and unsuitable for urban development and planning. From figure 11, the high areas were found to be around Atoabo, Bonsa, Awodwa, Nkwanta, and Animakrom requires much attention from planners to help mitigate future landslides. The results shown in this study can help geospatial professionals, developers, planners, governmental and non-governmental agencies, and engineers in slope management and land use planning. Moreover, there must be a consciously when utilizing the models for specific site development. This is because of the scale of the causative factors of the analysis since other causative factors such as geophysical and geotechnical analysis need to be considered. Therefore, the models used in this study are valid of generalized planning and assessment purpose.

5. Conclusions and recommendations

This paper aims at mapping the landslide susceptibility zones in Wassa West district using the AHP. In this study, a combined MCDA and GIS approach have been developed and implemented for landslide susceptibility mapping. The AHP mathematical decision rule-based concept has been proposed for identification of susceptible areas. The combined MCDA and GIS approach was based on an expert idea and reviewed literature for determining the weights and rankings of the causative factors and their categories for landslide occurrences. Restriction cost surfaces were also used as constraint surfaces for delineating suitable areas from unsuitable areas. It was observed from this present study that; the proposed raster optimal map shows some areas of the study area are very high and unsuitable for human settlement and developmental projects in the study area. The final susceptibility map depicts different classes of severity of risk from low, moderate, high and very high risk for various categories of landslides. The adopted AHP decision rule is an objective way of assigning weights for landslide susceptibility mapping and generating matrices, where a lot of subjectively and bias rules are involved. Additionally, implementing AHP concept in ArcGIS environment is quite easy as compared to other conventional techniques. Landslide studies are very important in developing countries including Ghana, since the landslide can result into a huge loss of lives and properties. This is due to rapid human inferences, climate changes, and anthropogenic activities influence the occurrence of landslides. Landslide susceptibility mapping helps to know about the relative likelihood of future land sliding based solely on the properties of the area which can put forward useful recommendation to minimize its effects. In addition, landslide studies provide planners with tools for selecting suitable areas for developmental projects. Moreover, it helps planners to decide the suitable site for the construction of roads, bridges, hydropower plants, and many others. It is obvious that the scientific studies of landslides put forward useful recommendation to reduce the loss of life and property. It is recommended that; the Town and Country Planning department should use this optimal raster map for future redevelopment and assessment of the study area. However, the Geological and Survey Department, Survey and Mapping Division Department, and Meteorological Department of the country should produce an up to date rainfall map, aspect map, and geomorphological map of the study area for further studies to review the affected areas and help give relevant solutions to mitigate the menace to prevent loss of lives and properties.

Acknowledgements

The authors would like to appreciate the anonymous reviewers for their helpful comments that made this piece of knowledge a better one. We also thank the Survey and Mapping Division Department of the Lands Commission of Ghana for providing us with data that was used in the investigation of the research findings.

References

Akay, A.E., and A. Erdogan (2017). GIS-based multi-criteria decision analysis for forest fire risk mapping, ISPRS Annals of the Photogrammetry, Remote Sensing and Spatial Information Sciences, Vol. IV-4/WA, 2017 4th International Geo Advances Workshop, 14-15 October 2014, Safranboln, Karabuk, Turkey, 25-30.

Akay, A.E., and B. Yilmaz (2017). Using GIS and AHP for planning primer transportation of forest products, ISPRS Annals of the Photogrammetry, Remote Sensing and Spatial Information Sciences, Vol. IV-4/WA, 2017 4th International Geo Advances Workshop, 14-15 October 2014, Safranboln, Karabuk, Turkey, 19-24.

Asante-Annor, A., S.A. Konadu, and E. Ansah (2018). Determination of potential landfill site in Tarkwa area using multi-criteria GIS, Geophysical and Geotechnical Evaluation. Journal of Geoscience and Environment Protection, 6, 1-27.

Asklunel, R., and B. Eldvall (2005). Contamination of water resources in Tarkwa mining area of Ghana, Published MSc Thesis, Department of Engineering Geology, Royal Institute of Technology, LTh Ekosystemteknk, 1-72.

Aslani, M., and A.A. Alesheikh (2011). Site selection for small gas stations using GIS, Scientific Research and Essays, 6(15), 3161-3171.

Aysen, A. (2003). Problem Solving in Soil Mechanics, A. A. Balkema Publishers, Lisse, Abingdom, Exton (PA), Tokyo, Japan, 1-77.

Boroushaki, S., and J. Malczewski (2008). implementing and extension of the analytical hierarchy process using ordered weighted averaging operators with fuzzy quantifiers in ArcGIS, Computers & Geosciences Journal, 34, 399-410.

Boye, C.B., M.S. Peprah, and N.K. Kodie (2018). Geographic assessment of telecommunication signals in a mining community: A case study of Tarkwa and its environs, Ghana Journal of Technology, 2(2), 41-49.

Broekhuizen, H., C.G.M. Groothuis-Oudshoorn, J.A. Van Til, J.M. Hummel, and M.J. Ijzerman (2015). A review and classification of approaches for dealing with uncertainty in multi-criteria decision analysis for healthcare decisions, Pharmaco Economics, 33, 445-455.

Budhu, M. (2011). Soil Mechanics and Foundations. 3rd Edition, John Wiley and Sonc, Inc., USA, 1-43.

Cadraku, H., and S. Bejta (2018). Landslide in Kosovo and necessity for their monitoring, International Journal of Natural and Engineering Sciences, 12(1), 14-18.

Cellek, S. (2018). The effect of water on landslide, ucuk landslide (Gerze/Sinop), International Participated Cappadocia Geosciences Symposium, 24-26 October 2018, NIGIDE, Turkey, 1-2.

Chaturvedi, P., and V. Dutt (2018). Interactive Landslide Simulator: Role of Contextual Feedback in Learning Against Landslide Risks, Springer Nature Switzerland AG2018, U. S. Tiwary (Ed.): IHCI 2018, LNSS 1128, 1-10.

Frost, B.R., and C.D. Frost (2014). Essentials of Igneous and Metamorphic Petrology. Cambridge University Press, UK, 1-40.

Hancock, G.R., J.F.M. Duque, and G.R. Willgoose (2019). Geomorphic design and modelling at catchment scale for best mine rehabilitation-The Drayton mine example (New South Wales, Australia), Environmental Modelling & Software, 114, 140-151.

Joe-Asare, T., M.S. Peprah, and M.M. Opoku (2018). Assessment of the potability of underground water from a small-scale underground mine: A Case study, Ghana Mining Journal, 18(2), 61-67.

Kanungo, D.P., M.K. Arora, S. Sarkar, and R.P. Gupta (2006). Remote sensing and GIS based landslide risk assessment using a linguistic rule based fuzzy approach, In Proceedings of SPIE, The International Society for Optical Engineering, December 2006, India, 1-13.

Khadka, A., S. Dhakal, and P. Budha (2018). GIS based landslide susceptibility mapping along the road section from Bandeu to Barahabise, Sindhupal Chonk district of Nepal, International Journal of Science and Research (IJSR), 7(11), 465-471.

Kihoro, J., N.J. Bosco, and H. Murage (2013). Suitability analysis for rice growing sites using a multi-criteria evaluation and GIS approach in Great Mwea Region, Kenya, Springer plus, 2(365), 1-9.

Kortatsi, B.K. (2004). Hydrochemistry of Groundwater in the Mining Area of Tarkwa Prestea, Ghana, Published PhD Thesis, University of Ghana, Legon-Accra, Ghana, 1-45.

Kouli, M., C. Loupasakis, P. Soupios, D. Rozos, and F. Vallianatos (2014). Landslide susceptibility mapping by comparing the WLC and WofE multi-criteria methods in the West Crete Island, Greece, Environmental Earth Sciences Journal, 72, 5197-5219.

Kumi-Boateng, B., and M.S. Peprah (2020). Modelling local geometric geoid using soft computing and classical techniques: A case study of the University of Mines and Technology (UMaT) local geodetic reference network, International Journal of Earth Sciences Knowledge and Applications, 2(3), 166-177.

Larbi, E.K., C.B. Boye, and M.S. Peprah (2018). A GIS approach in optimal route selection in the mining communities using the analytical hierarchy process and the least cost path analysis, 5th UMaT Biennial International Mining and Mineral Conference, Tarkwa, Ghana, GLM 50-62.

Malczewski, J. (1999). GIS and Multicriteria Decision Analysis. John Wiley and Sons, New York, 1-40.

Meshram, S.G., E. Alvandi, V.P. Singh, and C. Meshram (2019). Comparison of AHP and Fuzzy AHP models for prioritization of watersheds, Soft Computing, 1-12.

Mountjoy, J., and A. Micallef (2018). Submarine Landslides. In book: Submarine Geomorphology, 235-250. https://doi.org/10.1007/978-3-319-57852-1_13.

Myers, J.H., and M.I. Alpert (1968). Determinant buying attitudes: meaning and measurement, Journal of Marketing, 32, 13-20.

Njoku, C.G., and A.O. Alagbe (2015). Site suitability assessment of Petrol Filling Stations (PFSs) in Oyo Town, Oyo State, Nigeria: A Geographic Information Systems (GIS) approach, IOSR Journal of Environmental Science, Toxicology and Food Technology (IOSR-JESTFT), 9(12), 8-19.

Peprah, M. S., C.B. Boye, E.K. Larbi, and P. Opoku Appau (2018). Suitability analysis for siting oil and gas filling stations using multi-criteria decision analysis and GIS approach – A case study in Tarkwa and its Environs, Journal of Geomatics, 12(2), 158-166.

Peprah, M.S., and I.O. Mensah (2017). Performance evaluation of the Ordinary Least Square (OLS) and Total Least Square (TLS) in adjusting field data: An empirical study on a DGPS data, South African Journal of Geomatics, 6(1), 73-89.

Peprah, M.S., Y.Y. Ziggah, and I. Yakubu (2017). Performance evaluation of the Earth Gravitational Model (EGM2008) – A case study, South African Journal of Geomatics, 6(1), 47-72.

Politis, S., M. Klumpp, and D. Celebi (2010). Analytical hierarchy process in supplier evaluation. In: Grubbstrom, R. W./Hinterhuber, H. H. (Eds.): 16th International Working Seminar on Production Economics, Conference Proceedings, Innsbruck 01.-05.03.2010, Innsbruck (Eigenverlag), 3, 411-424.

Saaty, T.L. (1977). A scaling method for priorities in hierarchical structures, Journal of Mathematical Psychology, 15, 234-281.

Saaty, T.L. (1980). The Analytic Hierarchy Process: Planning, Priority Setting, Resource Allocation. McGraw-Hill, New York, USA, 641-658.

Saaty, T.L. (1983). Conflict resolution and the Falkland Island invasion, In: Interfaces, 13(6), 841-855.

Samia, J., A. Temme, A.K. Bregt, J. Wallinga, J. Stuiver, F. Guzzetti, F. Ardizzone, F., and M. Rossi (2018). Implementing landslide path dependency in landslide susceptibility modelling, Landslides, 15, 2129-2144.

Sara, R.G., C. Christine, G. Donn, and J. Brad (2011). The benefits of using Geographic Information Systems as a community assessment tool, Public Health Reports, 126(2), 298-303.

Shahabi, H., B.B. Ahmad, and S. Khezri (2012). Application of satellite remote sensing for detail landslide inventories using frequency ratio model and GIS, International Journal of Computer Science Issues, 9(4), 108-117.

Sidle, R.C., R. Greco, and T. Bogaard (2019). Overview of landslide hydrology, Water, 11(148), 1-3.

Silva, T. M., and N.S. Sooriya (2018). Impact of land cover changes on steep slopes in central highlands for accelerating the landslides in Sri Lanka, An experience from Aranayaka landslide, 1st International Conference on Social Sciences (ICSS 2018), 39-41.

Strom, A. (2010). Landslide dams in Central Asia Region, Landslide-Journal of the Japan Landslide Society, 47(6), 309-324.

Sumi, R.S. (2010). Analytical hierarchy process for higher effectiveness of buyer decision process, Global Journal of Management and Business Research, 10(2), 1-8.

Tanyas, H. (2019). Rapid Assessment of Earthquake-Induced Landslides. Published PhD Thesis, ITC Faculty of Geo-Information Science and Earth Observation, University of Twente, Ankara, Turkey, 1-186.

Umar, Z., B. Pradhan, A. Ahmad, M.N. Jebur, and M.S. Tehrany (2014). Earthquake induced landslide susceptibility mapping using an integrated ensemble frequency ratio and logistic regression models in West Sumatera Province, Indonesia. Catena, 118, 124-135.

Westen, C.J.V., R. Soeters, and K. Sijmons (2000). Digital geomorphological landslide hazard mapping of the Alpago Area Italy, International Journal of Applied Earth Observation and Geoinformation (JAG), 2(1), 51-60.

Westen, C.J.V., A.C. Seijmonsbergen, and F. Mantovani (1999). Comparing Landslide Hazards maps, Natural Hazards, 20, 137-158.

Yakubu, I., Y.Y. Ziggah, and M.S. Peprah (2018). Adjustment of DGPS data using artificial intelligence and classical least square techniques, Journal of Geomatics, 12(1), 13-20.

Yakubu, I., D. Mireku-Gyimah, and A.A. Duker (2015). Review of methods for modelling forest fire risk and hazard, African Journal of Environmental Science and Technology, 9(3), 155-165.

Journal of Geomatics Vol. 14, No. 2, October 2020

An assessment of urban growth of Delhi using geospatial techniques

Parul Singh[*,1], Sudha Ravindranath[2], Vidya A[2], K Ganesha Raj[2]
[*1]Banasthali Vidyapith, Tonk, Rajasthan, 304022.
[2]Regional Remote Sensing Centre - South, Bengaluru, Karnataka, 560037.
*Email: parulsinghkasyap@gmail.com

(Received: Jan 24, 2020; in final form Nov 07, 2020)

Abstract: The growing population and urbanization are the leading issue faced by the developing countries in the contemporary world. Due to rapid and unplanned urbanization it is imperative to study the urban growth and its pattern in order to properly plan the city's infrastructure in an environmentally substantial way. In the present study, urban growth and pattern of Delhi has been studied using geospatial techniques. Medium resolution satellite data covering two time periods viz., 1992 (Landsat 5) and 2019 (Landsat 8) have been used for the study. Supervised classification using Maximum Likelihood Classifier (MLC) have been used for generating broad urban land use/land cover and FRAGSTATS software for computing class and landscape metrics. It is seen that Delhi city is undergoing urban sprawling with aggregation at the core area and conversion of rural areas into urban patches at the periphery.

Keywords: Land Use/ Land Cover (LU/LC), spatial metrics, supervised classification, urban growth, urbanization

1. Introduction

Urbanization is a rampant phenomenon at all scales of development around the world. It is considered as an index of transformation from traditional rural economies to modern industrial one. Kingsley Davis has explained urbanization as process of switch from spread out pattern of human settlements to one of concentration in urban centers (Davis, 1962). Cities constantly undergo structural change, improvement and growth; such processes also involve the change in urban relationship with the surrounding environment. In recent years, cities have witnessed rapid urbanization and urban population growth resulting in haphazard sprawling of cities.

According to United Nations Reports (UN, 2018a; UN, 2018b) Delhi will overtake Tokyo as the world's largest city by 2030. Due to rapid growth of population in Delhi, the region is facing many problems associated with housing, waste disposal, air pollution, traffic congestion, shortage of electric power and security. Urban planning is essential because cities are becoming overpopulated and resources are depleting at alarming stage. The level of pollution i.e. air, water and land has increased due to poor environmental management. This has its direct impact on quality of urban environment, affecting efficiency of the people and their productivity in the overall development (Bhatta, 2010). Preservation and protection of the environmentally sensitive areas are mandatory. The study of land use and land cover changes is useful for managing natural resources and monitoring environmental changes (Anas et al., 1998).

The use of geospatial techniques involves visualization, modeling, analysis, computation, manipulation and interpretation of geospatial data using remote sensing, GIS, spatial statistics and GPS. These techniques play an important role in monitoring, quantifying and modeling of spatio- temporal fluctuations in the urban region over a period, identifying the pattern of urban sprawl, and planning for urban development (Coppin et al., 2004).

Delhi being the capital city of India and rapidly undergoing urbanization, there is an urgent need to study the urban growth and its patterns by analysis of spatial and temporal datasets using geospatial techniques. This will help in proper planning of the city and its infrastructure.

2. Scope and Objectives

The major scope of the study is to evaluate the urban growth dynamics from 1992 to 2019, which provides vital information on the urban expansion and its impact on the surrounding environment. To realize the scope, the study is divided into 3 main objectives which are listed below:

1. Generation of urban Land Use/ Land Cover map of Delhi using satellite data for two time periods (1992 and 2019)
2. Computation of spatial metrics to describe the urban growth pattern.
3. Change detection analysis of urban land use.

3. Study Area

The present study has been carried out within NCT-Delhi, the capital city of India located between the 28º24′17″ and 28º53′00″N latitudes and 76°45′30″ and 77º21′30″E longitudes (Figure 1). The study area covers a geographical area of 1,490 km² and Yamuna river divides the city into two parts east and west. Delhi city is located in northern part of India, bordered by Haryana on the north-west and south, Rajasthan on the south-west and Uttar Pradesh on the east. The Delhi Ridge is a remnant of the Aravalli ranges and functions as the green lung space of the city and protects the city from the hot winds coming from the deserts of Rajasthan to the west. The Delhi ridge is divided into four zones namely The Northern Ridge (The Old Delhi), Central Ridge (The New Delhi), South-Central Ridge (The Mehrauli) and Southern Ridge (The Tughlaqabad). The ridge has many forest and sanctuaries, of which Southern Ridge Forest, Sanjay Van, Jahanpapa City Forest, Rajokri Protected Forest and Mangar Bani Forest are ecologically important areas which needs to be protected. There are many historically significant monuments and heritage sites showing the rich history through their architecture viz., Humayun's Tomb, Lodhi Gardens, Qutub Minar, Safdarjung's Tomb, Jantar Mantar, Red Fort, Jama Masjid etc. which are global tourist spots. There is an urgent need to protect and preserve these culturally rich monuments from unplanned urban growth. Apart from this, Delhi is also the hub of education, employment, business and commerce generating enormous job opportunity for skilled and unskilled personnel. In the Proximity of Delhi, there are satellite towns like Gurugram, Noida, Faridabad and Ghaziabad which are the financial and industrial hubs due to which the city witnesses a large extent of migration from all parts of the country. According to the 2011 census, the population of Delhi city was around 16 million (Census of India, 2011) and the present estimated population is nearly 29 million (World Urbanization Prospects, 2018). The increasing population is one of the major driving elements for urban expansion in the region.

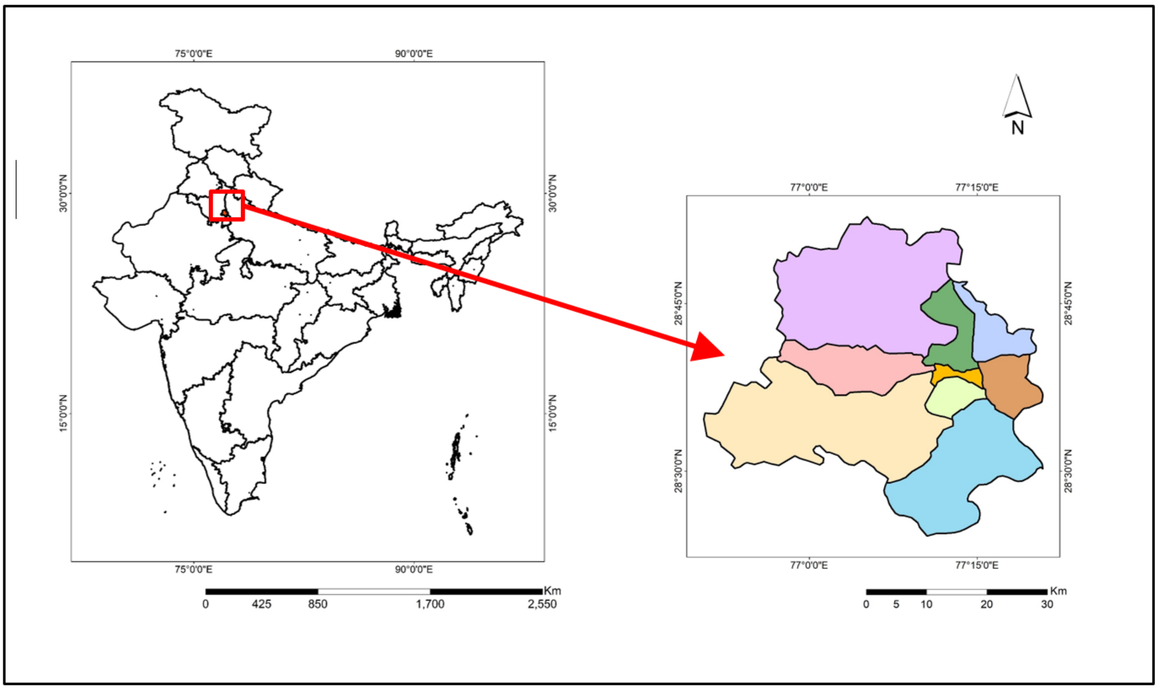

Figure 1: Study area showing NCT- Delhi

4. Data used

In the present study, two Landsat series satellite imageries have been utilized for LU/LC change detection. Satellite imageries have been downloaded from the USGS website (http://glovis.usgs.gov) for temporal study (1992, 2019). The details of the satellite data used is given in table 1.

Table 1: Details of satellite data used

Satellite Name	Sensor	Spatial resolution (meters)	Acquisition
Landsat 5	Thematic Mapper (TM)	30	April 06, 1992
Landsat 8	Operational land Imager (OLI)	30	May 30, 2019

5. Methodology

The satellite data has been pre-processed which includes atmospheric correction. The supervised classification using Maximum Likelihood classifier (MLC) has been adopted for generating broad urban land cover classes. The overall methodology adopted for the study is given in figure 2.

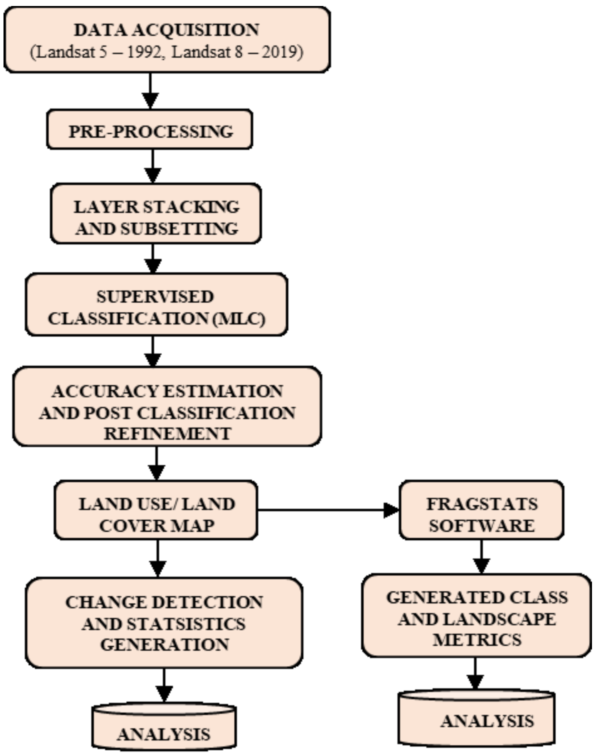

Figure 2: Methodology flowchart

Landsat series satellite images of 1992 and 2019 have been used for the generation of LU/LC maps (Figure 3). The classification scheme adopted has the following LU/LC classes viz., urban (built-up and transportation), water, vegetation, scrub land, open land, cultivated land, fallow land.

The broad steps involved are acquisition of temporal datasets (1992 and 2019) from the USGS website, layer stacking, study area extraction and atmospheric correction to improve the accuracy of the classification of imageries. Supervised classification has been adopted for delineating the broad LU/LC classes. Post classification refinement has been carried out to improve the accuracy of classification (Taubenböck et al., 2007). The description for all the land cover used in the study are mentioned in table 2.

Table 2: Land Use and Land Cover scheme

Land cover	Description
Built -up	Land cover by building and other man – made structures including transportation (railways, roads and airport)
Vegetation	It depicts the vegetation inside the city (parks, gardens, urban green space etc.)
Agriculture land 1. Fallow land 2.Cultivated land	Land covered with temporary crops followed by harvest period, crop fields and pastures. It is agriculture land with no cultivation It is agriculture land with crops
Open land	Open lands are the open space land inside the city with no built-up
Scrub land	It is an elevated land having natural vegetation with low trees (less than 2 meters tall), bushes etc.
Water body	River, lakes, reservoirs

In order to understand the changing urban landscape pattern, spatial metrics have been used for quantifying and categorizing complex landscape structure into simple and identifiable patterns (Herold et al., 2005). The use of these metrics in landscape studies helped in shifting of environmental ecology from a qualitative to quantitative analysis. This has been carried out using FRAGSTATS, a spatial pattern analysis program which uses the LU/ LC images as the input (Abebe, 2013). Seven metrics have been selected based on the literature review which has the potential to best describe urban growth pattern. They are Class Area (CA), Number of Patches (NP), Patch Density (PD), Largest Patch Index (LPI), Contagion Index (CONT), Shannon's Diversity Index (SHDI) and Landscape Shape Index (LSI). Class Area (CA) is a measure of landscape composition, specifically, how much of the landscape is comprised of a particular patch type. Number of Patches (NP) measure the patches in the landscape. Patch Density (PD) measure the number of patches per unit area. Largest Patch Index (LPI) is the percentage of the landscape comprised of the single largest patch (at the class or landscape level). LPI is the measure of dominance. CONTAG measure the tendency of patch type to be spatially aggregated. Landscape Shape Index (LSI) measures the class aggregation or clumpiness. Shannon's Diversity Index (SHDI) measures the diversity of the landscape. The interpretation of the selected spatial metrics is given in table 3 (McGarigal et al., 2002).

Table 3: Spatial metrics interpretation table

Spatial metrics	Pattern of urban growth
Class Area (CA) increases, Number of Patches (NP) increases	Scattered growth of city (Sprawling)
Class Area (CA) increases, Number of Patches (NP) decreases	Infilling & Edge expansion (Urban Growth)
Patch Density (PD) depends on Number of Patches (NP) (Direct relationship) Number of patches decreases, Patch Density decreases Number of Patches increases, Patch Density increases	Infilling & edge expansion happens Scattered growth happens
If Shannon's Diversity Index (SHDI) is 0 If SHDI > 0	No Diversity Diversity of a particular patch type.
If Largest Patch Index (LPI) ≥ 1, without limit Largest Patch Index I = 1	Landscape becomes aggregated Landscape pattern is maximum compact (almost square)
CONTAG decreases CONTAG increases	Landscape pattern is aggregated Landscape pattern is clumped

6. Results and discussion

6.1 Land Use/ Land Cover (LU/LC) map generation

Supervised classification has been carried out on both the satellite datasets (1992 and 2019) by taking appropriate training signatures for broad LU/LC classes viz., built-up, vegetation, open land, fallow land, cultivated land, water bodies and scrub land. The result of the LU/LC is given in table 4 and the classified outputs are given in figure 4. The classified map of 1992 shows concentration of built-up in the center and eastern part of Delhi, but from the 2019 LU/LC classified map it is seen that the direction of the urban growth is toward the south east, south west and north direction. The prominent reason for this urban spread is due to the presence of emerging technological and industrial hubs like Gurugram, Faridabad, Noida and Ghaziabad.

From the table 4, it is seen that the urban area, which was 338 km^2 (23%) in 1992, has increased to 605km^2 (41%) in 2019. The open land which was 130km^2 in 1992 has decreased to 86km^2 in 2019. The agriculture land (fallow and cultivated land) which was 742km^2 (50%) in 1992 has decreased to 533km^2 (36%) in 2019. There is 14% (209 km^2) decrease in the agriculture land from 1992 to 2019, which has been the consequence of conversion of agriculture land into new residential layouts like Dwarka, Rohini, Janakpuri etc.

Marginal changes in area are noticed in the scrub category, because these regions belong to Delhi ridge, which is restricted and preserved by the government authority and forest department, but still has been constantly under the pressures of urban development. The Delhi ridge is the remnant of Aravalli hills which is environmental sensitive region. The ridge has many forest and sanctuaries, of which Southern Ridge Forest, Sanjay Van, Jahanpapa City Forest, Rajokri Protected Forest, Mangar Bani Forest are ecologically important areas which needs to be protected. Minor development has been noticed in vegetation category. The vegetation category represents the greenery inside the city, such as urban green spaces, gardens, parks etc. Thus, an overall 18% increase is observed in the built-up category over 27 years of span.

One of the most important and final step at classification process is accuracy assessment. The aim of accuracy assessment is to quantitively assess how effectively the pixels were sampled into the correct land cover classes. Accuracy estimation has been done for all the classified outputs, with reference to Google Earth imagery. The accuracy assessment of both the classified images were carried out by taking 280 random points which were cross-verified, and the classification accuracy was 85% and 88% for 1992 and 2019 respectively. Post classification refinement was carried to improve the accuracy of LU/LC maps.

Table 4: Land Use/Land cover Statistics

Land Cover	Area in Km^2 and % (1992)	Area in Km^2 and % (2019)	Change in Km^2 (+/ -)
Built-up	338 km^2 23%	604 km^2 41%	+266
Cultivated Land	142 km^2 10%	121 km^2 8%	-21
Fallow Land	600 km^2 40%	412 km^2 27%	-188
Vegetation	143 km^2 9%	150 km^2 10%	+7
Scrub Land	112 km^2 7%	92 km^2 6%	-20
Open Land	130 km^2 9%	86 km^2 6%	-44
Water	25 km^2 2%	25 km^2 2%	No change

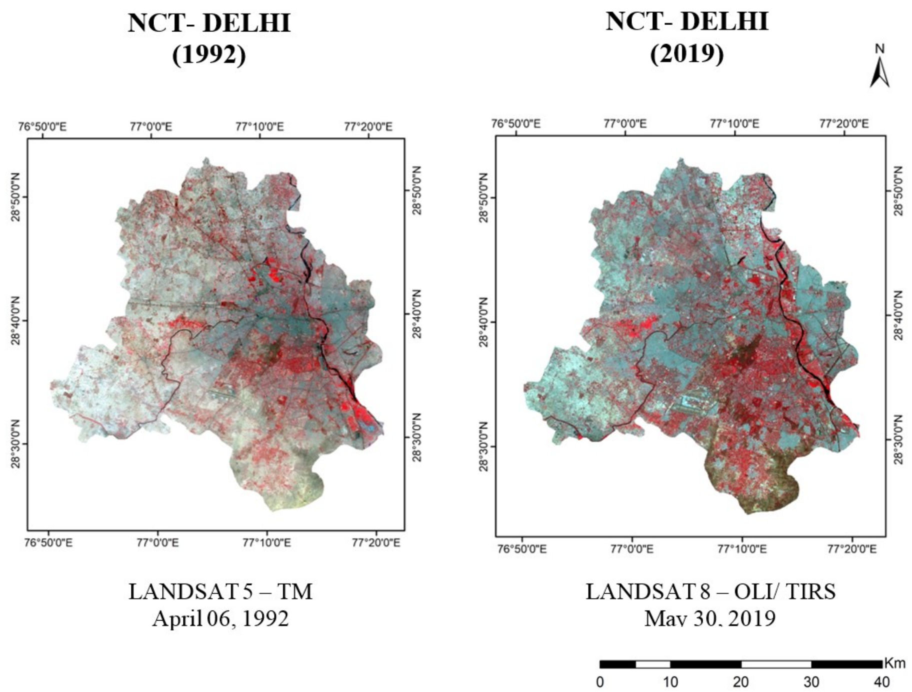

Figure 3: NCT-Delhi as seen in 1992 and 2019 Satellite images

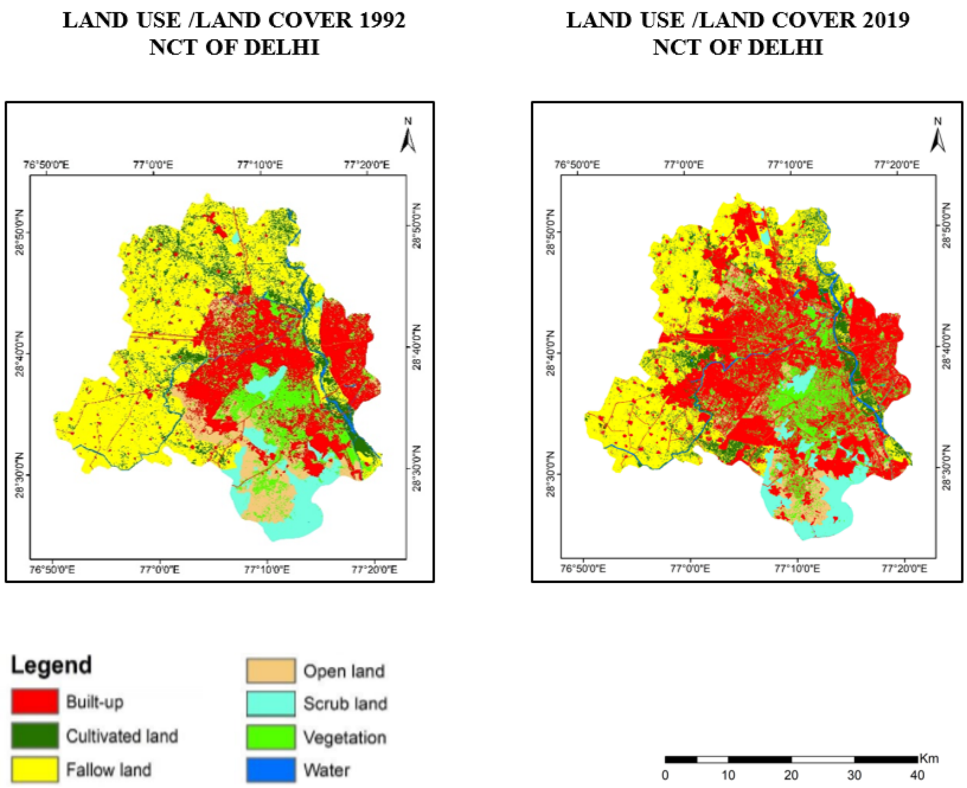

Figure 4: Classified images of NCT- Delhi

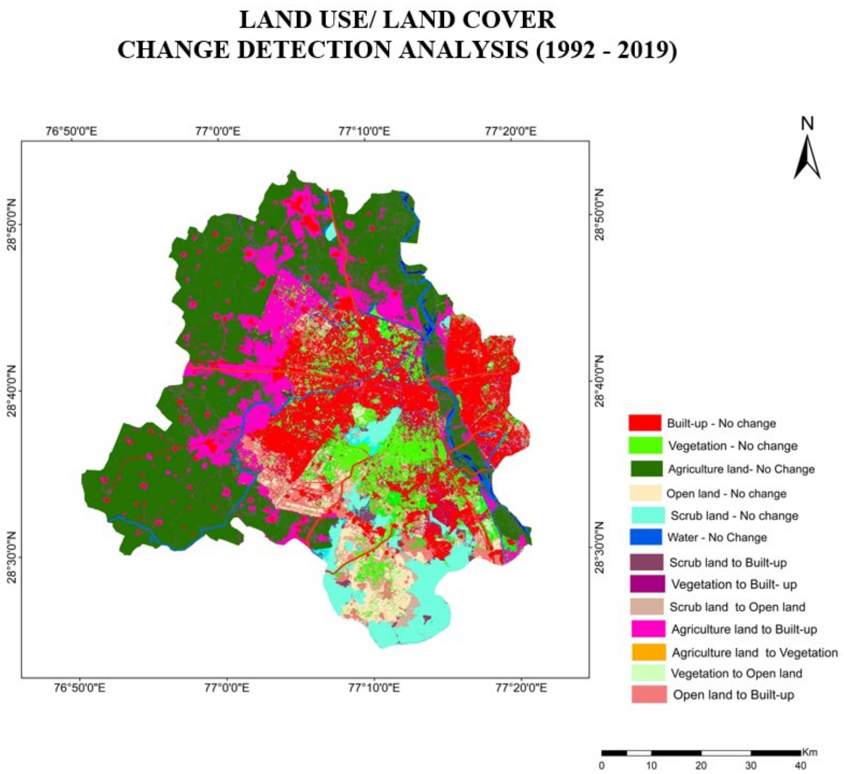

Figure 5: Map showing Land Use and Land Cover change detection analysis for NCT- Delhi (1992-2019)

6.2 Land Use/Land Cover change detection analysis

Change detection analysis has been carried using the LU/LC outputs (1992-2019) and conversion of land cover classes is given in figure 5. For the change detection analysis cultivated and fallow land has been merged as agriculture land. From the analysis, it is seen that 198km^2 agriculture land has been converted into built-up, due to new residential areas like Rohini, Dwarka, Paschim Vihar and Janakpuri. 46 km^2 of open land is also converted into built up area and some vegetation areas and scrub land also converted into built-up; further details are given in table 5. From the figure 5, it is seen that, between 1992-2019 high changes in the LU/LC is seen in the north, west and south part of Delhi, however low changes are seen in the scrub land (Delhi Ridge) and slight changes has been seen in the Yamuna floodplain.

Table 5: Land Use/Land Cover change detection statistics 1992 -2019

Class Name	Change in area (km^2)
Agriculture land to Built-up	198
Scrub land to Built-up	13
Vegetation to Built-up	8
Vegetation to Open land	3
Open land to Built-up	46
Agriculture land to Vegetation	9
Scrub land to Open land	10

6.3 Spatial metrics computation

Using the LU/LC classified maps of 1992, and 2019 in FRAGSTATS software, the class and landscape spatial metrics were computed for 7 classes as mentioned in table 2. The class spatial metrics for Built-up area indicated that, the total Class Area (CA) (1992-2019) has increased by 18% while the Number of urban Patches (NP) has increased by 133% between 1992-2019, indicating the scattered growth of the region. The same observation is confirmed from the increase in patch density value by 133.7% between 1992-2020, along with increase in number of patches, which indicates that the urban expansion is undergoing in a scattered manner. Large Patch Index (LPI) has increased 165% between 1992-2019 which indicates aggregation at the urban core area. The class metrics for LU/LC class is given in table 6.

Table 6: Class metrics for Land Use/Land Cover Classes

CLASS NAME	Number of Patches (NP)		Patch Density (PD) (Number per 100 hectares)		Largest Patch Index (LPI) (Percent)	
	1992	2019	1992	2019	1992	2019
Built-up	3866	9034	1.45	3.39	6.45	17.1
Open land	5507	11190	2.07	4.2	1.9	0.99
Fallow land	1835	3878	0.68	1.45	11.1	8
Cultivated land	7969	6810	2.99	2.5	0.29	0.32
Vegetation	5473	9693	2.05	3.6	2.7	1.5
Scrub land	91	578	0.03	0.21	8.9	1.72
Water	562	1367	0.21	0.51	0.2	0.23

From the landscape analysis with computation of spatial metric indicators, Contagion value (CONTAG) is decreased resulting in the tendency of patch types to be spatially aggregated, similar observation has been seen from Landscape Shape Index (LSI). The increase in Shannon's Diversity Index (SHDI), the richness in the number of different patches type. The landscape metrics for the LU/LC is given in table 7.

From the analysis of LU/LC map and spatial metrics it is seen that Delhi city is undergoing urban sprawling with aggregation at the core area and conversion of rural areas into urban patches at the periphery.

Table 7: Landscape metrics for Land Use/Land Cover Classes

Landscape Metrics	1992	2019
CONTAG	54.8	53.7
SHDI	1.61	1.59
LSI	60.9	80.15

7. Conclusion

From the study, it is seen that the urban growth has increased by nearly 18% over 27-year span with most of the increase is seen due to the conversion of agriculture land into built-up. The spatial metrics analysis has indicated that the city is sprawling with aggregation at the core. It is evident that the combined approach of using geospatial techniques and spatial metrics has helped in capturing the physical dimension of urban growth and pattern leading to better understanding and representation of the spatio-temporal dynamics of NCT-Delhi.

A proper planning is imperative as the available resources are depleting at an alarming rate due to unplanned urbanization. This has its direct impact on quality of urban environment, affecting efficiency of the people and their productivity in the overall development. Preservation and protection of the environmentally sensitive areas are mandatory. The present study is useful for managing natural resources and monitoring environmental changes and will be helpful in planning of the city and its infrastructure.

References

Abebe, G. A. (2013). Quantifying Urban growth Pattern in Developing countries using Remote Sensing and Spatial Metrics: a case study in Kampala, Uganda. Master of Science thesis. University of Twente.

Anas, A, R. Arnott, and K. Amall (1998). Urban spatial structure, Journal of Economic Literature, American Economic Association, 36(3), 1426-1464.

Bhatta, B. (2010). Analysis of Urban Growth and Sprawl from Remote Sensing Data. Advances in Geographic Science, Springer Heidelberg Dordrecht, London, New York. DOI10.1007/978-3- 642- 05299-6., 172 p.

Census, I. (2011). http://censusindia.gov.in/

Coppin, P., I. Jonckheere, K. Nackaerts, B. Muys, and E. Lambin (2004). Digital change detection methods in ecosystem monitoring: a review, International Journal of Remote Sensing, 25(9), 1565-1596.

Davis Kingsley (1962). Urbanization in India – Past and Future in India's Urban Future (R. Turner, Editor), University of California Press, Berkley.

Herold, M., H. Couclelis, and K.C. Clarke (2005). The role of spatial metrics in the analysis and modeling of urban land use change, Computers, Environ. & Urban Systems, 29, 369-399.

McGarigal, K., S.A., Cushman, M.C. Neel, and E. Ene (2002). FRAGSTATS: Spatial pattern analysis program for categorical maps. Amherst: Computer software produced by the authors at the University of Massachusetts.

Taubenbock, H., I. Pengler, B. Schwaiger, S. Cypra, M. Hiete, and A. Roth (2007). A multi-scale urban analysis of the Hyderabad metropolitan area using remote sensing and GIS. In 2007 Urban Remote Sensing Joint Event (pp. 1-6). IEEE.

UN (2018a). Revision of World Urbanization Prospects. United Nations: New York, NY, USA.

UN (2018b). The World's Cities in 2018: Data Booklet, Statistical Papers - United Nations (Ser. A), Population and Vital Statistics Report, UN, New York doi.org/10.18356/c93f4dc6-en

Reviewers for Journal of Geomatics, Volume 14 No. 1 and 2

Editorial Board places on record its sincere gratitude to the following peers for sparing their valuable time to review papers of the Journal of Geomatics, Volume 14.

Dr. A.S. Rajawat
Chief Editor

Dr. Markand Oza	Dr. Hitendra Padalia	Dr. Rojalin Tripathy
Dr. Shard Chander	Dr. Chandan Goswami	Dr. Shibendu S. Ray
Dr. Sameer Saran	Shri J.G. Patel	Dr. Rashmi Sharma
Dr. Ashutosh Bhardwaj	Prof. Sunil Kumar Wanchoo	Shri Rajendra N. Gaikwad
Prof. Ashraf Mousa	Prof. Mahmoud Salah	Shri R.J. Bhanderi
Dr. Praveen Kumar Gupta	Dr. Gaurav Jain	Mr. Rosly Boy Lingdoh
Dr. Vijay Kumar Baraik	Mr. Manish Parmar	Dr. Amit Kumar Dubey
Prof. Julian Smit	Dr. Cynthia Borkai Boye	Dr. Rohit Pradhan
Mr. Pankaj Dhote	Prof. C. Jeganathan	Dr. Asare Asante-Annor
Prof. G.P. Ganapathy	Dr. Bimal Kumar Bhattacharya	Dr. S.P. Vyas
Dr. Ranendu Ghosh	Mr. Amitabh	Mr. Jaya Prasad
Ms. Preeti Rajput	Mrs. Sunanda Trivedi	Dr. B. Karitkeyan

Author index (Vol. 14)

INDIAN SOCIETY OF GEOMATICS: AWARDS

National Geomatics Award for Excellence

This award has been instituted to recognize outstanding and conspicuously important contribution in promoting geomatics technology and applications at the country level. The contributions should have made major impact on the use of this technology for national development.
Areas of contribution considered for the award are:

1. Geographical Information System
2. Global Positioning System
3. Photogrammetry
4. Digital Cartography
5. Applications of Geomatics

The award shall consist of Rs. 50,000/- in cash, a medal and citation.

Eligibility

Any citizen of India, engaged in activities related to geomatics technology and its applications is eligible for this award. The prize is awarded on the basis of work primarily done in India.

The age limit for awardees is 45 years or above as on June 30 of the year of award.

Selection

A duly constituted Award Committee will evaluate all nominations received. The committee shall consist of eminent experts in the field of geo-spatial technology, to be identified by the Executive Council, ISG. The committee shall forward selected name/s to ISG – EC for approval and announcement. Apart from those persons, whose nominations have been received, the Committee may consider any person or persons who, in their opinion, have made outstanding contributions to development of geo-spatial technology and applications.

The award can be withheld in any year if, in the opinion of the committee, no candidate is found suitable in that particular year.

Presentation of the Award

The award shall be presented during the Annual Convention of ISG. Local Hospitality shall be taken care by ISG & Air fare (low cost) may be reimbursed if awardees request for it.

How to make Nomination

The nominations can be proposed by Head of a major research institute/ centre; Vice-Chancellor of a university; Secretary of Government Scientific Departments; President of a National Academy, President, Indian Society of Geomatics / Indian Society of Remote Sensing / Indian National Cartographic Association / ISG fellow or two life members of the society with more than 10 year old membership.

A candidate once nominated would be considered for a total period of two years. Nomination should be sent in the prescribed format to Secretary, ISG.

The last date for receiving nominations shall be September 30 or otherwise extended.

Format for nomination of Geomatics Award for Excellence

1. Name of the Nominee
2. Postal Address
3. Academic Background (Bachelor degree onwards)
4. Field of Specialisation
5. Important positions held (in chronological order)
6. Professional Experience including foreign assignments.
7. Important Awards / Honours
8. Important Publications/Patents: (A set of ten most important publications to be enclosed with this form)
9. Contributions of Nominee based on which the nomination is sent (in 1000 words, also provide a statement in 50 words which may be used for citation.):
10. Other Relevant Information:

Proposer:

Signature
Name
Address
Phone/ Fax
E-mail
Life Membership No. (in case of ISG Member):

Place & Date

Endorsed by (in case nomination is by 2 ISG Life members)

Signature
Name
Address
Phone/ Fax
E-mail
Life Membership No. (in case of ISG Member):

Place & Date
(The proposer should give a brief citation of the nominee's work)

National Geomatics Award

National Geomatics Award to be given each year: a) for original and significant contribution in Geomatics technology, b) for innovative applications in the field of Geomatics. Each award comprises a medal, a citation and a sum of Rs 25,000/- The guidelines for these awards are available on ISG website.

ISG Chapter Award for Best Performance

The best chapter award will be given to an active chapter of Indian Society of Geomatics, which has made significant contribution to further the mandate and goal of the society. The award consists of a citation and medal

President's Appreciation Medal for Contribution to the ISG

This award will be given to a member of the society, who has made noteworthy contribution to the growth of the ISG (its main body or any chapter). The Award consists of a Medal and a Citation.

Prof. Kakani Nageswara Rao Endowment Young Achiever Award

Indian Society of Geomatics instituted a new award from year 2013 named "Prof. Kakani Nageswara Rao Endowment Young Achiever Award", to encourage young researchers/scientists/academicians pursuing research in the field of geospatial technology/applications. The award carries a cash prize of Rs. 10,000/- along with a citation.

NATIONAL GEOMATICS AWARD

Indian Society of Geomatics has instituted two National Geomatics Awards to be given each year for (a) Original and significant contribution in Geomatics technology, (b) Innovative application(s) in the field of Geomatics. Each award comprises a medal, a citation and a sum of Rs. 25,000/-.

The guidelines for the award are as under

Areas of contribution considered for the award (both technology and applications)

1. Geographical Information System
2. Global Positioning System
3. Photogrammetry
4. Digital Cartography
5. Remote Sensing

Eligibility

Any citizen of India engaged in scientific work in any of the above-mentioned areas of research is eligible for the award.

The awards are to be given for the work largely carried out in India.

- First award will be given for original contribution in the field of Geomatics technology supported by publications in a refereed journal of repute.
- Second award will be given for carrying out innovative application(s). Supported by publications in rear reviewed Journals of repute.
- The contribution for the first award should have been accepted by peers through citation of the work.
- Work based on the applications of existing technologies will not be considered for the first award.
- The work should have made impact on the overall development of Geomatics.

How to Send Nomination

Nominations should be sent in the prescribed format, completed in all aspects to the Secretary, Indian Society of Geomatics, Space Applications Centre Campus, Ahmedabad 380 015 by August 31 of the year of award.

Selection Process

An expert committee, consisting of at least three members, constituted by the Executive Council of the Indian Society of Geomatics, will scrutinize the nominations and recommend the awardees' names to the Executive Council. The Council will decide on the award based on the recommendations.

FORMAT FOR AWARD NOMINATION

1. Name of the Candidate:
2. Present Position:
3. Positions held earlier (chronological order):
4. Academic qualifications (Bachelor's degree onwards):
5. Names of at least three Indian Scientists/Technologist in the area as possible referees *:
6. Brief write up on the work (500 words) for which award is claimed:
7. Publication(s) on the above work (reprint(s) to be enclosed):
8. List of other publications of the candidate:
9. Citation of the work for which award is claimed:
10. Impact of the work (for which award is claimed) on the development in the field of Geomatics (500 words):
11. Whether the work has already won any award? If so, give details:

The Applications in the above format (five copies) should be submitted (by Registered Post or Speed Post) to

The Secretary, Indian Society of Geomatics,
Space Applications Centre Campus,
Ahmedabad-380015

so as to reach by September 30 of the year of award

*ISG is, however, not bound to accept these names and can refer the nomination to other experts/peers

Journal of Geomatics Vol 14, No. 2, October 2020

INDIAN SOCIETY OF GEOMATICS: FELLOWS

Shri Pramod P. Kale, Pune
Dr George Joseph, Ahmedabad
Dr A.K.S. Gopalan, Hyderabad
Dr Prithvish Nag, Varanasi
Dr Baldev Sahai, Ahmedabad
Shri A.R. Dasgupta, Ahmedabad
Dr R.R. Navalgund, Bengaluru
Shri Rajesh Mathur, New Delhi
Dr Ajai, Ahmedabad
Prof P. Venkatachalam, Mumbai
Dr Shailesh Nayak
Prof I.V. Murli Krishna
Prof SM Ramasamy, Tiruchirapalli
Dr Ashok Kaushal, Pune
Shri A.S. Kiran Kumar, Bengaluru
Prof. P.K. Verma, Bhopal
Maj. Gen. Siva Kumar, Hyderabad

INDIAN SOCIETY OF GEOMATICS: PATRON MEMBERS

P-1 Director, Space Applications Centre (ISRO), Jodhpur Tekra Satellite Road, Ahmedabad - 380 015
P-2 Settlement Commissioner, The Settlement Commissioner & Director of Land Records-Gujarat, Block No. 13, Floor 2, Old Sachivalay, Sector-10, Gandhinagar – 382 010
P-3 Commissioner, Mumbai Metropolitan Region Development Authority, Bandra-Kurla Complex, Bandra East, Mumbai - 400 051
P-4 Commissioner, land Records & Settlements Office, MP, Gwalior - 474 007
P-5 Director General, Centre for Development of Advanced Computing (C-DAC), Pune University Campus, Ganesh Khind, Pune - 411 007
P-6 Chairman, Indian Space Research Organization (ISRO), ISRO H.Q., Antariksha Bhavan, New BEL Road,Bengaluru 560 231
P-7 Director General, Forest Survey of India, Kaulagarh Road, P.O. I.P.E., Dehra Dun – 248 195
P-8 Commissioner, Vadodara Municipal Corporation, M.S. University, Vadodara - 390 002
P-9 Director, Centre for Environmental Planning and Technology (CEPT), Navarangpura, Ahmedabad - 380 009
P-10 Managing Director, ESRI INDIA, NIIT GIS Ltd., 8, Balaji Estate, Sudarshan Munjal Marg, Kalkaji, New Delhi - 110 019
P-11 Director, Gujarat Water Supply and Sewerage Board (GWSSB), Jalseva Bhavan, Sector – 10A, Gandhinagar - 382 010
P-12 Director, National Atlas & Thematic Mapping Organization (NATMO), Salt Lake, Kolkata - 700 064
P-13 Director of Operations, GIS Services, Genesys International Corporation Ltd., 73-A, SDF-III, SEEPZ, Andheri (E), Mumbai - 400 096
P-14 Managing Director, Speck Systems Limited, B-49, Electronics Complex, Kushiaguda, Hyderabad - 500 062
P-15 Director, Institute of Remote Sensing (IRS), Anna University, Sardar Patel Road, Chennai - 600 025
P-16 Managing Director, Tri-Geo Image Systems Ltd., 813 Nagarjuna Hills, PunjaGutta, Hyderabad - 500 082
P-17 Managing Director, Scanpoint Graphics Ltd., B/h Town Hall, Ashram Road, Ahmedabad - 380 006
P-18 Secretary General, Institute for Sustainable Development Research Studies (ISDRS), 7, Manav Ashram Colony, Goplapura Mod, Tonk Road, Jaipur - 302 018
P-19 Commandant, Defense institute for GeoSpatial Information & Training (DIGIT), Nr. Army HQs Camp, Rao Tula Ram Marg, Cantt., New Delhi - 110 010
P-20 Vice President, New Rolta India Ltd., Rolta Bhavan, 22nd Street, MIDC-Marol, Andheri East, Mumbai - 400 093
P-21 Director, National Remote Sensing Centre (NRSC), Deptt. of Space, Govt. of India, Balanagar, Hyderabad - 500 037
P-22 Managing Director, ERDAS India Ltd., Plot No. 7, Type-I, IE Kukatpalli, Hyderabad - 500 072
P-23 Senior Manager, Larsen & Toubro Limited, Library and Documentation Centre ECC Constr. Gp., P.B. No. 979, Mount Poonamallee Road, Manapakkam, Chennai - 600 089.
P-24 Director, North Eastern Space Applications Centre (NE-SAC), Department of Space, Umiam, Meghalaya 793 103
P-25 Progamme Coordinator, GSDG, Centre for Development of Advanced Computing (C-DAC), Pune University Campus, Pune – 411 007
P-26 Chief Executive, Jishnu Ocean Technologies, PL-6A, Bldg. No. 6/15, Sector – 1, Khanda Colony, New Panvel (W), Navi Mumbai – 410 206
P-27 Director General, A.P. State Remote Sensing Applications Centre (APSRAC), 8th Floor, "B" Block, Swarnajayanthi Complex, Ameerpet, Hyderabad- 500 038
P-28 Director, Advanced Data Processing Res. Institute (ADRIN), 203, Akbar Road, Tarbund, Manovikas Nagar P.O., Secunderabad –500 009
P-29 Managing Director, LEICA Geosystems Geospatial Imaging Pvt. (I) Ltd., 3, Enkay Square, 448a Udyog Vihar, Phase-5, Gurgoan- 122 016
P-30 Director, Defense Terrain Research Limited (DTRL), Ministry of Defense, Govt. of India, Defense Research & Development Organisation, Metacafe House, New Delhi – 110 054
P-31 Chairman, OGC India Forum, E/701, Gokul Residency, Thakur Village, Kandivali (E), Mumbai – 400 101
P-32 Managing Director, ML Infomap Pvt. Ltd., 124-A, Katwaria Sarai, New Delhi – 110 016
P-33 Director, Rolta India Limited, Rolta Tower, "A", Rolta Technology Park, MIDC, Andheri (E), Mumbai – 400 093
P-34 Director, State Remote Sensing Applications Centre, Aizawl – 796 012, Mizoram

Instructions for Authors

The journal covers all aspects of Geomatics – geodata acquisition, pre-processing, processing, analysis and publishing. Broadly this implies inclusion of areas like GIS, GPS, Photogrammetry, Cartography, Remote Sensing, Surveying, Spatial Data Infrastructure and Technology including hardware, software, algorithm, model and applications. It endeavors to provide an international forum for rapid publication of developments in the field – both in technology and applications.

A manuscript for publication must be based on original research work done by the author(s). It should not have been published in part or full in any type of publication nor should it be under consideration for publication in any periodical. Unsolicited review papers will not be published.

The Editorial Board or the Indian Society of Geomatics is not responsible for the opinions expressed by the authors.

Language

The language of the Journal will be English (Indian). However, manuscripts in English (US) and English (British) are also acceptable from authors from countries located outside India.

Manuscript Format

Each paper should have a title, name(s) of author(s), and affiliation of each of the authors with complete mailing address, e-mail address, an abstract, four to six keywords, and the text. The text should include introduction/background, research method, results, discussion, followed by acknowledgements and references. The main text should be divided in sections. Section headings should be concise and numbered in sequence, using a decimal system for subsections. Figures, images and their captions should be inserted at appropriate points of the text. Figures, images and tables should fit in two column format of the journal. If absolutely necessary, figures, images and tables can spread across the two columns. Figures and images, however, should not exceed half a page in height. A title should be provided for each Table, Image and Figure. All figures and images should be in 600 dpi resolution and sized as per column/margin width. Authors must ensure that diagrams/figures should not lose easy readability upon reduction to column size. The SI (metric) units and international quantities should be used throughout the paper. In case measurements are given in any other system, equivalent measurements in SI (metric) units should be indicated in brackets.

Use MS Word with English (UK/US) or English (Indian) dictionary. The page size should be A4 paper, with 2 cm margin on all sides. Title, authors and affiliation should be centred. Abstract should be justified across margins. The manuscript text should be in two columns of 8.2 cm each with a gutter of 6mm between them. Use only Times New Roman fonts. Title should be 12 points bold. Authors and affiliation should be 9 points. All other text including headings should be 10 points. Heading numbering scheme should be decimal e.g. 1, 1.1, 1.2.3, etc. Headings should be in bold.

Normally length of a published paper should be about 6-10 pages in A4 size including figures. Use of illustrations in colour should be restricted and resorted to only where it is absolutely necessary and not for enhancing the look of the paper. If the number of colour illustrations exceeds five, authors' institution may be asked to reimburse the extra cost involved, which at current rates is about Rs. 2500 per coloured figure/diagram/plate/illustration.

Submission of Manuscript

Submissions should be in electronic form via email. The manuscript may be sent by email to drajai1953@gmail.com. In exceptional cases hard copy submission in camera ready form may be allowed with the prior permission of the Chief Editor. Submission in any other form will be returned to the author. To speed up the review process, authors are advised to provide a list of three probable reviewers with their institutional address and e-mail IDs.

Guidelines for Citing References

Names of all cited publications should be given in full. No abbreviations should be used. Following procedure is to be adopted.

Journal Publications

Bahuguna, I.M. and A.V. Kulkarni (2005). Application of digital elevation model and orthoimages derived from IRS-1C Pan stereo data in monitoring variations in glacial dimensions, Journal of the Indian Society of Remote Sensing, 33(1), 107- 112. (to be referred to in the text as Bahuguna and Kulkarni (2005) or if more than two sets of authors are to be referred to, as (Bahuguna and Kulkarni, 2005; Jain et al., 1994)) When more than two authors are to be referred to, use Jain et al. (1994). However, in References, all authors are to be mentioned.

Publication in a Book

Misra, V.N. (1984). Climate, a factor in the rise and fall of the Indus Civilization – Evidence from Rajasthan and Beyond in Frontiers of the Indus Civilization (B.B. Lal and S.P. Gupta: Chief Editors) Books and Books, New Delhi, pp. 461-489

Papers Published in Seminar/ Symposium Proceedings

Jain, A., A.R. Shirish, M. Das, K. Das, M.C. Porwal, and P.S. Roy (1994). Remote Sensing and Geographic Information System – An approach for the assessment of biotic interference in the forest ecosystem. Proceedings. 15th Asian Conference on Remote Sensing, Bangalore, November 17-23, 1994, pp. 65-72.

Books

Possehl, Gregory L. (1999). Indus Age: The beginnings. Oxford and IBH Publishing Corporation, New Delhi.

Reviewing

Each paper will be reviewed by three peers. Papers forwarded by members of the Editorial or Advisory Boards along with their comments would get processed faster and may be reviewed by two referees only.

Sample format for Authors is available in downloadable form at ISG website: www.isgindia.org/JOG/Sample_format.doc

Copyright

The copyright of the paper selected for publication will rest with the Indian Society of Geomatics. Corresponding author shall be required to sign a copyright assignment form, on behalf of all authors, once the paper is selected for publication. Authors are, however, at liberty to use this material elsewhere after obtaining permission from the Indian Society of Geomatics.

If the authors have used any copyright material in their manuscript, it is understood that they have obtained permission from the owner of the copyright material and they should convey the same along with the manuscript to the Chief Editor.

Certificate of Original Work

The authors will also provide a certificate that the paper is an original work, not published or being considered for publication elsewhere.

In the event the certificate turns out to be false, the Journal shall ban the author(s) from publishing in the Journal for a period of five years and inform the same to all other related publications.

Reprints

Authors will be allowed to download the (PDF) of their paper from ISG Website www.isgindia.org, No hard copy reprints will be provided.

ISG

To,
The Secretary, Indian Society of Geomatics
6202, Space Applications Centre (ISRO)
AHMEDABAD – 380 015. INDIA

Sir,

I want to become a Member/ Life Member/ Sustaining Member/ Patron Member/ Foreign Member/ Student Member of the Indian Society of Geomatics, Ahmedabad for the year _____. Membership fee of Rs. _____ /- is being sent to you by Cash/ DD/ Cheque. (In case of DD/ Cheque No.__________dated_________drawn on Bank _______________________________ . **I agree to abide by the Constitution of the Society.**

Date:

Place: **Signature**

- Name: Mr/Ms/Mrs/Dr____
- Address: ____

____PIN: _____________

Phone: ______________ Fax: ________________Email:
_______________________________________ • Date of Birth
____

•Qualifications____

- Specialisation: ____
- Designation: _________________________ Organisation. ____________________________
- Membership in other Societies: ____
- Mailing Address: ____

____PIN: ____________________

Proposed by:
(Member's Name and No)
Signature of Proposer

For Office Use: A/P/L Member No.		Receipt No.		Date:	

Indian Society of Geomatics (ISG), Room No. 6202 Space Applications Centre (ISRO), Ahmedabad-380015, Gujarat. Url: www.isgindia.org Phone: +91-79 26916202
Email: secretary@isgindia.org or sasharma@sac.isro.gov.in Fax +91-79-26916287

MEMBERSHIP FEES

Sr. No.	Membership Category	Life/Patron Membership fees ₹ Indian	US $ Foreign	Annual Subscription ₹ Indian
1.	Annual Member	10	---	300
2.	Life Member a) Admitted below 45 years of age	2500	250	
	b) Admitted after 45 years of age	2000	200	
3.	Sustaining Member	---	---	2000
4.	Patron Member	50000	3000	---
5.	Student Member	10	---	100

MEMBERSHIP GUIDELINES

- Subscription for Life Membership is also accepted in two equal instalments payable within duration of three months, if so desired by the applicant. In such a case, please specify that payment will be in instalments and also the probable date for the second instalment (within three months of the first instalment).
- A Member of the Society should countersign application of membership as proposer.
- Subscription in DD or Cheque should be made out in the name of **'Indian Society of Geomatics'** and payable at Ahmedabad.
- Direct deposit in ISG A/Cs must include bank fee RS. 25/- for cash payment.
- Financial year of the Society is from April 1 to March 31.
- For further details, contact Secretary, Indian Society of Geomatics at the address given above.
- ISG has chapters already established at the following places. Ahmedabad, Ajmer, Bhagalpur, Bhopal, Chennai, Dehradun, Delhi, Hissar, Hyderabad, Jaipur, Ludhiana, Mangalore, Mumbai, Mysore, Pune, Shillong, Trichi, Srinagar, Vadodara, Vallabh Vidya Nagar, Visakhapatnam and Trivandrum. Applicants for membership have the option to contact Secretary/Chairman of the local chapter for enrolment. Details can be found at the website of the Society: www.isgindia.org.
- Journal of the Society will be sent to Life Members by softcopy only.

Indian Society of Geomatics (ISG), Room No. 6202 Space Applications Centre (ISRO), Ahmedabad-380015, Gujarat. Url: www.isgindia.org Phone: +91-79 26916202
Email: secretary@isgindia.org or sasharma@sac.isro.gov.in Fax +91-79-26916287

Geomatics Revealed

IGiS

Integrated GIS & IP Software

VERSION 2.0

MAKE IN INDIA

National Awards on Technology
By The Former President of India,
Dr. A. P. J. Abdul Kalam

Launch of IGiS Version 2.0
By Padam Shri AS Kiran Kumar, Chairman, ISRO and
Shri Tapan Mishra, DIRECTOR, SAC, ISRO.

What's new in IGiS

IGiS Version 2.0 is full of enhancements which you'll appreciate every day. New advanced GIS/IP and SAR modules are vital now a days. New COM Based Architecture makes you even more productive. The more you do with IGiS Version 2.0, the more you'll wonder how you ever did without it.

Enhancements in IGiS Version 2.0

- Advanced GIS / Image Processing
- Microwave SAR Analysis
- Meteorological Analysis
- COM Based Scalable Architecture
- New Ribbon Bar GUI
- Python Customization
- OGC Standards

Product Development Partner

इसरो isro
Government of India | Department of Space
Indian Space Research Organisation - (ISRO)

SGL Scanpoint Geomatics Ltd.
www.scanpointgeomatics.com

Scanpoint Geomatics Ltd.
Corporate Office : 12, Abhishree Corporate Park, Iskcon - Ambli Road, Ahmedabad - 380 058. Gujrat (India)
[P] +91 2717 297096-98 [F] +91 2717 297039 [E] info@scanpointgeomatics.com [W] www.scanpointgeomatics.com

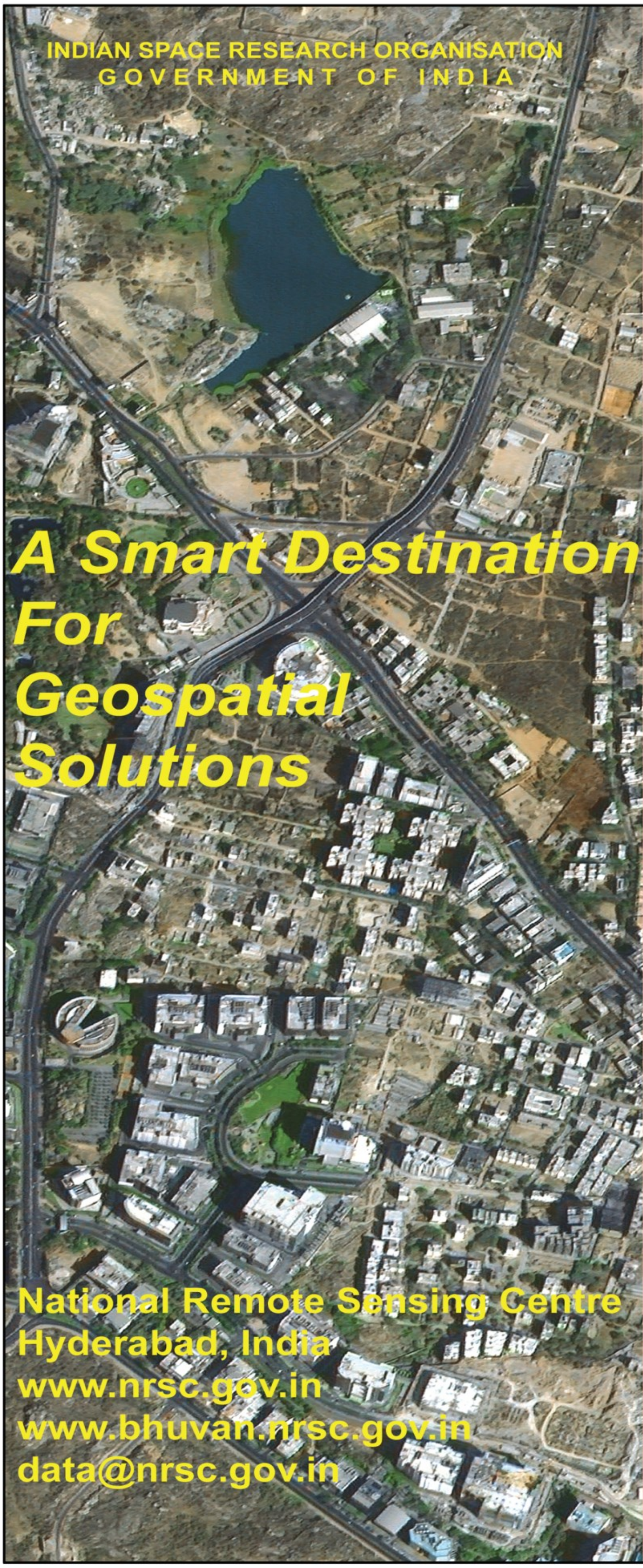

INDIAN SPACE RESEARCH ORGANISATION
GOVERNMENT OF INDIA

A Smart Destination For Geospatial Solutions

National Remote Sensing Centre
Hyderabad, India
www.nrsc.gov.in
www.bhuvan.nrsc.gov.in
data@nrsc.gov.in

nrsc

इसरो isro

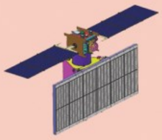

Only Organization in the Country to Acquire & Supply Satellite Data to Users

Aerial Acquisition for Specific User Demands & Disaster Management Support

Open Data & Value Added Products Dissemination Through Bhuvan

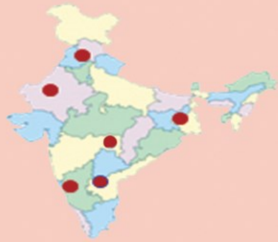

Region Specific Solutions

Capacity Building in Remote Sensing Applications